AD-A165 055 CONCEPTS FOR THE DEVELOPMENT OF A NONDESTRUCTIVE TESTING AND EVALUATION S..(U) ILLINOIS UNIV AT URBANA NEWMARK CIVIL ENGINEERING LAB P T FOXWORTHY NOV 85 1/3

UNCLASSIFIED AFESC/ESL-TR-85-46 F08637-84-M-1743 F/G 14/2 NL

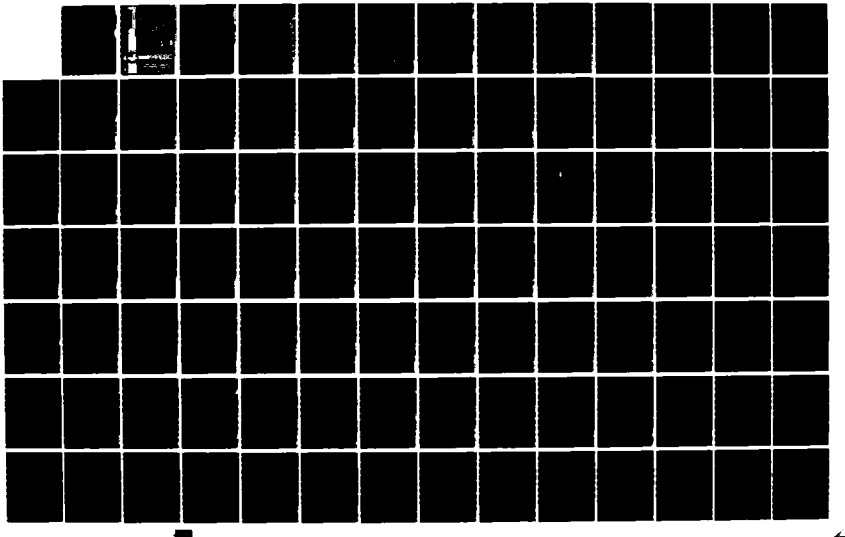

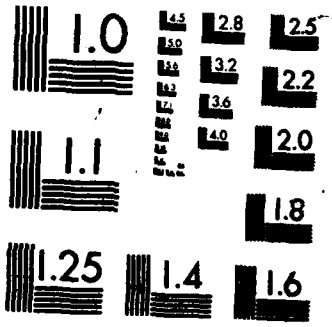

ESL-TR-85-46

Concepts for the Development of a Nondestructive Testing and Evaluation System for Rigid Airfield Pavements

P. T. FOXWORTHY
UNIVERSITY OF ILLINOIS
1211 NEWMARK CIVIL ENGINEERING LAB
208 N. ROMINE ST.
URBANA, IL 61801

NOVEMBER 1985

FINAL REPORT

JANUARY 1983 - MAY 1985

AFESC

ENGINEERING & SERVICES LABORATORY
AIR FORCE ENGINEERING & SERVICES CENTER
TYNDALL AIR FORCE BASE, FLORIDA 32403

NOTICE

PLEASE DO NOT REQUEST COPIES OF THIS REPORT FROM HQ AFESC/RD (ENGINEERING AND SERVICES LABORATORY). ADDITIONAL COPIES MAY BE PURCHASED FROM:

NATIONAL TECHNICAL INFORMATION SERVICE
5285 PORT ROYAL ROAD
SPRINGFIELD, VIRGINIA 22161

FEDERAL GOVERNMENT AGENCIES AND THEIR CONTRACTORS REGISTERED WITH DEFENSE TECHNICAL INFORMATION CENTER SHOULD DIRECT REQUESTS FOR COPIES OF THIS REPORT TO:

DEFENSE TECHNICAL INFORMATION CENTER
CAMERON STATION
ALEXANDRIA, VIRGINIA 22314

UNCLASSIFIED
SECURITY CLASSIFICATION OF THIS PAGE

AD-A165055

REPORT DOCUMENTATION PAGE

1a. REPORT SECURITY CLASSIFICATION: UNCLASSIFIED	1b. RESTRICTIVE MARKINGS
2a. SECURITY CLASSIFICATION AUTHORITY	3. DISTRIBUTION/AVAILABILITY OF REPORT: Approved for Public Release. Distribution Unlimited
2b. DECLASSIFICATION/DOWNGRADING SCHEDULE	
4. PERFORMING ORGANIZATION REPORT NUMBER(S): ESL-TR-85-46	5. MONITORING ORGANIZATION REPORT NUMBER(S)
6a. NAME OF PERFORMING ORGANIZATION: University of Illinois; 6b. OFFICE SYMBOL (If applicable)	7a. NAME OF MONITORING ORGANIZATION: Air Force Engineering and Services Center
6c. ADDRESS (City, State and ZIP Code): 1211 Newmark Civil Engineering Lab, 208 N. Romine St., Urbana, IL 61801	7b. ADDRESS (City, State and ZIP Code): HQ AFESC/RDCS, Tyndall AFB, FL 32403
8a. NAME OF FUNDING/SPONSORING ORGANIZATION; 8b. OFFICE SYMBOL (If applicable)	9. PROCUREMENT INSTRUMENT IDENTIFICATION NUMBER: F08637-84-M-1743
8c. ADDRESS (City, State and ZIP Code)	10. SOURCE OF FUNDING NOS.

PROGRAM ELEMENT NO.	PROJECT NO.	TASK NO.	WORK UNIT NO.
62601F	2673	00	42

11. TITLE (Include Security Classification): Concepts for the Development of a Nondestructive Testing and Evaluation System for Rigid Airfield Pavements

12. PERSONAL AUTHOR(S): Foxworthy, P. T.

13a. TYPE OF REPORT	13b. TIME COVERED	14. DATE OF REPORT (Yr., Mo., Day)	15. PAGE COUNT
Final	FROM Jan 83 TO May 85	November 1985	269

16. SUPPLEMENTARY NOTATION: Availability of this report is specified on reverse of front cover.

17. COSATI CODES			18. SUBJECT TERMS (Continue on reverse if necessary and identify by block number)		
FIELD	GROUP	SUB. GR.			
13	02		Nondestructive Testing	Operation	Environment
			Pavements	Distribution	Geology
			Aircraft	Computer Applications	

19. ABSTRACT (Continue on reverse if necessary and identify by block number)

This technical report develops a complete system for nondestructive testing and evaluation of rigid airfield pavements. An extensive review of present destructive and nondestructive equipment and methodologies is made to form the basis for selection of the equipment and analytical model used in this research. A brief description of the selected Dynatest Model 8000 Falling Weight Deflectometer (FWD) and the ILLISLAB finite element computer model is presented. Three Air Force installations were chosen for in-depth study of pavement response to FWD loads under a variety of environmental and geological conditions. Techniques are presented to determine the location of maximum damage to rigid pavement slabs for one or any combination of aircraft, and the validity of the calculated stresses is established through comparisons of measured and predicted deflections at joints. Major study findings include: (1) new designations for pavement features based on actual loading conditions, (2) guidelines for planning and conducting large-scale evaluations of major airfield systems, (3) a computer-based determination of E and K (continued on back of page)

20. DISTRIBUTION/AVAILABILITY OF ABSTRACT	21. ABSTRACT SECURITY CLASSIFICATION
UNCLASSIFIED/UNLIMITED ☒ SAME AS RPT. ☐ DTIC USERS ☐	Unclassified

22a. NAME OF RESPONSIBLE INDIVIDUAL	22b. TELEPHONE NUMBER (Include Area Code)	22c. OFFICE SYMBOL
Major Robert Costigan	904-283-6264	RDCS

DD FORM 1473, 83 APR — EDITION OF 1 JAN 73 IS OBSOLETE.

UNCLASSIFIED
SECURITY CLASSIFICATION OF THIS PAGE

Block 19 (continued)

(4) joint behavior prediction under fluctuating temperatures and their effect on generated slab stresses, (5) procedures to account for the annual distribution of traffic over the range of temperatures normally experienced at any facility, (6) a simplistic means of estimating total past damage from aircraft operations, and (7) development of computer programs to predict remaining structural life of rigid airfield pavements.

PREFACE

This report was submitted as a doctoral thesis to the Department of Civil Engineering, University of Illinois funded under Job Order Number 2673-0042 by the Air Force Engineering and Services Center, Engineering and Services Laboratory, Tyndall AFB, Florida 32403.

This thesis is being published in its original format by this laboratory because of its interest to the worldwide scientific and engineering community. This thesis covers work performed between January 1983 and May 1985. AFESC/RD project officer was Major Robert Costigan.

This report has been reviewed by the Public Affairs Officer (PA) and is releasable to the National Technical Information Service (NTIS). At NTIS, it will be available to the general public, including foreign nationals.

This technical report has been reviewed and is approved for publication.

ROBERT R. COSTIGAN, Major, USAF
Project Officer

JAMES R. VAN ORMAN
Deputy Director of Engineering
and Services Laboratory

EVERETT L. MABRY, Lt Col, USAF
Chief, Engineering Research
Division

(THE REVERSE OF THIS PAGE IS BLANK)

TABLE OF CONTENTS

CHAPTER			Page
1	INTRODUCTION		1
	1.1	Purpose	1
	1.2	Authority	2
	1.3	Background	3
	1.4	Limitations	5
	1.5	Sources of Information	5
	1.6	Brief Conclusions	6
	1.7	Thesis Format	6
2	TESTING EQUIPMENT AND PAVEMENT CHARACTERIZATION MODEL		8
	2.1	Destructive Evaluation Methods	8
	2.2	Nondestructive Testing Devices	14
	2.3	Nondestructive Evaluation Methods	18
	2.4	Description of Selected Equipment and Model	21
3	THE FIELD RESEARCH PROGRAM		28
	3.1	Major Concerns	28
	3.2	Selection of Field Test Sites	29
	3.3	FWD Measurement Repeatability	31
4	JOINT LOAD TRANSFER		55
	4.1	Load Transfer Efficiency	55
	4.2	Effect of Load Magnitude on Load Transfer Efficiency	59
	4.3	Variation of Load Transfer Efficiency Along the Joint	59
	4.4	The Effect of Temperature on Load Transfer Efficiency	72
	4.5	Load Transfer Efficiency Prediction	84
5	BACKCALCULATION OF CONCRETE ELASTIC MODULUS AND MODULUS OF SUBGRADE REACTION		88
	5.1	The Center Slab Deflection Basin	88
	5.2	The Graphical Solution for Dynamic E and k	93
	5.3	A Computer-based Iterative Solution for Dynamic E and k	95
	5.4	Comparison of Measured and Predicted Deflection Basins	99
	5.5	Repeatability of Backcalculated Dynamic E and k Moduli	107
6	THE CRITICAL STRESS AND JOINT CONSIDERATIONS		118
	6.1	Edge Versus Interior Stresses	118
	6.2	The Aggregate Interlock Factor	122
	6.3	Application of Center Slab Dynamic E and k Values to Joints	124
	6.4	Iterating to Determine the Aggregate Interlock Factor	125
	6.5	Calculating the Critical Stress	130

Page

7 RELATING CRITICAL STRESS TO PERFORMANCE 132

7.1 The Fatigue Damage Concept 132
7.2 Nondestructive Determination of Slab Concrete Flexural Strength 138
7.3 Performance Criteria 142
7.4 The Full-Scale Accelerated Traffic Tests 145
7.5 Developing the Field Performance Curve 155

8 THE NONDESTRUCTIVE TESTING AND EVALUATION PROCESS 160

8.1 Planning and Conducting the Field Testing Program 162
8.2 Data Preparation 174
8.3 Backcalculation of E, k, and the Aggregate Interlock Factors 175
8.4 Determination of the Critical Stress Location for Each Feature 185
8.5 Accounting for Temperature and Past Traffic Effects .. 189
8.6 Development of the Final Evaluation Data Base 198
8.7 Predicting the Remaining Life 202
8.8 Sensitivity of the Results 219

9 SUMMARY, CONCLUSIONS, AND NEEDED RESEARCH 225

9.1 Summary of the Research 225
9.2 Findings and Conclusions 228
9.3 Suggestions for Further Research 233

REFERENCES 236

APPENDIX

A EXAMPLE COMPUTER PRODUCTS 243

LIST OF TABLES

TABLE		Page
3-1.	PHYSICAL PROPERTY DATA FOR TEST FEATURES	35
3-2.	FWD LOAD AND DEFLECTION MEASUREMENT REPEATABILITY AT CONSTANT TEMPERATURE FOR SHEPPARD FEATURE T04A, SLAB NO. 1, AT THE CORNER POSITION	38
3-3.	FWD LOAD/DEFLECTION RATIO REPEATABILITY AT CONSTANT TEMPERATURE FOR SHEPPARD FEATURE T04A, SLAB NO. 1, AT THE CORNER POSITION	39
3-4.	FWD LOAD AND DEFLECTION MEASUREMENT REPEATABILITY AT CONSTANT TEMPERATURE FOR SHEPPARD FEATURE T04A, SLAB NO. 1, AT THE CENTER SLAB POSITION	40
3-5.	FWD LOAD AND DEFLECTION MEASUREMENT REPEATABILITY AT CONSTANT TEMPERATURE FOR SHEPPARD FEATURE T04A, SLAB NO. 1, ALONG THE LEFT LONGITUDINAL JOINT	41
3-6.	FWD LOAD AND DEFLECTION MEASUREMENT REPEATABILITY AT CONSTANT TEMPERATURE FOR SHEPPARD FEATURE T04A, SLAB NO. 1, AT THE TRANSVERSE JOINT	42
3-7.	FWD LOAD AND DEFLECTION MEASUREMENT REPEATABILITY AT CONSTANT TEMPERATURE FOR SHEPPARD FEATURE T04A, SLAB NO. 1, AT THE RIGHT LONGITUDINAL JOINT	43
3-8.	FWD LOAD AND DEFLECTION MEASUREMENT REPEATABILITY AT CONSTANT TEMPERATURE FOR SHEPPARD FEATURE A03B, SLAB NO. 2, AT THE CENTER SLAB POSITION	44
3-9.	FWD LOAD AND DEFLECTION MEASUREMENT REPEATABILITY AT CONSTANT TEMPERATURE FOR SHEPPARD FEATURE A05B, SLAB NO. 4, AT THE TRANSVERSE JOINT	45
3-10.	FWD LOAD AND DEFLECTION MEASUREMENT REPEATABILITY UNDER VARYING TEMPERATURES FOR SHEPPARD FEATURE T04A, SLAB NO. 1, AT THE CENTER SLAB POSITION	49
3-11.	FWD LOAD/DEFLECTION RATIO REPEATABILITY UNDER VARYING TEMPERATURES FOR SHEPPARD FEATURE T04A, SLAB NO. 1, AT THE CENTER SLAB POSITION	50
3-12.	FWD LOAD AND DEFLECTION MEASUREMENT REPEATABILITY UNDER VARYING TEMPERATURES FOR SHEPPARD FEATURE A03B, SLAB NO. 2, AT THE CENTER SLAB POSITION	51
3-13.	FWD LOAD AND DEFLECTION MEASUREMENT REPEATABILITY UNDER VARYING TEMPERATURES FOR SHEPPARD FEATURE A05B, SLAB NO. 4, AT THE CENTER SLAB POSITION	52

Page

3-14. FWD LOAD AND DEFLECTION MEASUREMENT REPEATABILITY UNDER VARYING TEMPERATURES FOR SHEPPARD FEATURE T04A, SLAB NO. 1, AT THE CENTER SLAB POSITION 53

4-1. THE RELATIONSHIP BETWEEN MAGNITUDE OF LOAD AND LOAD TRANSFER EFFICIENCY AS MEASURED AT UNDOWELED TRANSVERSE CONTRACTION JOINTS AND KEYED LONGITUDINAL CONSTRUCTION JOINTS 60

5-1. REPEATABILITY OF BACKCALCULATED DYNAMIC E AND k MODULI AT CONSTANT TEMPERATURE 108

5-2. REPEATABILITY OF BACKCALCULATED DYNAMIC E AND k MODULI AT VARIOUS TEMPERATURES 115

6-1. COMPARISON OF MEASURED AND PREDICTED FWD DEFLECTIONS ACROSS LONGITUDINAL AND TRANSVERSE JOINTS 126

7-1. DEVELOPMENT OF THE CORRELATION BETWEEN THE BACKCALCULATED DYNAMIC E MODULUS AND CONCRETE FLEXURAL STRENGTH 140

7-2. DEVELOPMENT OF THE CORRELATION BETWEEN THE PLATE BEARING-DERIVED STATIC k MODULUS AND THE FWD-DERIVED DYNAMIC k MODULUS 153

8-1. MAXIMUM AND MINIMUM MEAN DAILY TEMPERATURES FOR SEYMOUR-JOHNSON AIR FORCE BASE 193

8-2. THE DISTRIBUTION OF TOTAL ANNUAL TRAFFIC WITHIN EACH OF TWELVE TEMPERATURE ZONES 194

8-3. PASS PER COVERAGE RATIOS FOR SELECTED AIRCRAFT AT VARIOUS STANDARD DEVIATIONS OF WANDER WIDTH FOR RIGID PAVEMENTS 210

LIST OF FIGURES

FIGURE		Page
2-1.	The Dynatest Model 8000 FWD System	23
2-2.	Typical Force Output of the FWD	24
2-3.	Typical Location of the Loading Plate and Deflection Sensors of the FWD	26
3-1.	Sheppard Air Force Base Testing Locations	32
3-2.	Plattsburgh Air Force Base Testing Locations	33
3-3.	Seymour-Johnson Air Force Base Testing Locations	34
3-4.	FWD Testing Pattern for the Study of Load and Deflection Measurement Repeatability	36
3-5.	Recommended FWD Testing Pattern for Network Level Evaluations	48
4-1.	The Concept of Joint Load Transfer Efficiency	57
4-2.	Measurement of Joint Load Transfer Efficiency with the FWD	58
4-3.	FWD Testing Pattern for Determination of Directional Effects of Traffic on Load Transfer Efficiency and Consistency of Load Transfer Efficiency Along Joints	62
4-4.	Joint Load Transfer Efficiencies at Various Locations for Feature T04A, Slab No. 1	63
4-5.	Joint Load Transfer Efficiencies at Various Locations for Feature T04A, Slab No. 2	64
4-6.	Joint Load Transfer Efficiencies at Various Locations for Feature T04A, Slab No. 3	65
4-7.	Joint Load Transfer Efficiencies at Various Locations for Feature A05B, Slab No. 1	66
4-8.	Joint Load Transfer Efficiencies at Various Locations for Feature A05B, Slab No. 2	67
4-9.	Joint Load Transfer Efficiencies at Various Locations for Feature A05B, Slab No. 4	68
4-10.	Joint Load Transfer Efficiencies at Various Locations for Feature A08B, Slab No. 1	69
4-11.	Joint Load Transfer Efficiencies at Various Locations for Feature A08B, Slab No. 2	70
4-12.	Joint Load Transfer Efficiencies at Various Locations for Feature A08B, Slab No. 3	71
4-13.	The Relationship Between Air Temperature and Transverse Joint Load Transfer Efficiency for Feature T04A	74
4-14.	The Relationship Between Air Temperature and Transverse Joint Load Transfer Efficiency for Feature A03B	75
4-15.	The Relationship Between Air Temperature and Transverse Joint Load Transfer Efficiency for Feature A05B	76
4-16.	The Relationship Between Air Temperature and Transverse Joint Load Transfer Efficiency for Feature A06B	77
4-17	The Relationship Between Air Temperature and Transverse Joint Load Transfer Efficiency for Feature A08B	78
4-18.	The Relationship Between Air Temperature and Longitudinal Joint Load Transfer Efficiency for Feature T04A	79
4-19.	The Relationship Between Air Temperature and Longitudinal Joint Load Transfer Efficiency for Feature A03B	80

Page

4-20. The Relationship Between Air Temperature and Longitudinal Joint Load Transfer Efficiency for Feature A05B 81
4-21. The Relationship Between Air Temperature and Longitudinal Joint Load Transfer Efficiency for Feature A06B 82
4-22. The Relationship Between Air Temperature and Longitudinal Joint Load Transfer Efficiency for Feature A08B 83
4-23. The Generalized S-Shaped Curve and Its Fundamental Parameters 86
5-1. The Concept of the Deflection Basin 89
5-2. The Characteristic Shape of a Deflected Slab with High Stiffness and Weak Subgrade Support 90
5-3. The Characteristic Shape of a Deflected Slab with Low Stiffness and Strong Subgrade Support 90
5-4. The Deflection Basin "Area" Concept 92
5-5. A Typical ILLI-SLAB Grid for the Backcalculation of E and k . 94
5-6. The ILLI-SLAB Finite Element Mesh for the Analysis of FWD Data 97
5-7. The First Iteration in the Computer Solution of E and k 98
5-8. An Enlarged View of the Second Iteration in the Computer Solution of E and k 100
5-9. Comparison of Measured and Predicted FWD Deflections for Feature T04A 101
5-10. Comparison of Measured and Predicted FWD Deflections for Feature A03B 102
5-11. Comparison of Measured and Predicted FWD Deflections for Feature A05B 103
5-12. Comparison of Measured and Predicted FWD Deflections for Feature A06B 104
5-13. Comparison of Measured and Predicted FWD Deflections for Feature A08B 105
5-14. Comparison of Measured and Predicted FWD Deflections for Feature R08A 106
5-15. The Effect of a Small Change in Deflection (Load) on the Elastic Modulus of Concrete 110
5-16. Pavement Temperature versus Backcalculated E and k for Feature T04A 112
5-17. Pavement Temperature versus Backcalculated E and k for Feature A05B 113
5-18. Pavement Temperature versus Backcalculated E and k for Feature A08B 114
5-19. The Typical Variation in E and k at Constant Temperature Applied to Single Observations of E and k at Various Temperatures 116

6-1. The Effect of Slab Size on ILLI-SLAB-Generated Interior Stresses 120
6-2. The Change in Maximum Tensile Stress Under an Aircraft Gear as the Gear Travels Closer to the Longitudinal Joint 121
6-3. The Range of Possible Load Transfer Efficiencies and Aggregate Interlock Factors 123
6-4. Measured Versus Predicted Joint Load Transfer Efficiencies .. 128
6-5. The Iterative Solution for the Aggregate Interlock Factor ... 129

Page

7-1. Flexural Beam Fatigue Response Curves for Various Cemented Materials 133
7-2. Summary of Various PCC Fatigue-Based Design Models Using Laboratory Beams and Accelerated Full-Scale Tests 136
7-3. Determination of the Concrete Flexural Strength (3rd Point Loading) from the Backcalculated FWD Dynamic E Modulus 141
7-4. Typical Data Sheet for Reanalysis of Accelerated Traffic Test Results 150
7-5. Relationship Between the Conventional Static k Modulus and the Backcalculated FWD Dynamic k Modulus 154
7-6. Relationship Between the Strength and Stress of Concrete Slabs and Their Field Performance - The Transfer Function ... 156
7-7. Comparison of Field Performance Models Based on Accelerated Traffic Tests 157
7-8. Comparison of PCC Fatigue Models Based on Laboratory Beam Tests 159

8-1. Flow Chart of the Nondestructive Testing and Evaluation Process 161
8-2. Proposed Feature Designations for Runway 17-35 at Plattsburgh Air Force Base 165
8-3. Proposed Feature Designations for the SAC Apron at Seymour-Johnson Air Force Base 166
8-4. Determination of FWD Testing Requirements 170
8-5. Recommended Stratified Testing Sequences 171
8-6. Crack Development and Testing Sequence for Feature A20T 173
8-7. Unformatted FWD-Generated Data File 176
8-8. Reformatted Field Data File for Feature A20T, Slab No. 1 177
8-9. Backcalculated E and k Result and Predicted Sensor Deflection for the Center Slab Position 180
8-10. Iterated Aggregate Interlock Factors, and Measured and Predicted Deflections and Load Transfer Efficiencies at the Transverse Joint 182
8-11. Iterated Aggregate Interlock Factors, and Measured and Predicted Deflections and Load Transfer Efficiencies at the Longitudinal Joint 183
8-12. Iterated Aggregate Interlock Factors, and Measured and Predicted Deflections and Load Transfer Efficiencies at the Slab Corner 184
8-13. Determining the Location of Maximum Accumulated Damage for Two or More Aircraft 187
8-14. The Effect of Load Transfer Efficiency on Maximum Tensile Stress at the Bottom of a PCC Slab 190
8-15. Typical Hourly Temperature Variations in the Spring and Summer at Sheppard AFB 195
8-16. Modified Field Data Base for Use with AIFCALC to Iterate Transverse and Longitudinal Aggregate Interlock Factors 200
8-17. Typical AIFCALC Output Showing Aggregate Interlock Factors for Each of Twelve Temperature Zones 201
8-18. Modified AIFCALC Output for Use with DAMAGE 204

8-19. Typical DAMAGE Output Showing Miner's Accumulated Damage for One Coverage of the C-141 at Six Gross Weight Levels 206
8-20. Summary of Lateral Distributions of Commercial Aircraft Along Runways at Nine Major Airports 209
8-21. Summary of Predicted Remaining Passes for Each Gross Weight Category of the C-141 212
8-22. Input File to DAMAGE for a 40 Percent Mix of the C-141 214
8-23. Input File to DAMAGE for a 60 Percent Mix of the KC-135 215
8-24. Cumulative Miner's Damage Numbers for the C-141 216
8-25. Cumulative Miner's Damage Numbers for the KC-135 217
8-26. Remaining Passes for a 40/60 Mix of C-141/KC-135 Aircraft ... 218
8-27. The Effect of Aircraft Type on the Remaining Life of Feature A20T 220
8-28. The Effect of Pass to Coverage Ratio on Remaining Structural Life for the C-141 Aircraft 221
8-29. The Effect of Miner's Damage Number on the Remaining Structural Life of Feature A20T 223
8-30. The Effect of Different Mix Proportions on the Total Available Aircraft Operations 224

A-1. Reformatted Field Data File for Feature A20T 244
A-2. Backcalculated E and k Results and Predicted Sensor Deflections for the Center Slab Position 246
A-3. Iterated Aggregate Interlock Factors, and Measured and Predicted Deflections and Load Transfer Efficiencies at the Transverse Joints 247
A-4. Iterated Aggregate Interlock Factors, and Measured and Predicted Deflections and Load Transfer Efficiencies at the Longitudinal Joints 248
A-5. Iterated Aggregate Interlock Factors, and Measured and Predicted Deflections and Load Transfer Efficiencies at the Slab Corners 249
A-6. Modified Field Data Base for Use with AIFCALC to Iterate Transverse and Longitudinal Aggregate Interlock Factors 250
A-7. Typical AIFCALC Output Showing Aggregate Interlock Factors for Each of Twelve Temperature Zones 251
A-8. Modified AIFCALC Output for Use with DAMAGE 252
A-9. Typical DAMAGE Output Showing Miner's Accumulated Damage for One Coverage of the C-141 at Six Gross Weight Levels 253
A-10. Summary of Predicted Remaining Passes for Each Gross Weight Category of the C-141 254
A-11. Input File to DAMAGE for a 40 Percent Mix of the C-141 255
A-12. Input File to DAMAGE for a 60 Percent Mix of the KC-135 256
A-13. Cumulative Miner's Damage Numbers for the C-141 257
A-14. Cumulative Miner's Damage Numbers for the KC-135 258
A-15. Remaining Passes for a 40/60 Mix of C-141/KC-135 Aircraft ... 259

CHAPTER 1

INTRODUCTION

The mission of the United States Air Force is to "preserve the United States as a free nation with its fundamental institutions and values intact, by preparing aerospace forces for the conduct of prompt and sustained combat operations" (1). The success of this global commitment is highly dependent on the ability of the Air Force to project its airpower into any theater of operations. Thus, the importance of structurally adequate, well maintained airfield pavements in supporting mission aircraft loads at operational levels becomes obvious.

To properly prepare for and carry out this mission, Air Staff planners must have accurate, up to date information concerning the structural adequacy of not only our own major installations but those of our allies abroad, as well. This information is crucial in planning future maintenance and repair activities and in determining the feasibility of proposed mission changes at an installation. At present, this needed information is, at best, inadequate and inaccurate, and in most instances nonexistent.

1.1 Purpose

The current destructive test methodologies for obtaining critical airfield evaluation data and conducting the analyses are costly and time-consuming, but most importantly, severely impact the operation of the base. In many cases the structural evaluation is neglected because base operations cannot live with the mission degradation that would occur with extensive down time of the pavements. It should be emphasized that many of these same problems exist in evaluating commercial airfields, as well.

Fortunately in recent years, great strides have been made in the development of equipment that can rapidly and nondestructively collect data upon which an evaluation of load-carrying capacity and future life can be made. Of particular importance in the evaluation of rigid airfield pavements was the development of impulse loading devices, such as the Falling Weight Deflectometer, that reasonably approximate actual moving aircraft wheel loads. Simultaneously, researchers have been developing analytical models that could describe the response of a pavement system to specific loading conditions.

This report presents several concepts in the overall process of nondestructive testing and evaluation (NDT & E) of rigid airfield pavements and integrates them into a complete system, including field testing, analyses, and prediction of future performance. Implementation of the system will permit rapid completion of field testing with little or no interruption of installation operations, and analysis of field data and presentation of results is possible within hours. The advantages of such a system in peacetime applications are numerous, but its value in rapidly assessing airfields in a contingency situation can not be overestimated.

1.2 Authority

The research described in this report was conducted at the Department of Civil Engineering at the University of Illinois at Urbana-Champaign, in cooperation with the United States Air Force Engineering and Services Center, Tyndall Air Force Base, Florida. The concepts presented and the computer codes developed are intended for public release, with the hope they will advance the state of the art in rigid pavement evaluation and foster additional research into specific aspects of the methodology.

1.3 Background

There are three broad categories of military airfields, critical to the successful accomplishment of the Air Force mission, which must be evaluated for structural and functional adequacy. First, over 150 major installations worldwide are directly operated and maintained by the Air Force, most of which have airfield facilities that were constructed during World War II or in the early 1950's. These pavements were originally designed to support B-29 and B-47 aircraft for 20 years at normal levels of operation. Competition for limited Military Construction Program and Operations and Maintenance funding has prevented their reconstruction and, coupled with the introduction of the B-52, C-141, and C-5 aircraft, has dictated that Air Force engineers repair, restore, and rehabilitate these overloaded pavements by the most economical means available. NDT & E provides the most feasible means upon which to base such critical decisions.

Second, within the past decade the concept of Collocated Operating Bases (COBS) has been introduced as a means of reducing the vulnerability of our main bases to attack. This concept centers around the development of numerous host-nation airfields, for use in launch and recovery of aircraft, which would be too costly or impractical to destroy. Information regarding the structural capacity of each of these airfields must be obtained before contingency plans can be finalized. Oftentimes this information is not available from the host country. With over 250 COB's in western Europe alone, a program for NDT & E is mandatory.

Third, captured enemy airfields must be evaluated quickly for structural adequacy to take fullest advantage of their strategic importance in support of ground forces. NDT & E can provide the theater commander with rapid guidance on the type and quantity of aircraft that can use the facility.

With the need for a viable NDT & E system firmly established during the mid 1960's, both the Army and the Air Force embarked on separate research programs to develop the equipment and computer codes required for a complete system. Both efforts resulted in large, vibratory devices used for determining the dynamic stiffness modulus of the pavement system, but differed in their approach to the analysis of the pavement's response. The Air Force elected to use newly-emerging finite element techniques for determining stresses, strains, and deflections within the pavement (2), while the Army pursued the linear-elastic approach (3). Neither system utilized air transportable equipment, however, which limited their use to well planned, peacetime situations. Such limitations did not severely impact the Army's use of their system, confined primarily to stateside applications. The Air Force, on the other hand, required a system that was rapidly deployable and reliable, two areas that exhibited great weaknesses during initial field trials. Consequently, efforts were initiated to develop a smaller, durable, C-130 transportable system. The resulting system, developed in the late 1970's, was an impulse loading device that uses wave propagation techniques to characterize the various layers of the paving system. This new system has been undergoing field testing and verification since 1982, and preliminary results indicate general agreement with other widely used NDT & E systems (4).

Despite improvements in transportability, several problem areas still exist with the system that limit its utility:

1) The uniqueness of the system makes verification of results with other widely accepted methods difficult and field repairs of critical components nearly impossible.

2) Thirty to forty-five minutes are required to perform one test.

3) Considerable judgment and experience are required of the engineer to properly interpret the wave dispersion curves.

4) Unmanageable quantities of computer time are required by the finite element code to generate output that is comparable to linear elastic or even Westergaard-based H-51 programs.

5) The effects of repeaced loadings on joint systems are ignored.

For these reasons, research was undertaken to develop a complete NDT & E system, based on simplistic, widely used equipment, that would combine the best mechanistic response models available with empirical field performance data to predict future performance of rigid airfield pavements.

1.4 Limitations

The field testing techniques and other methodologies presented herein were developed from testing and analysis of plain jointed concrete pavements using dummy groove longitudinal and transverse contraction joints and keyed longitudinal construction joints. Although it is felt that the techniques will apply equally well to reinforced slabs and to dowelled joints, additional research is required to verify this. In addition, only unbound base courses were available at the test locations, and no overlays, either flexible or rigid, are included in the study.

Finally, only a limited range of soil and environmental conditions was experienced during the field testing program. Applicability of the system for a variety of such conditions must be verified through much more extensive field testing and analysis.

1.5 Sources of Information

Information presented throughout this report was obtained from a wide variety of sources. U.S. Government agencies such as the U.S. Air Force,

U.S. Army, and the Federal Aviation Administration have conducted the bulk of the previous research in NDT & E and, therefore, are a prime source for technical reports. Research at the university level also has been extensive and well documented. State and foreign governmental agency reports were utilized to some extent as well.

Field data was collected at three Air Force installations representing a reasonable cross section of geological, environmental, and operational conditions.

1.6 Brief Conclusions

Based on the results of this effort, it is now possible to rapidly test and evaluate the rigid airfield pavements at any major facility, utilizing a combination of mechanistic modeling and empirical transfer functions, to predict performance and future pavement life. The structural capacity of pavement systems for any given aircraft or mix of aircraft can be determined quickly, and for a wide variety of environmental conditions. In addition, the research has uncovered potential methods for locating voids, determining pavement thicknesses nondestructively, and accounting for temperature variation effects on load transfer at joints.

1.7 Thesis Format

The results of this study will be presented in the following sequence:

Chapter 2 - Selection of the test data collection device and mechanistic model for the study.

Chapter 3 - Design of the testing program to investigate various aspects of the structural evaluation process.

Chapter 4 - Investigation of joint load transfer efficiencies and their dependence upon temperature.

Chapter 5 - Development of the backcalculation procedure for determining subgrade modulus and pavement stiffness.

Chapter 6 - Comparison of interior and edge stresses and the development of the computer program to calculate the critical stress.

Chapter 7 - Analysis of full-scale accelerated traffic tests and their use in developing a field performance curve for airfield pavements.

Chapter 8 - Formulation of the various components into a comprehensive system for predicting remaining pavement life, and illustration of the entire process.

Chapter 9 - Conclusions, recommendations, and suggestions for further research.

CHAPTER 2

TESTING EQUIPMENT AND PAVEMENT CHARACTERIZATION MODEL

During recent years several nondestructive pavement evaluation systems have been developed by various governmental and private organizations to analyze the load-carrying capability of highway and airfield pavements. The use of NDT & E devices is seen as a great advance over costly and time-consuming destructive techniques. Although NDT & E devices do not permit the in-depth analysis of pavement materials that destructive testing does, the benefits of minimal operational impact, comprehensive testing of every pavement feature, and reduced effort to produce a final report are particularly attractive. In 1981, the Transportation Research Board formed a Task Force (A2T56) to make a state-of-the-art review of available methodologies (5). As of 1983, some 15 different procedures have been brought before the Task Force, representing a wide range of equipment and analytical tools. The following discussion briefly summarizes the presently available testing and analysis techniques, including their strengths and weaknesses, and forms the basis for selection of the equipment and mechanistic model used in this study.

2.1 Destructive Evaluation Methods

Although destructive testing of airfield pavements is now almost exclusively limited to very special investigations of pavement distress, any discussion of evaluation methodologies leading to equipment and model selection would be incomplete if past techniques are not presented and appreciated. The following procedures evolved during the 1940's and form the basis for many of the techniques in use today.

The evaluation process was begun by dividing the airfield pavement system into individual sections, or features, that were nearly identical in their construction, soil conditions, and traffic usage. The physical properties of the pavement and foundation materials needed to conduct a rigid pavement evaluation of each feature, based on procedures developed by the U.S. Army Corps of Engineers in the mid-1950's (6), include: pavement layer thicknesses, flexural strength and modulus of elasticity of the concrete, Poisson's ratio of the concrete, and Westergaard's modulus of base course and/or subgrade reaction (K-value). Since the modulus of elasticity and Poisson's ratio of concrete do not vary widely in static determinations, it was assumed, for the preparation of the evaluation charts, that they equal 4 x 10^6 psi and 0.20, respectively. These values are typical of those measured during testing of a large number of pavements built by the Corps of Engineers. The remaining three properties must be established for each feature by excavating test pits and extracting core samples. Since an airfield typically contains between 75 and 125 distinct features, actual testing of each feature is time and cost prohibitive. Thus, information to make the evaluation is obtained by testing 20 to 25 features, selected for their representative nature, and then extrapolating the results to similar features elsewhere.

2.1.1 Full Scale Testing

The destructive investigation begins by opening 4 by 5 foot test pits to expose the supporting material for plate bearing tests. Extreme care must be exercised to preserve the integrity of this material during removal of the concrete. Disturbance of this base course or subgrade surface can adversely affect the results of the plate bearing test. A complete description of the

test and the calculations required to obtain the modulus of subgrade reaction are found in Reference 7. In addition to the plate load test, in situ moisture and density measurements are made for each material layer, and bulk disturbed soil samples are obtained from each layer for laboratory testing. Concrete thickness can be obtained at the test pit, and flexural strengths can be determined by sawing beam samples from the excavated concrete. In most cases, however, this process is extremely expensive. Thus, the number of tests that can reasonably be performed is very limited, which increases the probability of error in estimating the flexural strength. Therefore, six-inch diameter core samples are usually extracted for thickness and splitting tensile strength. A relationship developed by the U.S. Army Waterways Experiment Station (8) and discussed in Chapter 7 is then used to obtain the flexural strength from the splitting tensile strength. The relative ease in extracting these cores permits sampling of each feature at least once. With the information obtained from selected test pit locations and extracted core samples, the evaluation can be performed. The additional moisture and density data and material samples are used to identify potential sources of future problems and as the basis for design of repair and reconstruction projects.

Full scale destructive testing has several advantages over NDT & E, but these must be weighed against the cost of procuring the information and the inaccuracies in the assumptions. On the positive side, underlying causes for pavement distress can be explored more fully by exposing each layer of the system. Subsidence and plastic deformation of any layer is easily detected on the vertical walls of the pit, and elevated water tables become immediately evident. Collection of sufficient quantities of each material permits a full range of laboratory tests, including classification and

moisture-density-CBR relationships, to verify compaction deficiencies. Joint load transfer systems can be examined closely for deterioration, and visual evidence of suspected concrete alkali-aggregate reactions can be obtained. Finally, and probably most importantly, the as-built physical properties of the pavement system can be established. Without this information, the solid data base needed for future design and evaluation would be unreliable.

Once the physical properties of each feature have been established, however, there is very little justification for retesting destructively in the future. Only in very special circumstances, where specific causes for a pavement failure must be firmly established, would excavation of a test pit be warranted. The tremendous rate that NDT & E equipment can perform, from 200 to 500 tests per day, means not only that every feature can be tested, but many slabs within each feature can be tested. Statistical concepts can thus be utilized to shed light on the variability associated with the evaluation of each feature, and the need to extrapolate the results of testing at one location to many other locations is avoided.

Finally, the benefits derived by eliminating the closure of critical runway and taxiway pavements and costly excavation and repair procedures are difficult to measure.

2.1.2 Small Aperture Testing

The advent of modern, multiple-wheel, heavy gear load aircraft has created an increased need to determine the load carrying capability of airfield pavements. With ever increasing volumes of aircraft traffic, it is now nearly impossible to close a major facility, such as a runway or primary taxiway, long enough to complete a test pit. Recognizing this two-fold problem, the Corps of Engineers developed a methodology (13) to determine

pavement and soil properties at depths through small access holes, thus eliminating the excavation of test pits. Six-inch core samples are extracted from the concrete for usual strength and thickness determinations, but then the holes are used to perform California Bearing Ratio (CBR) tests on each layer under the pavement. Correlations developed by the Corps for three different soil groupings are then applied to the CBR results to obtain appropriate modulus of subgrade reaction values.

The distinct advantage of small aperture testing lies in the minimal impact on airport operations. The entire procedure requires about 45 minutes to complete, and repair of the hole is rapid. The procedure has been used extensively throughout Europe by the U.S. Air Force in situations where test pit operations would have been impossible. The major weaknesses of the method, however, cast some doubt on the accuracy of the results. Unavoidable saturation of the base or subgrade during the drilling operation may severely influence the CBR test results. Attempts to correlate the results of a CBR test to those of a plate bearing test are somewhat dubious. And finally, preserving the integrity of the surface of subgrade materials while extracting coarse-grained base material through a six-inch opening is very difficult.

2.1.3 Analysis of Destructive Test Data

Establishing allowable gross loads for an airfield feature from destructive test data has traditionally been a reverse application of the design charts developed by the Corps of Engineers (9). These charts are based on limiting the tensile stress at the bottom of the slab with the load adjacent to the slab edge. Westergaard's analytical model of a thin plate on a dense liquid foundation, in conjunction with influence charts (14) and

computer solutions (15) for multiple-wheel gear configurations, is used to calculate the magnitude of the stress (10,11). Built in to the design charts, and therefore assumed for evaluation, is a standard 25 percent reduction in this calculated free edge stress to account for the assumed load transfer that takes place across the joints. This maximum edge stress, coupled with the strength of the concrete, has been related to the number of coverages to initial crack failure through the accelerated traffic tests discussed in detail in Chapter 7. The desired allowable gross loads for specific levels of aircraft operation are obtained by applying pass per coverage ratios developed by the Corps of Engineers (12).

The classical Westergaard approach based on destructive plate bearing tests has several advantages in the evaluation of rigid pavements. First, a composite subbase and subgrade modulus is obtained directly from the plate test. This composite static modulus measures the cumulative effects of moisture, density, and strength of the supporting structure and eliminates the need to evaluate each layer. Second, although not theoretically rigorous, a single Winkler idealization of the supporting layers permits the closed-form calculation of stresses and deflections under interior, edge, and corner loading positions. Third, the contribution of load transfer mechanisms at joints can be taken into account, although arbitrarily, through a predetermined reduction in the maximum calculated edge stress in the loaded slab. The ability of the plate theory approach to account for edge loading conditions, coupled with the fact that nearly all load associated distress in jointed concrete pavements initiates at the joint (16), has prompted the Federal Aviation Administration (FAA) to revise their design criterion from maximum interior stress to maximum edge stress (17).

The advantages of the plate theory approach outlined above have also introduced two weaknesses into the analysis which must be noted. First, the dense liquid idealization does not take into account the effect of shear interaction between adjacent support elements. Consequently, displacements of the subgrade are discontinuous at the edge of the loaded area. Second, Westergaard's assumption of an infinite slab cannot be met with the large radius of relative stiffness values typical of airfield pavements. This can lead to calculated deflections and stresses that do not agree very closely with measured values.

2.2 Nondestructive Testing Devices

As mentioned previously in this report, major shortcomings in the present U.S. Air Force NDT & E equipment prompted the search for a simplistic, widely used device that could measure the response of rigid airfield pavements to standardized loading conditions. Several recent publications (18,19, and 20) provide excellent descriptions of the commercially available equipment, and these references should be consulted for specific details. The following discussion summarizes the five general classes of equipment and highlights their strengths and deficiences.

2.2.1 Static Deflection Equipment

Devices which measure the deflection response of a pavement to slowly applied loads are generally classed as static deflection equipment. The most commonly used devices in this class are the Benkelman Beam and its various modifications. Plate bearing equipment and the Curvature Meter also fall into this class but are seldom used.

The Benkelman Beam requires a loaded truck or aircraft to create the deflection to be measured. Deflection basins have been measured with the device; however, this is a cumbersome procedure requiring multiple beams or multiple recordings at known distances as the vehicle moves from the center of the deflection basin. The device is relatively inexpensive, but the requirement to manuallly record data precludes its use for extensive evaluations.

2.2.2 Automated Beam Deflection Equipment

Two pieces of equipment that attempt to automate the Benkelman Beam are placed into this class. The La Croix Deflectograph is a commercially available device that has been used widely in Europe and other parts of the world, but not in the United States. The Traveling Deflectometer is a similar device that was custom built for the California Department of Transportation. It is not used by any other agencies responsible for the evaluation of pavements.

Although these devices are capable of making several hundred measurements daily, several disadvantages exist that limit their utility. First, if the deflection basin is large, as is the case for rigid airfield pavements, the point on the beam used for a reference may be in the basin. Second, it is difficult to test a specific point on the pavement, particularly joint locations. Third, the size of the vehicle required to obtain prototype loadings would severely restrict its air transportability.

2.2.3 Steady State Dynamic Deflection Equipment

Any device which produces a sinusoidal vibration in the pavement with a dynamic force generator falls into this category. The most widely used,

commercially available devices in this group are the Dynaflect and various models of the Road Rater. Two custom built devices, the WES 16-kip Vibrator and the Federal Highway Administration's NDT van, or Thumper, have also been used extensively on airfields and highways, respectively.

The Dynaflect has several advantages over other NDT devices, including its low cost, its wide acceptance, its mobility, and its speed of operation. In addition, an inertial reference is used, eliminating the need to establish a reference point outside the deflection basin. It has several major weaknesses, however, that cast doubt as to its ability to correctly characterize a pavements response to actual loadings. First, it requires a static preload that is relatively large in comparison to the maximum peak-to-peak loading. The stress sensitive stiffnesses of paving materials can be altered by this preloading prior to testing, although this effect is limited primarily to the thinner airfield pavements. Second, the 1000-pound maximum peak-to-peak force generated can hardly simulate the deflections expected under actual aircraft loading conditions. Third, the actual contact area of the steel wheels used to impart the load is difficult to determine for the analysis. Finally, the limit of about 50 inches for the measured deflection basin radius is not adequate for the large basins encountered on rigid airfield pavements.

The various models of the Road Rater retain all of the advantages of the Dynaflect, but can cost up to three times as much. The more expensive models are capable of generating peak-to-peak forces as high as 8000 pounds, but this merely increases the static preload that must be used. The ability to vary the load and the frequency of application are important advantages over the Dynaflect, but measurement of deflection basins greater than three feet in radius are not possible.

The WES and FHWA custom built vibrators can generate peak-to-peak loadings that correspond more closely to actual aircraft load conditions, but again the preload requirement can not be avoided. Their size and cost have excluded them from consideration for this study.

2.2.4 Impulse Deflection Equipment

Any piece of equipment which delivers a transient force impulse to the pavement is included in this group. The most commonly used equipment is the Dynatest Falling Weight Deflectometer (FWD); however, the KUAB FWD has been recently introduced into the United States, and the Phoenix FWD has been in use in Europe for several years. In addition to the advantages listed for the Dynaflect and Road Rater, the FWD has a relatively small preload when compared to the impulse force that is imparted. Most importantly, however, these devices are specifically designed to simulate the deflections under moving wheel loads. Finally, deflection basins with radii up to 96 inches can be measured.

2.2.5 Other Equipment

There are several other devices currently in various stages of research and development that should be noted. Wave velocity equipment, such as the Air Force impact device and the system developed by the University of Texas Center for Transportation Research, shows promise for determining the elastic modulus of layered systems. Their major weaknesses lie in collecting and interpreting the data and in analyzing joint behavior.

Laser technology and photogrammetry techniques are being investigated to measure deflections under moving loads. These devices will require mounting

on loaded trucks or aircraft and, therefore, are not well suited for the purposes of this research.

2.3 Nondestructive Evaluation Methods

In contrast to the wide variety of NDT equipment available, there are just two widely used approaches to the mechanistic analysis of rigid pavement systems, elastic layered theory and plate theory. Within each theory, however, researchers have developed engineering models to meet specific requirements of the pavement systems being evaluated. For example, finite element and other numerical analysis techniques have been applied to both theories to substantially enhance their capabilities. The following discussion provides a brief description of each approach and appropriate references for further detail.

2.3.1 Elastic Layered Theory

The characterization of supporting layers in pavement systems as elastic solids finds its origins in the work done by Boussinesq circa 1885. In his approach, soil is regarded as a linearly elastic, isotropic, homogeneous solid of infinite extent in both horizontal and vertical directions. In the mid-1940's, Burmister (21,22) extended this concept to two and three layer systems for the analysis of stresses and deflections in flexible pavements. He found that stiff upper layers reduced stresses and deflections in the subgrade from those predicted by Boussinesq, and further, that this reduction was proportional to the ratio of the elastic moduli. Yoder and Witczak (23) provide an excellent summary of the early work in elastic layered concepts, but they chose to limit their coverage to those solutions that could be hand calculated.

The recent advances in the elastic layered approach have centered around the development of computer solutions to multi-layered problems. Ioannides et al (24) and Parker and Gunkel (25) present a thorough review of the basic codes released since 1963. Initially used for design of flexible pavements and flexible overlays, these codes are now being modified to iteratively backcalculate layer moduli for prediction of pavement response to loading conditions in both flexible and rigid systems. Hall (20), Bush (26), and Uddin (27) describe several methods currently in use.

Elastic-layered programs have been particularly attractive for rigid pavement evaluation for several reasons. First, they allow the characterization of the pavement as a multi-layered system, a more realistic approach than the use of a composite subgrade modulus, k, when plate theory is employed. Second, elastic-layered theory has been proposed by many engineers as the single, unified procedure that can best accommodate both flexible and rigid design and evaluation philosophies. Third, characterization of the supporting materials with fundamental properties that can be verified in the laboratory is seen as an advantage over the reliance on a single, field-determined modulus. Finally, elastic-layered programs are very efficient to run and have been adapted to the micro-computer. Thus, results can be obtained quickly in the field without relying on a mainframe computer.

The most serious drawback to elastic-layered analysis of rigid pavements lies in the inability of these programs to analyze the most critical element of the entire system, the joints. They can not provide any information on pavement response under edge and corner loads, or the efficiency of load transfer systems at the joints. In addition, they do not take into account the stress dependency of granular materials or the effect of slab size.

2.3.2 Plate Theory

The calculation of stresses and deflections using plate theory for slab-on-grade pavements regards the soil medium as a bed of closely spaced, independent, linear springs. Each spring deforms in response to the load applied directly to it, while neighboring ones remain unaffected. Thus, the vertical stress at any point is directly related to the deflection at that point by the modulus of subgrade reaction, k. This idealization is commonly referred to as a "dense liquid" and is attributed to Winkler (28). In the mid-1920's, Westergaard (10) developed the closed form solutions for slab-on-grade response to circular loads that form the basis for design practices still in use today. Again, both Ioannides (24) and Yoder and Witczak (23) present excellent summaries of the original work done by Westergaard and others.

The determination of stresses and deflections in pavement slabs with joints and other discontinuities has been a subject of major concern for several years. For many pavement structures, it has been virtually impossible to obtain closed-form solutions because of the complexities in boundary conditions, geometry, and material properties. Certain simplifying assumptions could be made to permit analytical solutions, such as those used by Westergaard, but these have always resulted in significant modification of the characteristics of the problem. As in the case of elastic-layered theory, however, major advances in plate theory, centered around the computer, have resolved many of these concerns. First, influence charts (14) were developed to handle multiple wheel applications of Westergaard's equations. Then computerized procedures (15) were formulated to facilitate these calculations. Now, numerical methods such as the finite element (29,30), finite difference (31), and discrete element models (32) are

available to accommodate a wide range of complex boundary conditions, including load transfer at joints and cracks, stress-sensitive granular materials, and multiple wheel loads. Thus, the major drawback of elastic layered methods is avoided.

The primary weaknesses of plate theory, and particularly the modern numerical methods, are more apparent in the design of pavement structures than in their evaluation. Unlike laboratory-based elastic moduli, it can be difficult to achieve a specific design modulus of subgrade reaction when several material layers are used in construction. In evaluation of rigid pavements, however, the item of interest is usually the total support provided to the PCC layer, such as a k value, for prediction of pavement response. Second, the return to plate theory represents a departure from the "unified" approach sought by many engineers. Unfortunately, this philosophically sound and practically desirable approach has been reduced to the mere elimination of one of the two theories. Eventually, a single approach will probably be developed that will incorporate the most desirable features of each. In the interim, plate theory remains a useful and imperative option. Finally, the rapid advances in computer technology are quickly dispelling any concerns regarding memory requirements and execution time of these modern numerical models.

2.4 Description of Selected Equipment and Model

In light of the above investigation of available nondestructive equipment and engineering models, the Dynatest Model 8000 Falling Weight Deflectometer and the ILLI-SLAB finite element program were selected for this research. Each represents the latest advancements in the state of the art, but more importantly, they were selected because of the confidence the author and

other research and field engineers have in their ability to simulate actual loading conditions on airfield pavements. A brief description of each is presented below.

2.4.1 The Dynatest Model 8000 FWD

The Dynatest Model 8000 FWD is the most widely used FWD in the United States. It is manufactured in Denmark and distributed by Dynatest Consulting of Ojai, California. The testing system is trailer-mounted and weighs between 1323 and 1875 pounds depending on the weight of the falling mass used. The entire unit can be towed by a standard automobile, as shown in Figure 2-1.

The impulse force is created by dropping masses from different heights. The system is equipped with four mass levels weighing 110, 220, 440, and 660 pounds. By varying the drop heights and mass levels, impulse forces ranging between 1500 and 24000 pounds can be achieved. The masses are raised hydraulically and released on an electronic signal. The drop heights can be varied from 0.8 to 15.0 inches. The system is equipped with four electronic triggers to allow four drop heights without changing trigger locations. These heights are calibrated to give the desired range of loads.

The masses drop onto a rubber buffer system to provide a load pulse in approximately a half-sine wave form with 25 to 30 millisecond duration (see Figure 2-2). The load is transmitted to the pavement through an 11.8 inch diameter loading plate, and measured using a strain gauge-type load transducer. Deflections are measured using up to seven velocity transducers mounted on a bar which is lowered automatically with the loading plate. The bar places six transducers at locations up to 90 inches from the center of the load plate. The seventh sensor is located at the center of the plate. A

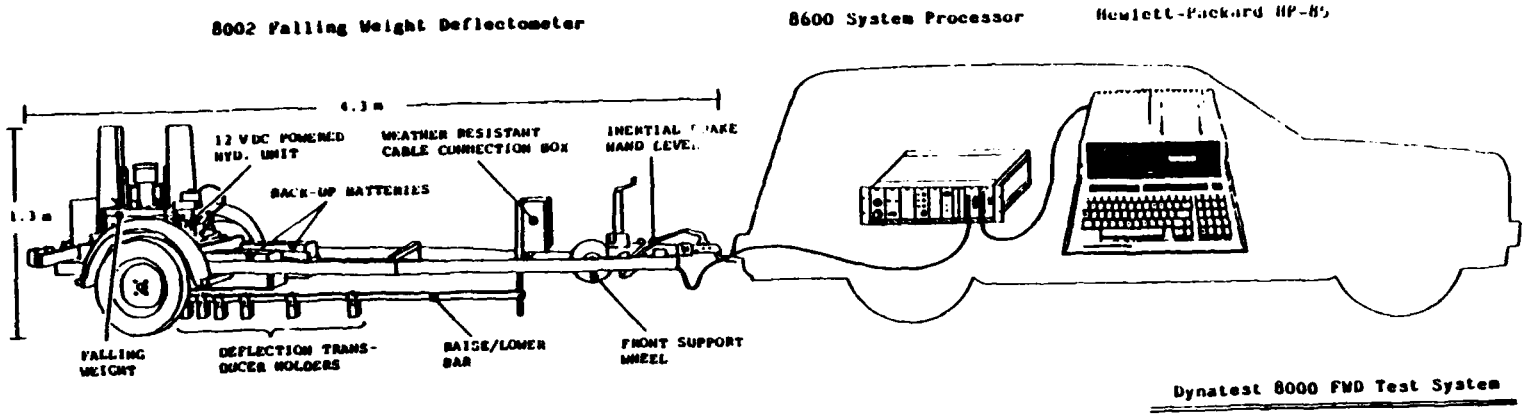

Figure 2-1. The Dynatest Model 8000 FWD System

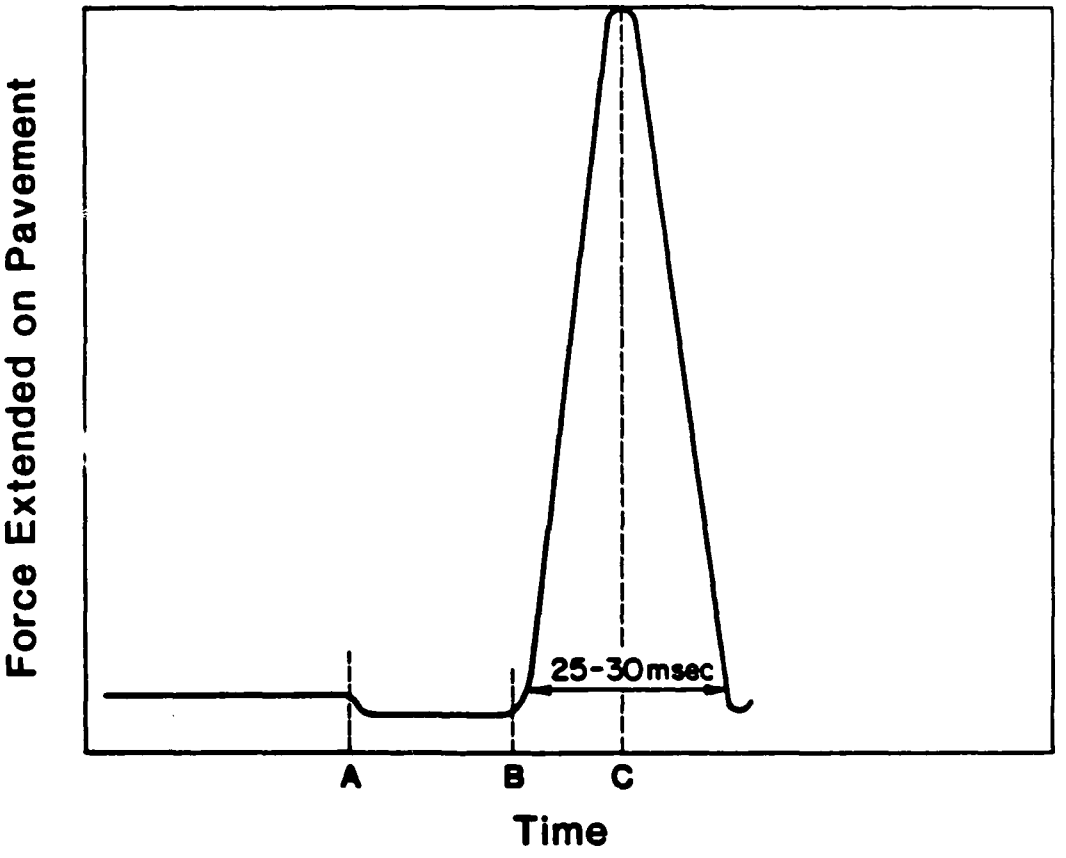

A - Time at which weights are released
B - Time at which weight package make first contact load plate
C - Peak load reached

Figure 2-2. Typical Force Output of the FWD

typical configuration is shown in Figure 2-3. The velocity transducers are specifically designed to insure a linear response with the 25 to 30 millisecond rise time.

The information from the transducers and load cell are fed into a microprocessor-based control and registration unit. The signals from the velocity transducers are processed through an integrating preamplifier, then through an amplifier, and finally through a rectifier to produce a direct current signal which is directly proportional to displacement. The signal from the load cell is processed in much the same way, except it does not require integration. The results are then fed into a Hewlitt-Packard Model 85 computer (HP-85) which records them on paper tape and magnetic cassette. The HP-85 also controls the complete operation, including lowering the plate and deflection sensors to the pavement surface, raising the mass to predetermined drop heights, releasing the mass, recording the results, raising the loading plate and sensors, and signalling the operator at completion of the test. Results are processed in metric units but can be stored in either metric or British units. The entire operation can be controlled by one person from the front seat of the tow vehicle, and typically requires 45 seconds to complete an entire test sequence.

Power to operate the trailer hydraulics is supplied by heavy duty batteries mounted on the trailer and continuously charged by the special alternator system installed in the tow vehicle. The computer is powered by a separate battery that is charged independently from the trailer batteries.

2.4.2 The ILLI-SLAB Finite Element Program

ILLI-SLAB was developed at the University of Illinois in the late 1970's for structural analysis of jointed, one- or two-layer concrete pavements with

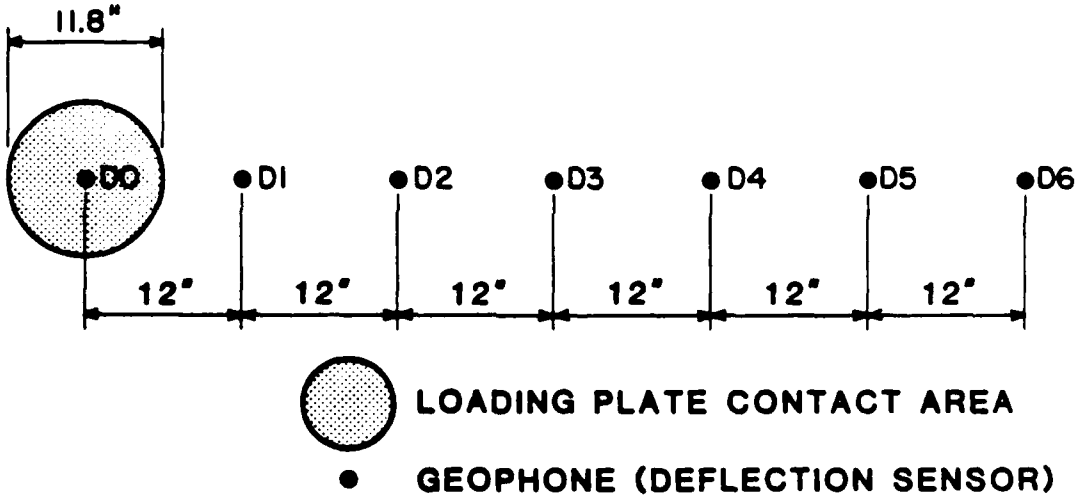

Figure 2-3. Typical Location of the Loading Plate and Deflection Sensors of the FWD

load transfer systems at the joints (33). The ILLI-SLAB model is based on the classical theory of a medium-thick plate on a Winkler foundation, and can evaluate the structural response of a concrete pavement system with joints and/or cracks. It employs the 4-noded, 12-dof plate bending (ACM or RPB12) element. The Winkler-type subgrade can be modeled either as a uniformly or variably distributed pressure subgrade through an equivalent mass formulation. This is a more realistic representation than the four concentrated spring elements used in other finite element programs such as WESLIQID and FINITE, because it eliminates discontinuities in the deflection profiles. Two stabilized layers, in addition to the unbound supporting layers, can be accommodated, which adds immensely to its versatility in analyzing rigid pavements with stabilized bases or rigid overlays.

Recent efforts by Ioannides (24) to revise and expand ILLI-SLAB have produced a versatile, easy to use tool with improved accuracy. Three new foundation models have been added to provide the capability to analyze a slab on a stress dependent subgrade, a semi-infinite half space, or a two-parameter foundation. Guidelines for proper mesh construction have been provided, and a global coordinate system is now in place for easy use in analysis. Finally, a reexamination of the time-honored Westergaard solutions in light of the finite element method has conclusively established the correct form of the equations and their limitations. The work by Ioannides et al,(24) has been instrumental in the development of the procedures used throughout this study.

CHAPTER 3

THE FIELD RESEARCH PROGRAM

The engineer performing NDT & E of an airfield pavement system is invariably faced with what must seem like an overwhelming task of planning and executing the data collection program. The tremendous number of tests that are possible in a relatively short time period with the FWD permits great flexibility in evaluating many features and distress patterns. However, this flexibility also leads to a certain amount of perplexity in trying to plan the most efficient manner in which to collect and organize such a vast quantity of data. Adding to this confusion are the inevitable variabilities associated with the testing of nonhomogeneous, anisotropic paving materials subjected to wide ranges in climatic conditions. A major objective of this research was to provide specific guidelines to the engineer for conducting the field testing program in light of these inherent variations, and, to this end, the field research program was designed.

3.1 Major Concerns

With the introduction of NDT & E in the early 1960's, engineers began to experience significant variation in field test measurements over relatively short time periods. Such variations surely existed with destructive testing methods, but were largely ignored because of the expense involved in performing repeated testing. To date, little has been formally written on this problem, particularly in regards to rigid airfield pavements, either because equipment manufacturers were reluctant to publicize such information, or because testing firms did not have the impetus to explore the problem. This research effort has attempted to quantify this variation for several

aspects of the rigid pavement evaluation process. The following specific concerns have been addressed:

1. What is the repeatability of FWD deflection and load measurements at the center, edge, and corner of a slab over any given minute, hour, day, month, or season?

2. What is the effect of pavement or air temperature on FWD deflection and load measurements, backcalculated slab and subgrade moduli, and load transfer efficiencies at joints?

3. How much variation exists in PCC elastic modulus, subgrade modulus, and load transfer efficiency from slab to slab within the same feature?

4. How does the magnitude of load affect backcalculated moduli and load transfer efficiency?

5. How does the type of joint construction influence the load transfer efficiency-temperature relationship?

6. Is load transfer efficiency relatively constant along the joint?

The remainder of this chapter describes the field research test program, the specific procedures developed to address each of the major concerns, and the results pertaining to variability of load and deflection measurements. Chapters 4 and 5 will deal specifically with load transfer efficiency and moduli variation, respectively.

3.2 Selection of Field Test Sites

Several factors were considered in selecting suitable locations to collect data, but of utmost concern was repeated access to pavement sections that were typical of those in service at any major airfield. Such access is normally not available for extended periods of time unless the airfield, or major portions of it, are shut down for maintenance. Fortunately, the U.S. Air Force Engineering and Services Center Pavement Evaluation Team routinely

coordinates the closure of entire runway, taxiway, and apron facilities for three day periods to perform destructive evaluations, and it was their scheduling that dictated the final selection of test sites.

With the cooperation of the Pavement Evaluation Team, three Air Force installations were visited between March and June 1984, representing a wide cross section of environmental, geographic, and operational conditions. Sheppard Air Force Base (AFB) in Wichita Falls, Texas is a pilot training base with an even mix of T-37 and T-38 aircraft presently using the airfield pavements. The base, however, was originally designed for heavy load bomber aircraft, and as such contained a wide range of PCC thicknesses, including some very thick, little used apron and taxiway features. These pavements were selected for most of the repeated FWD testing because of their unlimited access. Testing began on 13 March 1984 using a Dynatest Model 8000 FWD furnished by the U.S. Army Waterways Experiment Station at Vicksburg, Mississippi.

On 5 May 1984 testing continued on the Runway, Parallel taxiway, and Operational Apron at Plattsburgh AFB, New York, a Strategic Air Command base with an F-111 and KC-135 mission. Again, variability of FWD measurements was investigated, but greater emphasis was placed on verification of the revised traffic area concepts presented in Chapter 8.

Seymour-Johnson AFB, North Carolina was visited in mid-June 1984. This Tactical Air Command base supports primarily F-4 aircraft on 15 to 21 inch PCC pavement. The major thrust at this location was to simulate an actual evaluation program by testing as many different features as possible in a three day period. Each feature was tested between 9:00 am and 3:00 pm and again between 3:00 am and 7:00 am to provide additional information on temperature effects and to establish the feasibility of night testing.

At the conclusion of this portion of the field research program, it became evident that hourly and daily temperature variations could effect NDT measurements, but nothing was known about monthly or seasonal changes. As a result, Sheppard AFB was revisited in mid-July 1984 to retest the same locations but at much higher temperatures. Figures 3-1 through 3-3 point out the features selected for testing at each installation, and Table 3-1 summarizes their physical properties.

3.3 FWD Measurement Repeatability

The first major concern addressed during the field research program was the repeatability of the FWD load and deflection measurements. If the validity of these measurements can be established, then confidence can be expressed in the equipment, and a firm foundation can be laid for the analysis. To investigate this aspect of the data collection process, a testing program was conducted at Sheppard AFB to measure loads and deflections for several combinations of load, temperature, and thickness.

3.3.1 Constant Temperatures

Testing for repeatability began by devising a test pattern for the FWD consisting of five points on each slab, three load levels, and four complete repetitions. This pattern was repeated for three slabs in each feature and for three features of different thickness. Figure 3-4 illustrates the test pattern used.

The sequence of events for a complete pattern was as follows: 1) the loading plate was lowered over Point 1, a series of three drops at low, medium and high load levels was performed, and then the plate was raised to the travel position; 2) this same sequence was performed a second time

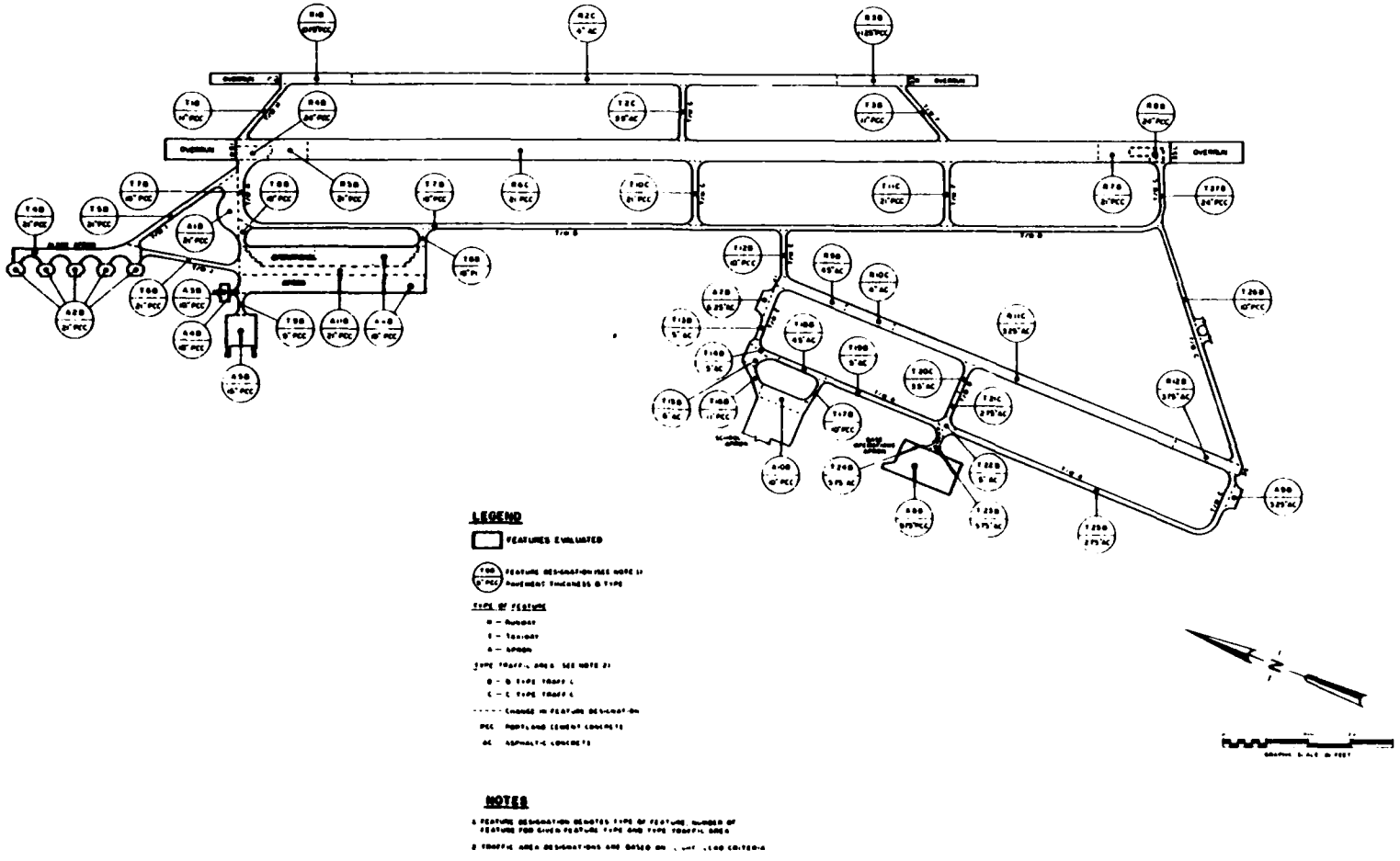

Figure 3-1. Sheppard Air Force Base Testing Locations

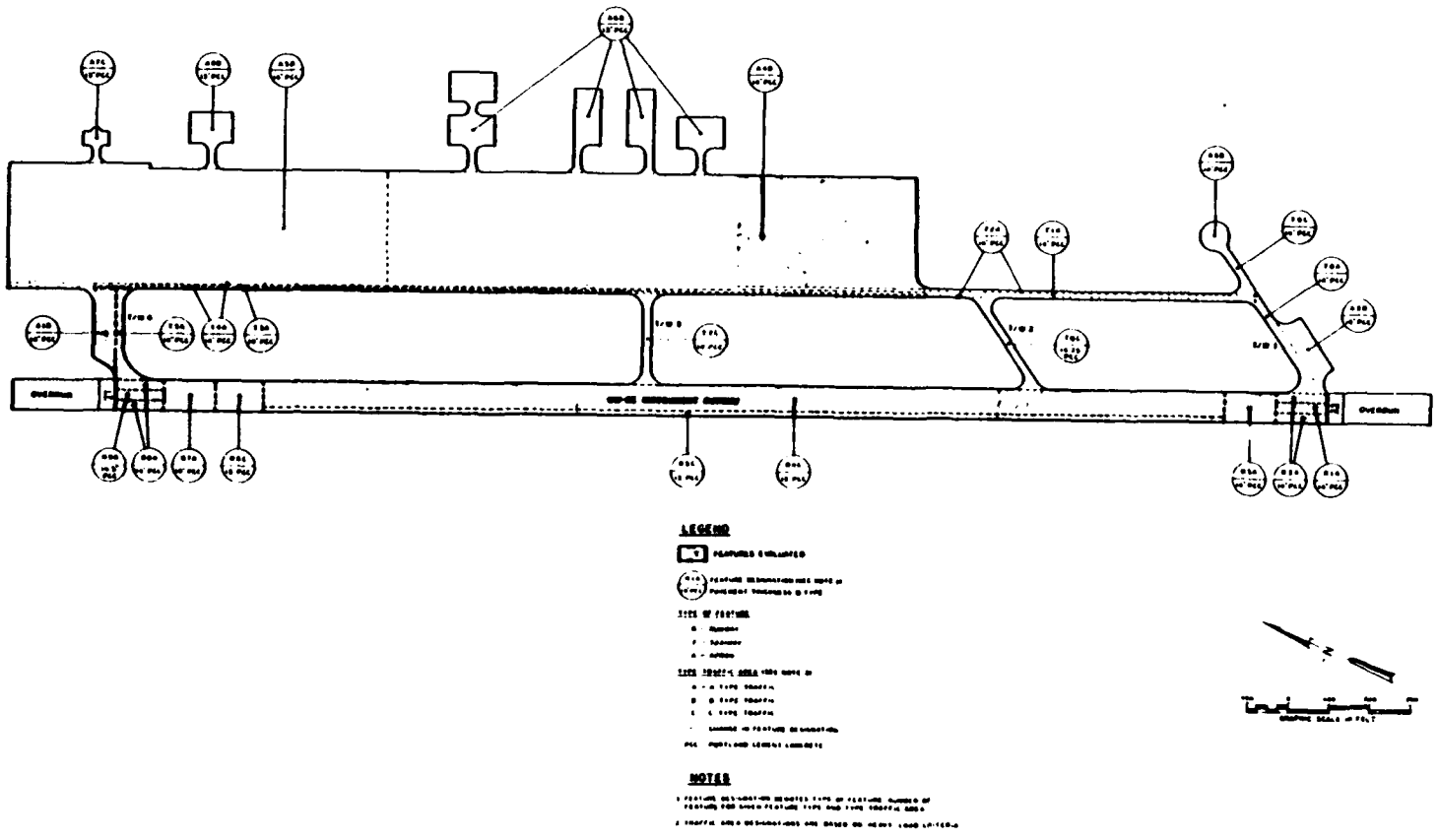

Figure 3-2. Plattsburgh Air Force Base Testing Locations

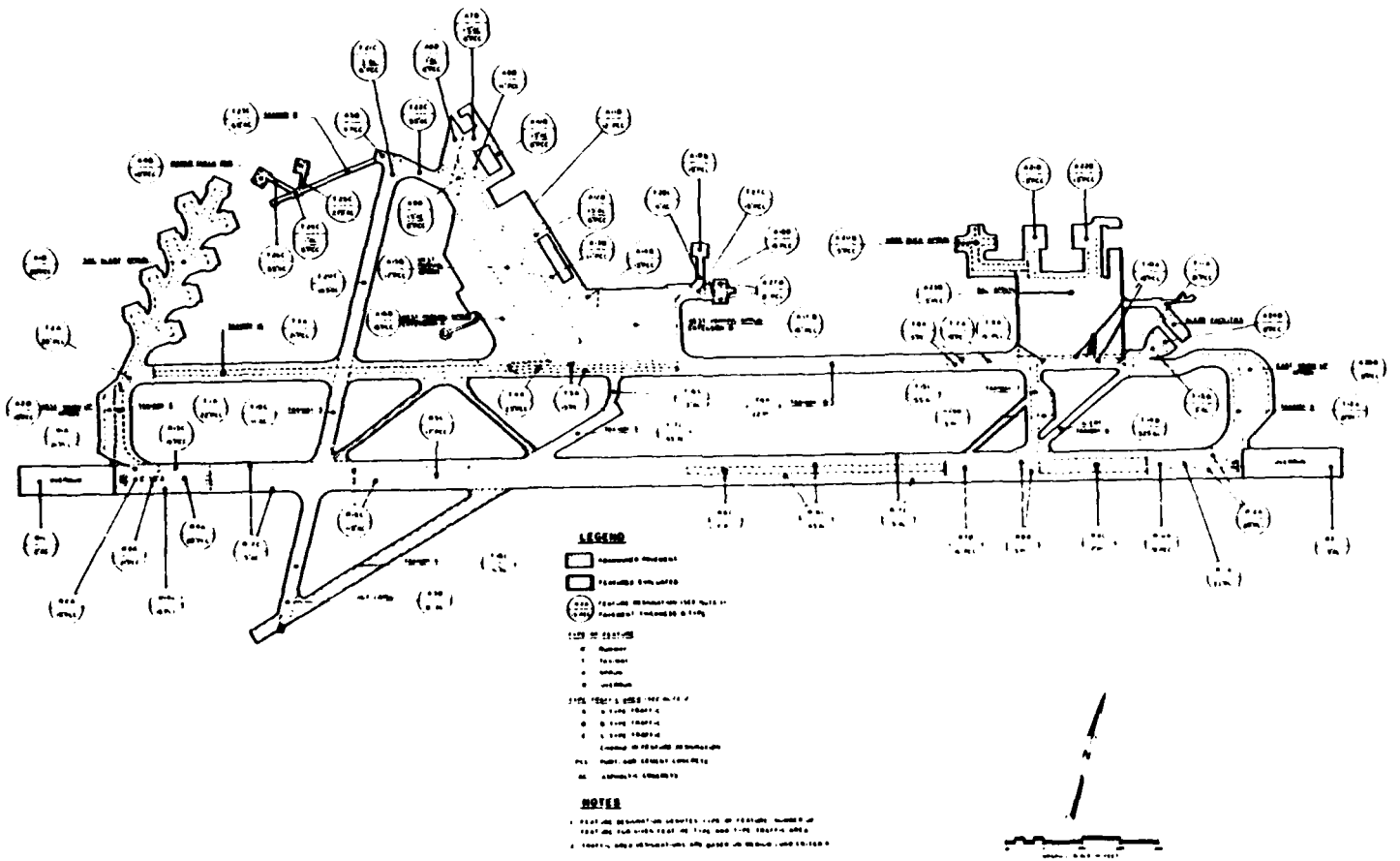

Figure 3-3. Seymour-Johnson Air Force Base Testing Locations

TABLE 3-1. PHYSICAL PROPERTY DATA FOR TEST FEATURES

Base	Feature	Slab Thick. (ins.)	Slab Widths Tran. (ft.)	Slab Widths Long. (ft.)	Base Course Thick. (ins.)	Base Course Class.	Subgrade Class.(1)	PCI(2)
Sheppard	T04A	21.0	25.0	25.0	12.0	SP	CL	85
	A03B	10.0	19.3	16.7	----	--	CL	95
	A05B	15.0	25.0	25.0	----	--	CL	70
	A06B	19.0	25.0	25.0	----	--	CL	95
	A08B	10.0	20.0	12.5	----	--	CL	85
	R08A	24.0	25.0	25.0	----	--	CL	95
Plattsburgh	R01A	14.0	25.0	25.0	----	--	SP	91
	R02A	14.5	25.0	25.0	----	--	SP	91
	R03A	14.5	25.0	25.0	----	--	SP	94
	R04C	13.0	25.0	25.0	----	--	SP	94
	R05C	13.0	25.0	25.0	----	--	SP	91
	R06C	13.0	25.0	25.0	----	--	SP	88
	R07A	14.0	25.0	25.0	----	--	SP	91
	R08A	14.0	25.0	25.0	----	--	SP	91
	R09A	14.5	25.0	25.0	----	--	SP	88
	T01A	14.0	20.0	20.0	----	--	SM	63
	T03A	14.0	20.0	20.0	----	--	SM	63
	T05A	14.0	25.0	25.0	----	--	SM	63
	A01B	14.0	25.0	25.0	----	--	SM	63
	A04B	13.5	20.0	20.0	----	--	SM	81
Seymour-Johnson	R03A	21.0	25.0	25.0	----	--	SW-SM	67
	R06C	17.0	25.0	25.0	6.0	GP-GM	SM	63
	R09C	17.0	25.0	25.0	----	--	SM	29
	T01A	22.0	25.0	25.0	----	--	SW-SM	25
	T03A	21.5	25.0	25.0	----	--	SW-SM	63
	T05A	21.5	25.0	25.0	6.0	GP-GM	SM	63
	T07A	15.0	25.0	25.0	5.0	SM	SC	100
	A20B	15.0	25.0	25.0	----	--	SM	82
	A23B	15.5	25.0	25.0	----	--	SM	80

(1) Unified Soil Classification
(2) Pavement Condition Index (see Reference 69)

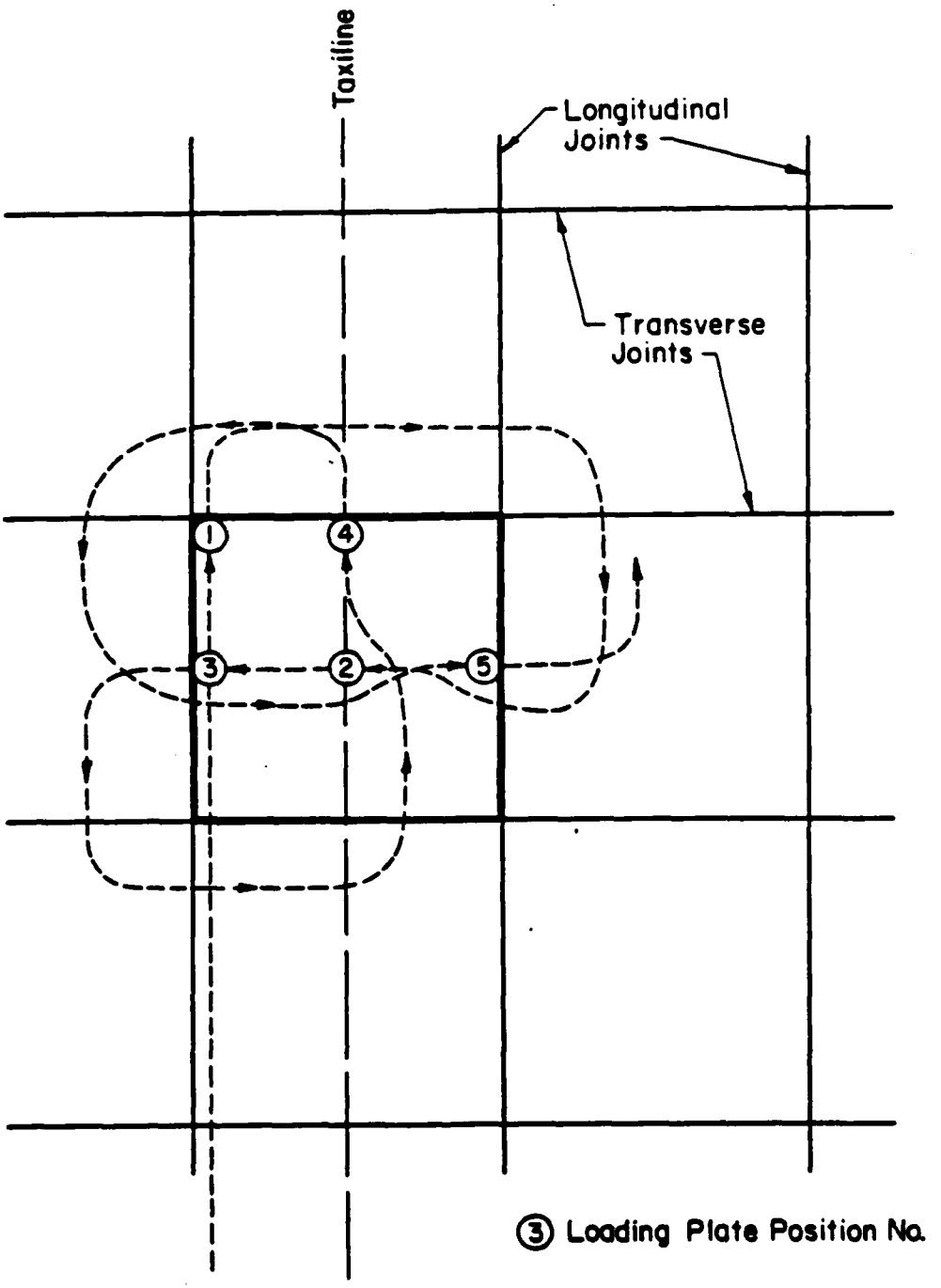

Figure 3-4. FWD Testing Pattern for the Study of Load and Deflection Measurement Repeatability

without moving the FWD: 3) steps 1 and 2 were repeated at each of the five locations on the slab; 4) steps 1, 2, and 3 were repeated for the entire slab; 4) steps 1 through 4 were repeated for each of three slabs in Feature T4A; and 6) steps 1 through 5 were repeated for Features A3B and A5B. The entire test sequence for one slab took approximately 45 minutes to complete, thus minimizing the effects of temperature change on the measurements. Each of the four series of drops at each point on the slab could have been performed consecutively, but by moving the FWD and then returning to approximately the same spot, it was felt that a more realistic measure of repeatability could be achieved.

The results of this study on FWD measurement repeatability are presented in the form of tables. Tables 3-2 through 3-7 show the results of three different load levels on each of the five positions in a slab. Slab 1 of Feature T4A was selected to illustrate the degree of repeatability typical of each slab. Tables 3-8 and 3-9 are presented to verify that the same trends continue for various PCC thicknesses.

An examination of each of these tables reveals that appreciable improvement in the coefficient of variation can be expected as the load level increases. Typically, load measurements average about 2 1/2 percent variation in the 7000 pound range while deflections average about 6 percent. As loads increase to 15000 pounds, the variation in load measurement drops to about 2 percent with deflections dropping to near 5 percent. Finally, 23000 pound loads display about a 1 percent variation, and their corresponding deflections about 4 percent. These typical values apply to the joints as well as to the center slab positions. Table 3-3 shows typical results of the attempt to eliminate the influence of small differences in load magnitude on the deflection sensor readings by comparing load/deflection ratios. The

TABLE 3-2. FWD LOAD AND DEFLECTION MEASUREMENT REPEATABILITY AT CONSTANT TEMPERATURE FOR SHEPPARD FEATURE T04A, SLAB NO. 1, AT THE CORNER POSITION

Load[1] Range	Test No.	Load (lbf)	Sensor Deflections D0 (mils)	D1	D2	D3	D4	D5	D6
Low	1	7568	3.4	1.7	1.6	1.4	1.2	1.1	0.9
	2	7360	3.3	1.5	1.5	1.3	1.1	1.1	0.9
	3	6880	2.9	1.7	1.5	1.3	1.1	1.1	0.9
	4	7088	3.0	1.6	1.5	1.3	1.2	1.0	0.9
Average		7224	3.15	1.63	1.53	1.35	1.18	1.05	0.90
Coef. of Var.		.04	.08	.06	.03	.04	.04	.05	<.005
Medium	1	15536	8.5	3.4	3.1	2.8	2.4	2.2	1.9
	2	15540	8.7	3.4	3.1	2.7	2.4	2.2	1.8
	3	14912	7.6	3.7	3.3	3.0	2.6	2.2	2.0
	4	14936	7.9	3.7	3.4	3.0	2.6	2.3	2.0
Average		15206	8.18	3.55	3.23	2.98	2.50	2.23	1.93
Coef. of Var.		.02	.06	.05	.05	.05	.05	.02	.05
High	1	22801	13.2	5.1	4.5	4.0	3.5	3.1	2.7
	2	22817	13.4	5.0	4.5	4.1	3.6	3.2	2.7
	3	22196	12.1	5.5	4.8	4.3	3.8	3.5	2.9
	4	22483	12.3	5.5	4.8	4.3	3.9	3.4	2.9
Average		22574	12.75	5.28	4.65	4.18	3.70	3.30	2.80
Coef. of Var.		.01	.05	.05	.04	.04	.05	.06	.04

(1) Load ranges - Low: 6000- 9000 lbf
Medium: 14000-16000 lbf
High: 22000-25000 lbf

TABLE 3-3. FWD LOAD/DEFLECTION RATIO REPEATABILITY AT CONSTANT TEMPERATURE FOR SHEPPARD FEATURE T04A. SLAB NO. 1, AT THE CORNER POSITION

Load(1) Range	Test No.	Load (lbf)	Sensor Load/Deflection Ratios (lbf/mil) D0	D1	D2	D3	D4	D5	D6
Low	1	7568	2225	4451	4370	5405	6306	6880	8408
	2	7360	2230	4906	4906	5661	6690	6690	8177
	3	6880	2372	4047	4586	5292	6254	6254	7644
	4	7088	2362	4430	4725	5452	5906	7088	7875
Average		7224	2297	4458	4646	5452	6289	6728	8026
Coef. of Var.		.04	.04	.08	.05	.03	.05	.05	.04
Medium	1	15536	1804	4510	4947	5477	6390	6970	8071
	2	15540	1828	4570	5012	5550	6475	7063	8178
	3	14912	1962	4030	4518	4970	5735	6778	7456
	4	14936	1890	4036	4392	4978	5744	6493	7468
Average		15206	1871	4286	4717	5243	6086	6826	7793
Coef. of Var.		.02	.04	.07	.07	.06	.07	.05	.05
High	1	22801	1727	4470	5066	5700	6514	7355	8444
	2	22817	1702	4563	5070	5565	6338	7130	8450
	3	22196	1834	4035	4624	5161	5841	6341	7653
	4	22483	1827	4087	4683	5228	5764	6612	7752
Average		22574	1772	4288	4860	5413	6114	6859	8074
Coef. of Var.		.01	.04	.06	.05	.05	.06	.07	.05

(1) Load ranges - Low: 6000- 9000 lbf
Medium: 14000-16000 lbf
High: 22000-25000 lbf

TABLE 3-4. FWD LOAD AND DEFLECTION MEASUREMENT REPEATABILITY AT CONSTANT TEMPERATURE FOR SHEPPARD FEATURE F04A, SLAB NO. 1, AT THE CENTER SLAB POSITION

Load Range	Test No.	Load (lbf)	Sensor Deflections (mils) D0	D1	D2	D3	D4	D5	D6
Low	1	7304	1.1	1.0	0.9	0.9	0.7	0.7	0.6
	2	7176	1.1	1.0	0.9	0.8	0.8	0.7	0.7
	3	7152	1.0	0.9	0.9	0.8	0.7	0.6	0.5
	4	7128	1.0	0.9	0.9	0.8	0.7	0.6	0.6
Average		7190	1.05	0.95	0.90	0.83	0.73	0.65	0.58
Coef. of Var.		.01	.05	.06	<.005	.06	.07	.09	.09
Medium	1	15432	2.4	2.1	2.0	1.8	1.7	1.5	1.4
	2	15208	2.4	2.0	2.0	1.9	1.7	1.4	1.4
	3	15056	2.3	2.2	2.0	1.9	1.7	1.5	1.3
	4	15016	2.3	2.1	2.0	1.8	1.7	1.5	1.3
Average		15178	2.35	2.10	2.00	1.85	1.70	1.48	1.35
Coef. of Var.		.01	.02	.04	<.005	.03	<.005	.03	.04
High	1	23532	3.6	3.2	3.0	2.8	2.5	2.3	2.0
	2	23055	3.6	3.1	3.0	2.7	2.6	2.3	2.0
	3	22864	3.5	3.2	3.0	2.8	2.5	2.3	2.0
	4	23135	3.5	3.1	3.0	2.8	2.6	2.3	2.0
Average		23147	3.55	3.15	3.00	2.78	2.55	2.30	2.00
Coef. of Var.		.01	.02	.02	<.005	.02	.02	<.005	<.005

(1) Load ranges - Low: 6000- 9000 lbf
Medium: 14000-16000 lbf
High: 22000-25000 lbf

TABLE 3-5. FWD LOAD AND DEFLECTION MEASUREMENT REPEATABILITY AT CONSTANT TEMPERATURE FOR SHEPPARD FEATURE T04A, SLAB NO. 1, ALONG THE LEFT LONGITUDINAL JOINT

Load Range	Test No.	Load (lbf)	Sensor Deflections D0 (mils)	D1	D2	D3	D4	D5	D6
Low	1	6936	1.8	1.2	1.0	0.9	0.8	0.7	0.6
	2	6960	1.8	1.2	1.0	0.9	0.8	0.7	0.6
	3	6656	1.8	1.1	1.0	0.9	0.7	0.6	0.5
	4	6632	1.8	1.1	1.0	0.9	0.8	0.6	0.6
Average		6796	1.80	1.15	1.00	0.90	0.78	0.65	0.58
Coef. of Var.		.03	<.005	.05	<.005	<.005	.06	.09	.09
Medium	1	15208	4.4	2.0	2.0	1.9	1.7	1.4	1.4
	2	15032	4.3	2.4	2.2	1.9	1.7	1.4	1.2
	3	14296	4.4	2.3	2.2	1.9	1.6	1.4	1.3
	4	14368	4.5	2.3	2.1	1.8	1.6	1.4	1.2
Average		14726	4.40	2.25	2.13	1.88	1.65	1.40	1.28
Coef. of Var.		.03	.02	.08	.04	.03	.03	<.005	.07
High	1	23103	6.7	3.4	3.1	2.7	2.4	2.0	1.8
	2	22960	7.4	3.4	3.0	2.7	2.4	2.1	1.8
	3	22944	6.9	3.3	3.0	2.7	2.4	2.0	1.7
	4	22912	7.0	3.3	3.0	2.6	2.3	2.0	1.7
Average		22980	7.00	3.35	3.03	2.68	2.38	2.03	1.75
Coef. of Var.		<.005	.04	.02	.02	.02	.02	.02	.03

(1) Load ranges - Low: 6000- 9000 lbf
Medium: 14000-16000 lbf
High: 22000-25000 lbf

TABLE 3-6. FWD LOAD AND DEFLECTION MEASUREMENT REPEATABILITY AT CONSTANT TEMPERATURE FOR SHEPPARD FEATURE T04A, SLAB NO. 1, AT THE TRANSVERSE JOINT

Load Range (lbf)	Test No.	Load (lbf)	Sensor Deflections (mils) D0	D1	D2	D3	D4	D5	D6
Low	1	7456	1.6	1.2	1.1	1.0	0.9	0.7	0.6
	2	7416	1.8	1.2	1.1	1.0	0.9	0.7	0.6
	3	7184	1.5	1.2	1.1	1.0	0.9	0.7	0.6
	4	7184	1.6	1.2	1.1	1.0	0.9	0.7	0.7
Average		7310	1.63	1.20	1.10	1.00	0.90	0.70	0.63
Coef. of Var.		.02	.08	<.005	<.005	<.005	<.005	<.005	.08
Medium	1	15400	3.0	2.6	2.3	2.1	1.8	1.6	1.4
	2	15336	4.0	2.5	2.3	2.0	1.8	1.6	1.4
	3	15168	3.7	2.7	2.4	2.1	1.9	1.7	1.5
	4	15120	3.8	2.7	2.4	2.1	1.9	1.7	1.4
Average		15256	3.85	2.63	2.35	2.08	1.85	1.65	1.43
Coef. of Var.		.01	.03	.04	.02	.02	.03	.03	.03
High	1	23055	6.1	3.7	3.3	3.0	2.6	2.3	2.0
	2	23214	6.2	3.7	3.2	3.0	2.6	2.2	2.0
	3	22880	5.7	3.7	3.5	3.2	2.8	2.4	2.1
	4	22546	5.8	3.7	3.5	3.2	2.8	2.2	2.1
Average		22923	5.95	3.70	3.38	3.10	2.70	2.28	2.05
Coef. of Var.		.01	.04	<.005	.04	.04	.04	.04	.03

(1) Load ranges - Low: 6000- 9000 lbf
Medium: 14000-16000 lbf
High: 22000-25000 lbf

TABLE 3-7. FWD LOAD AND DEFLECTION MEASUREMENT REPEATABILITY AT CONSTANT TEMPERATURE FOR SHEPPARD FEATURE T04A, SLAB NO. 1, AT THE RIGHT LONGITUDINAL JOINT

Load Range	Test No.	Load (lbf)	Sensor Deflections D0 (mils)	D1	D2	D3	D4	D5	D6
Low	1	7200	1.6	1.3	1.2	1.0	0.9	0.8	0.6
	2	7152	1.6	1.3	1.1	1.0	0.8	0.7	0.6
	3	6936	1.6	1.2	1.1	1.0	0.8	0.7	0.7
	4	6992	1.6	1.2	1.1	1.0	0.9	0.7	0.6
Average		7070	1.60	1.25	1.13	1.00	0.85	0.73	0.60
Coef. of Var.		.02	<.005	.05	.04	<.005	.07	.07	<.005
Medium	1	15424	3.6	2.9	2.5	2.2	2.0	1.7	1.5
	2	15360	3.8	2.7	2.4	2.1	1.8	1.6	1.4
	3	15040	3.7	2.7	2.4	2.1	1.8	1.6	1.4
	4	14920	3.8	2.6	2.3	2.1	1.8	1.6	1.3
Average		15186	3.73	2.73	2.40	2.13	1.85	1.63	1.40
Coef. of Var.		.02	.03	.05	.03	.02	.05	.03	.06
High	1	23103	5.7	4.0	3.5	3.1	2.8	2.4	2.0
	2	23262	5.9	3.9	3.4	3.0	2.7	2.3	2.0
	3	23421	5.9	3.9	3.4	3.0	2.6	2.3	2.0
	4	23389	5.8	3.9	3.4	3.1	2.7	2.4	2.0
Average		23294	5.83	3.93	3.43	3.05	2.70	2.35	2.00
Coef. of Var.		.01	.02	.01	.01	.02	.03	.02	<.005

(1) Load ranges - Low: 6000- 9000 lbf
Medium: 14000-16000 lbf
High: 22000-25000 lbf

TABLE 3-8. FWD LOAD AND DEFLECTION MEASUREMENT REPEATABILITY AT CONSTANT TEMPERATURE FOR SHEPPARD FEATURE A03B, SLAB NO. 2, AT THE CENTER SLAB POSITION

Load Range	Test No.	Load (lbf)	Sensor Deflections D0 (mils)	D1	D2	D3	D4	D5	D6
Low	1	7752	5.4	5.1	4.5	3.9	3.2	2.5	1.9
	2	7608	5.6	5.4	4.6	3.9	3.3	2.5	1.9
	3	7464	5.1	4.7	4.2	3.6	2.9	2.3	1.8
	4	7456	5.4	5.0	4.4	3.7	3.1	2.4	1.8
Average		7570	5.38	5.05	4.43	3.78	3.13	2.43	1.85
Coef. of Var.		.02	.04	.06	.04	.04	.05	.04	.03
Medium	1	15656	11.1	10.3	9.1	7.8	6.4	5.0	3.8
	2	15656	11.0	10.6	8.9	7.6	6.2	5.0	3.8
	3	15440	10.2	9.6	8.3	7.5	5.9	4.8	3.6
	4	15408	10.5	9.6	8.5	7.2	6.0	4.8	3.6
Average		15540	10.70	10.03	8.70	7.53	6.13	4.90	3.70
Coef. of Var.		.01	.04	.05	.04	.03	.04	.02	.03
High	1	23612	16.2	15.0	13.1	11.1	9.2	7.2	5.4
	2	23405	15.8	14.8	12.8	10.9	9.0	7.2	5.4
	3	23341	14.9	13.9	12.0	10.4	8.5	6.8	5.0
	4	23294	15.0	13.9	12.0	10.2	8.5	6.8	5.0
Average		23413	15.48	14.40	12.48	10.65	8.80	7.03	5.20
Coef. of Var.		.01	.04	.04	.05	.04	.04	.03	.04

(1) Load ranges - Low: 6000- 9000 lbf
Medium: 14000-16000 lbf
High: 22000-25000 lbf

TABLE 3-9. FWD LOAD AND DEFLECTION MEASUREMENT REPEATABILITY AT CONSTANT TEMPERATURE FOR SHEPPARD FEATURE A05B, SLAB NO. 4, AT THE TRANSVERSE JOINT

Load Range	Test No.	Load (lbf)	Sensor Deflections (mils) D0	D1	D2	D3	D4	D5	D6
Low	1	7696	2.1	2.0	1.8	1.5	1.3	1.2	1.0
	2	7616	2.1	2.1	1.7	1.5	1.2	1.1	1.1
	3	7600	2.1	2.0	1.8	1.8	1.4	1.2	1.2
	4	7456	2.1	2.0	1.8	1.6	1.4	1.2	1.0
Average		7592	2.10	2.03	1.78	1.60	1.33	1.18	1.08
Coef. of Var.		.01	<.005	.02	.03	.09	.07	.04	.09
Medium	1	15584	4.5	4.2	3.7	3.2	2.9	2.5	2.2
	2	15464	4.4	4.3	3.6	3.2	3.0	2.6	2.2
	3	15448	4.5	4.2	3.7	3.3	2.9	2.5	2.2
	4	15368	4.5	4.2	3.7	3.3	3.0	2.5	2.2
Average		15466	4.48	4.23	3.68	3.25	2.95	2.53	2.20
Coef. of Var.		.01	.01	.01	.01	.02	.02	.02	<.005
High	1	23532	6.6	6.2	5.5	4.8	4.2	3.7	3.2
	2	23548	6.6	6.3	5.4	4.8	4.2	3.7	3.2
	3	22626	6.5	6.1	5.4	4.7	4.1	3.5	3.1
	4	22499	6.5	6.0	5.3	4.6	4.1	3.5	3.1
Average		23051	6.55	6.15	5.40	4.73	4.15	3.60	3.15
Coef. of Var.		.02	.01	.02	.02	.02	.01	.03	.02

(1) Load ranges - Low: 6000- 9000 lbf
Medium: 14000-16000 lbf
High: 22000-25000 lbf

results show no improvement in coefficients of variation for deflection measurements when "normalized" by load.

Of particular interest in these tables is the consistency of the first and second drops (made within 30 seconds of each other) and the third and fourth drops (also made within 30 seconds of each other but nearly 30 minutes after the first two drops). Generally, the second pair of drops produced slightly lower deflections and loads, a definite trend that is attributable to increased temperatures in the rubber buffers. Further evidence of this phenomenon will be presented later in this chapter.

Differences in the drops can also be partially accounted for by slight inaccuracies in repositioning the FWD, and by rounding of the deflection values to the nearest one-tenth mil. Overall, however, the FWD exhibits remarkable consistency in measuring very transient loads and small deflections on such nonuniform materials.

3.3.2 Changing Temperatures

Results of the previous section indicate that good consistency exists in FWD measurements at relatively constant temperature for all points on the slab, thus minimizing the influence of the equipment on the variability of the end product, the backcalculated moduli and load transfer efficiency. This section looks at the contribution of time, temperature, and, to some extent, seasonal changes toward the variation in FWD load and deflection measurements at center slab within hourly and daily periods. Moisture is presumed to play a modest role in the variations observed, but it is very difficult to account for it apart from temperature over short time periods. Therefore, only time and temperature differences are used in the comparisons. Seasonal variations in FWD measurements are also presumed to

exist, as a logical extension of daily variations, but unless the drop heights on the FWD remained unchanged from March through July, which was not possible in this case, this effect can only be examined using backcalculated moduli. Chapter 5 will deal with this aspect in detail.

The testing pattern developed for the repeatability study was specially designed for that purpose, but was not well suited for the routine collection of large amounts of information for many pavement slabs. As a result, the pattern of Figure 3-4 was reduced to that shown in Figure 3-5. This "normal" pattern permitted sampling at each key location on a slab while assisting the transition to the next slab. Using this modified pattern, load and deflection measurements were taken at the same points on each slab, under several temperature conditions, but within the same three-day period. Tables 3-10 through 3-14 provide examples of the influence of temperature fluctuations on FWD measurements made at center slab positions only. Joints and corners, as will be seen later, are significantly affected by temperature changes, and therefore would not provide a meaningful comparison to the constant temperature case.

The trends displayed in Tables 3-10 through 3-13 closely parallel the findings for the constant temperature cases presented earlier. These measurements were taken in July with only a 20-degree spread between maximum and minimum temperatures. The coefficients of variation for load and deflection measurements are nearly identical to those of the constant temperature case, and significant improvement in these coefficients can be obtained at the higher load levels. Table 3-11 is again presented as a typical result of the effort to see if any improvement in deflection measurement consistency could be obtained by normalizing with load, but the results show only slight reductions in the coefficients of variation.

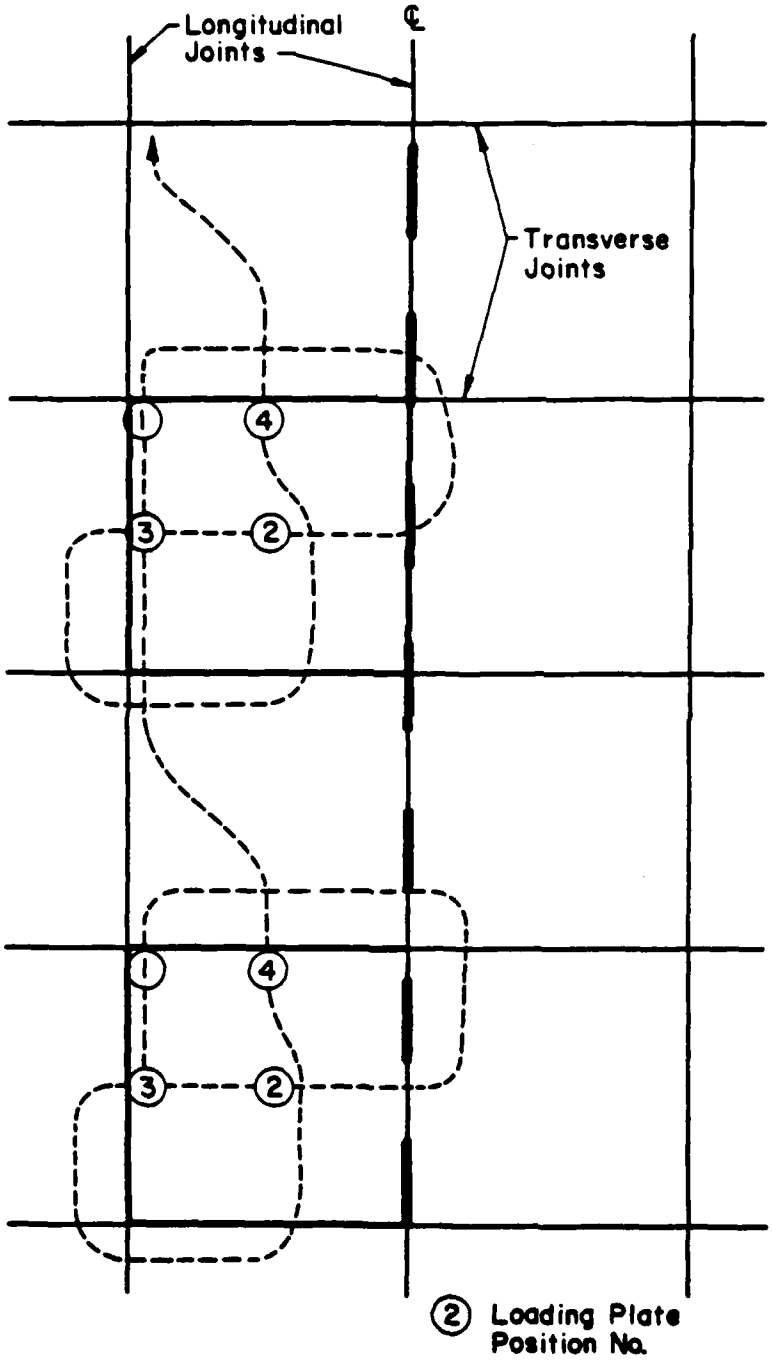

Figure 3-5. Recommended FWD Testing Pattern for Network Level Evaluations

TABLE 3-10. FWD LOAD AND DEFLECTION MEASUREMENT REPEATABILITY UNDER VARYING TEMPERATURES FOR SHEPPARD FEATURE T04A, SLAB NO. 1, AT THE CENTER SLAB POSITION

Load Range	Temp. Cond. No.	Load (lbf)	Sensor Deflections (mils) D0	D1	D2	D3	D4	D5	D6
Low	1	8395	1.1	1.0	1.0	0.9	0.8	0.7	0.6
	2	8300	1.1	1.0	1.0	0.9	0.9	0.8	0.6
	3	8125	1.1	1.0	0.9	0.9	0.8	0.8	0.7
	4	7998	1.0	1.0	0.9	0.9	0.8	0.7	0.7
Average		8205	1.08	1.00	0.95	0.90	0.83	0.75	0.65
Coef. of Var.		.02	.05	<.005	.06	<.005	.06	.08	.09
Medium	1	15534	2.4	2.1	2.0	1.9	1.7	1.6	1.4
	2	15582	2.4	2.2	2.1	2.0	1.8	1.7	1.5
	3	15852	2.3	2.2	2.0	1.9	1.8	1.7	1.4
	4	15964	2.3	2.1	2.0	1.9	1.8	1.6	1.4
Average		15733	2.35	2.15	2.03	1.93	1.78	1.65	1.45
Coef. of Var.		.01	.02	.03	.02	.03	.03	.03	.04
High	1	23389	3.6	3.0	2.9	2.8	2.5	2.2	2.0
	2	23484	3.4	3.1	3.0	2.8	2.5	2.4	2.0
	3	23357	3.3	3.0	3.0	2.7	2.5	2.2	2.0
	4	23071	3.3	3.0	2.9	2.7	2.5	2.2	2.0
Average		23325	3.40	3.03	2.95	2.75	2.50	2.25	2.00
Coef. of Var.		.01	.04	.02	.02	.02	.00	.04	<.005

Notes: Temperature Condition No. 1 existed on 10 July at 1:55p at an air temperature of 101 degrees F.

Temperature Condition No. 2 existed on 11 July at 8:45a at an air temperature of 89 degrees F.

Temperature Condition No. 3 existed on 11 July at 9:20a at an air temperature of 91 degrees F.

Temperature Condition No. 4 existed on 12 July at 10:00a at an air temperature of 82 degrees F.

TABLE 3-11. FWD LOAD/DEFLECTION RATIO REPEATABILITY UNDER VARIYING TEMPERATURES FOR SHEPPARD FEATURE T04A. SLAB NO. 1, AT THE CENTER SLAB POSITION

Load Range	Temp. Cond No.	Load (lbf)	Sensor Load/Deflection Ratios (lbf/mil) D0	D1	D2	D3	D4	D5	D6
Low	1	8395	7631	8395	8395	9327	10493	11992	13991
	2	8300	7545	8300	8300	9222	9222	10375	13833
	3	8125	7386	8125	9027	9027	10156	10156	11607
	4	7998	7998	7998	8886	8886	9997	11425	11425
Average		8205	7640	8204	8652	9115	9967	10987	12714
Coef. of Var.		.02	.03	.02	.04	.02	.05	.08	.11
Medium	1	15534	6472	7397	7767	8175	9137	9708	11095
	2	15582	6492	7082	7420	7791	8656	9165	10388
	3	15852	6892	7205	7926	8343	8806	9324	11322
	4	15964	6940	7601	7982	8402	8868	9977	11402
Average		15733	6699	7321	7773	8177	8866	9543	11051
Coef. of Var.		.01	.04	.03	.03	.03	.02	.04	.04
High	1	23389	6496	7796	8065	8353	9355	10631	11694
	2	23484	6907	7575	7828	8387	9393	9785	11742
	3	23357	7077	7785	7785	8650	9342	10616	11678
	4	23071	6991	7690	7955	8544	9228	10486	11535
Average		23325	6867	7711	7908	8483	9329	10379	11662
Coef. of Var.		.01	.04	.01	.02	.02	.01	.04	.01

Notes: Temperature Condition No. 1 existed on 10 July at 1:55p at an air temperature of 101 degrees F.

Temperature Condition No. 2 existed on 11 July at 8:45a at an air temperature of 89 degrees F.

Temperature Condition No. 3 existed on 11 July at 9:20a at an air temperature of 91 degrees F.

Temperature Condition No. 4 existed on 12 July at 10:00a at an air temperature of 82 degrees F.

TABLE 3-12. FWD LOAD AND DEFLECTION MEASUREMENT REPEATABILITY UNDER VARYING TEMPERATURES FOR SHEPPARD FEATURE A03B, SLAB NO. 2, AT THE CENTER SLAB POSITION

Load Range	Temp. Cond. No.	Load (lbf)	Sensor Deflections D0 (mils)	D1	D2	D3	D4	D5	D6
Low	1	7886	3.9	3.5	3.1	2.6	2.2	1.7	1.3
	2	8014	4.4	4.1	3.7	3.2	2.7	2.2	1.7
	3	7807	4.2	3.8	3.3	2.9	2.3	1.9	1.4
Average		7902	4.17	3.80	3.37	2.90	2.40	1.93	1.47
Coef. of Var.		.01	.06	.08	.09	.10	.11	.13	.14
Medium	1	14819	8.4	7.5	6.7	5.7	4.8	3.9	2.9
	2	15884	9.0	8.3	7.6	6.5	5.5	4.5	3.4
	3	15487	9.1	8.2	7.3	6.2	5.0	4.1	3.1
Average		15397	8.83	8.00	7.20	6.13	5.10	4.17	3.13
Coef. of Var.		.03	.04	.05	.06	.07	.07	.07	.08
High	1	22085	11.8	10.8	9.6	8.1	6.7	5.4	4.1
	2	22546	12.8	11.8	10.6	9.1	7.6	6.2	4.8
	3	22276	12.9	11.8	10.4	8.7	7.1	5.7	4.3
Average		22302	12.13	11.47	10.20	8.63	7.13	5.77	4 40
Coef. of Var.		.01	.05	.05	.05	.06	.06	.07	.08

Notes: Temperature Condition No. 1 existed on 10 July at 10:00a at an air temperature of 92 degrees F.

Temperature Condition No. 2 existed on 10 July at 2:45p at an air temperature of 101 degrees F.

Temperature Condition No. 3 existed on 11 July at 1:55p at an air temperature of 104 degrees F.

TABLE 3-13. FWD LOAD AND DEFLECTION MEASUREMENT REPEATABILITY UNDER VARYING TEMPERATURES FOR SHEPPARD FEATURE A05B, SLAB NO. 4, AT THE CENTER SLAB POSITION

Load Range	Temp. Cond. No.	Load (lbf)	Sensor Deflections D0 (mils)	D1	D2	D3	D4	D5	D6
Low	1	7966	1.8	1.6	1.5	1.5	1.3	1.2	1.1
	2	7632	1.7	1.7	1.6	1.4	1.3	1.1	1.0
	3	8348	1.9	1.7	1.6	1.5	1.3	1.2	1.1
Average		7982	1.80	1.67	1.57	1.47	1.30	1.17	1.07
Coef. of Var.		.04	.06	.03	.04	.04	<.005	.05	.05
Medium	1	15455	3.7	3.4	3.2	3.0	2.8	2.4	2.2
	2	15391	3.7	3.5	3.3	3.1	2.8	2.6	2.2
	3	15900	3.8	3.5	3.3	3.1	2.8	2.6	2.2
Average		15582	3.73	3.47	3.27	3.07	2.80	2.53	2.20
Coef. of Var.		.02	.02	.02	.02	.02	<.005	.05	<.005
High	1	23166	5.1	4.8	4.5	4.2	3.7	3.4	3.0
	2	22705	5.3	5.0	4.7	4.3	3.9	3.5	3.1
	3	22928	5.3	4.9	4.7	4.3	3.9	3.5	3.1
Average		22933	5.23	4.90	4.53	4.27	3.83	3.47	3.07
Coef. of Var.		.01	.02	.02	.06	.01	.03	.02	.02

Notes: Temperature Condition No. 1 existed on 10 July at 10:38a at an air temperature of 96 degrees F.

Temperature Condition No. 2 existed on 10 July at 3:25p at an air temperature of 101 degrees F.

Temperature Condition No. 3 existed on 12 July at 2:00p at an air temperature of 91 degrees F.

Table 3-14, however, highlights an interesting phenomenon that occurs as temperatures fall. As air temperatures approach freezing, the FWD loads measured by the load cell increase significantly, but without a proportionate increase in the deflections. Loads that typically showed less than 2 percent variation in warm temperatures display 8 to 9 percent variation in cold temperatures, while deflections remain relatively unaffected.

It appears that for center slab conditions only, the moderate temperature fluctuations (15 to 20 ^{o}F) experienced throughout the course of a normal test day do not add to the existing, constant temperature variation found in the equipment and pavement materials, unless testing is done below 40 degrees. At these lower temperatures, the rubber buffers of the FWD apparently stiffen and impart a more sharply-spiked impulse load to the pavement, creating higher load measurements. This same effect also appears early in the morning, even if the temperature is above 60 degrees, if the FWD has been stored overnight in cool conditions and not allowed to "warm up" prior to testing. The 8:00 am reading on 15 March in Table 3-14 is a good example of this. These higher loads, however, do not increase deflections appreciably. The results of this phenomenon on backcalculated moduli will be examined more closely in Chapter 5.

TABLE 3-14. FWD LOAD AND DEFLECTION MEASUREMENT REPEATABILITY UNDER VARYING TEMPERATURES FOR SHEPPARD FEATURE T04A, SLAB NO. 1, AT THE CENTER SLAB POSITION

Load Range	Temp. Cond. No.	Load (lbf)	Sensor Positions D0 (mils)	D1	D2	D3	D4	D5	D6
Low	1	7304	1.1	1.0	0.9	0.9	0.7	0.7	0.6
	2	8376	1.1	1.0	1.0	0.9	0.9	0.7	0.7
	3	8848	1.2	1.0	1.0	1.0	0.9	0.8	0.7
	4	9632	1.1	1.0	1.0	1.0	0.8	0.8	0.7
Average		8540	1.13	1.00	0.98	0.95	0.83	0.75	0.68
Coef. of Var.		.11	.04	<.005	.05	.06	.12	.08	.07
Medium	1	15432	2.4	2.1	2.0	1.8	1.7	1.5	1.4
	2	16504	2.4	2.1	2.1	1.9	1.8	1.6	1.5
	3	17720	2.5	2.3	2.1	2.0	1.9	1.7	1.5
	4	18824	2.5	2.2	2.2	2.0	1.8	1.7	1.4
Average		17120	2.45	2.18	2.10	1.93	1.75	1.63	1.45
Coef. of Var.		.09	.02	.04	.04	.05	.03	.06	.04
High	1	23532	3.6	3.2	3.0	2.8	2.5	2.3	2.0
	2	24295	3.6	3.2	3.1	2.8	2.6	2.4	2.1
	3	25965	3.8	3.2	3.1	2.9	2.7	2.4	2.2
	4	28318	3.7	3.3	3.2	2.9	2.7	2.4	2.0
Average		25527	3.68	3.23	3.10	2.85	2.63	2.38	2.08
Coef. of Var.		.08	.03	.02	.03	.02	.04	.02	.05

Notes: Temperature Condition No. 1 existed on 13 March at 12:30p at an air temperature of 61 degrees F.

Temperature Condition No. 2 existed on 15 March at 8:00a at an air temperature of 65 degrees F.

Temperature Condition No. 3 existed on 17 March at 4:15a at an air temperature of 45 degrees F.

Temperature Condition No. 4 existed on 19 March at 8:20a at an air temperature of 36 degrees F.

CHAPTER 4

JOINT LOAD TRANSFER

Joints have long been recognized as the major focal point for pavement distress in jointed concrete pavements, and yet are largely ignored in most of today's evaluation schemes. As is shown in Chapter 8, the load transfer efficiency of a joint has a tremendous effect on the stresses that are developed at the bottom of the slab, and therefore, on the performance of the slab under load. In the previous chapter, the excellent reproducibility of FWD center slab load and deflection measurements was established for the range of temperatures normally encountered throughout the testing day. This same high degree of repeatability was also obtained at longitudinal and transverse joints, but only if the temperature remained constant. It quickly became evident during the field testing program that this same degree of repeatability did not exist at the joints as temperatures changed. Both the magnitude of the deflections and the load transfer efficiencies were affected. This chapter will describe the relationship between load transfer efficiency and the magnitude of load, the variation in load transfer efficiency along a joint, the influence of temperature on joint behavior, and the techniques to predict joint load transfer efficiency for any temperature.

4.1 Load Transfer Efficiency

The importance of load transfer at joints on the overall performance of rigid airfield pavements has been well documented. A perfectly efficient system for transferring load from one side of the joint to the other can reduce the free edge stress by 50 percent. Many different systems have been

developed and tested for establishing and maintaining high degrees of load transfer across joints during the life of the pavement. The objective of these systems is simple: to minimize the tensile stresses and deflections in the concrete that result when loads are applied at the edge of the slab. keeping concrete edge stresses at a minimum dramatically reduces fatigue damage and greatly increases pavement life, while reducing deflections minimizes the potential for pumping.

In the evaluation of remaining pavement structural life, the level of stress developed under an aircraft gear at the slab joint must be determined. Unfortunately, it is impractical to quickly or economically measure actual stresses developed at joints. It is possible, however, to determine how well the load transfer mechanism is performing by measuring the relative deflection on both sides of the joint. This relative deflection is a direct indication of the load transfer efficiency of the joint, as shown in Figure 4-1. Normally, a correction is applied to the deflection measured by the D1 sensor to account for slab curvature due to bending, but the finite element mesh is designed to automatically make this adjustment. Coupling the load transfer efficiency with a good analytical model of joint behavior, such as ILLI-SLAB, the edge stresses under actual loads can be calculated.

The FWD is an excellent tool for measuring relative deflections at joints. As illustrated in Figure 4-2, the loading plate is positioned as nearly tangent to the joint as possible. This will automatically place the D0 and D1 sensors about 6 inches either side of the joint. Maneuvering the FWD into this position normally requires a spotter for the vehicle operator, unless a closed circuit camera system is employed. Such a system reduces the data collection crew requirement to one person and eliminates the inevitable communication difficulties between spotter and driver. Whichever arrangement

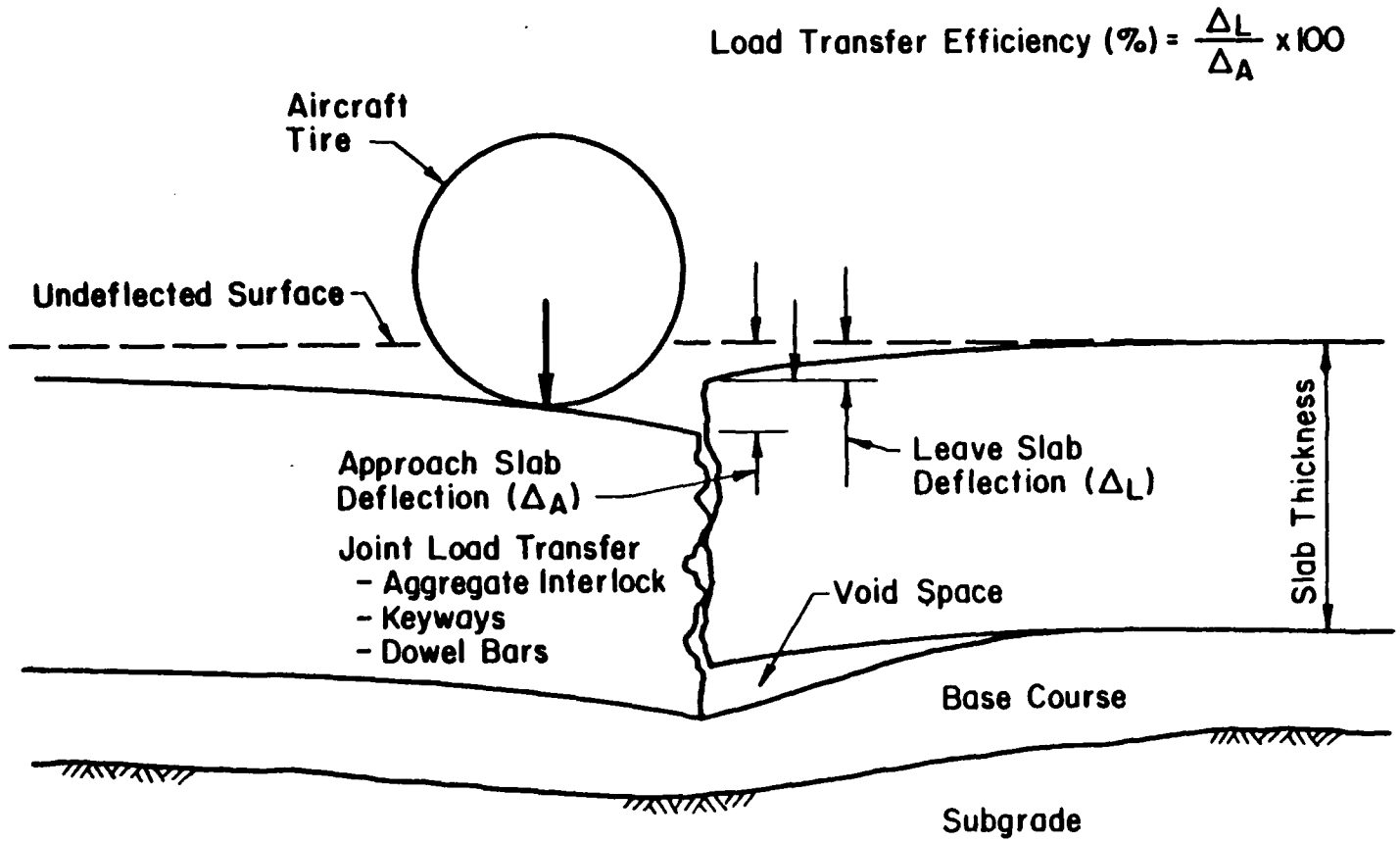

Figure 4-1. The Concept of Joint Load Transfer Efficiency

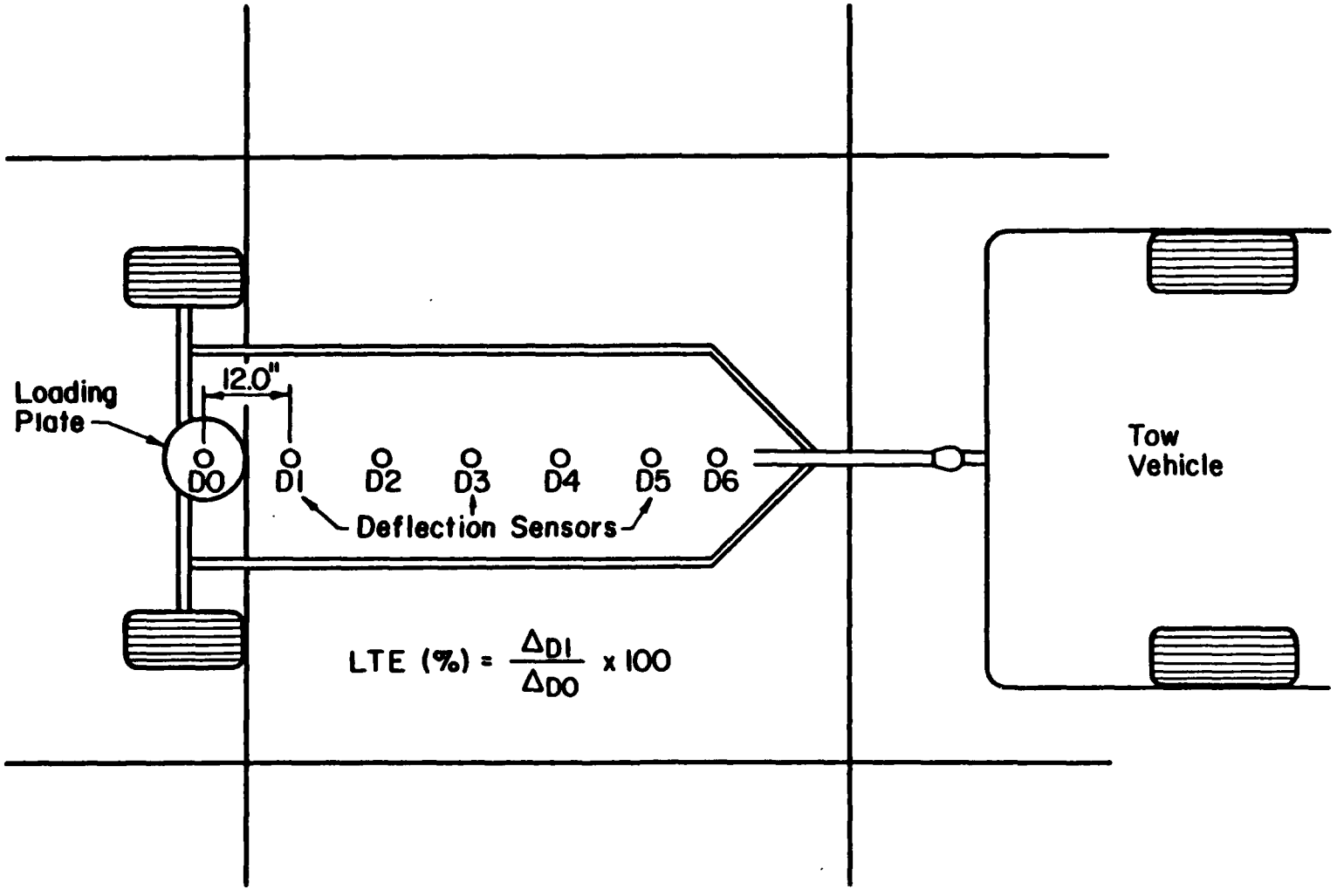

Figure 4-2. Measurement of Joint Load Transfer Efficiency with the FWD

is used, the FWD can collect and store load transfer efficiency data quickly and easily. This information will prove to be the key to the successful evaluation of any rigid pavement system.

4.2 Effect of Load Magnitude on Load Transfer Efficiency

It has been suggested by some researchers that the determination of load transfer efficiency at joints is dependent on the magnitude of the loads used to create the relative deflections. To investigate this possibility, the data presented in Table 4-1 were extracted from the constant temperature repeatability study discussed in Chapter 3. These data represent three slab thicknesses, two joint types, loads from 6500 to 24000 pounds, and load transfer efficiencies between 30 and 100 percent.

The results displayed in Table 4-1 support the conclusion that load transfer efficiency is independent of the load magnitude, at least within the load range of the FWD (this may not be true for light load devices, such as the Dynaflect, that generate loads near 1000 pounds). With the exception of Slab 1 in Feature T4A, load transfer efficiencies are remarkably consistent, especially in view of the inherent variation in the equipment and materials highlighted earlier. With this result, the extrapolation of load transfer efficiencies under actual aircraft loadings can be made confidently.

4.3 Variation of Load Transfer Efficiency Along the Joint

Two additional aspects of joint load transfer that the engineer must be concerned with during field testing are 1) the direction in which the relative deflections are measured, and 2) the location of the measurement along the joint. It has been shown on highway pavements, for example, that load transfer efficiency measured with the loading plate on the approach slab

TABLE 4-1. THE RELATIONSHIP BETWEEN MAGNITUDE OF LOAD AND LOAD TRANSFER EFFICIENCY AS MEASURED AT UNDOWELED TRANSVERSE CONTRACTION JOINTS AND KEYED LONGITUDINAL CONSTRUCTION JOINTS

Feature	Slab No.	Undoweled Transverse Contraction				Keyed Longitudinal Construction			
		Load (lbf)	D0 (mils)	D1	LTE (%)	Load (lbf)	D0 (mils)	D1	LTE (%)
T04A	1	7456	1.6	1.2	75	6936	1.8	1.2	67
		15400	3.9	2.6	67	15032	4.3	2.4	56
		23055	6.1	3.7	61	23103	6.7	3.4	51
	2	6840	1.1	0.9	82	6968	1.3	1.2	92
		14648	2.6	2.2	85	14640	3.0	2.7	90
		22514	3.9	3.4	87	22673	4.4	4.1	93
	3	6752	1.2	1.2	100	6688	1.5	1.3	87
		14656	2.8	2.7	96	14808	3.4	3.1	91
		23150	4.2	4.1	98	22848	5.2	4.6	88
A03B	1	7496	1.8	1.7	94	7216	2.3	0.9	39
		16296	4.0	3.8	95	15496	4.9	2.2	45
		23914	6.0	5.7	95	23421	7.3	3.4	47
	2	7528	5.0	2.7	54	7400	4.5	4.0	89
		15368	11.4	5.2	46	15512	9.6	8.3	86
		23246	17.6	7.3	41	23373	14.4	12.2	85
	3	6872	3.1	1.0	32	6936	2.8	1.0	36
		14992	7.4	2.3	31	15064	6.4	1.9	30
		23071	11.3	3.6	32	23150	9.5	2.8	29
A05B	1	6888	1.6	1.5	94	6896	2.1	1.8	86
		14936	3.6	3.3	92	14944	4.8	4.3	90
		22801	5.4	5.0	93	22976	7.2	6.5	90
	2	6680	1.9	1.9	100	6792	2.2	1.9	86
		14840	4.5	4.3	96	14824	5.1	4.4	86
		22928	6.6	6.4	97	22769	7.6	6.6	87
	4	7696	2.1	2.0	95	7240	2.3	2.1	91
		15584	4.5	4.2	93	15280	4.8	4.4	92
		23532	6.6	6.2	94	23007	7.2	6.5	90

is much different than when measured from the leave slab. In addition, the highly channelized nature of highway traffic causes variation in load transfer efficiency along the joint. To investigate these concerns, a third testing pattern, shown in Figure 4-3, was utilized on nine slabs at Sheppard AFB. This pattern consisted of 21 FWD measurements and required about 45 minutes per slab to complete. The results of this investigation are presented in Figures 4-4 through 4-12. Two sets of measurements are included to dramatize the effect that temperature has on load transfer efficiency.

Several general trends can be seen from these figures. First, there appears to be very little difference in load transfer efficiency at transverse joints when measured from the approach or leave slabs. This conclusion is not too surprising for the airfield situation where traffic is usually bi-directional along taxilines and centerlines. For longitudinal joints, however, this is not the case. Several slabs show marked increases in load transfer efficiency when measured from the leave slab, indicating that loading history can influence joint behavior. Again, this result is not surprising when one considers that aircraft gears ride consistently along the same side of the longitudinal joint, regardless of the direction of travel. Therefore, the engineer must determine where the majority of the gears track and adjust his test pattern accordingly. The mirror image of the normal pattern in Figure 3-5, for instance, can be used if it is more appropriate.

Load transfer efficiencies are consistent, for the most part, along the joint. This permits some lattitude in trying to position the FWD somewhere near the midspan of the slab. In several instances, however, the efficiencies drop off as the corner of the slab is approached. This tendency could result from loss of subbase support at the corner, and thus the effect of shear in the base or subgrade, or it could be due to the absence of dowel

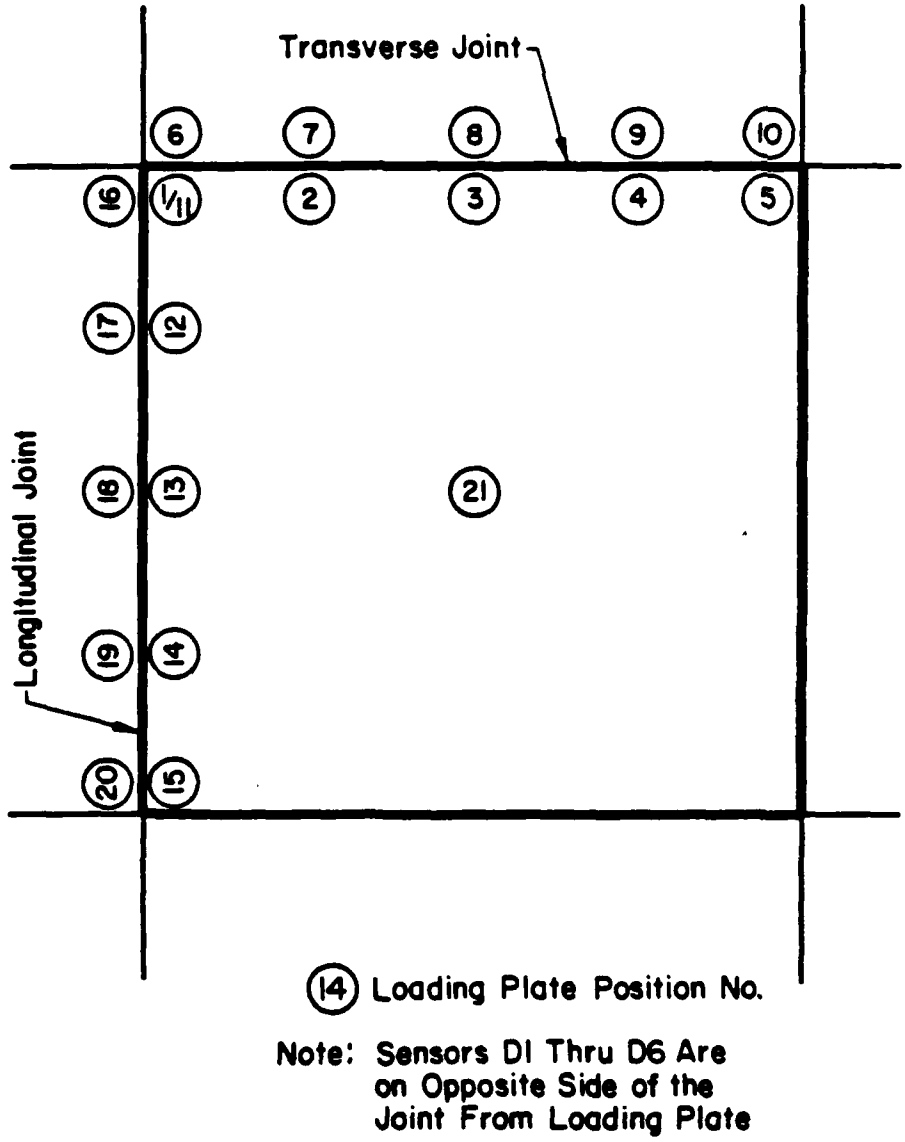

Figure 4-3. FWD Testing Pattern for Determination of Directional Effects of Traffic on Load Transfer Efficiency and Consistency of Load Transfer Efficiency Along Joints

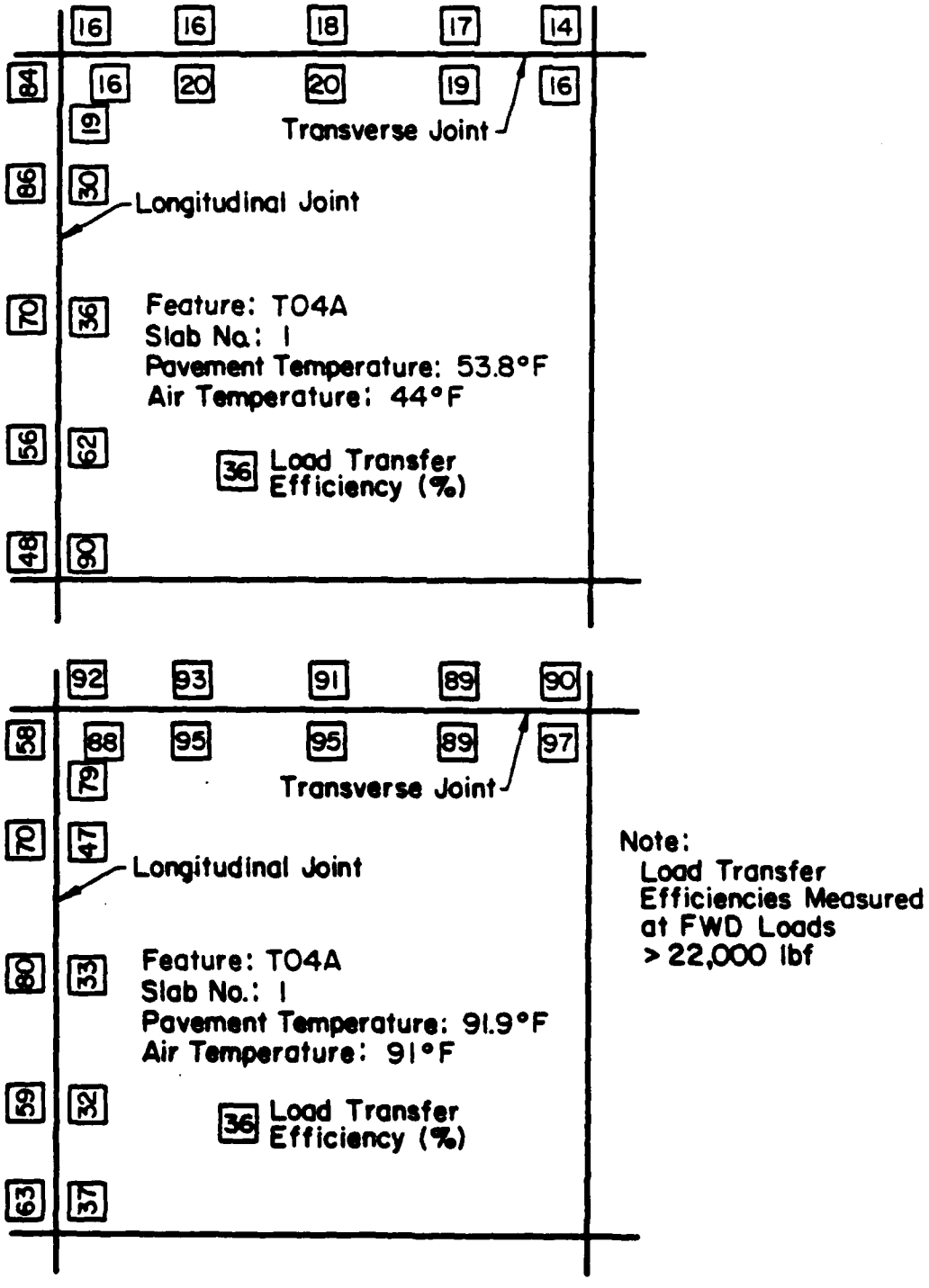

Figure 4-4. Joint Load Transfer Efficiencies at Various Locations for Feature T04A, Slab No. 1

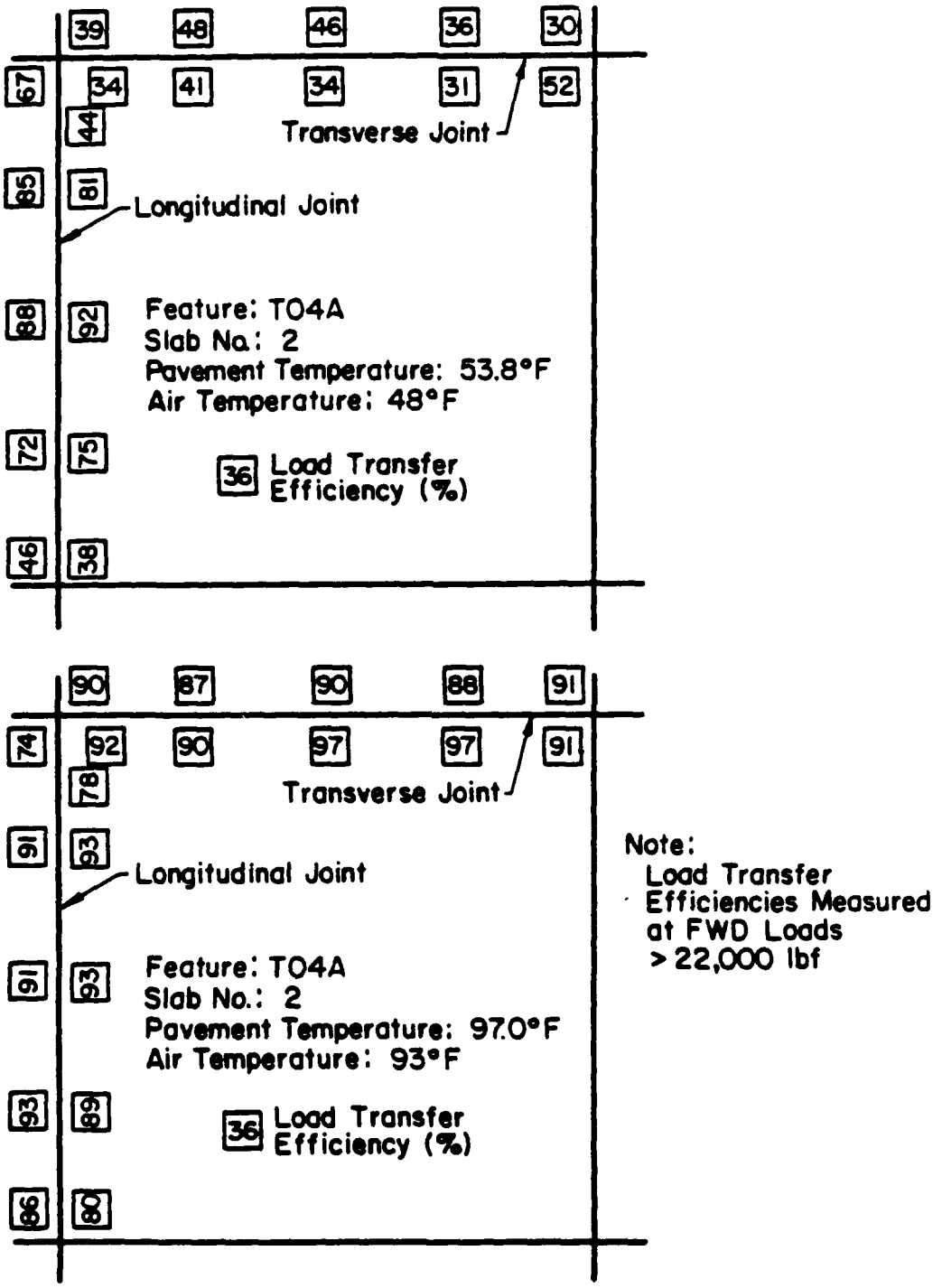

Figure 4-5. Joint Load Transfer Efficiencies at Various Locations for Feature T04A, Slab No. 2

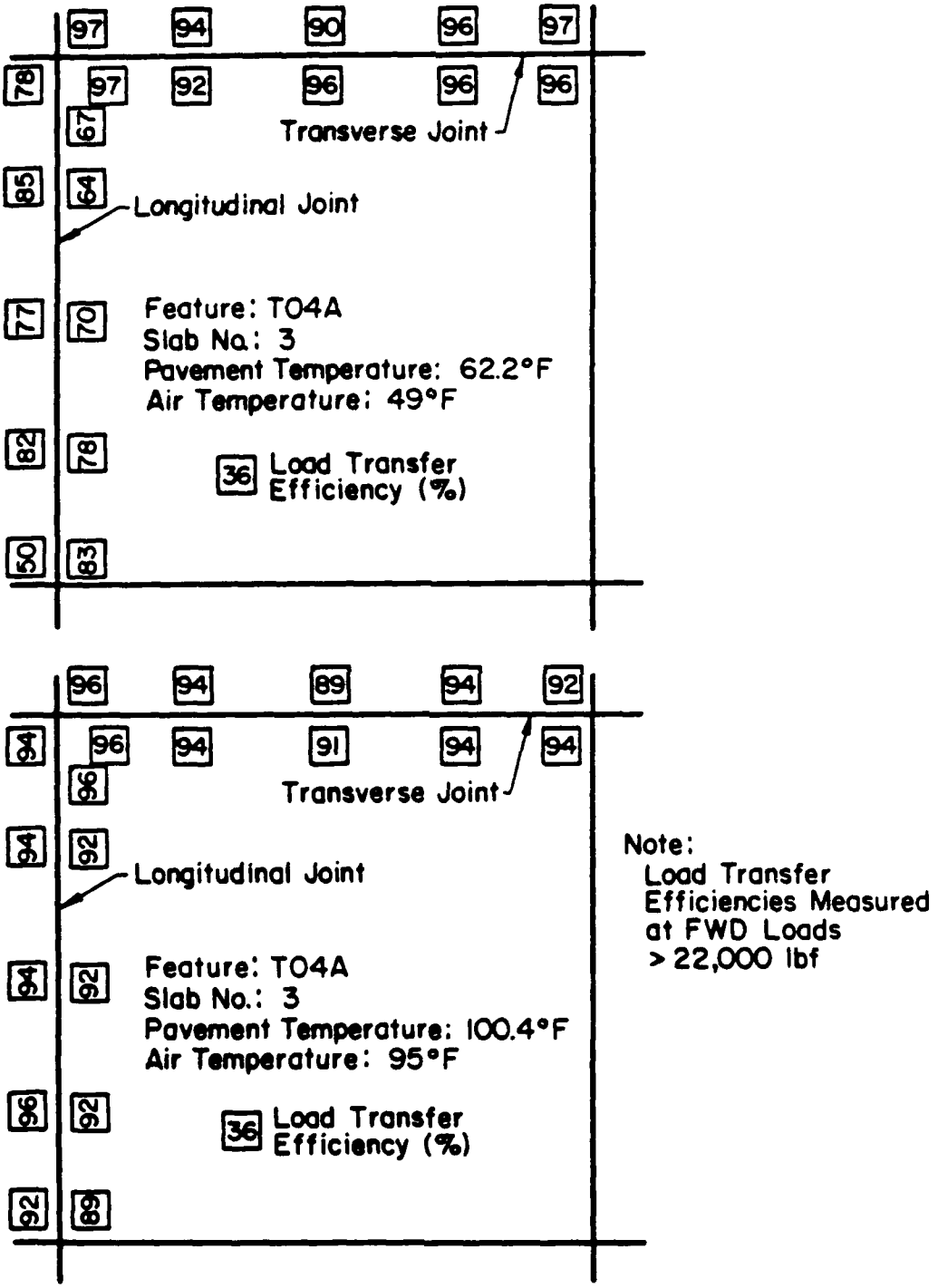

Figure 4-6. Joint Load Transfer Efficiencies at Various Locations for Feature T04A, Slab No. 3

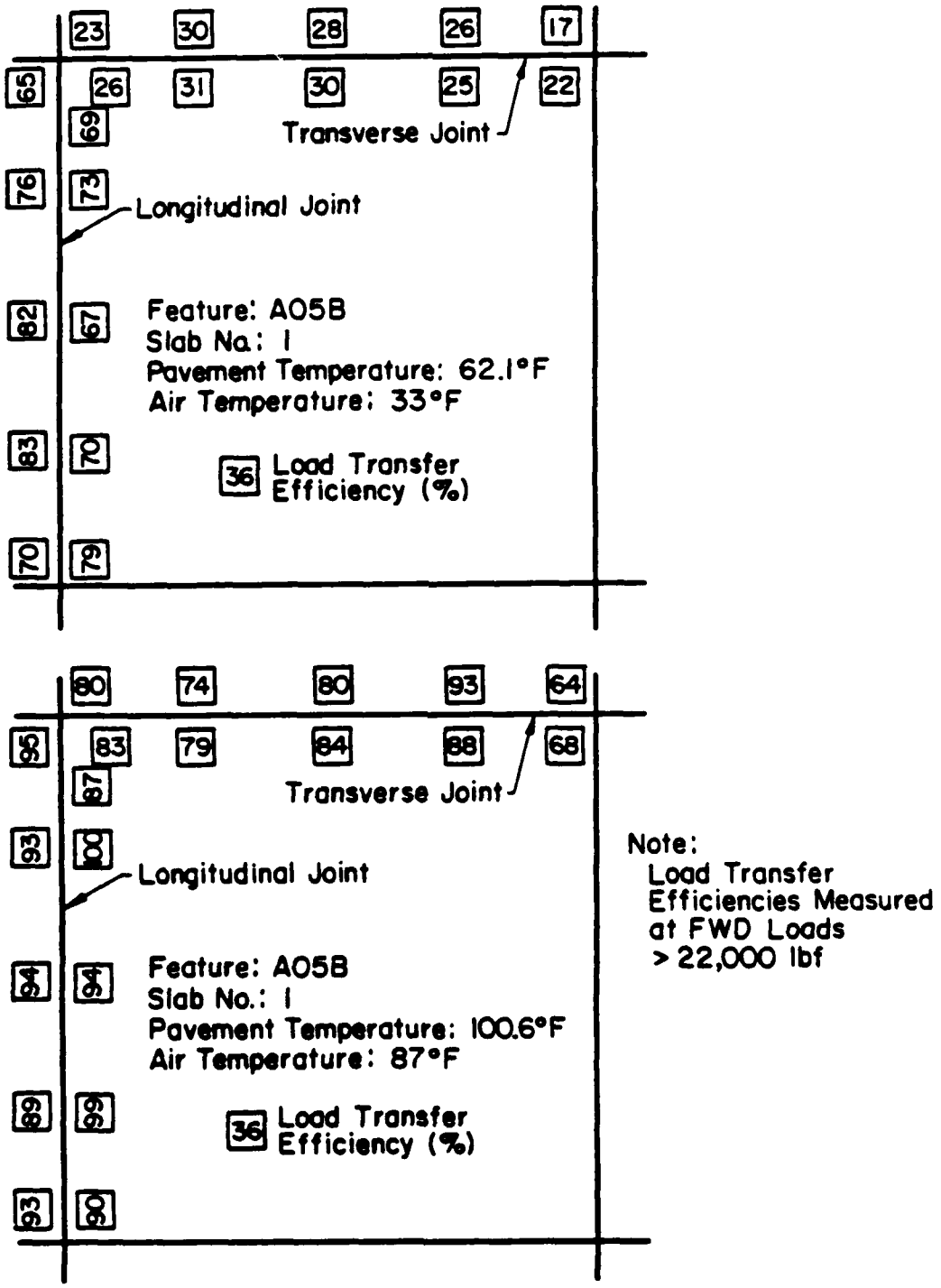

Figure 4-7. Joint Load Transfer Efficiencies at Various Locations for Feature A05B, Slab No. 1

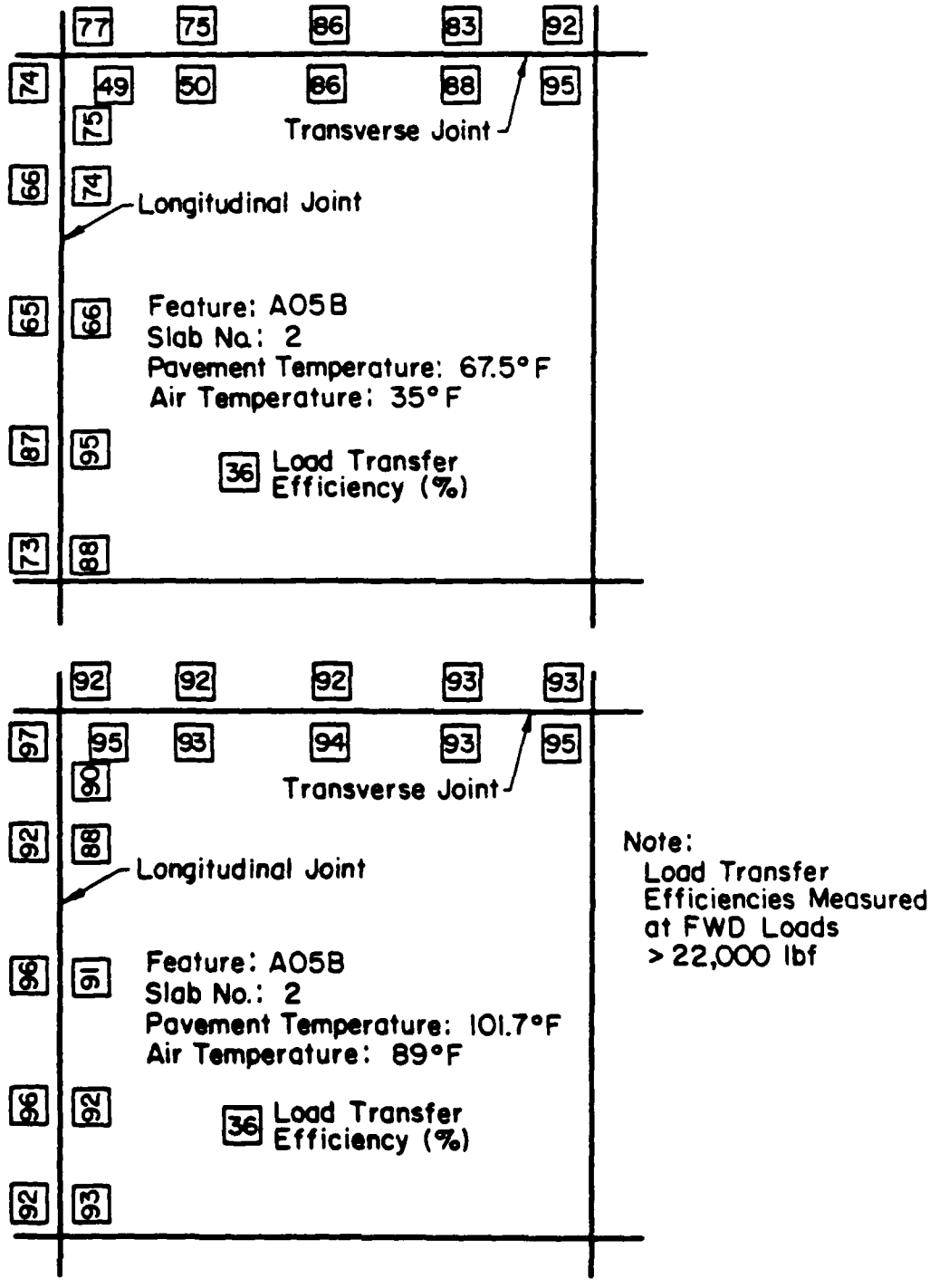

Figure 4-8. Joint Load Transfer Efficiencies at Various Locations for Feature A05B, Slab No. 2

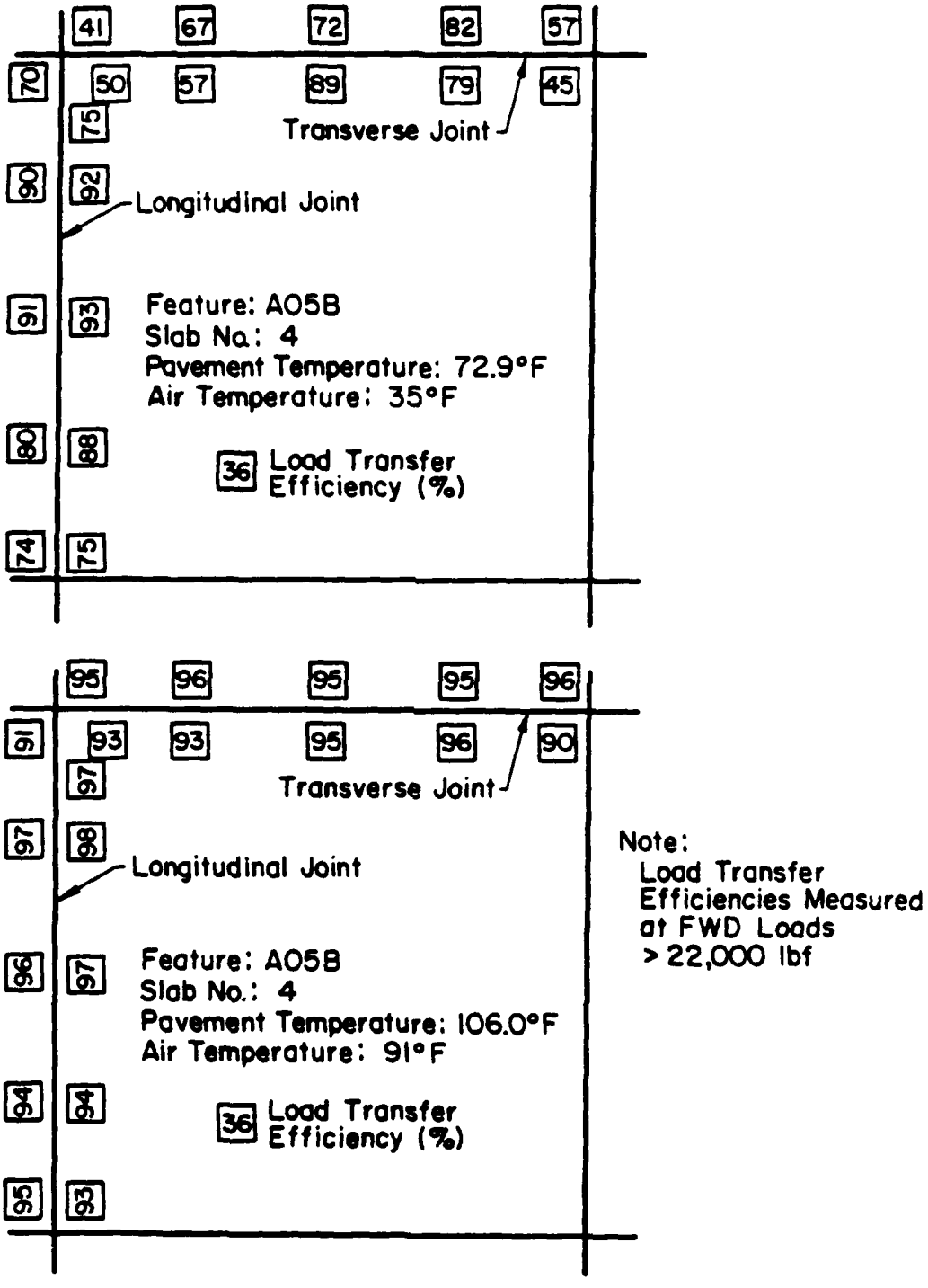

Figure 4-9. Joint Load Transfer Efficiencies at Various Locations for Feature A05B, Slab No. 4

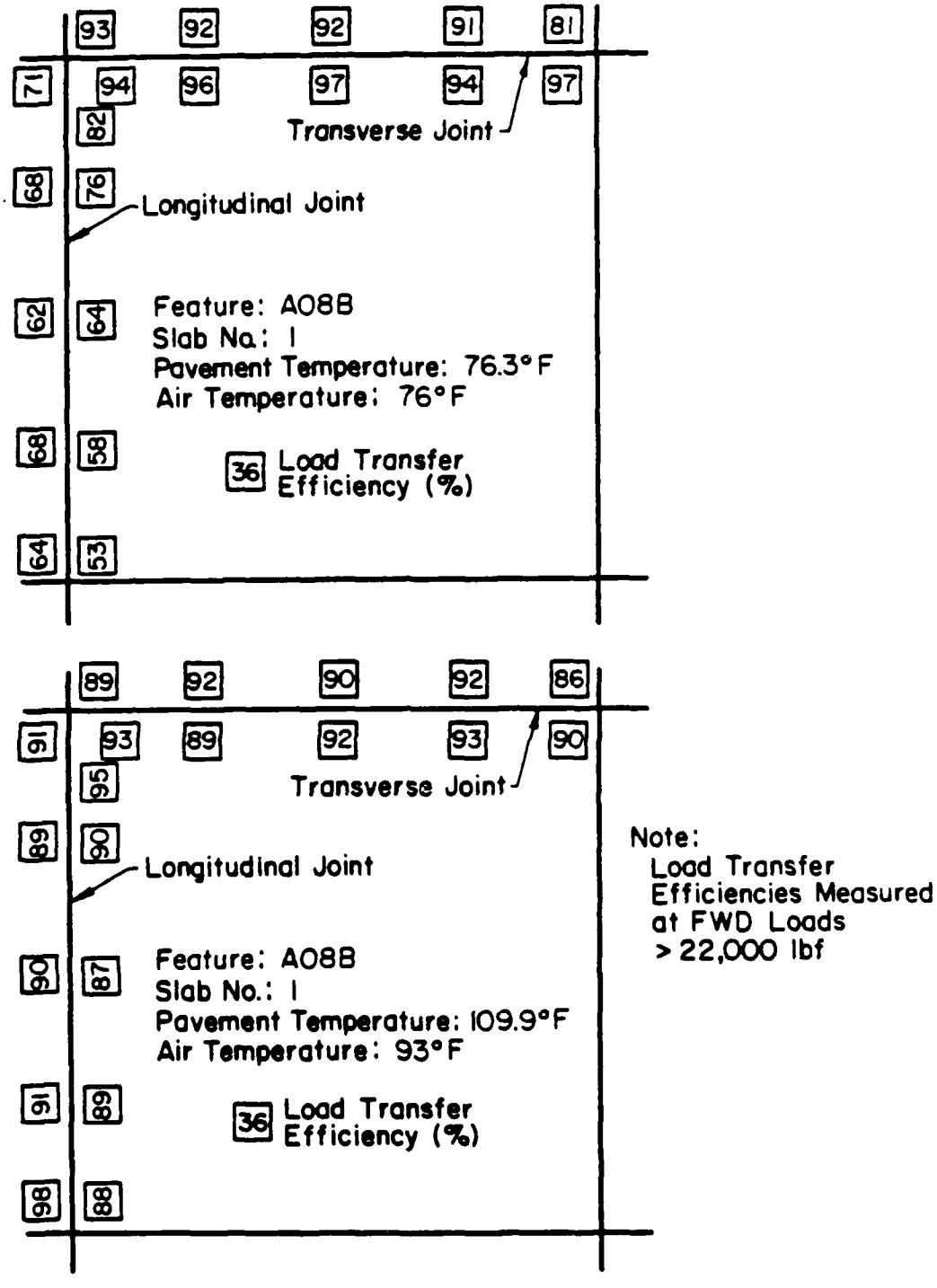

Figure 4-10. Joint Load Transfer Efficiencies at Various Locations for Feature A08B, Slab No. 1

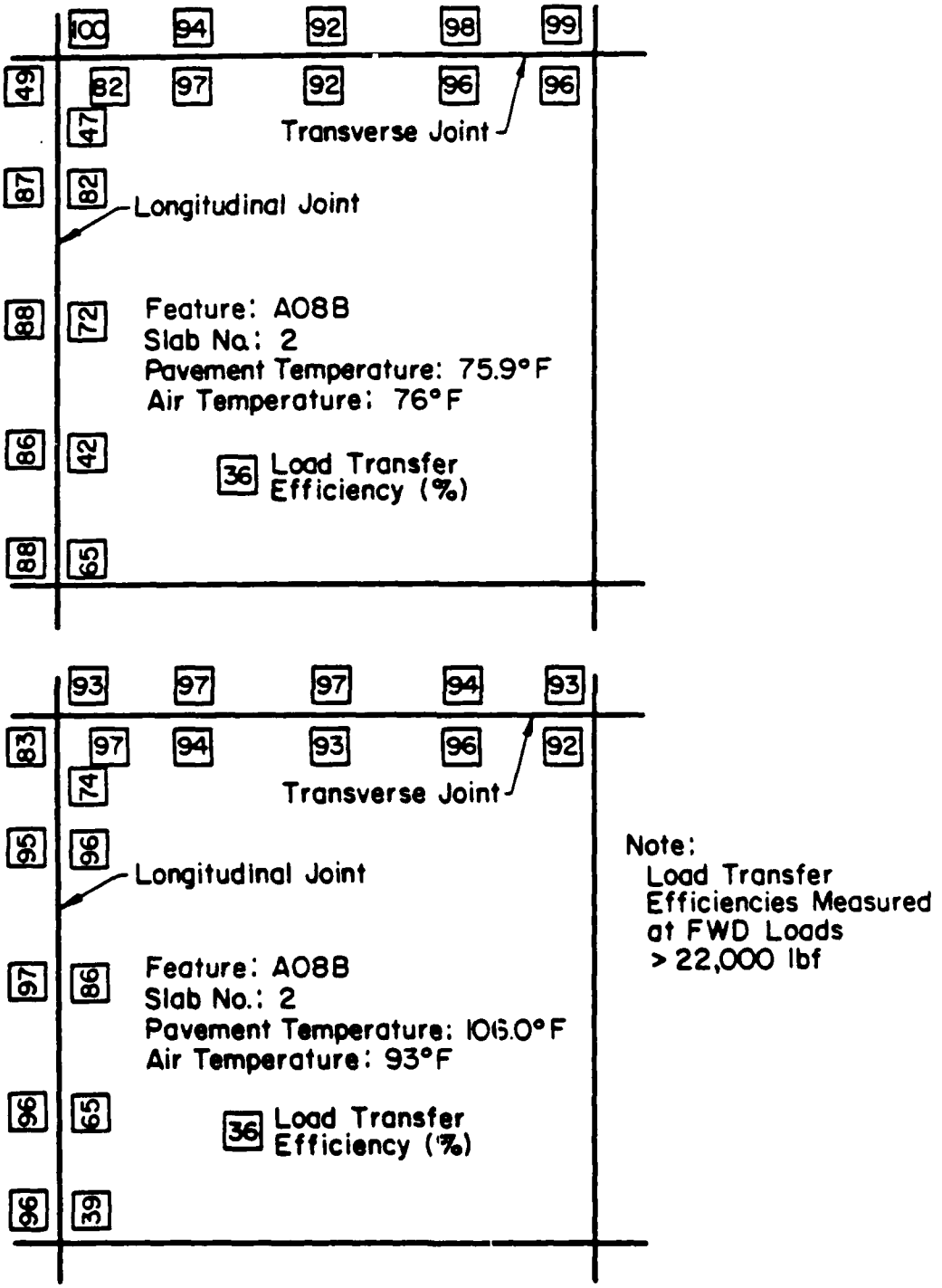

Figure 4-11. Joint Load Transfer Efficiencies at Various Locations for Feature A08B, Slab No. 2

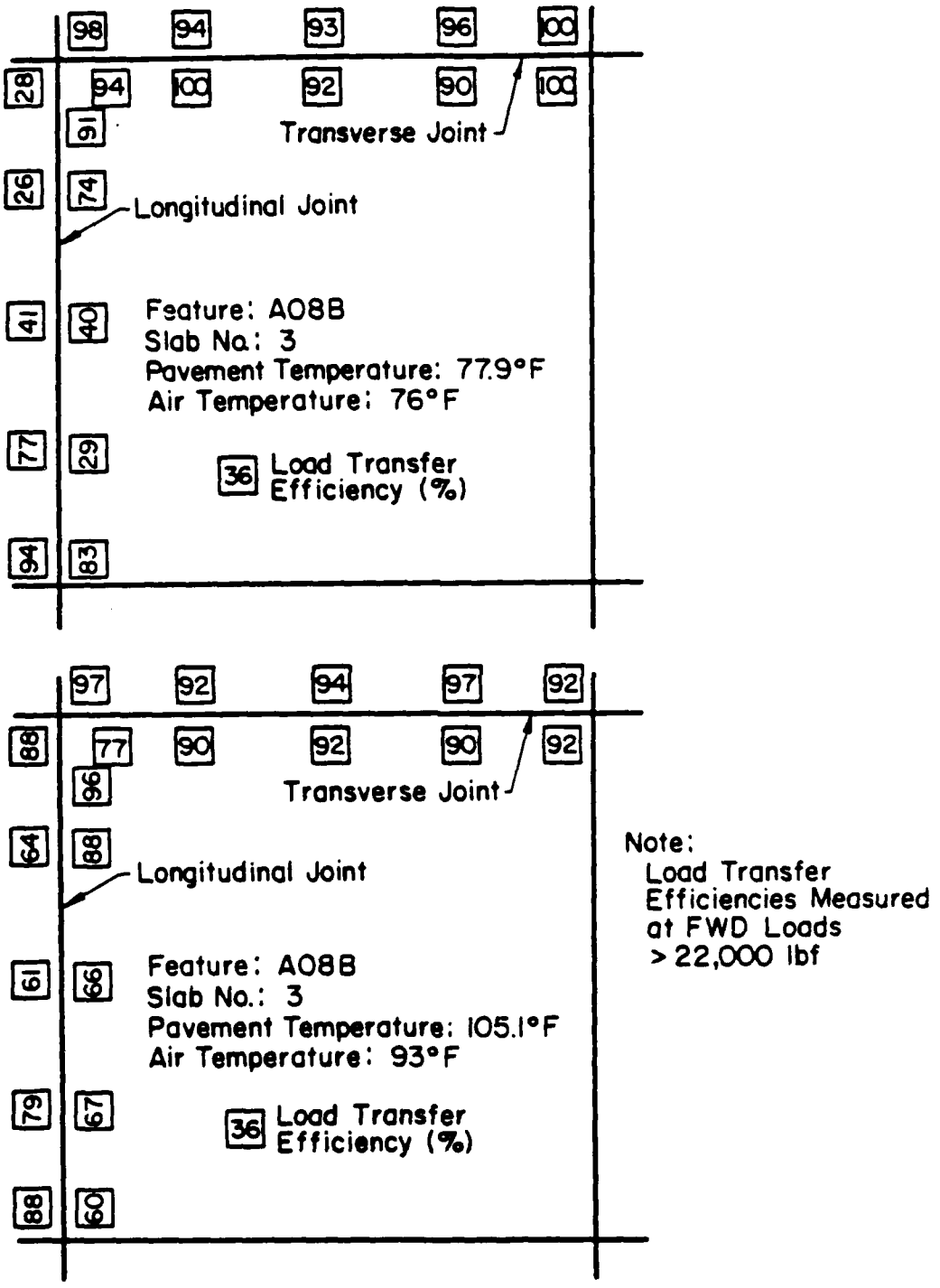

Figure 4-12. Joint Load Transfer Efficiencies at Various Locations for Feature A08B, Slab No. 3

bars near the corners in each of the adjacent slabs. In any event, Position 1 of the normal test pattern is intended to identify potential problem areas near corners.

Finally, the effect of increased temperature on load transfer efficiency is unmistakeable; significant increases in joint performance accompany higher temperatures. This effect will be examined closely in the next section.

4.4 The Effect of Temperature on Load Transfer Efficiency

One of the most disturbing aspects of NDT & E of any pavement system is the variability of results due to temperature. In flexible pavement systems, this effect is most pronounced on the stiffness of the asphaltic concrete materials. In rigid pavements, temperature changes influence load transfer efficiency more than any other characteristic of the system. Although temperature has been known to affect load transfer for some time, no attempts have been made to accurately quantify this phenomenon. One of the major objectives of this research effort was to describe the behavior of different joint types under changing temperature conditions. From this background, it was expected that a technique could be developed to account for the temperature effect in predicting the remaining life of rigid pavements.

The repetitive nature of the FWD testing at Sheppard AFB, coupled with the extremes in temperature that are routinely experienced in field testing, provided the basis upon which to quantify load transfer changes with temperature. Load transfer efficiencies were measured at 20 dummy groove transverse joints and 20 keyed longitudinal joints, encompassing the entire range of pavement thicknesses available. Pavement surface temperatures were recorded for each test by inserting a digital thermometer probe into a

predrilled, one inch deep, 1/8-inch diameter, oil-filled hole in each slab. Air temperatures were also obtained from the base weather station for each hour in the hope that either could be used for analysis. A minimum of 5, and generally 12, temperature levels were obtained for each joint.

Figures 4-13 through 4-22 graphically display the distinct relationship between joint load transfer efficiency and air temperature over a wide spectrum. The highly significant aspect of this behavior lies in the characteristic shape of this relationship, an S-shaped curve. Each joint appears to take on the same shape and is nearly identical for both pavement temperature and air temperature. The variety of horizontally shifted positions for joints within the same slab is typical, and makes it difficult to select a "representative" joint for the entire feature. This wide disparity in joint behavior within a single feature will be specifically addressed in Chapter 8.

Each joint tends toward a maximum load transfer efficiency of 100 percent as temperatures increase, and toward a minimum value of 25 to 30 percent as temperatures decrease. In many instances, such as the transverse joint of Slab 3 in Feature T4A (Figure 4-13), the joint opening is so small that good load transfer exists throughout the temperature range, regardless of how much the slab contracts. On the other hand, some joints have such poor load transfer at all temperatures in the normal range (see Slab 2 of Figure 4-14) that they display a nearly flat response between 30 and 50 percent. This behavior, however, does not mean that the characteristic shape of the load transfer efficiency-temperature curve can not be described by an S-shaped curve. It merely means the curve is shifted significantly, in either direction, from the norm.

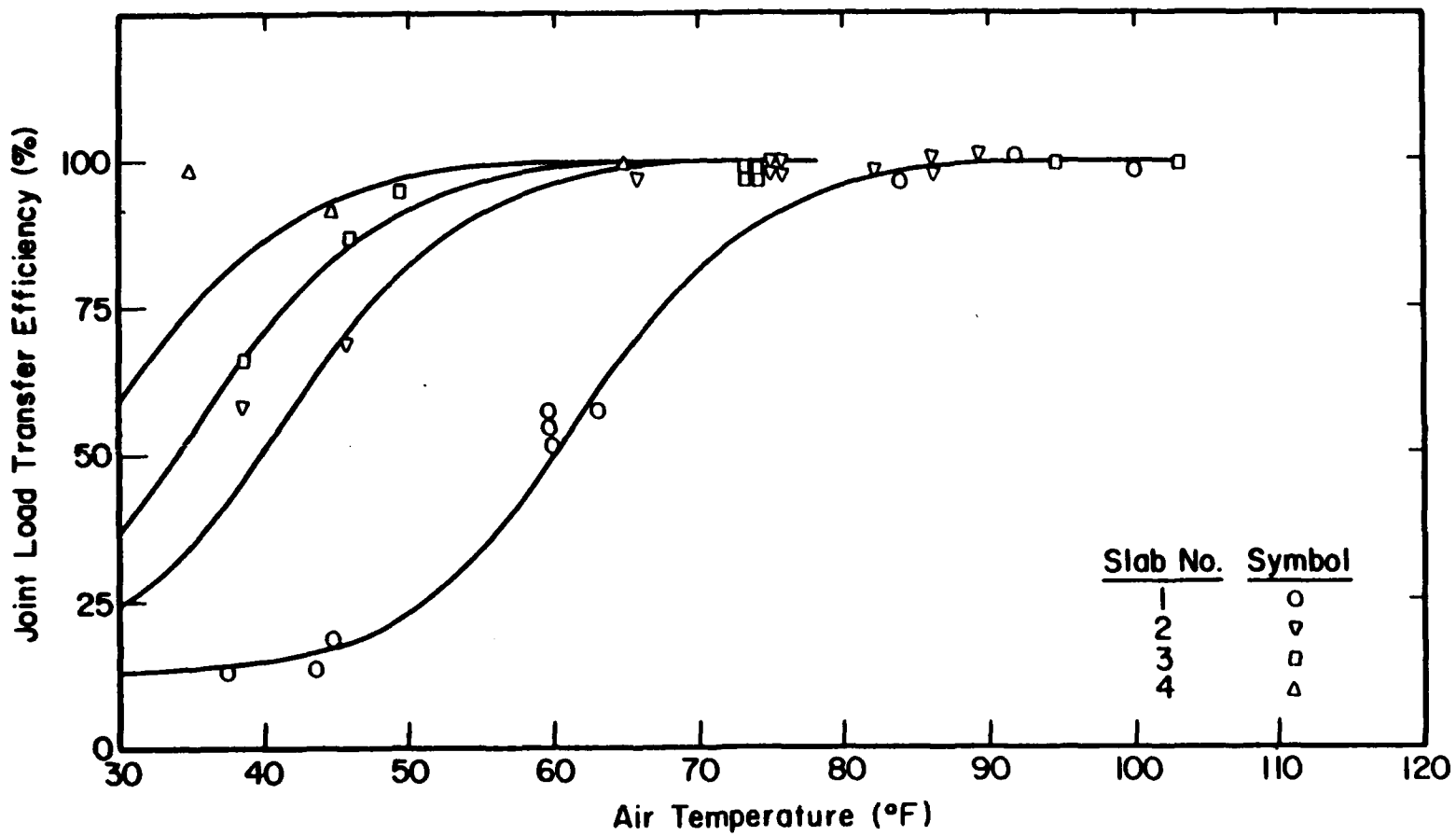

Figure 4-13. The Relationship Between Air Temperature and Transverse Joint Load Transfer Efficiency for Feature T04A

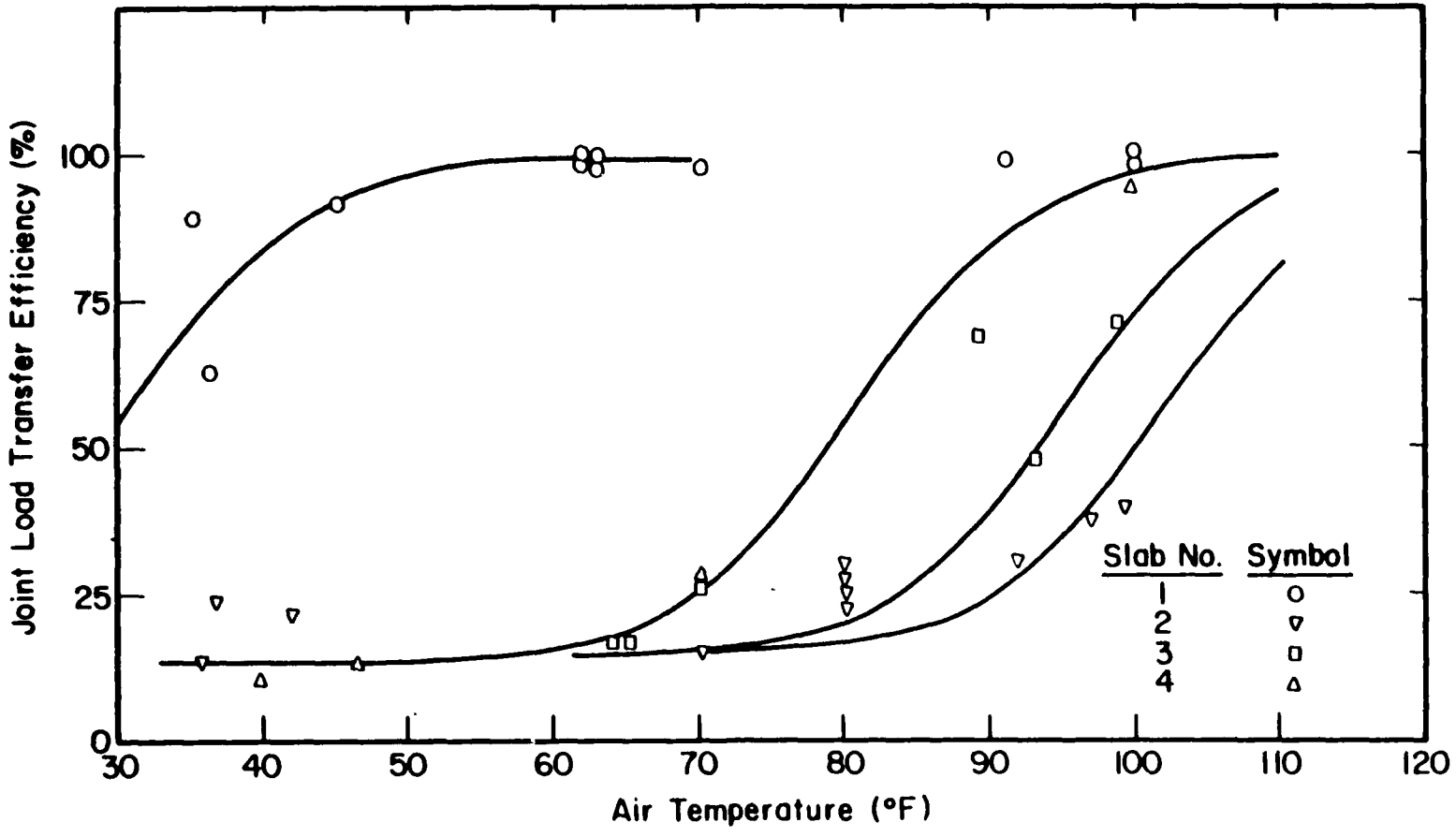

Figure 4-14. The Relationship Between Air Temperature and Transverse Joint Load Transfer Efficiency for Feature A03B

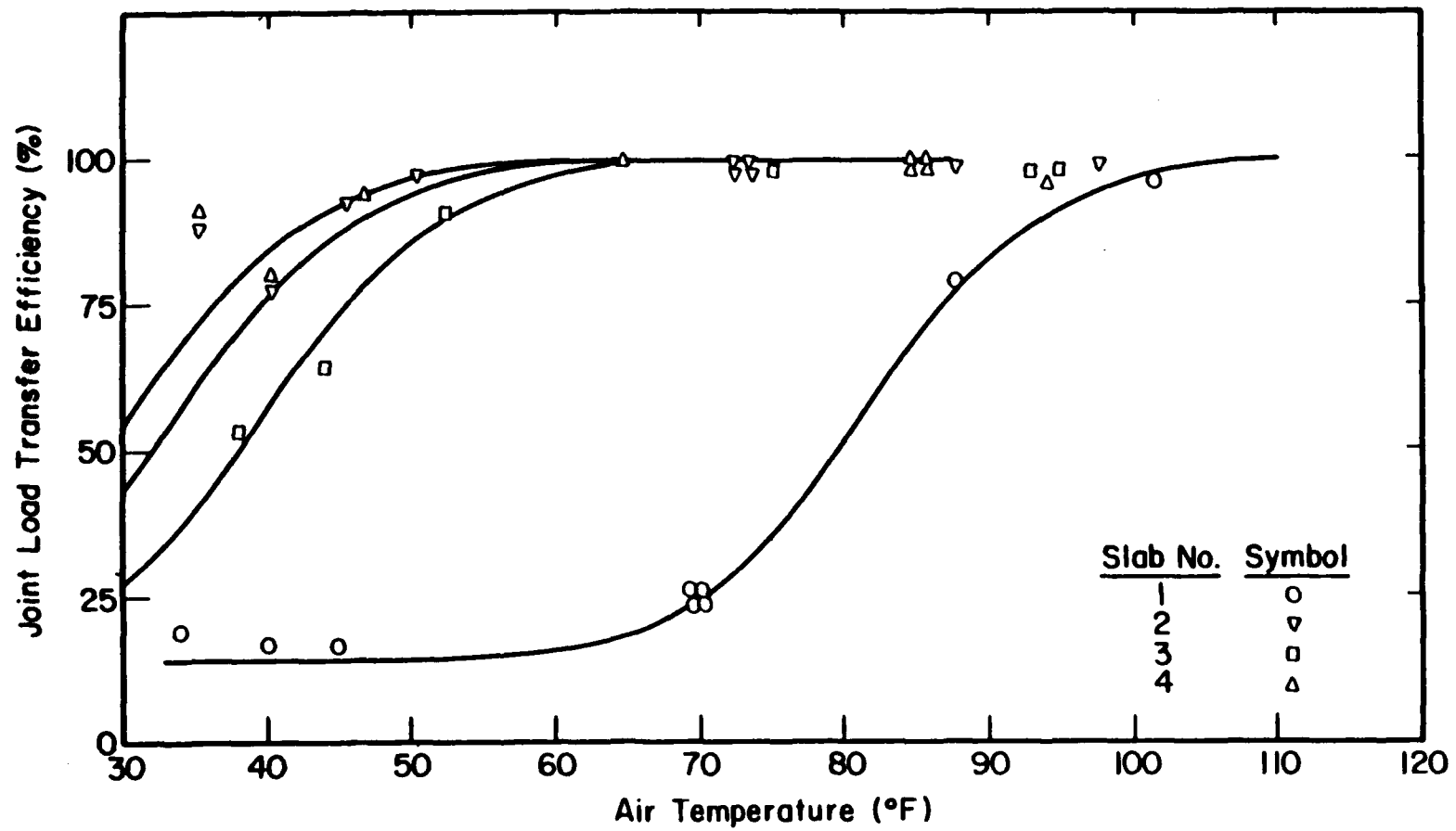

Figure 4-15. The Relationship Between Air Temperature and Transverse Joint Load Transfer Efficiency for Feature A05B

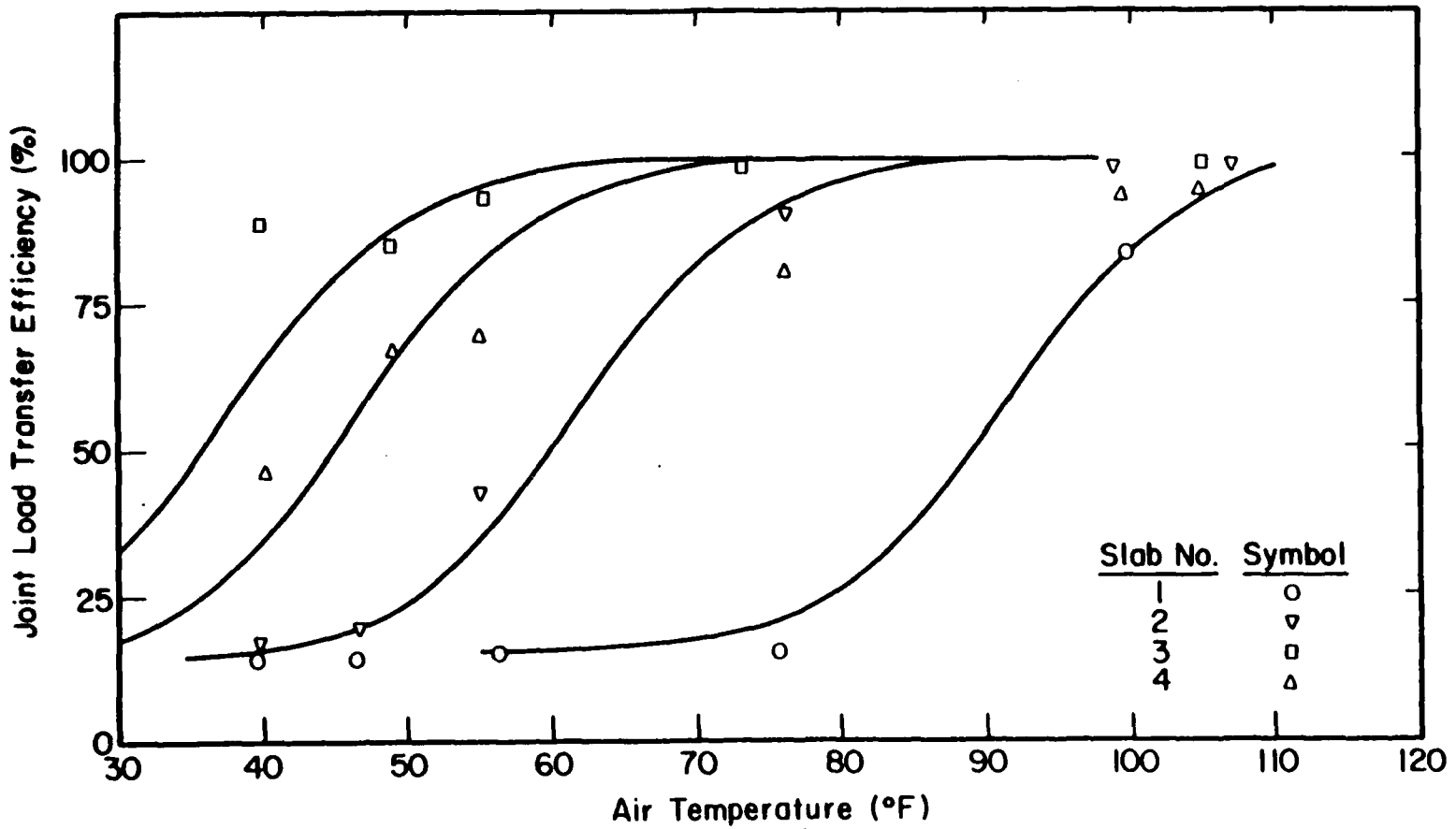

Figure 4-16. The Relationship Between Air Temperature and Transverse Joint Load Transfer Efficiency for Feature A06B

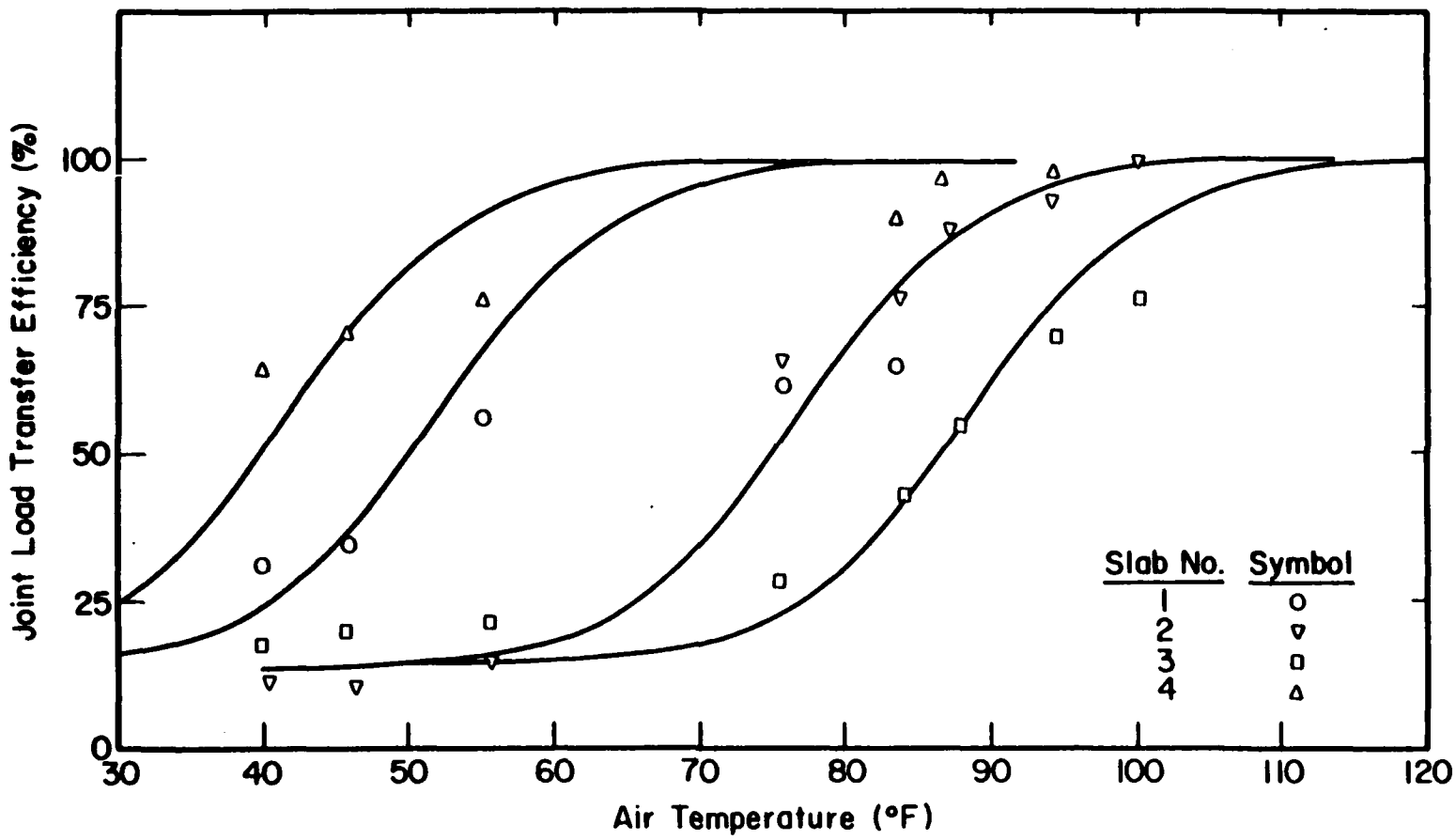

Figure 4-17. The Relationship Between Air Temperature and Transverse Joint Load Transfer Efficiency for Feature A08B

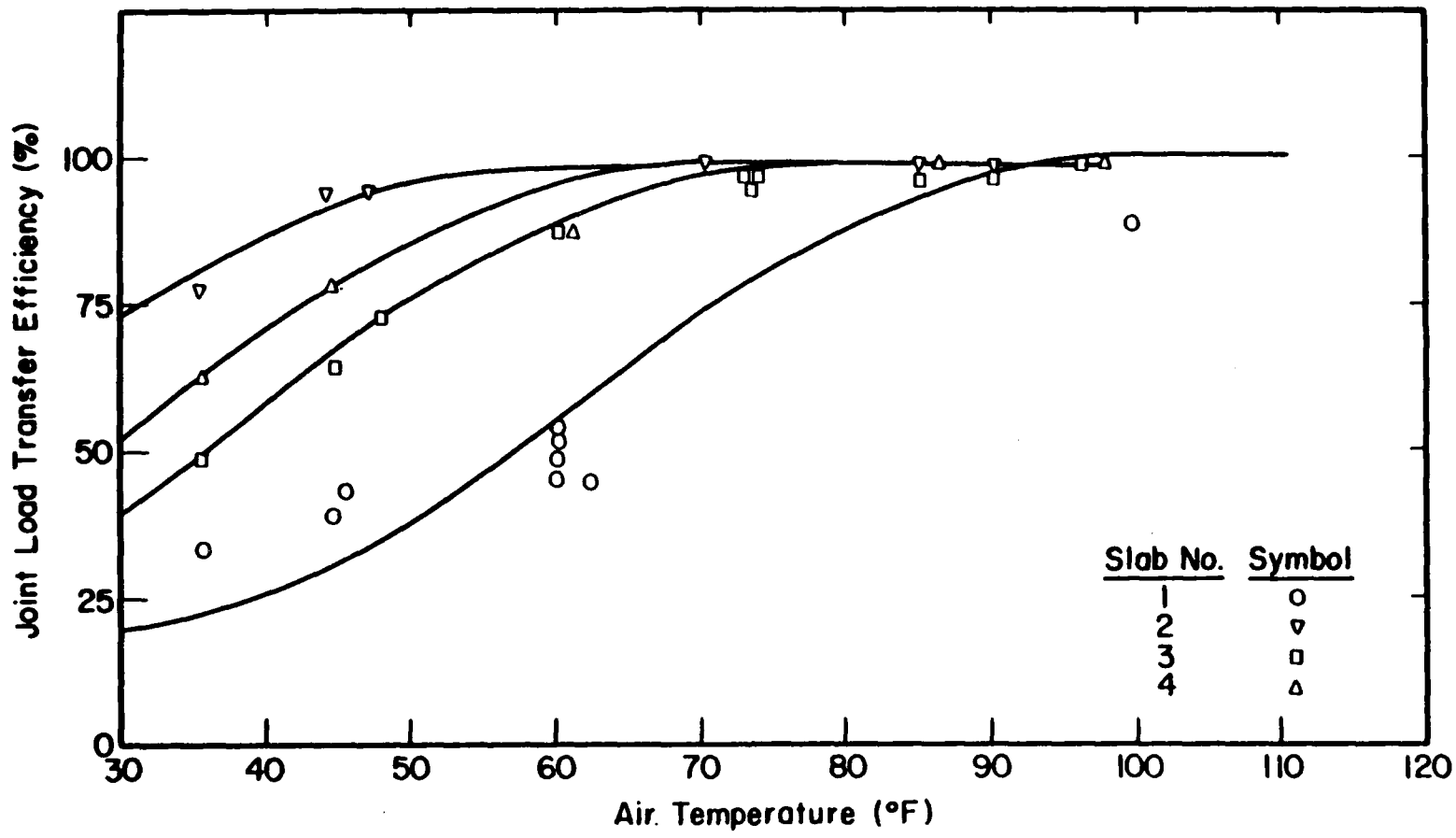

Figure 4-18. The Relationship Between Air Temperature and Longitudinal Joint Load Transfer Efficiency for Feature T04A

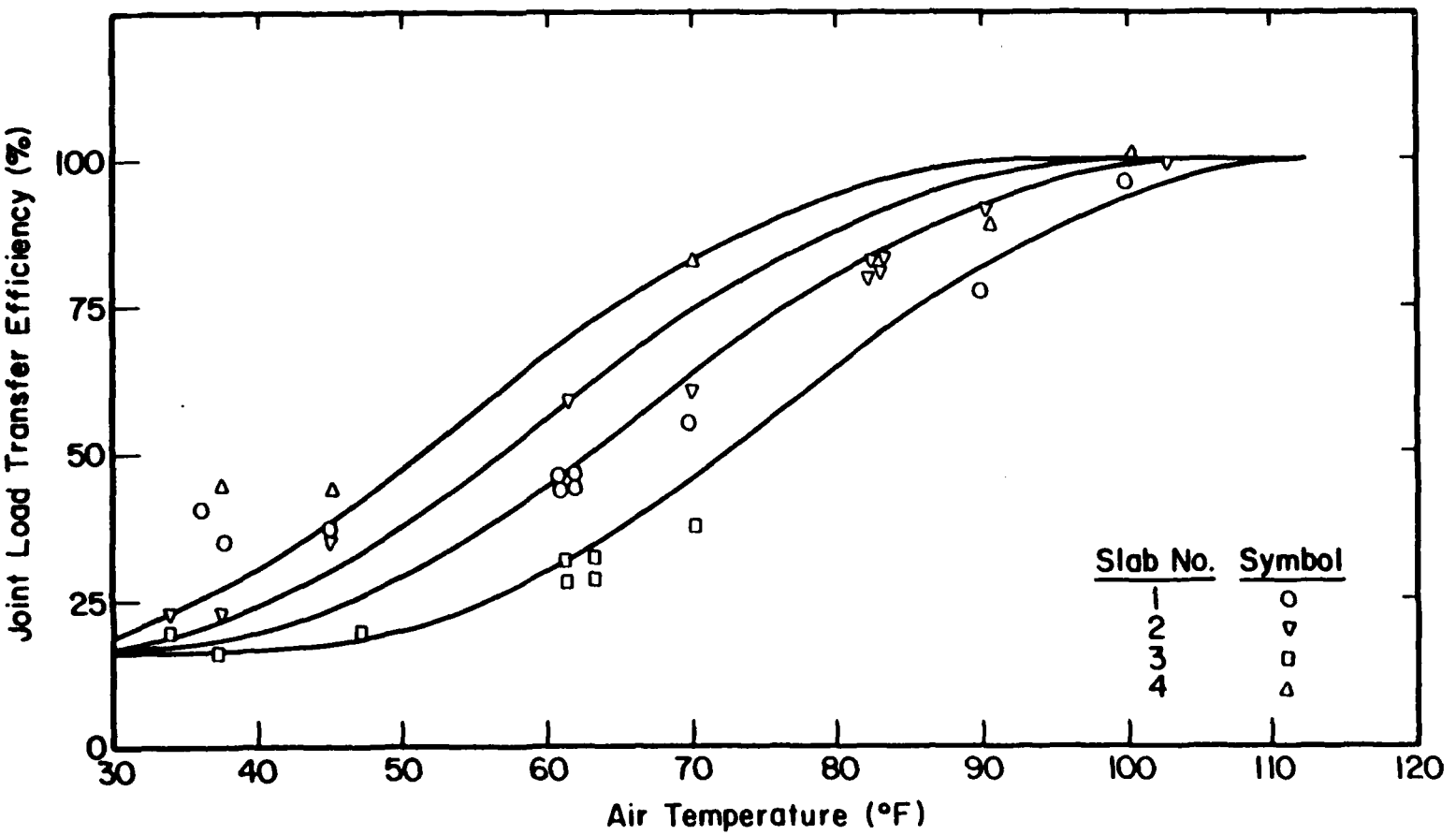

Figure 4-19. The Relationship Between Air Temperature and Longitudinal Joint Load Transfer Efficiency for Feature A03B

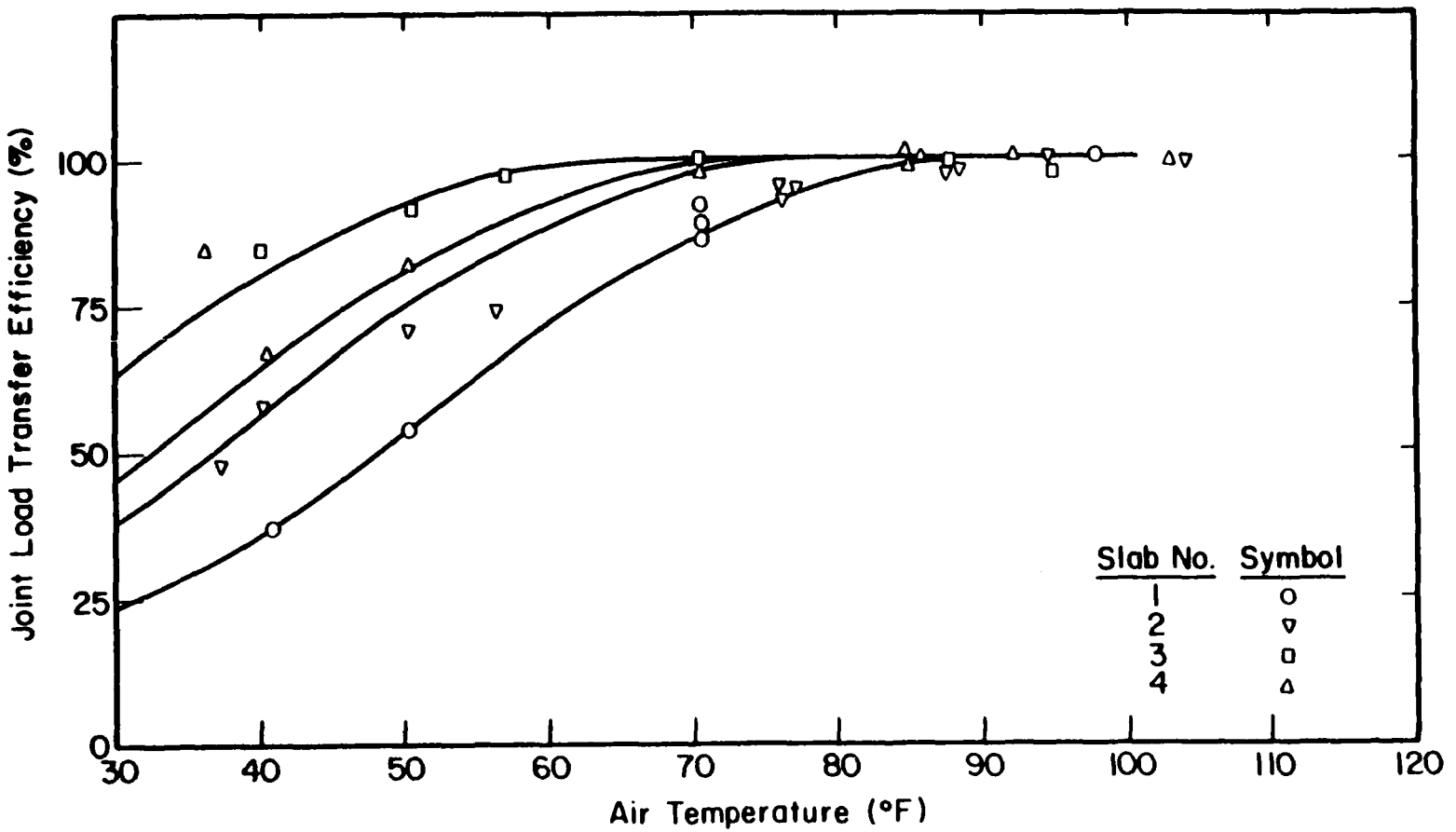

Figure 4-20. The Relationship Between Air Temperature and Longitudinal Joint Load Transfer Efficiency for Feature A05B

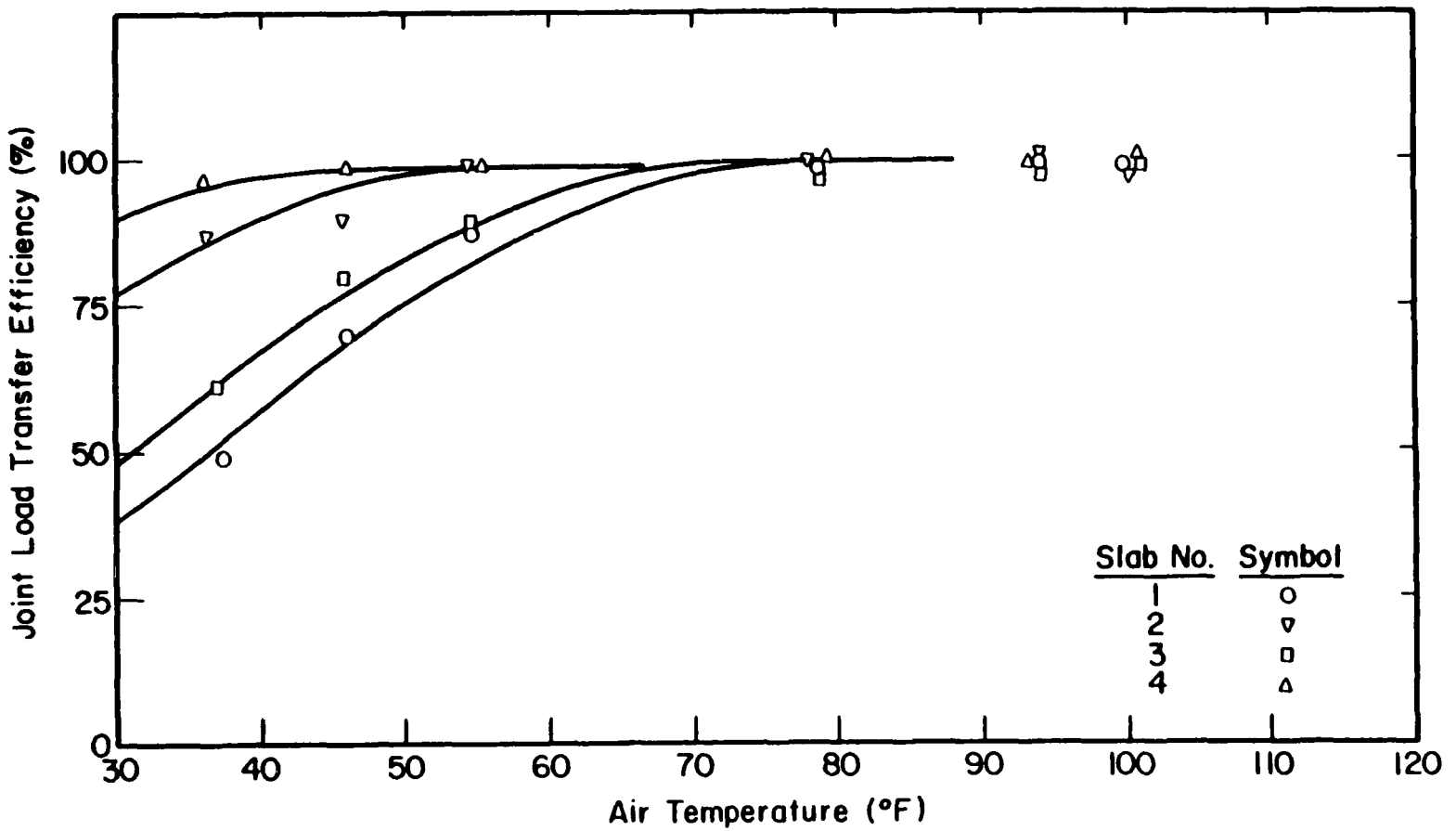

Figure 4-21. The Relationship Between Air Temperature and Longitudinal Joint Load Transfer Efficiency for Feature A06B

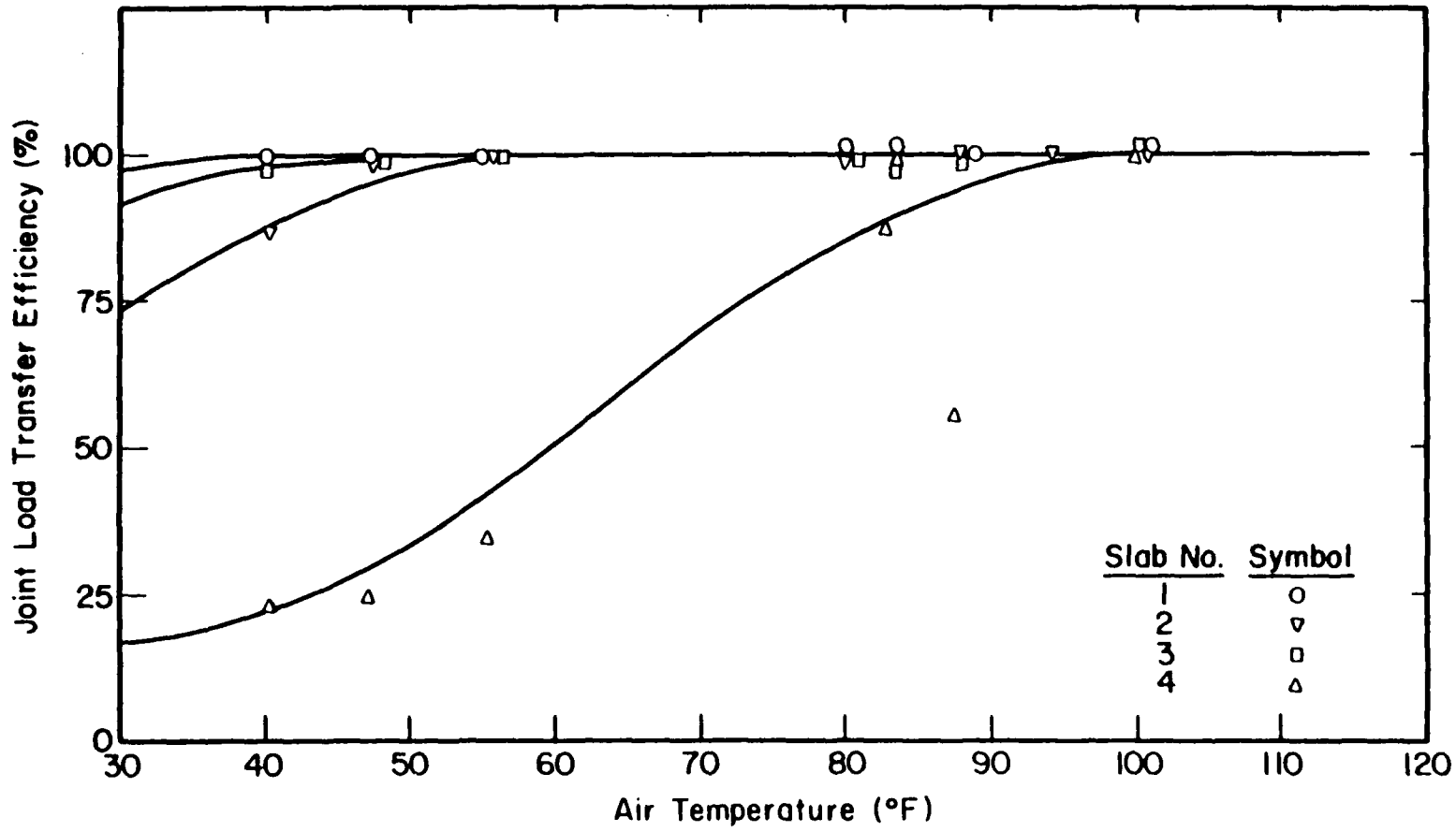

Figure 4-22. The Relationship Between Air Temperature and Longitudinal Joint Load Transfer Efficiency for Feature A08B

AD-A165 055 CONCEPTS FOR THE DEVELOPMENT OF A NONDESTRUCTIVE TESTING AND EVALUATION S..(U) ILLINOIS UNIV AT URBANA NEWMARK CIVIL ENGINEERING LAB P T FOXWORTHY NOV 85 2/3

UNCLASSIFIED AFESC/ESL-TR-85-46 F08637-84-M-1743 F/G 14/2 NL

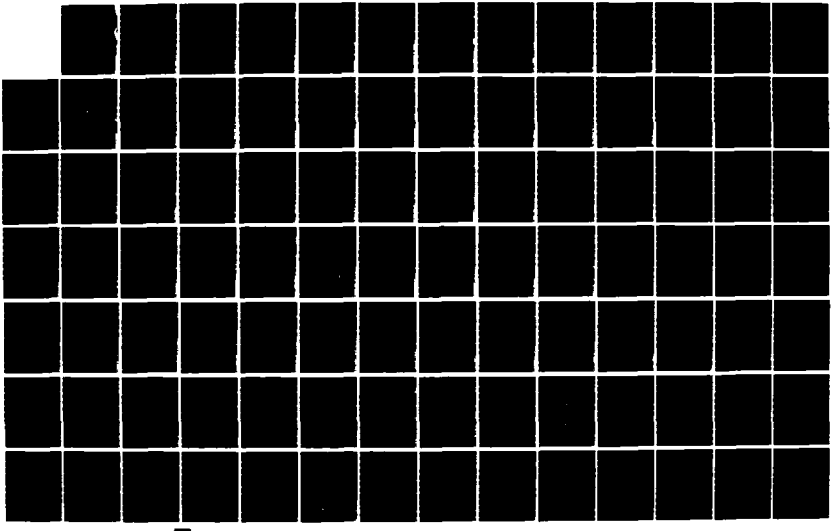

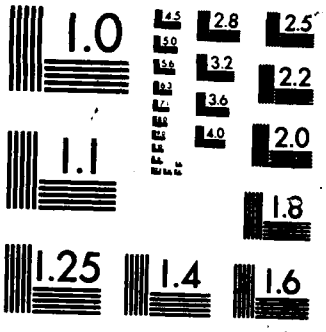

The explanation for this consistent behavior is undoubtedly complex and involves the interaction of aggregate particles along the face of the transverse crack, or the contact between the male and female portions of the longitudinal keyed joint. Presumably, as the joint opens up under falling temperatures, less concrete surface area is available for contact and deflection resistance. When the joint opens completely, a certain minimum amount of load transfer is still available through the shear strength of the base course or subgrade material. Thus, the upper bound of 100 percent and a somewhat variable lower bound of 25 to 30 percent are reasonable. Additional research might correlate the lower bound with the material type used directly beneath the PCC surface.

With upper and lower bounds established, the only remaining characteristic of the curve to identify is the slope, or rate at which the load transfer efficiency approaches the bounds. Inspection of Figures 4-13 to 4-22 reveals that each curve of similar joint type has approximately the same slope, and that a distinctly steeper slope exists for transverse dummy groove joints than for the longitudinal keyed joints. It appears that the type of joint construction affects the rate at which load transfer diminishes with temperature, a not too surprising result.

4.5 Load Transfer Efficiency Prediction

The discovery that the load transfer efficiency-temperature relationship of a given joint type closely follows an S-shaped curve with certain upper and lower bounds and diminishing rate makes it possible to establish the horizontal location of this curve for any joint, if the load transfer efficiency at some temperature is known. But this is precisely what is determined in the field with the FWD. Therefore, it becomes possible to rely

on only one measurement of load transfer efficiency for a joint to predict what that efficiency will be for any temperature that joint might experience. Only in those instances when measured load transfer efficiency is near the upper or lower bound are additional measurements recommended. This can mean tremendous savings in personnel and equipment costs in field data collection; retesting of the same joint at several temperatures to determine its behavior pattern is eliminated. In addition, as will be described in detail in Chapter 8, knowing the load transfer efficiency for the entire temperature range permits a much more accurate determination of cumulative fatigue damage from aircraft operations over an entire year.

An S-shaped curve with a positive slope has the following general form:

$$LTE = A_1 + (A_2 - A_1)\, e^{-(SF/AT)^{A_3}} \qquad (4.1)$$

where: LTE = Load Transfer Efficiency
A_1 = Lower Bound
A_2 = Upper Bound
SF = Shift Factor in Degrees Kelvin
AT = Air Temperature in Degrees Kelvin
A_3 = Slope at Inflection Point

Note that the air temperature and shift factor must be converted to the absolute scale in order to avoid the mathematical impossibilities that would occur when temperatures at or below zero on either the Fahrenheit or Centigrade scale are encountered. Figure 4-23 illustrates the generalized form of the S-shaped curve and its five fundamental parameters.

In Equation 4.1, the values of the constants A_1 and A_2 were determined by inspection of Figures 4-13 to 4-22, whereas the value of A_3 must be determined for each type of joint construction. This was done using the Statistical Package for the Social Sciences' (SPSS) Nonlinear Computer

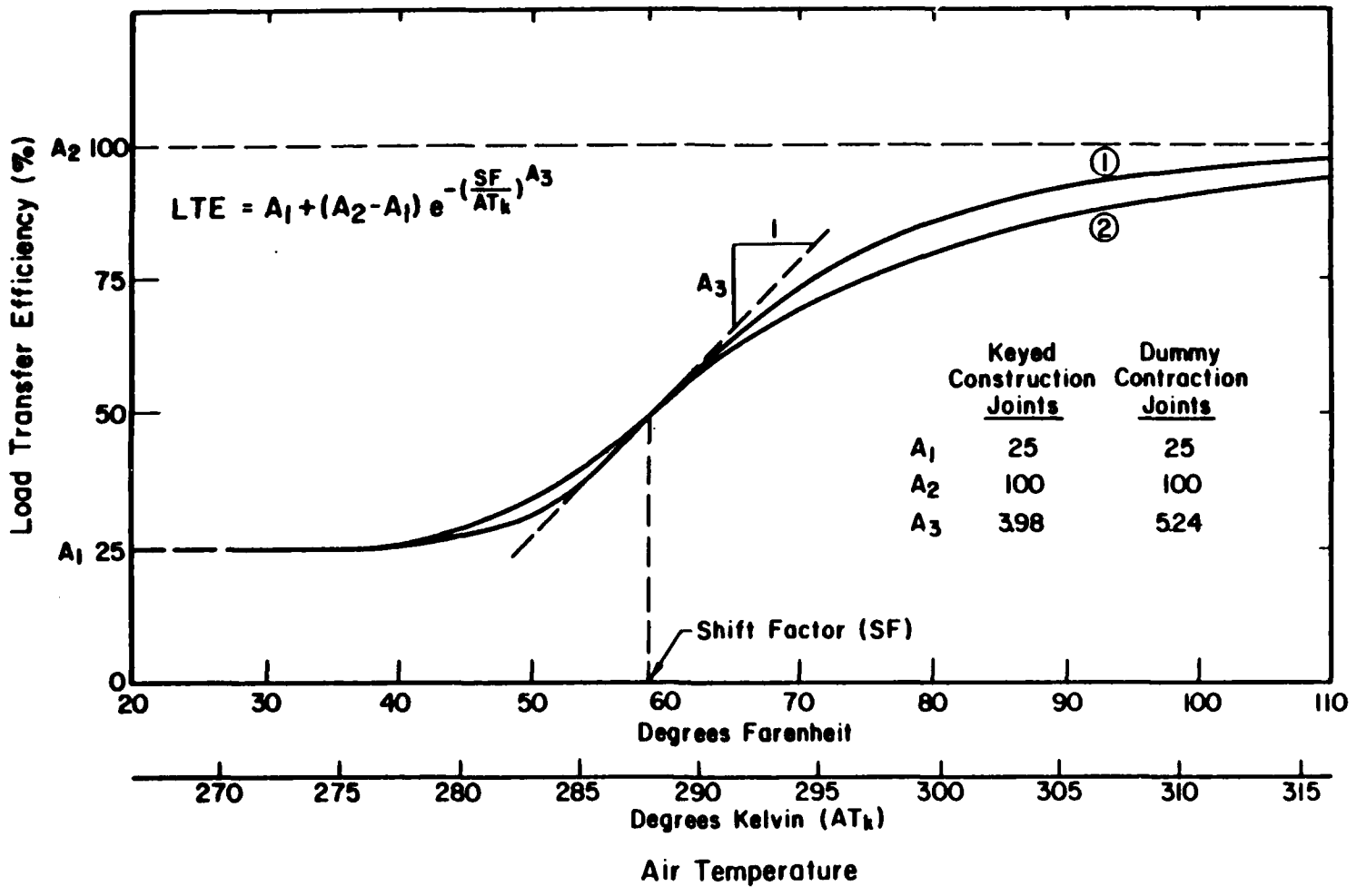

Figure 4-23. The Generalized S-Shaped Curve and Its Fundamental Parameters

Analysis (34). The value of A_3 was calculated for each of the 20 transverse joints and 20 longitudinal joints and averaged to obtain a single curve that describes the load transfer efficiency versus temperature relationship for that joint type. The following equations were developed for each joint type:

For transverse dummy groove joints:

$$LTE = 0.25 + 0.75\, e^{(SF/AT)^{40.0}} \qquad (4.2)$$

For longitudinal keyed joints:

$$LTE = 0.25 + 0.75\, e^{(SF/AT)^{25.0}} \qquad (4.3)$$

The above equations can now be used to predict the load transfer efficiency that will exist at a given joint for any temperature if the load transfer efficiency is known for just one temperature. In making this calculation, it is assumed that the load transfer efficiency measured in the field lies somewhere between 25 and 100 percent, exclusive. Otherwise, the shift factor can not be determined uniquely for that joint. Chapter 8 will discuss the alternatives available in this circumstance.

CHAPTER 5

BACKCALCULATION OF CONCRETE ELASTIC MODULUS AND MODULUS OF SUBGRADE REACTION

Up to this point in the development of the NDT & E procedure for rigid airfield pavements, the focus of attention has been on the selection of a piece of equipment to gather field data, and then on its use to characterize the behavior of pavement slabs to changing environmental conditions. In this chapter, a technique will be presented which uses the ILLI-SLAB analysis model to backcalculate two essential parameters of the pavement system, Young's modulus of elasticity of the Portland cement concrete (E) and Westergaard's modulus of subgrade reaction (k), from FWD-generated deflections. The backcalculated moduli will then be used to compare predicted pavement deflections with FWD measured deflections. Finally, the moduli will be examined for repeatability at constant temperature, and variability within pavement features.

5.1 The Center Slab Deflection Basin

When any type of load is placed on a rigid pavement slab, whether it be an aircraft gear or a bicycle, the slab will deflect nearly vertically to form a basin, as shown in Figure 5-1. The deflected shape of that basin is a function of several variables, including the thickness and stiffness of the slab, the stiffness of the underlying materials, and the magnitude of the load. For example, a slab with a high elastic modulus on a weak subgrade material will produce the nearly flat deflected shape of Figure 5-2. On the other hand, a flexible slab on a strong foundation will deflect as seen in Figure 5-3. This interaction between E and k results in a characteristic deflection basin for a given magnitude and duration of load and thickness of

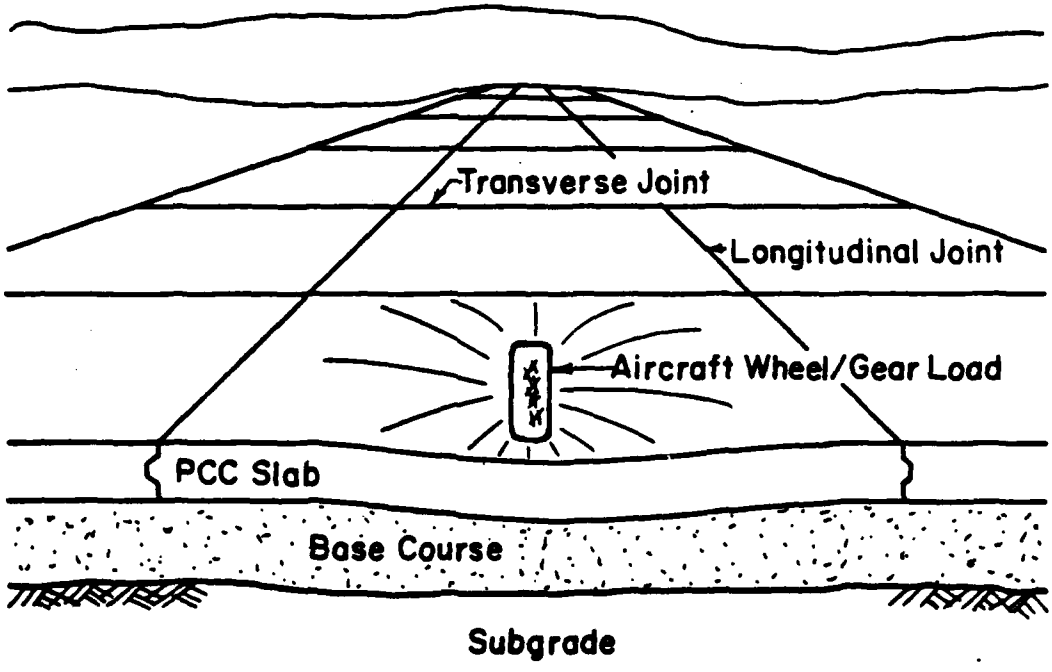

Figure 5-1. The Concept of the Deflection Basin

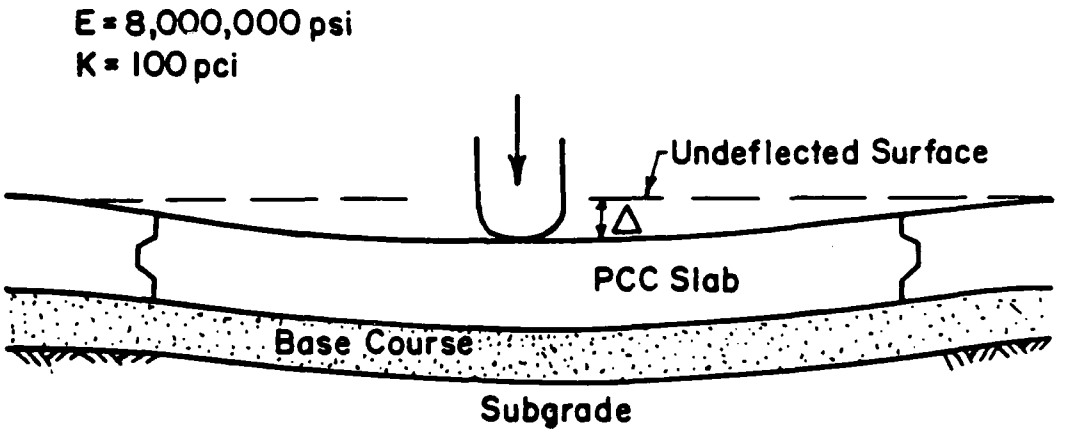

Figure 5-2. The Characteristic Shape of a Deflected Slab with High Stiffness and Weak Subgrade Support

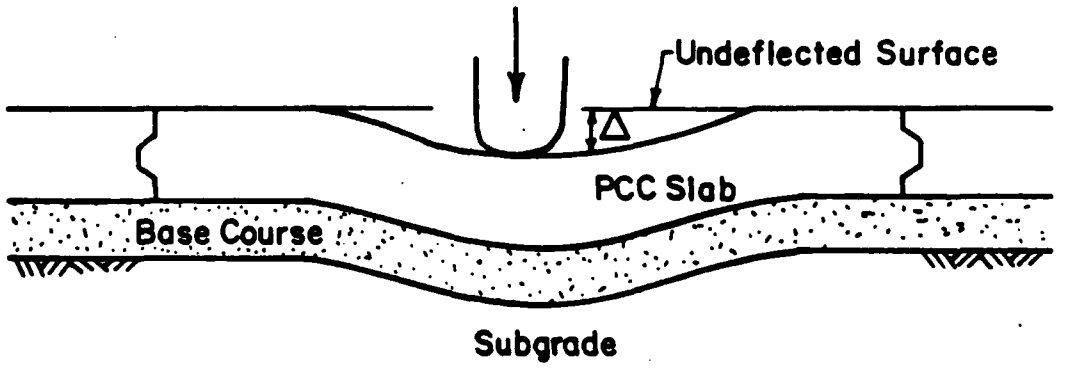

Figure 5-3. The Characteristic Shape of a Deflected Slab with Low Stiffness and Strong Subgrade Support

concrete. If the exact shape of the basin can be measured under loading conditions similar to an aircraft gear, and if two independent parameters describing the shape of the basin can be developed, then a unique value for both E and k can be backcalculated for a given load and slab configuration.

It must be emphasized that these backcalculated values are "dynamic" or time dependent in nature because they were derived from rapid FWD impulse loadings as opposed to static plate loadings. As a result, they will undoubtedly exhibit higher values than their static counterparts. Throughout this report, the term "dynamic" will be used to describe these backcalculated moduli; however, it is important to distinguish between rapid FWD impulses (25-30 msec rise times) and normal dynamic load testing (1-2 msec rise times) that occurs in the laboratory for resilient modulus or other types of fatigue testing.

Hoffman and Thompson (35) found that it was possible to characterize a two-parameter model for flexible pavements using the maximum deflection under the load (D0) and a parameter they called the basin "area". This "area" concept, illustrated in Figure 5-4, combines all the measured deflections in the basin into a single number to minimize the effect of an erroneous geophone reading. The "area" being determined is essentially 1/2 of the cross sectional area of the deflection basin taken through the center of the load. To eliminate the effect of variable loads and to restrict the maximum and minimum values of the "area", each deflection reading is normalized with respect to the maximum D0 deflection. Thus, the basin "area" has the units of length and is a function of the number and location of the sensors. Using the Dynatest Model 8000 FWD with 7 sensors spaced 12 inches apart, and the trapezoidal rule, the following equation is employed to calculate "area" for rigid pavements:

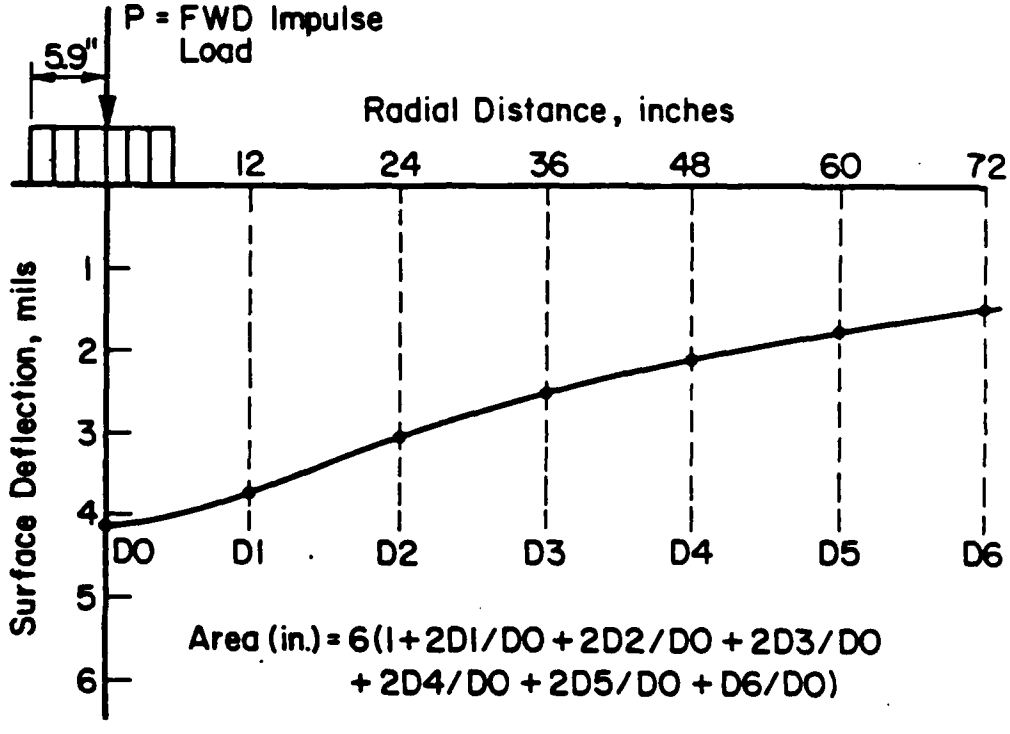

Figure 5-4. The Deflection Basin "Area" Concept

$$\text{"Area"(ins.)} = 6 \times (1 + 2 \times D1/DC + 2 \times D2/D0 + 2 \times D3/D0 + 2 \times D4/D0 + 2 \times D5/D0 + D6/D0) \quad (5.1)$$

By visualizing a perfectly stiff slab, the maximum "area" possible from Equation 5.1 is 72 inches. Conversely, a practical minimum "area" of about 11 is obtained if Boussinesq techniques are employed (the slab is as stiff as the foundation).

The independence of the D0 and "area" parameters is assured by the normalizing process. The same D0 could produce an "area" of 72 inches just as easily as 11 inches. With the deflection basin "area" and the maximum deflection D0, it is possible to solve for that unique combination of dynamic E and k that produces the same characteristic basin as measured with the FWD.

5.2 The Graphical Solution for Dynamic E and k

The determination of dynamic E and k from deflection basin measurements can be accomplished graphically for any given slab configuration, Poisson's ratio of the concrete, and magnitude of load. The following steps must be performed and are illustrated in Figure 5-5:

1) A finite element ILLI-SLAB mesh incorporating the slab dimensions is generated, with care taken to place nodal points at corresponding FWD sensor locations. Figure 5-6 depicts this particular mesh and how the inherent symetry can be used to reduce the computer memory requirements.

2) A minimum of nine ILLI-SLAB computer runs is made using various combinations of dynamic E and k that are expected to bracket the in situ values.

3) For each computer run, the deflections at the seven sensor locations are used to establish the D0 and "area" parameters.

4) These D0-"area" points are plotted, showing their inherent E and k values, to develop a grid of constant dynamic E and k lines.

5) The actual FWD-generated deflection basin "area" and D0 are then plotted on the grid, and the unique dynamic E and k values are interpolated.

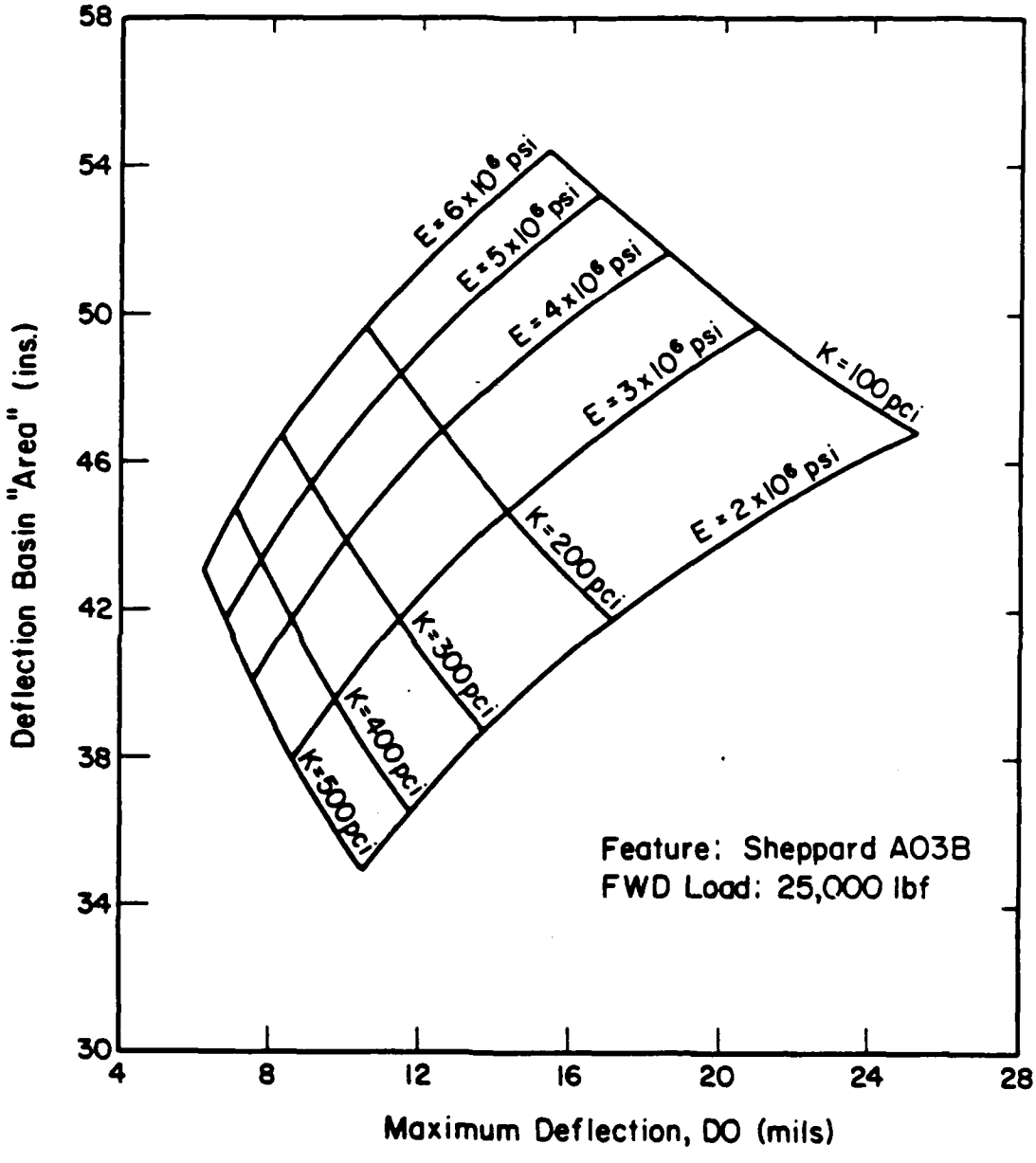

Figure 5-5. A Typical ILLI-SLAB Grid for the Backcalculation of E and k

This technique has proven successful in backcalculating dynamic E and k values that, when reinput back into the ILLI-SLAB model, reproduce FWD-measured deflections very accurately (36). However, its use has been limited primarily to thinner highway pavements where only four sensors on the FWD are needed to describe the deflection basin accurately.

There are several drawbacks to this graphical technique that should be noted because they severely limit its application for large airfield evaluation programs. First, the method requires hand plotting of the backcalculation grid which can only be done after several ILLI-SLAB computer runs have been manually inputted. Secondly, a new grid must be developed for each pavement thickness and slab size encountered. This can mean up to 25 separate grid formulations for each airfield. Third, individual FWD deflections must be normalized to a standard load, usually 24,000 pounds, to avoid a separate grid for each drop of the FWD. Finally, inaccuracies can easily be introduced through poor interpolation of dynamic E and k values within the grid. This source of error can be minimized somewhat, but only if more ILLI-SLAB runs are made to develop a finer grid.

5.3 A Computer-based Iterative Solution for Dynamic E and k

One of the major objectives of this research was to develop a complete, computer-based rigid pavement evaluation system that would relieve the engineer of hand manipulation of large amounts of data. Initially, efforts centered around the development of algorithms for estimating dynamic E and k given the deflection basin characteristics and the geometry of the slab. Although showing some potential, these efforts failed to produce any greater degree of accuracy than could be obtained from the graphical solutions.

Consequently, a simple iterative scheme was devised, using ILLI-SLAB as a computer subroutine, that very accurately calculates the unique dynamic E and k combination. Figure 5-6 depicts the finite element mesh that was devised for this scheme, while Figure 5-7 describes the first iteration.

1) The field measured DO and "area" parameters (Point f) are calculated from the deflection basin generated at the center slab location.

2) Three points, representing extremes in E and k, are selected arbitrarily and input, along with the slab dimensions, into the ILLI-SLAB model. A corresponding DO and "area" are calculated for each of these points (1,2,3) as shown.

3) The distances between points f and 2 (SL_1), f and 3 (SL_2), 2and 3 (SL_3), and 1 and 2 (SD_2) are calculated. This establishes the values of angles A_1, A_2, and A_3.

4) The vector V_1 must be resolved into its two components along lines 1-2 and 2-3. This is done by locating Point a along line 2-3 so that line f-a is parallel to line 1-2. The lengths of lines f-a and 2-a are the required components.

5) The slopes of lines 1-2 and 2-3 are calculated and used to find angle Psi. Once Psi is known, angle B_2 becomes its compliment. Angle B_3 is then found by subtraction. With each angle of triangle f-a-2 and one of its sides, V_1, known, the lengths of vectors V_2 and V_3 are calculated.

6) The first estimate of the dynamic E and k represented by Point f is obtained from the ratio of V_3 to SL_3 for E and the ratio of V_2 to SD_2.

The backcalculation grids generated by the ILLI-SLAB model each display the characteristic curvatures of the constant E and k lines that are pictured in Figures 5-5 and 5-7. Thus, the first estimate of E and k in this iterative scheme will always be greater than the true value by an amount dependent on this degree of curvature near the field data point. This fact is utilized in the second iteration, illustrated in Figure 5-8. Two more combinations of E and k (Points 5 and 6) are selected at an arbitrary distance from the initial estimate (Point 4), and the vector W_1 is again

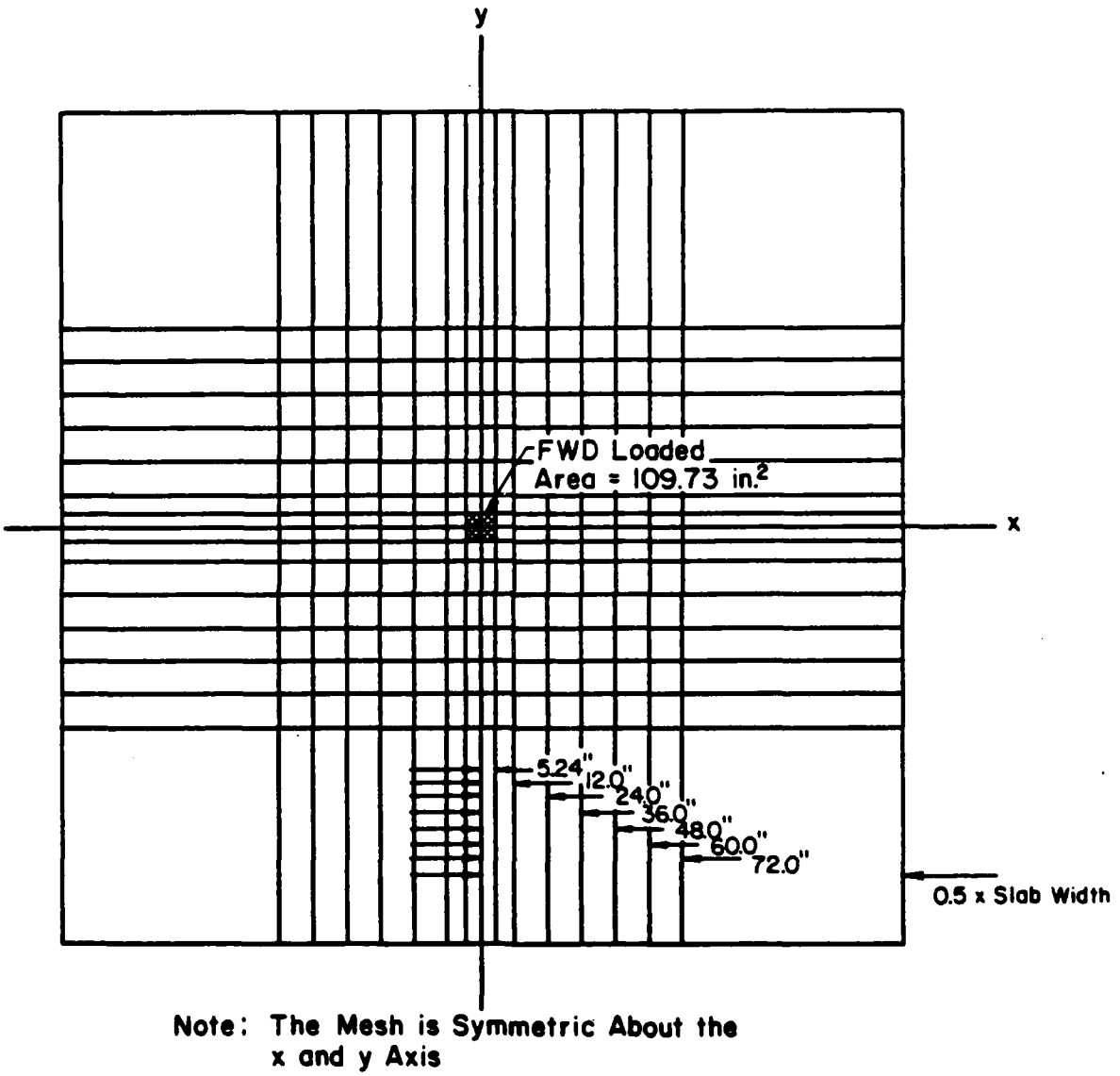

Figure 5-6. The ILLI-SLAB Finite Element Mesh for the Analysis of FWD Data

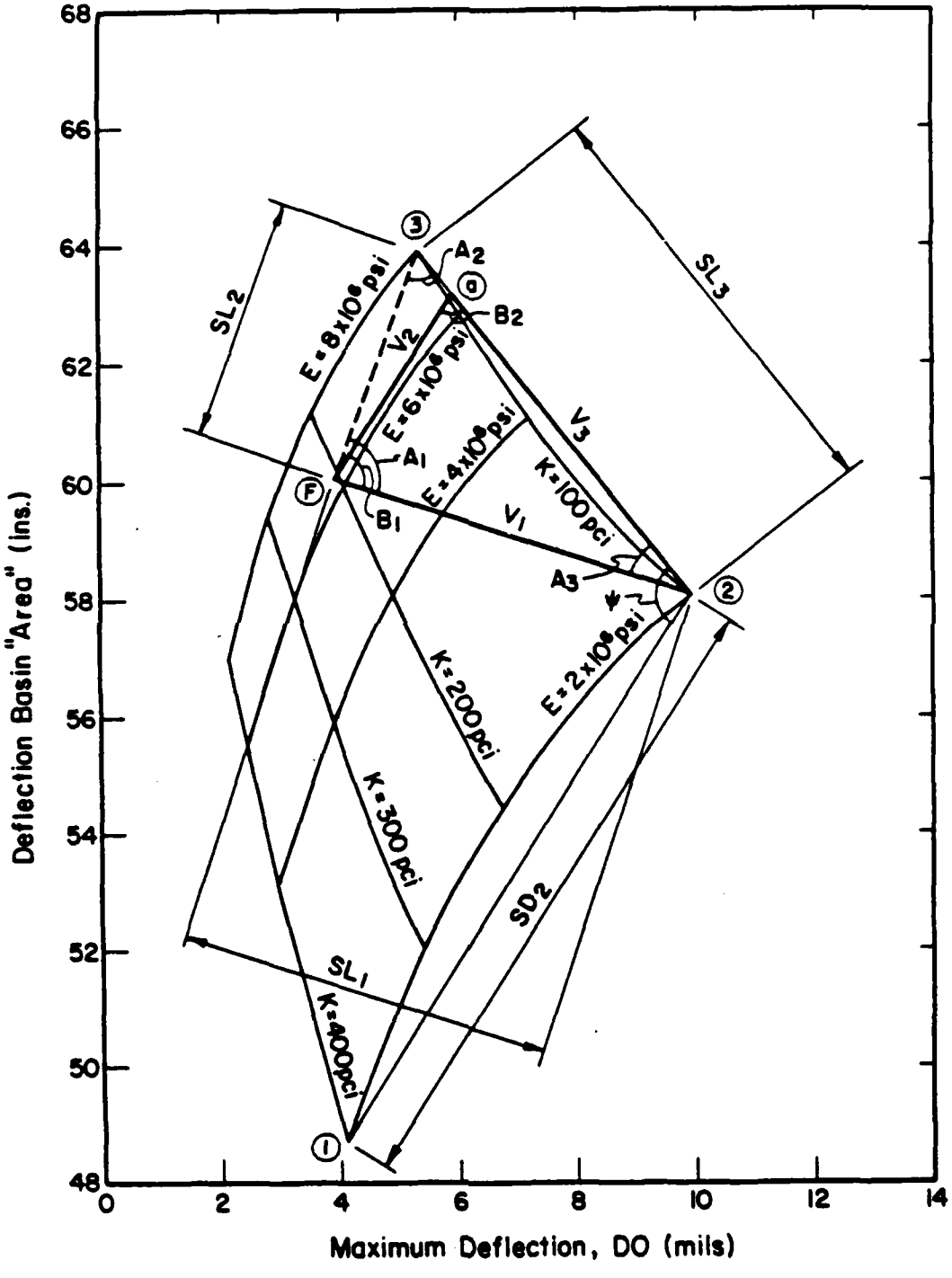

Figure 5-7. The First Iteration in the Computer Solution of E and k

resolved into its two components, W_2 and W_3. The new estimate of f will be much closer to, but slightly less than the true value. The process is repeated until the "area" is within 0.01 inches and the D0 within 0.05 mils of the true value measured in the field.

The program contains checks after each iteration and will terminate when the tolerances are satisfied. Up to five iterations may be required to close within these tolerances, but 3 or 4 iterations are typical. The greater sensitivity of both "area" and D0 in the higher ranges of E and k will dictate just how many iterations are ultimately required.

5.4 Comparison of Measured and Predicted Deflection Basins

The validity of any analytical model is truely tested when predicted response is compared with measured response. To verify the accuracy of ILLI-SLAB and the backcalculated dynamic E and k moduli, each individual slab at Sheppard AFB was used to compare measured and predicted deflections for FWD loads in excess of 22,000 pounds. Figures 5-9 through 5-14 graphically present some selected results for each feature. These figures illustrate the outstanding precision with which ILLI-SLAB models a pavement's response to load.

An analysis of the deflection data reveals very similar trends to those established during the FWD repeatability study. As deflections decrease away from the loaded area, the percent error between measured and predicted deflection at each sensor tends to increase. This is reasonable if each sensor carries about the same built-in error (the sensors are accurate to within .0005 ins.). Typically, one to two percent error is observed for the D0 reading while five to six percent is common for the D6 value. In most cases, however, this match in measured and predicted deflection basins is

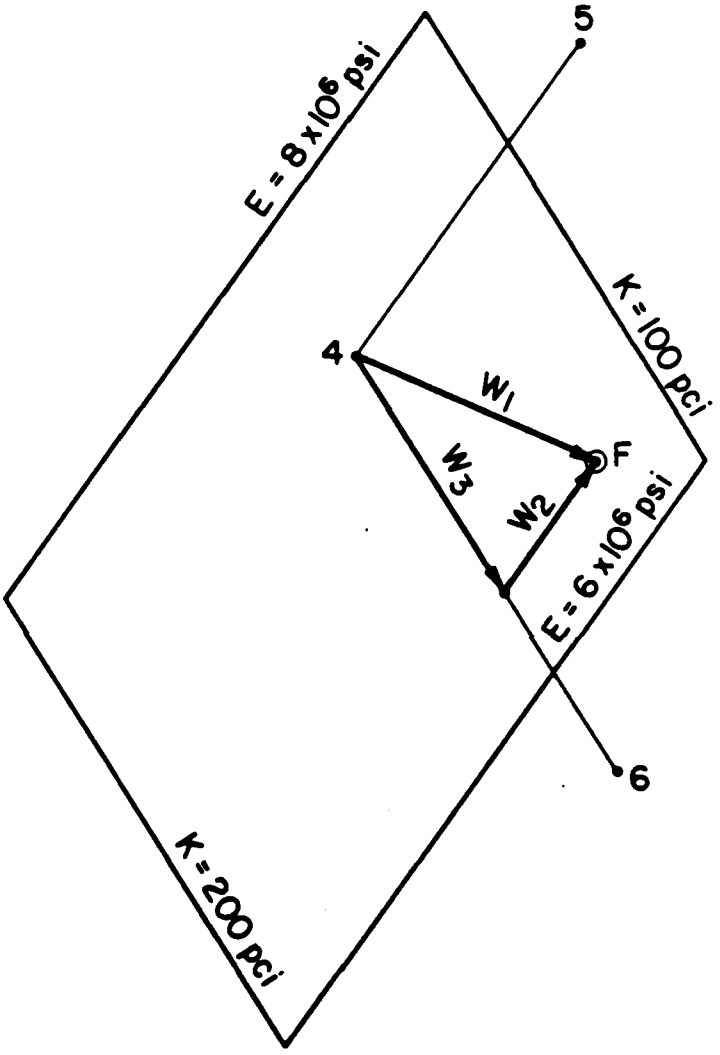

Figure 5-8. An Enlarged View of the Second Iteration in the Computer Solution of E and k

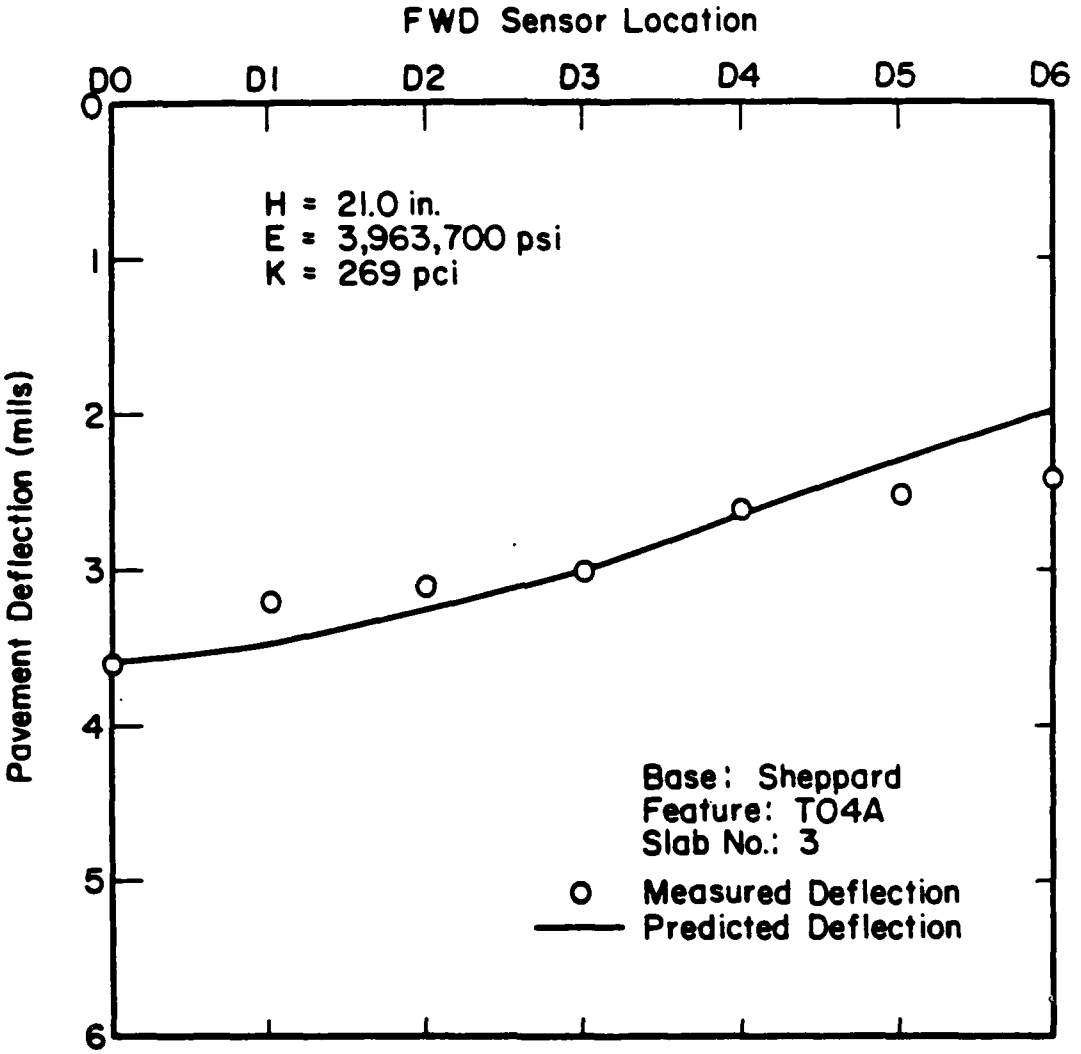

Figure 5-9. Comparison of Measured and Predicted FWD Deflections for Feature T04A

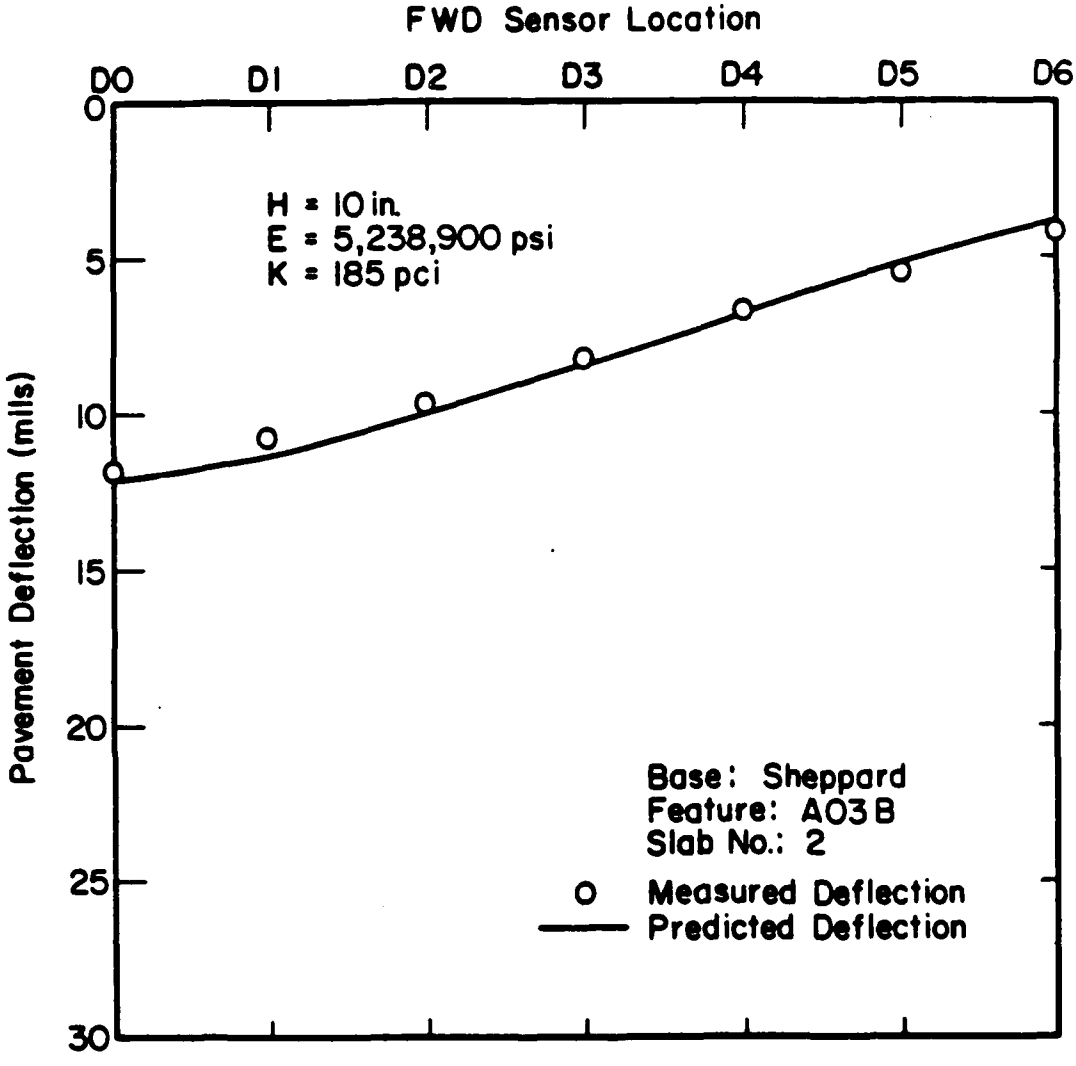

Figure 5-10. Comparison of Measured and Predicted FWD Deflections for Feature A03B

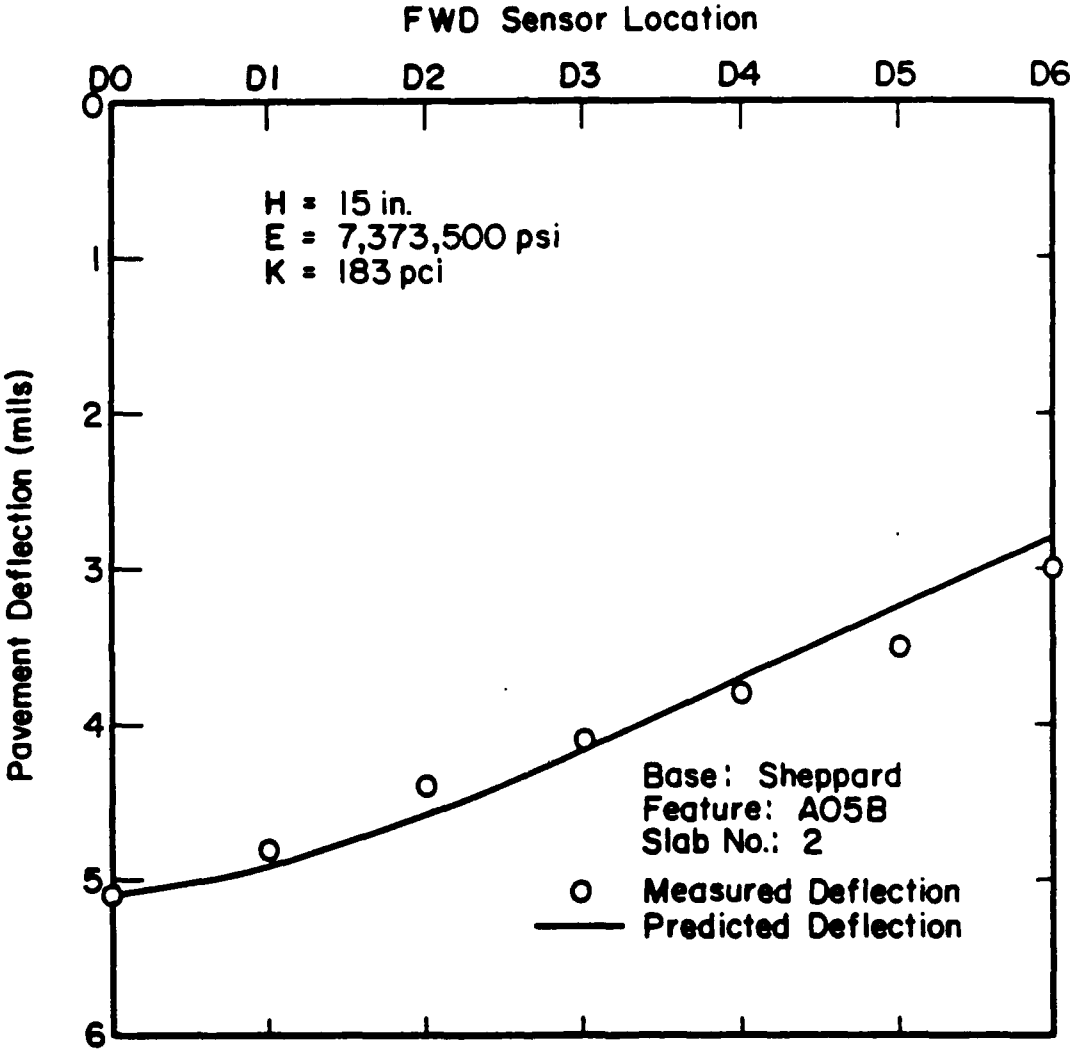

Figure 5-11. Comparison of Measured and Predicted FWD Deflections for Feature A05B

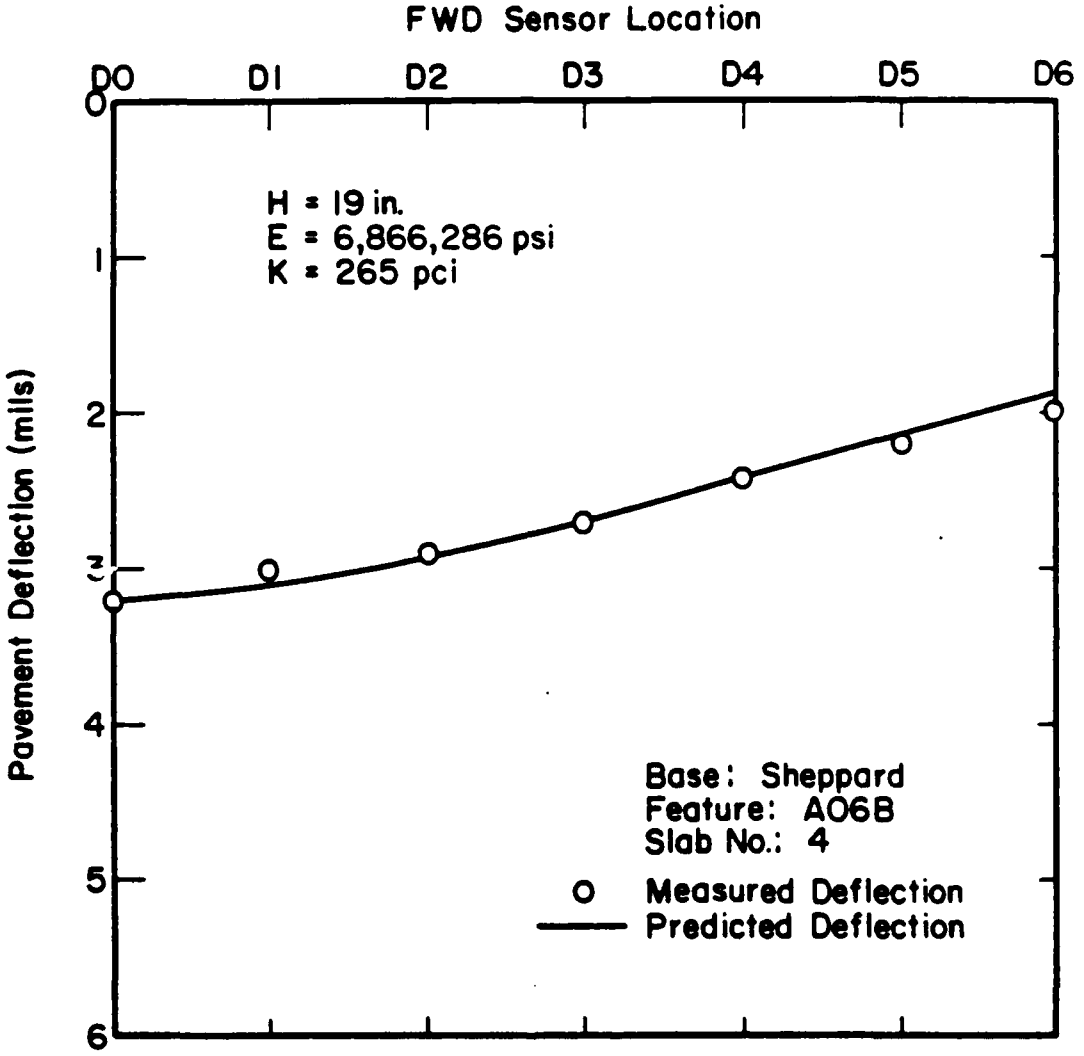

Figure 5-12. Comparison of Measured and Predicted FWD Deflections for Feature A06B

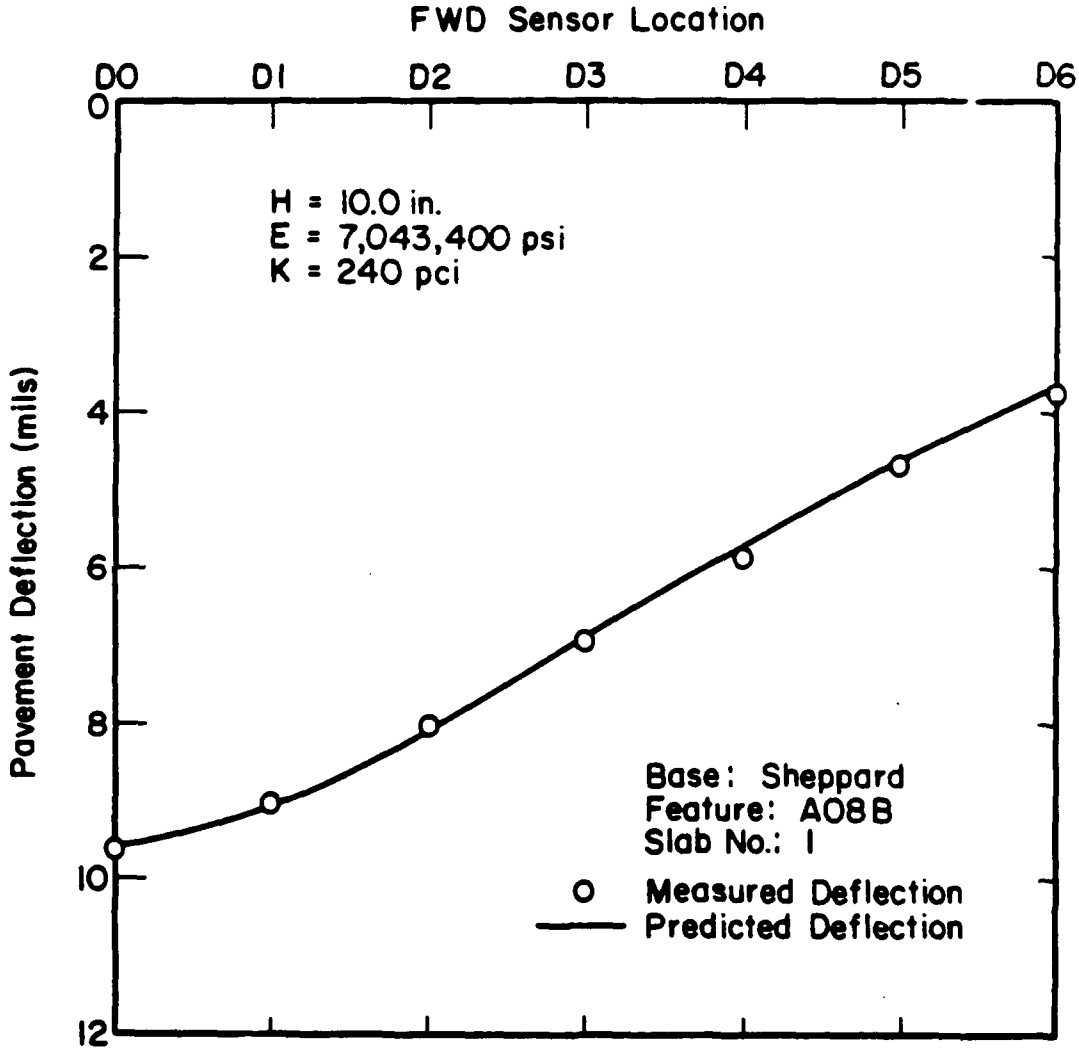

Figure 5-13. Comparison of Measured and Predicted FWD Deflections for Feature A08B

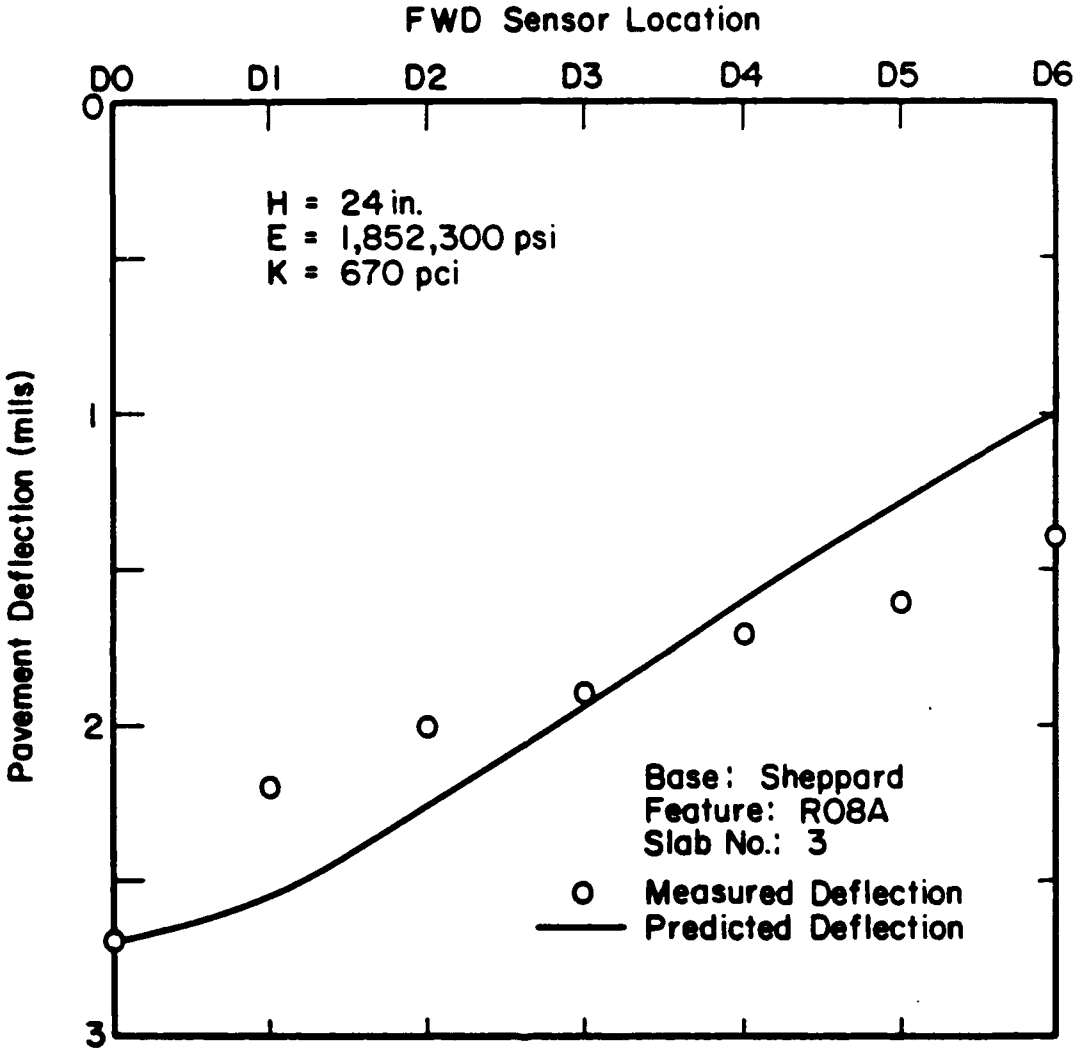

Figure 5-14. Comparison of Measured and Predicted FWD Deflections for Feature R08A

remarkable, especially in light of the inherent variation in the sensors and paving materials, and the very small deflections involved.

5.5 Repeatability of Backcalculated Dynamic E and k Moduli

In Chapter 3 the excellent repeatability of FWD load and deflection measurements at constant temperature was verified. In addition, nearly identical deflections were found over the normal (15-20 ^{o}F) temperature fluctuations that are encountered during daily testing. With the ability to accurately backcalculate dynamic E and k values, it is now possible to examine the effects of temperature and load on these two parameters without the confounding effects of interpolation errors that arose due to the "logarithmic" nature of the grid. The constant temperature case will be investigated to determine the extent of inherent variation in E and k due to equipment and materials, and then backcalculated moduli at several temperatures will be examined to see if any patterns develop.

5.5.1 Constant Temperatures

Table 5-1 contains the results of backcalculated dynamic moduli at constant temperature for two features at Sheppard AFB. Each table entry for the given temperature (eg., 78.6, 82.2, ...) represents at least eight tests performed within 45 minutes of each other (the results for other temperatures will be discussed in Section 5.5.2). Several important conclusions can be drawn from this table and the results of extensive analyses of variance. First, at slab center, no apparent relationship exists between the magnitude of load and k, other than a decrease in the coefficient of variation of k as load increases for these features. This indicates that the dynamic k is not stress sensitive for the interior FWD loads used or the base and subgrade

TABLE 5-1. REPEATABILITY OF BACKCALCULATED DYNAMIC E AND k MODULI AT CONSTANT TEMPERATURE

Feature	Slab No.	Pvmt Temp. (°F)	Load[1] Range	k Average (pci)	k Coef. of Var.	E x 10^6 Average (psi)	E x 10^6 Coef. of Var.	No. of Tests
T04A	1	78.6	Low	294	.19	4.2	.33	8
			Medium	280	.15	3.8	.26	8
			High	286	.11	3.6	.18	8
	2	82.2	Low	434	.09	2.9	.13	8
			Medium	349	.07	3.3	.14	8
			High	358	.07	3.2	.12	8
	3	80.8	Low	206	.14	5.5	.15	8
			Medium	205	.17	4.7	.27	8
			High	215	.12	4.6	.22	8
A05B	1	68.4	Low	181	.11	6.6	.18	9
			Medium	178	.16	6.0	.11	9
			High	190	.05	5.8	.12	9
	2	74.5	Low	156	.12	7.9	.17	8
			Medium	158	.04	6.9	.04	8
			High	181	.06	6.2	.08	8
	4	89.1	Low	125	.18	7.9	.29	8
			Medium	141	.07	6.0	.13	8
			High	150	.05	5.7	.07	8

(1) Load ranges - Low: 6000- 9000 lbf
Medium: 14000-17000 lbf
High: 22000-26000 lbf

materials involved. This makes sense when considering the very low levels of stress that ultimately reach these supporting materials from FWD loadings. Typical stress-strain curves for subgrade materials at high rates of loading display maximum elastic and shear moduli at low levels of strain, and resilient modulus is capped at a maximum value at deviator stress levels below about two psi.

Second, although the coefficients of variation decrease with increased load, they remain somewhat higher for backcalculated k than those observed for FWD-measured loads and deflections. Typical variations at high load levels ranged between 4 and 12 percent and averaged about 8 percent, whereas low load levels experience variation averaging 15 percent. Thus, higher load levels produce more consistent back calculated k results.

Third, a pattern does exist with regard to dynamic E values and magnitude of load. Consistently higher, and often unrealistic, dynamic E values are backcalculated for low load levels, as evidenced by Feature A05B in Table 5-1. The differences are much more pronounced between low and medium loads than between medium and high loads. The coefficients of variation for dynamic E values display much the same tendencies, with the higher loads showing significantly greater consistency. Again, higher load levels appear to give more realistic and reliable results. Figure 5-15 offers a reasonable explanation for the greater inconsistency in E values than k values, when conceptually, the modulus of subgrade reaction for granular materials should be much more variable than the elastic modulus of fairly uniform concrete. This plot of deflection (or load) versus concrete elastic modulus illustrates that small variations in deflection (load) at the lower levels can result in large changes in E.

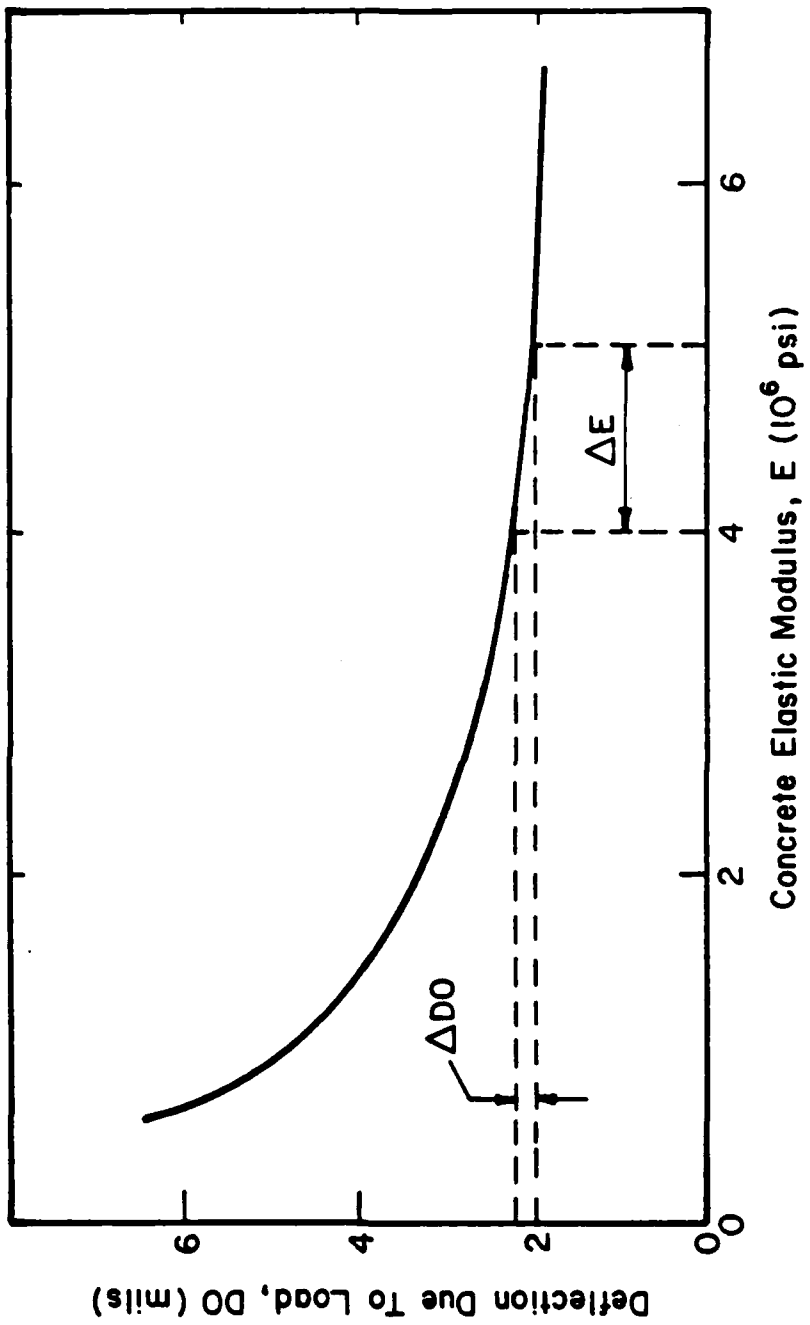

Figure 5-15. The Effect of a Small Change in Deflection (Load) on the Elastic Modulus of Concrete

5.5.2 Various Temperatures

One of the most puzzling aspects of NDT & E is the effect of changing environmental conditions on the parameters that characterize the pavement system. Figures 5-16 through 5-18, which show individual E- and k-value trends with pavement temperature, indicate that all slabs within a feature display similar tendencies, but no overall predictable pattern is discernable. Dynamic k values tend to be slightly higher at colder temperatures, level off in the mid-range, and then increase again slightly at the higher temperatures. This sort of pattern would seem to be related more to moisture levels than temperature, but additional research into this aspect is needed to reach any meaningful conclusions. In any event, the fluctuation in k is not significant enough to affect the stresses generated to any great extent. Dynamic E values also exhibit a pattern similar to k values, tending to be moderately higher at colder temperatures and then leveling off. At higher temperatures, however, the pattern is inconsistent.

Table 5-2 presents a summary of the results of backcalculated dynamic k and E values for 8 slabs at pavement temperatures ranging from 36 to 101 ^{o}F. With at least five cases per slab, this table shows that the introduction of temperature as a variable has increased the coefficients of variation above the levels established by the constant temperature situation, particularly for dynamic E values at low load levels. At recommended high load levels, this increase in the coefficient of variation is modest, averaging about 4 percent. Dynamic k values remain relatively unaffected by temperature fluctuations, with coefficients of variation very similar to the constant temperature case. Figure 5-19 illustrates how the normal variation in E and k at constant temperatures is great enough to encompass the variation in E and k at different temperatures.

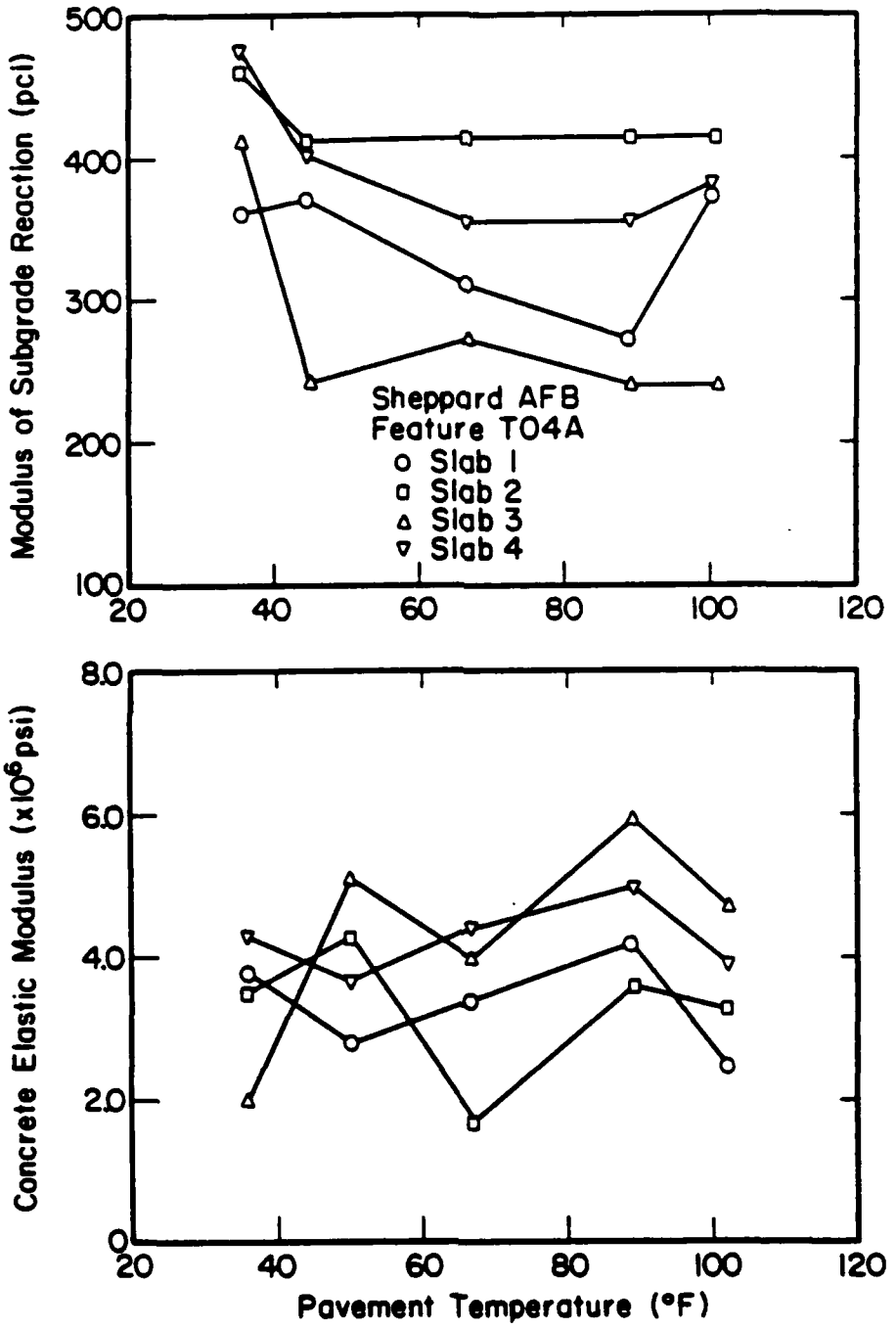

Figure 5-16. Pavement Temperature versus Backcalculated E and k for Feature T04A

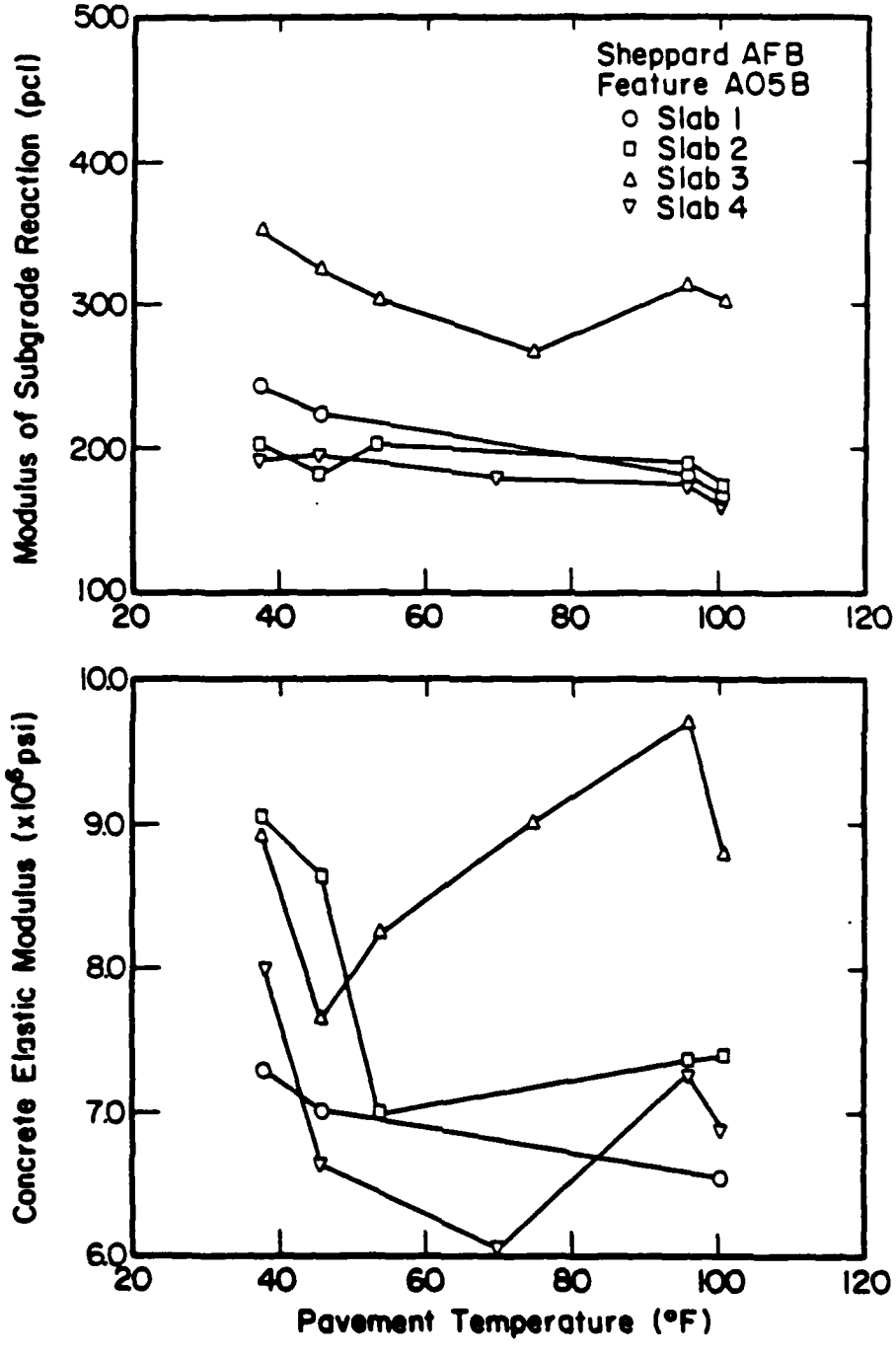

Figure 5-17. Pavement Temperature versus Backcalculated E and k for Feature A05B

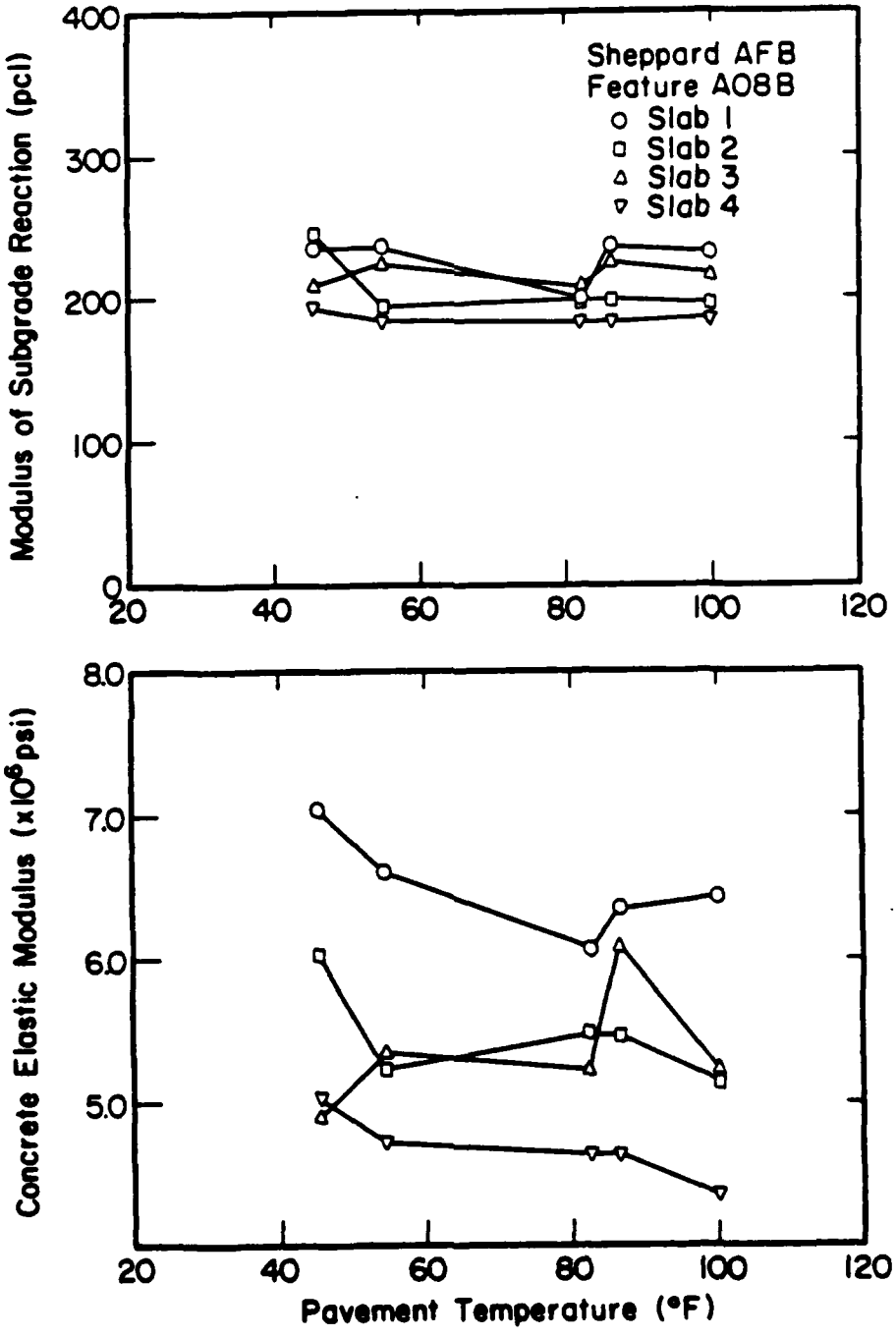

Figure 5-18. Pavement Temperature versus Backcalculated E and k for Feature A08B

TABLE 5-2. REPEATABILITY OF BACKCALCULATED DYNAMIC E AND k MODULI AT VARIOUS TEMPERATURES

Feature	Slab No.	Pvmt Temp. Range (°F)	Load(1) Range (lbf)	k Average (pci)	k Coef. of Var.	E x 10^6 Average (psi)	E x 10^6 Coef. of Var.	No. of Cases
T04A	1	33.1	Low	275	.19	5.9	.31	8
		to	Medium	276	.15	4.2	.16	8
		121.8	High	316	.13	3.6	.19	8
	2	33.1	Low	422	.13	4.7	.26	8
		to	Medium	348	.12	4.4	.27	8
		121.8	High	396	.10	3.8	.27	8
	3	33.1	Low	268	.29	5.8	.38	8
		to	Medium	243	.27	1.3	.27	8
		121.8	High	261	.25	4.6	.26	8
	4	33.1	Low	448	.24	2.9	.53	5
		to	Medium	370	.13	4.4	.08	5
		121.8	High	391.	.12	4.2	.12	5
A05B	1	34.2	Low	209	.17	7.1	.13	6
		to	Medium	189	.16	7.2	.13	6
		119.3	High	208	.18	6.5	.09	6
	2	34.2	Low	194	.31	9.1	.33	7
		to	Medium	176	.16	7.7	.21	7
		119.3	High	188	.08	7.6	.14	7
	3	34.2	Low	327	.23	10.0	.19	6
		to	Medium	287	.12	9.3	.24	6
		119.3	High	310	.09	8.8	.09	6
	4	34.2	Low	189	.14	7.5	.27	7
		to	Medium	173	.10	6.8	.15	7
		119.3	High	182	.07	6.8	.11	7

(1) Load ranges - Low: 6000- 9000 lbf
Medium: 14000-16000 lbf
High: 22000-25000 lbf

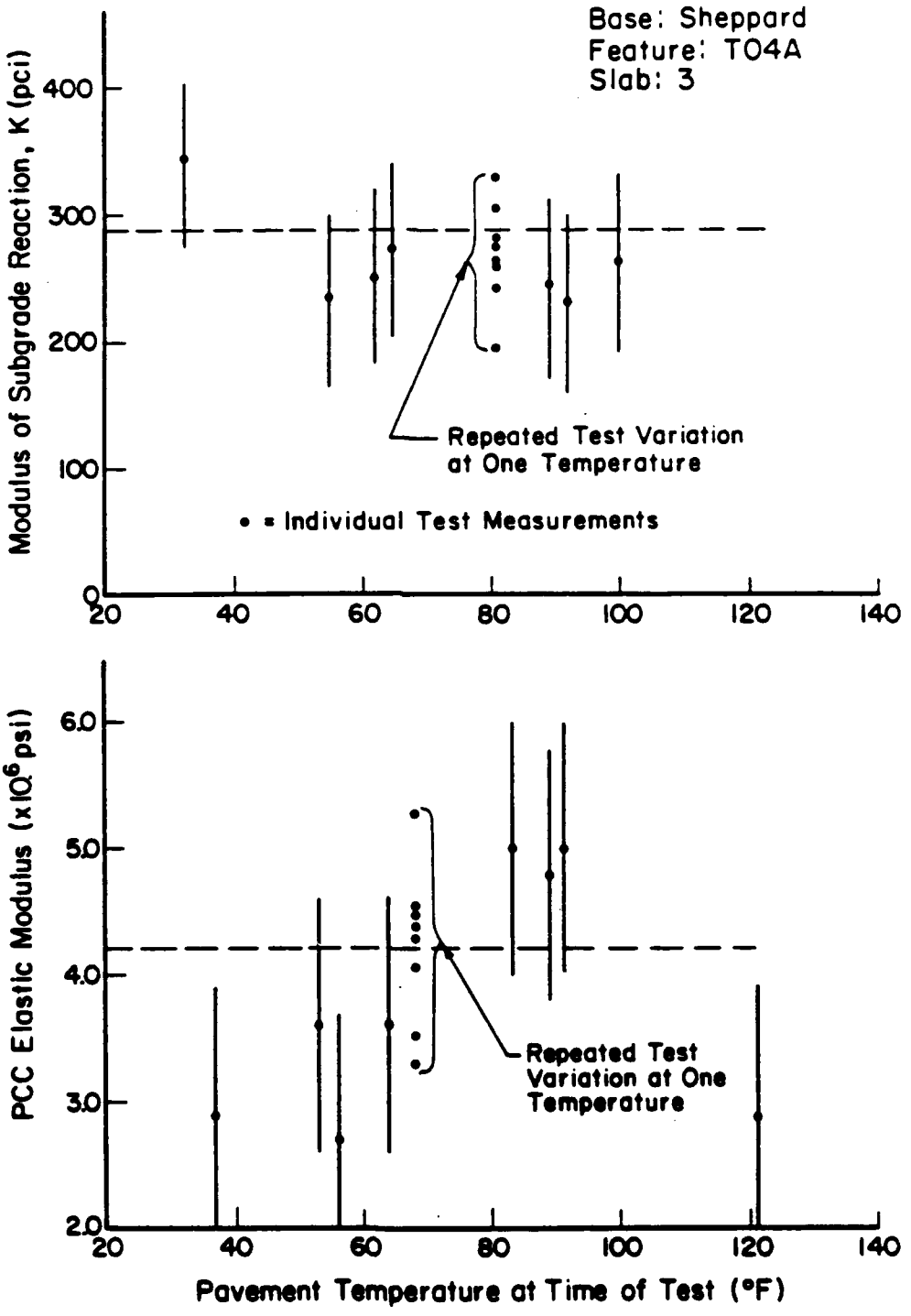

Figure 5-19. The Typical Variation in E and k at Constant Temperature Applied to Single Observations of E and k at Various Temperatures

In summary, it appears that only temperature extremes substantially influence backcalculated dynamic E and k values. Temperature fluctuations between 45 and 90 ^{o}F are relatively insignificant, producing very little additional variation over and above that which is already inherent in the equipment and pavement materials. As will be emphasized throughout the remainder of this report, the overwhelming temperature effect occurs at the joints where load transfer plays an important role in the pavement response to load.

CHAPTER 6

THE CRITICAL STRESS AND JOINT CONSIDERATIONS

The backcalculation of the elastic modulus of the concrete and the subgrade reaction modulus is a critical step in the determination of the actual stresses that develop under aircraft loadings. If only the interior stresses are desired, it merely remains to formulate the proper ILLI-SLAB mesh for the aircraft gear in question, and then have the program calculate the maximum tensile stress at the bottom of the slab. The elastic-layered programs discussed in Chapter 2 could have accomplished this calculation almost as accurately and certainly with greater speed. But the value of the ILLI-SLAB finite element model lies in its ability to calculate edge stresses under any gear configuration and joint load transfer type, given a reasonable approximation of the E and k values. This chapter will discuss the complexities of using edge stresses over interior stresses, and the computer program developed for this calculation.

6.1 Edge Versus Interior Stresses

Historically, either adjusted edge or interior streses have been used in various rigid pavement design procedures. The decision to use interior stresses rather than edge stresses in some design procedures was made for simplicity more than anything else. Interior stresses are easily calculated using either elastic layered theory or Westergaard's equations. In some instances, it has been justified by assuming all joints have high load transfer. Only just recently has it been feasible, with the advent of the high speed computer, to consider actual boundary conditions and their effect on stress calculations. The fact that most of the rigid pavement slabs

constructed to date violate the major assumptions of elastic layered and Westergaard theory with regard to slab dimensions has largely been ignored. As an example of the effect that slab size has on the interior stress, Figure 6-1 illustrates how the maximum tensile stress under a C-141 aircraft gear changes as slab size increases. This analysis is for a single slab with free edges all around. Obviously, this type of sensitivity analysis would not even be possible without a finite element or similar computer model, but it serves to point out the variation that can occur even in interior stresses. Figure 6-2 shows how the maximum tensile stress in the concrete increases as the same C-141 gear is moved toward the transverse edge of a typical airfield slab. This dramatic increase in maximum tensile stress must be accounted for if our rigid pavements are to be properly designed and evaluated.

Recent shifts in policy with regard to design of rigid pavements by the FAA (17) and others have given credence to the importance and validity of using edge stress for design. Again, as a matter of convenience and a lack of better information, a standard 25 percent reduction in free edge stress is applied to account for load transfer, in whatever form it may take. Perhaps for design purposes, this approach is reasonable. The results of load transfer studies conducted during this research effort and presented in the discussion to follow, however, will suggest that this standard 25 percent reduction in free edge stress used in design is too high in light of the actual performance of joint load transfer systems throughout their design life.

The evaluation of rigid pavement systems, on the other hand, affords the engineer the opportunity to atone for the shortcomings in the design and construction of concrete slabs and joints. The equipment and analytical models now available render it feasible to identify poorly performing slabs

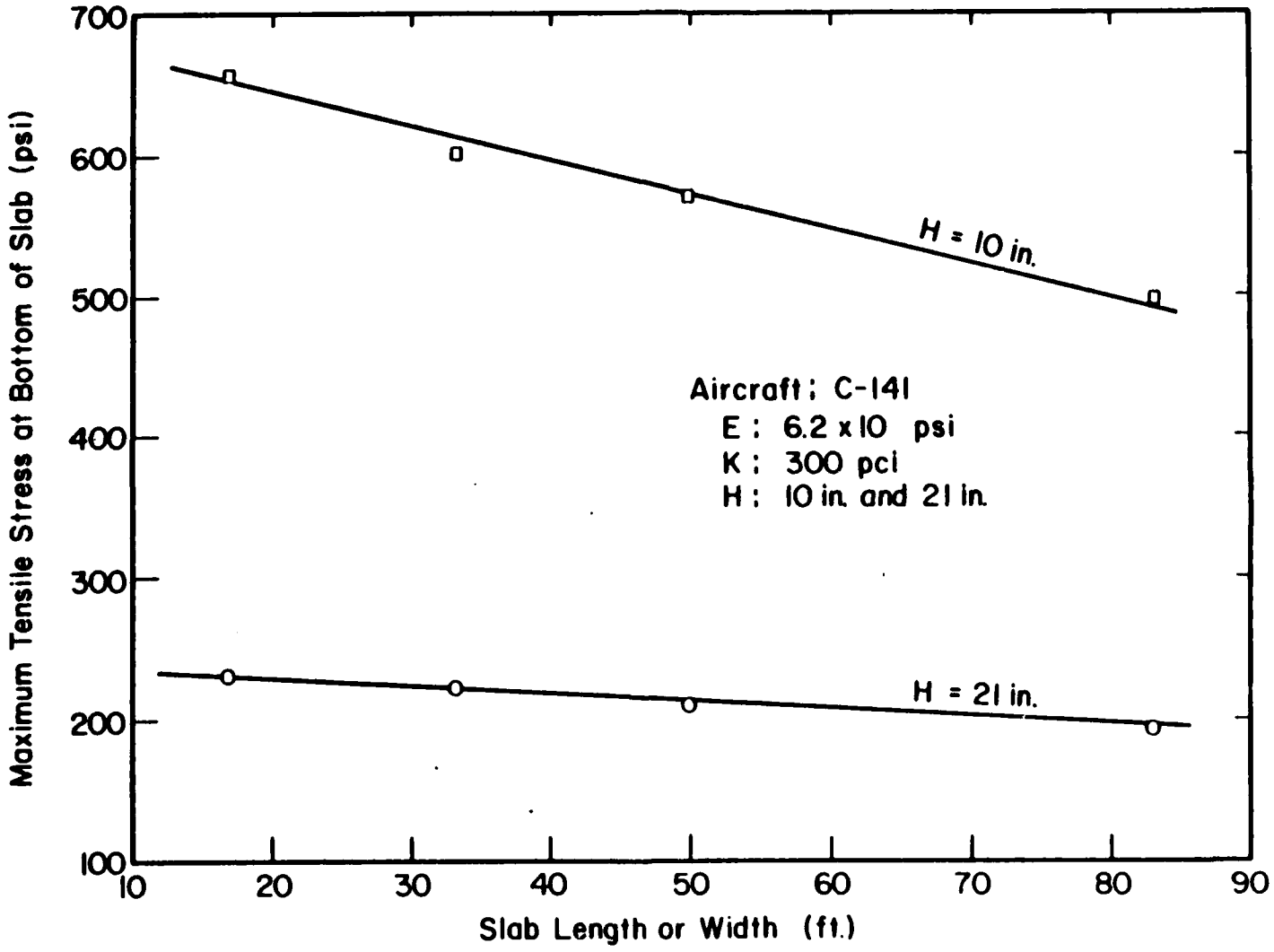

Figure 6-1. The Effect of Slab Size on ILLI-SLAB-Generated Interior Stresses

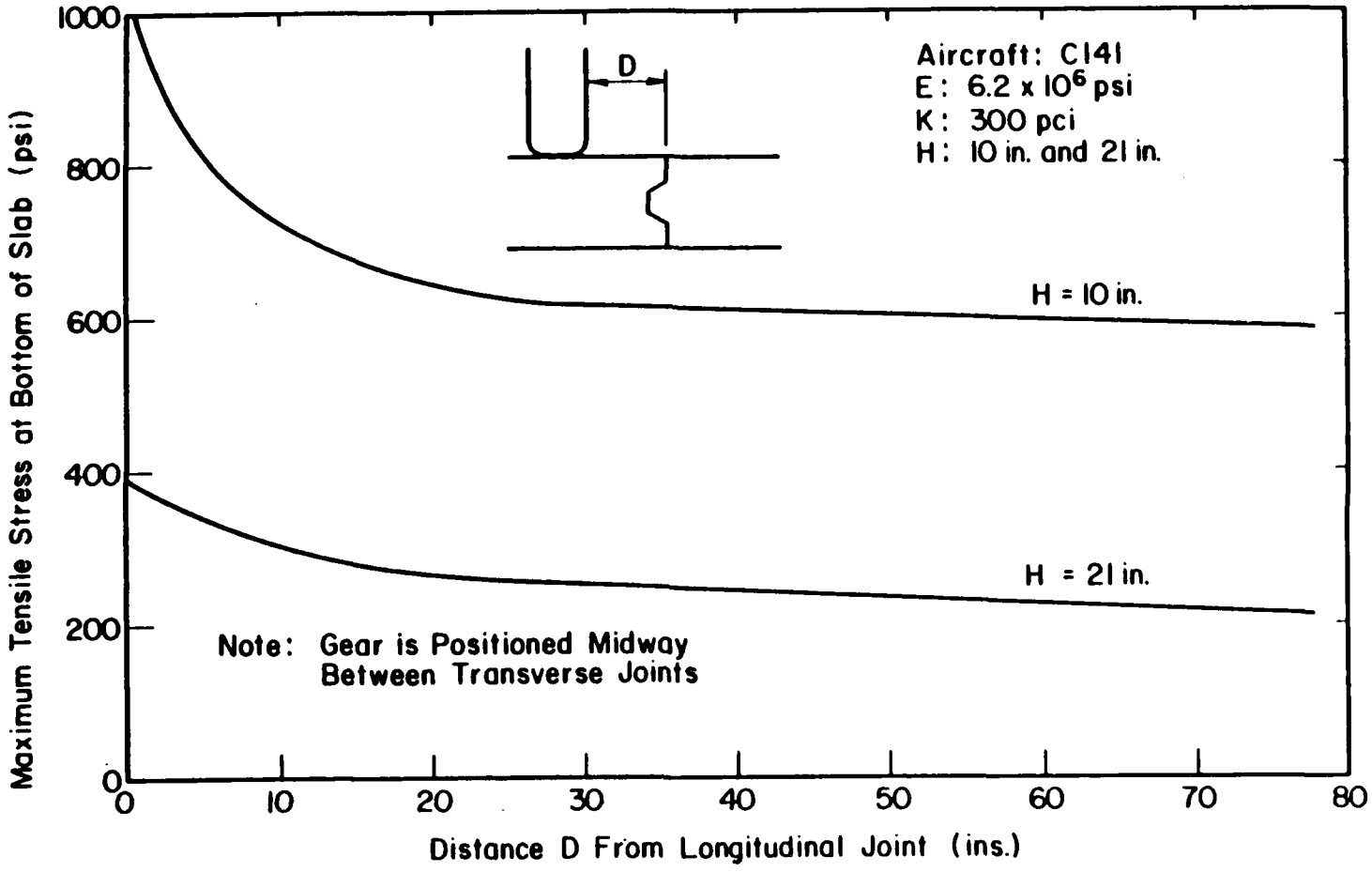

Figure 6-2. The Change in Maximum Tensile Stress Under an Aircraft Gear as the Gear Travels Closer to the Longitudinal Joint

and joints. Preventative maintenance techniques or allowable load restrictions can then be implemented to preserve and protect individual slabs and features for their full design life. The key to achieving the greatest return on the investment in millions of square yards of rigid pavement is the realistic assessment of the damage caused by aircraft loads, a process that begins with the calculation of the critical stress.

6.2 The Aggregate Interlock Factor

In the ILLI-SLAB finite element model, keyway and aggregate interlock load transfer mechanisms are modeled as a series of vertical springs adjoining two adjacent slabs at the joint (37). The stiffness of these springs, expressed in pounds per inch per inch of thickness, is known as the aggregate interlock factor and is applicable to both mechanisms. The magnitude of the aggregate interlock factor can be directly related to the joint efficiency, but is a function of slab and subgrade properties. Figure 6-3 illustrates how a given aggregate interlock factor can produce a wide range of joint load transfer efficiencies, depending on the thickness and stiffness of the concrete and the modulus of subgrade reaction. This figure was developed from a data base of over 1000 ILLI-SLAB runs, representing concrete thicknesses from 6 to 32 inches, elastic moduli from 1 to 10 million psi, and subgrade reaction moduli from 50 to 1000.

For the designer, this dependency poses no particular problem since an aggregate interlock factor is chosen by trial and error that results in some standard percentage of the free edge stress for assumed slab stiffness and support conditions. For the evaluator, however, the task of selecting the appropriate aggregate interlock factor is more involved. Each joint has its own unique load transfer efficiency, and each slab has its own unique

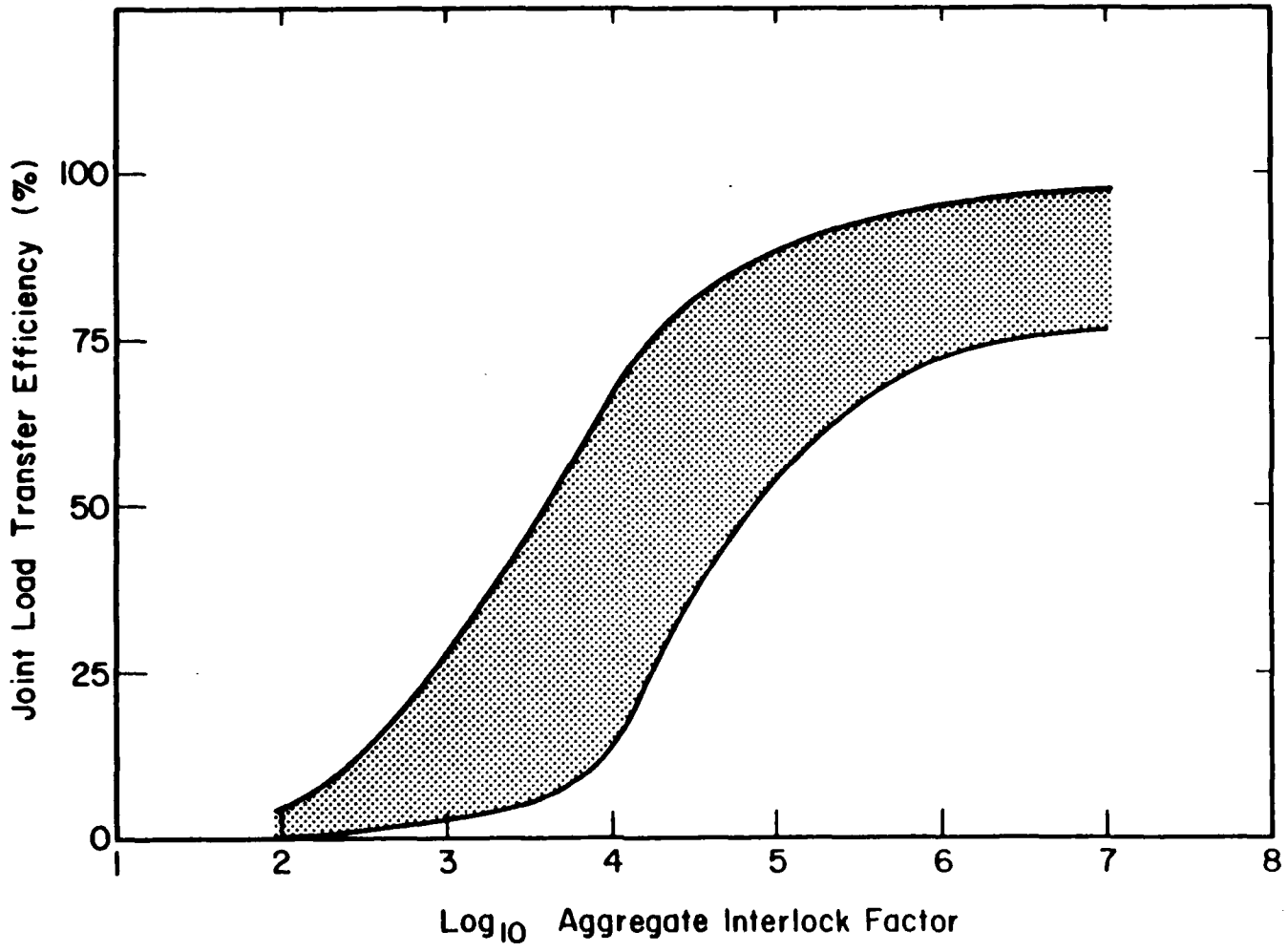

Figure 6-3. The Range of Possible Load Transfer Efficiencies and Aggregate Interlock Factors

combination of dynamic E and k, both measured or backcalculated from FWD loads and deflections. This trial and error selection of the aggregate interlock factor that best models actual joint efficiency is well suited for computer determination.

6.3 Application of Center Slab Dynamic E and k Values to Joints

The techniques presented earlier for backcalculation of dynamic E and k values for each slab were based upon deflection basins generated at the center of the slab. Ideally, of course, it would be desirable to use actual joint measurements for the determination of E, k, and the aggregate interlock factor, but the complexities surrounding support conditions at the joints makes such an undertaking impractical at this point in time. However, if the center slab backcalculated values could be assumed to exist at the joints as well, then selection of the proper aggregate interlock factor is reduced to an iterative computer solution. The impact of making this assumption is much more significant for k than for E. Obviously, making this assumption for k ignores the potential loss of support that can occur at the joint from plastic deformation, pumping, etc. It also ignores the assumed nonexistance of shear across joints in the Winkler foundation. However if this assumption will permit reasonably accurate ILLI-SLAB modeling of the joint's behavior under FWD loads, great confidence can then be placed in the calculated stresses under actual gear loads.

This approach was tested, and a trial and error procedure was used to determine the aggregate interlock factor that would reproduce the FWD-measured load transfer efficiencies. This factor, along with the center slab E and k values and actual FWD load used at the joint, were then reinput into ILLI-SLAB to compare measured with predicted deflections across the

joint. Table 6-1 presents the results of this investigation for a variety of pavement thicknesses and joint load transfer efficiencies, while Figure 6-4 illustrates the high degree of correlation between measured and predicted load transfer efficiencies. This remarkable agreement between measured and predicted deflections, across such a stark discontinuity as a keyed construction joint or dummy contraction joint, further reinforces ILLI-SLAB's ability to accurately model behavior at joints. In addition, these encouraging results fostered the development of an iterative computer scheme to determine aggregate interlock factors for use in calculating the critical stress.

6.4 Iterating to Determine the Aggregate Interlock Factor

The tremendous variation in load transfer efficiency from joint to joint within a single feature, vividly illustrated in Figures 4-13 through 4-22, dictates that the critical stress be calculated for each slab in the field testing program. To facilitate this requirement, an iterative computer solution was developed that utilizes backcalculated slab moduli and the aggregate interlock factor to reproduce the load transfer efficiency measured by the D0 and D1 deflection sensors of the FWD, six inches either side of the joint. The basis upon which the technique was developed is shown in Figure 6-5 and described below.

The load transfer efficiency of a rigid pavement joint with specific thickness and moduli values displays a characteristic S-shape when plotted against the $\log_{10}$ of the aggregate interlock factor. The exact location of that curve within the limits illustrated in Figure 6-3, however, is not known and must be determined from the single load transfer efficiency measured by the FWD. To accomplish this, a nonlinear regression model was developed from

TABLE 6-1. COMPARISON OF MEASURED AND PREDICTED FWD DEFLECTIONS ACROSS LONGITUDINAL AND TRANSVERSE JOINTS

Feature	Slab No.	Load (lbf)	Meas. or Pred.	Sensor Deflections (mils) D0	D1	D2	D3	D4	D5	D6	LTE (%)
Longitudinal Joints											
T04A	1	23182	M	5.3	4.1	3.6	3.2	2.8	2.4	2.0	77
			P	5.6	4.4	3.6	2.9	2.3	1.7	1.1	79
	2	23087	M	4.3	3.9	3.5	3.0	2.6	2.3	1.9	91
			P	4.3	3.9	3.3	2.6	2.1	1.6	1.1	92
	3	22626	M	5.0	4.5	4.1	3.6	3.1	2.8	2.3	90
			P	4.9	4.5	3.9	3.3	2.8	2.2	1.7	92
	4	23071	M	4.3	3.9	3.5	3.0	2.7	2.3	2.0	91
			P	4.2	3.9	3.3	2.7	2.2	1.7	1.2	92
A05B	1	25170	M	9.1	6.0	5.1	4.3	3.6	2.9	2.4	66
			P	8.5	5.7	4.8	4.0	3.2	2.5	1.8	67
	2	22896	M	7.6	7.2	6.3	5.4	4.6	3.9	3.3	95
			P	7.2	6.9	5.8	4.8	4.0	3.2	2.4	95
	3	26871	M	5.7	5.2	4.4	3.9	3.3	2.9	2.5	91
			P	5.5	5.1	4.2	3.4	2.8	2.1	1.5	93
	4	26505	M	8.6	6.9	5.9	5.0	4.3	3.7	3.1	80
			P	8.2	6.9	5.8	4.8	4.0	3.2	2.4	83
A08B	1	23055	M	17.2	10.4	8.5	6.7	5.2	4.1	3.1	60
			P	16.8	10.4	8.1	6.0	4.5	2.9	1.4	62
	2	24136	M	34.1	6.4	5.2	4.3	3.3	2.8	2.3	19
			P	28.1	4.1	3.1	2.3	1.7	1.0	0.4	15
	3	23898	M	22.9	6.7	5.7	4.7	3.9	3.2	2.7	29
			P	22.8	5.9	4.4	3.2	2.3	1.4	0.5	26
	4	22578	M	15.9	14.8	11.9	9.1	6.9	5.4	3.7	93
			P	15.5	14.5	11.1	8.2	6.1	3.9	1.8	94

TABLE 6-1. (continued)

Feature	Slab No.	Load (lbf)	Meas. or Pred.	Sensor Deflections (mils) D0	D1	D2	D3	D4	D5	D6	LTE (%)
				Transverse Joints							
T04A	1	23914	M	6.2	4.0	3.5	3.2	2.8	2.5	2.1	65
			P	6.1	4.0	3.3	2.7	2.2	1.7	1.2	65
	2	26537	M	5.0	3.4	3.0	2.7	2.3	2.0	1.7	68
			P	5.0	3.5	2.9	2.4	2.0	1.5	1.1	69
	3	25520	M	4.5	4.1	3.8	3.5	3.1	2.8	2.6	91
			P	5.2	4.8	4.1	3.5	2.9	2.4	1.9	93
	4	25726	M	8.7	2.2	2.0	1.9	1.5	1.4	1.3	25
			P	8.6	2.2	1.8	1.4	1.1	0.9	0.6	25
A05B	1	25631	M	11.9	3.4	3.1	2.7	2.4	2.1	1.8	29
			P	11.7	3.0	2.5	2.1	1.7	1.3	0.9	26
	2	25138	M	7.7	7.0	6.0	5.2	4.5	3.8	3.3	91
			P	7.5	6.9	5.9	5.0	4.2	3.4	2.6	92
	3	25106	M	6.7	4.3	3.8	3.3	3.0	2.6	2.2	64
			P	6.8	4.4	3.6	3.0	2.4	1.8	1.2	64
	4	25822	M	8.1	7.3	6.3	5.4	4.5	3.9	3.3	90
			P	8.3	7.6	6.4	5.3	4.3	3.4	2.5	92
A08B	1	24359	M	11.6	11.4	9.3	7.5	6.3	4.8	3.8	98
			P	12.2	11.6	8.9	6.7	5.0	3.3	1.6	95
	2	23580	M	13.8	13.4	11.2	9.2	7.1	5.9	4.6	97
			P	14.1	13.5	10.4	7.7	5.8	3.8	1.9	95
	3	25615	M	12.5	11.8	9.7	7.6	5.9	5.0	4.2	94
			P	13.0	12.3	9.4	6.9	5.1	3.3	1.5	95
	4	23739	M	25.7	8.6	7.3	6.2	5.1	4.4	3.6	33
			P	23.1	7.0	5.4	4.0	2.9	1.9	0.8	30

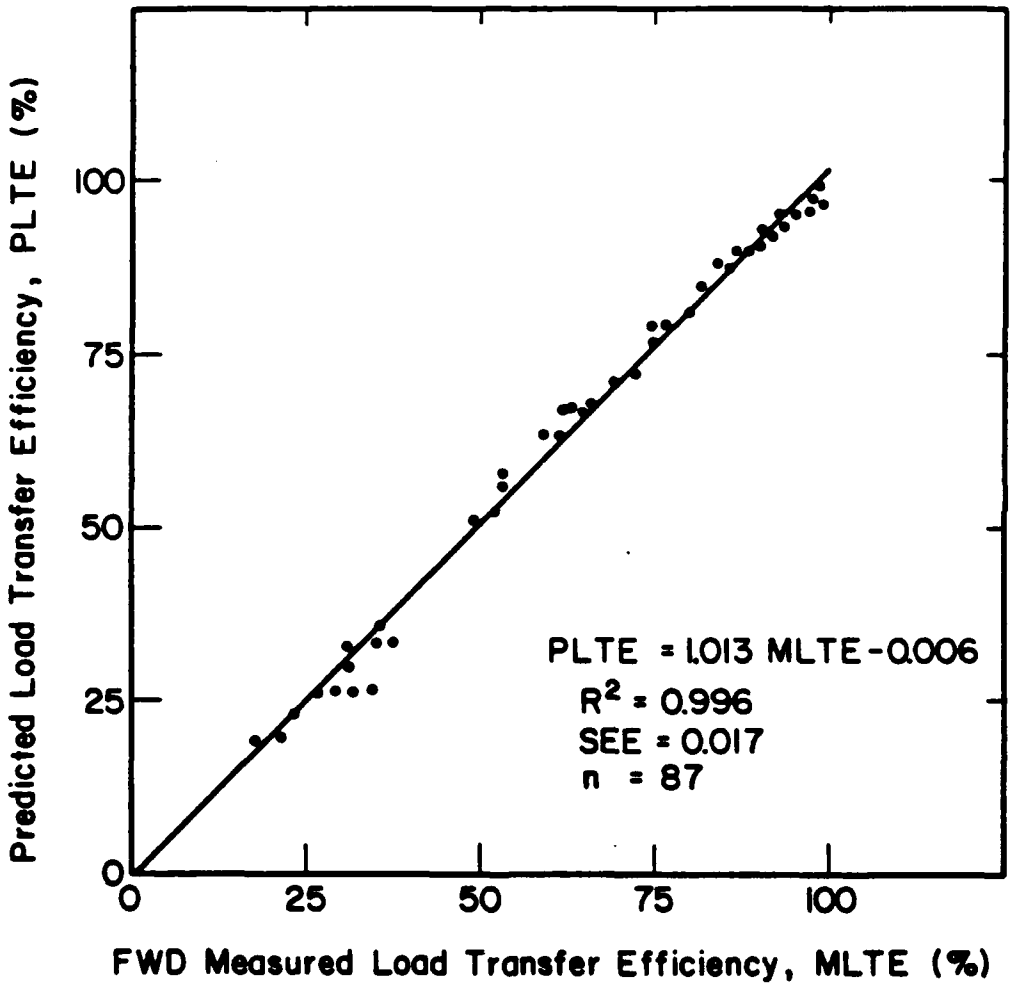

Figure 6-4. Measured Versus Predicted Joint Load Transfer Efficiencies

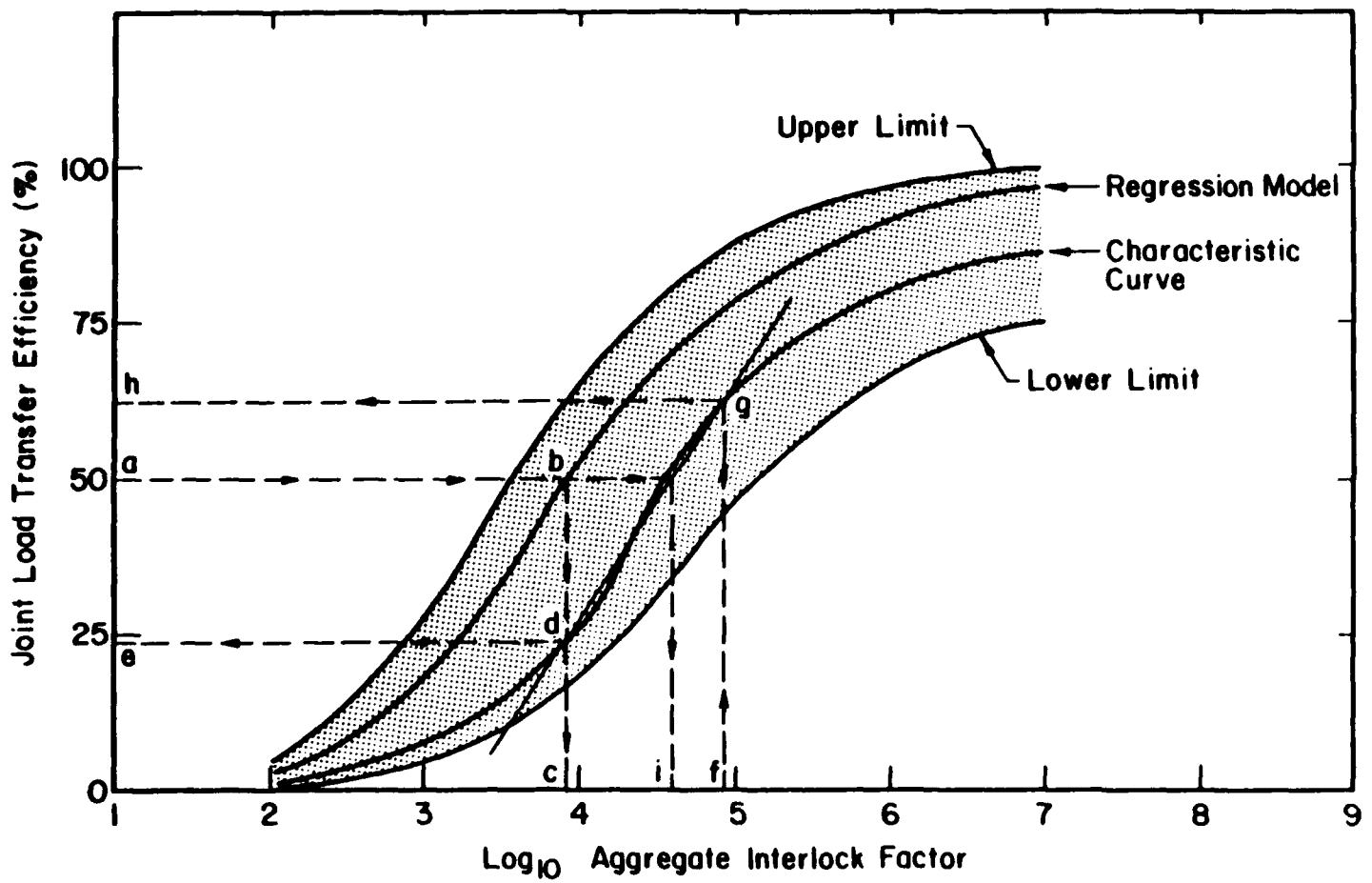

Figure 6-5. The Iterative Solution for the Aggregate Interlock Factor

the load transfer efficiency-aggregate interlock factor data base discussed in Section 6.2. This model provides a starting point for the iterative scheme by predicting a rough approximation of the aggregate interlock factor (Point c) from the measured load transfer efficiency (Point a). This factor is then input to ILLI-SLAB which calculates a load transfer efficiency (Point e) for that particular factor from the joint's characteristic curve at Point d. Depending on the position of Point e from Point c, one order of magnitude is either added to (Point f) or subtracted from Point c and reinput to ILLI-SLAB to calculate a new load transfer efficiency (Point h), again from the joint's characteristic curve (Point g). The line d-g can now be used to calculate Point i, the proper aggregate interlock factor for the measured load transfer efficiency at Point a. The straight line approximation of the S-shaped curve can introduce slight errors into the final result, particularly at higher load transfer efficiencies where curvature is greatest. Fortunately, load transfer efficiencies become less sensitive to the aggregate interlock factor in this region, and predicted deflections at the joint are relatively unaffected.

The results of this analysis will provide the appropriate aggregate interlock factor that, for a specific slab thickness, E, and k, will give the correct load transfer efficiency across the joint.

6.5 Calculating the Critical Stress

Calculation of the critical stress developed under the gear of an aircraft at any given time combines the procedures and techniques described in Chapters 3 through 6. The complete response of the rigid pavement slab to prototype loads is first determined by FWD testing at the corner, center, and transverse and longitudinal joints. The center slab deflections are then

used to backcalculate the dynamic elastic concrete modulus and modulus of subgrade reaction. Next, the these center slab moduli are transferred to each joint where load transfer efficiencies for any temperature can be used to calculate aggregate interlock factors. Finally, all three of these unique slab characteristics are input to the ILLI-SLAB finite element program, along with the gear weight and configuration of the desired aircraft, to calculate the maximum tensile stress generated at the bottom of the slab. The next chapter will describe how these critical stresses can be related to the field performance of the slab.

CHAPTER 7

RELATING CRITICAL STRESS TO PERFORMANCE

The precise determination of the critical stress at the bottom of a concrete slab due to a specific aircraft load and set of environmental conditions would merely be an academic exercise if it could not be related to the anticipated field performance of the slab. Only through this relationship, or transfer function as it is commonly referred to, can projections of remaining pavement life be made. Up to this point, strictly mechanistic concepts have been employed, with the exception of the dynamic k to describe support conditions, in the evaluation of rigid pavements. Unfortunately, this idealistic approach must now be tempered with empirical procedures to reach the objective, simply because all the factors affecting pavement performance can not be separately accounted for. This chapter will focus on the development of the transfer function, with emphasis on its empirical components of concrete flexural strength, fatigue damage, accelerated traffic testing, and pass per coverage ratio.

7.1 The Fatigue Damage Concept

The performance of many materials subjected to repeated loadings below ultimate static strength levels can often be described by some functional relationship between the repeated tensile stress or strain and the number of load applications to failure. For concrete paving materials, this "fatigue approach" frequently relates the maximum tensile stress/static flexural strength ratio to the $\log_{10}$ of the number of applications of load. Figure 7-1 depicts this concept for a variety of cemented materials.

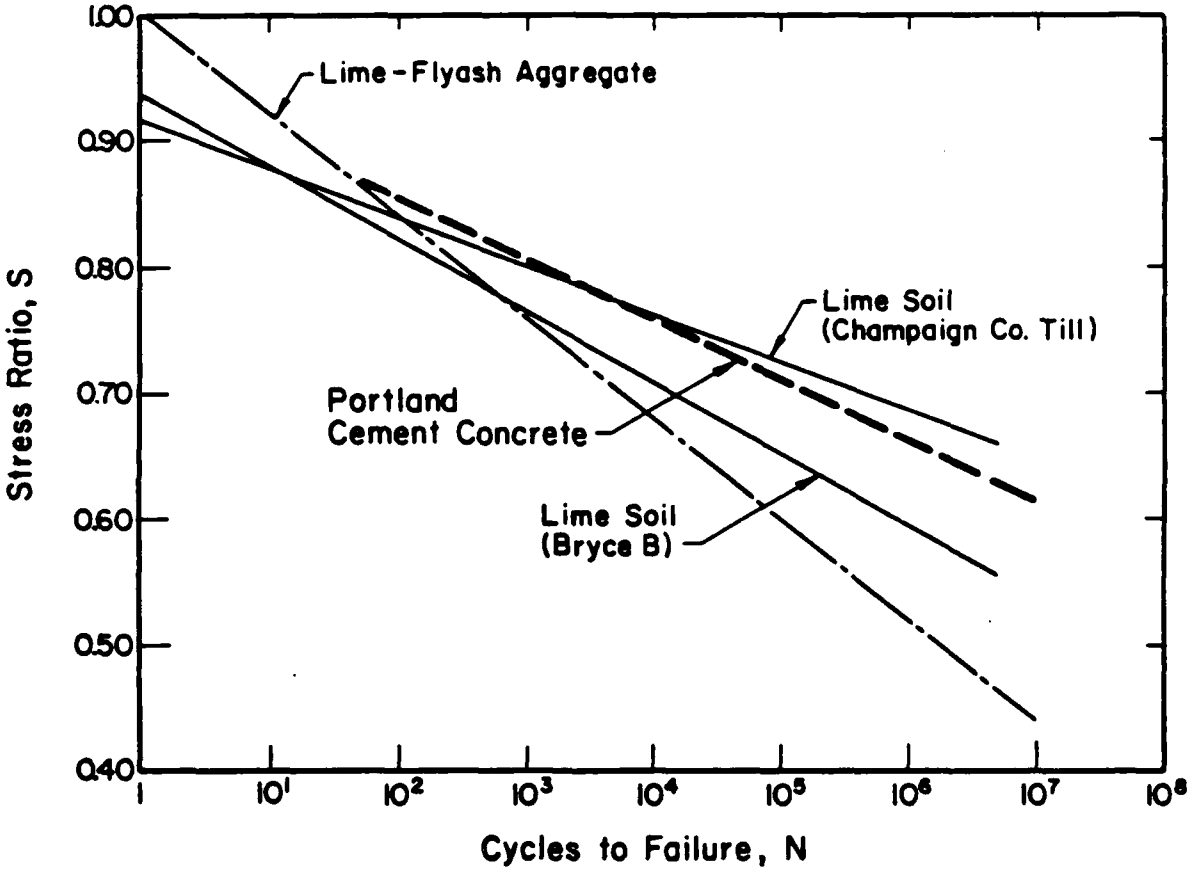

Figure 7-1. Flexural Beam Fatigue Response Curves for Various Cemented Materials (38)

The volume of research into the fatigue of concrete materials has truly been prolific, and is of interest in this research in selecting the basis for the transfer function. In his review of published investigations on concrete fatigue, Nordby (39) includes over 100 pertinent publications, beginning with the work of Considere and DeJoly in 1898. He summarizes many important findings pertaining to laboratory testing of specimens, but concludes that "research on the fundamental properties of concrete fatigue to describe the mechanism of fatigue failure may be particularly fruitful." The American Concrete Institute (ACI) review (40) contains 114 bibliographical entries and concludes by stating, "the most important need at the present is an understanding of the mechanism of fatigue in concrete." Murdock's review (41) of previous investigations of the fatigue behavior of plain concrete makes frequent reference to the use of statistics to confirm test results and adequately describe fatigue failure. Finally, Ople and Hulsbos (42) conclude that "there seems to be no knowledge as to whether or not the fatigue characteristics of one-dimensional, simply supported test systems can be translated directly to structural systems, such as fully supported pavement slabs."

Despite the lack of understanding of the mechanisms of concrete fatigue, even in the highly controlled laboratory environment, the results of laboratory fatigue studies on concrete beams have been employed by various investigators (45,46) for development of design procedures for rigid pavements. The reason for doing so is simple: it's the best information available, particularly when dealing with the number of load applications appropriate for highway design. Efforts have been made by other researchers (47,48,49) to analyze results of the AASHO Road Test performance data for use in design. These efforts at least attempt to incorporate actual field

performance of concrete slabs into the design, but may be significantly influenced by special modes of failure, such as pumping, that are not highly relevant to rigid airfield pavements. A graphical representation of several of these models was made by Darter (45) and Majidzadeh (50) and is presented as Figure 7-2.

The wide disparity in the models for stress ratios below 0.60 and above 0.70 in this figure can be explained by differences in the source of the data, the procedures for counting stress repetitions, the method of analysis used in calculating stresses, and the definition of failure. For example, the PCA curve represents a lower bound of laboratory test results and assumes a fatigue limit at the 0.50 stress ratio. A stress repetition is counted each time the beam is loaded, and the stress is calculated from simple bending equations. Failure occurs when the beam fractures. Darter's curves are 25th percentile probabilistic fatigue failure models based on the results of 140 laboratory beam tests conducted by three researchers and reported in References 39, 51, and 52. The ARE curve is based on the road test data using elastic layered theory to compute fully supported mid-slab stresses and AASHO equivalency factors to account for mixed traffic. A stress repetition occurred with each tandem axle pass, and failure was based on a Present Serviceability Index (PSI) of 2.5. The USAF curve is based on full scale, accelerated traffic tests of rigid airfield pavements where one coverage is equated to one load application. The analysis was based on plate theory with a 25 percent reduction in edge stress for load transfer, and failure was defined as 50 percent of the slabs exhibiting an initial crack. The Vesic model was developed by analyzing the AASHO road test data using Westergaard plate theory to determine stresses, but two repetitions were counted for each pass of a tandem axle. Finally, the RII model uses plate theory on an

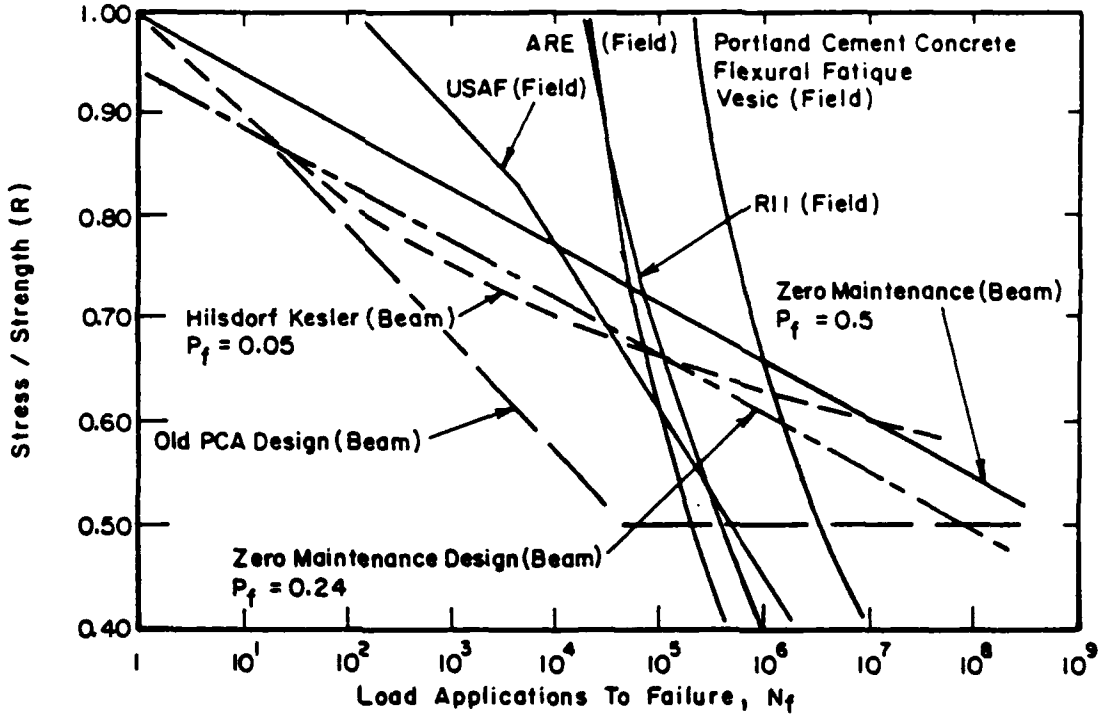

Figure 7-2. Summary of Various PCC Fatigue-Based Design Models Using Laboratory Beams and Accelerated Full-Scale Tests (50)

elastic solid foundation and incorporates load placement effects, slab geometry, and materials properties into the analysis.

With such a broad spectrum for analyses, it is not surprising to find this large discrepency in the available models. Darter (45) presents a thorough discussion of the difficulties in relating laboratory fatigue analysis to fatigue of actual slabs under field conditions. He concludes by stating that "the complexities are so great and available information so limited that any laboratory curves used to estimate fatigue damage in field slabs must be calibrated based on field data."

Two primary conclusions can be drawn from this review of concrete fatigue and performance research. First, our knowledge of fatigue mechanisms is not sufficient enough at present to warrant any basis other than empirical, full scale field testing for the development of the critical stress/flexural strength/pavement performance relationship. Although the most controlled full scale tests have certain shortcomings that cannot be avoided, the effects of the environment, construction deficiencies, material variations, loading conditions, and slab geometries just cannot be properly modeled by 6 x 6 x 24 inch, unsupported laboratory beams.

Second, it is imperative that the methods of testing, analysis, and model development be consistent. If testing is accomplished at mid-slab and stresses analyzed at mid-slab with elastic layered techniques, then the performance curve must be based on an elastic layered analysis of the loads imparted at mid-slab. Similarly, if joints are to be tested and analyzed with finite element techniques, then the transfer function must be based on that same finite element analysis of the original full-scale traffic data.

These two fundamental conclusions have guided the development of a "field performance" curve based on full scale, accelerated traffic tests conducted

over a thirty year period that have been completely reanalyzed using the ILLI-SLAB finite element model.

7.2 Nondestructive Determination of Slab Concrete Flexural Strength

One of the most fundamental, but often underemphasized, elements of the transfer function is the flexural strength of the concrete. This essential property shares an equally important part with the critical stress in the determination of the stress ratio, yet is often erroneously assumed from design specifications or laboratory-cured 28 day specimens. Several consistent conclusions have been reached by many investigators concerning the flexural strength of concrete. These have been summarized by Nordby (39) and Murdock (41) as follows:

1) The order in which varying load levels are applied can affect the flexural strength. Higher loads applied before lower ones is more detrimental than vice versa.

2) Rest periods between load applications serve to increase flexural strength.

3) Inadequately aged or cured specimens produce lower strengths.

Since this preponderance of evidence suggests that use of laboratory beam flexural strength test results to describe the in situ strength of field cured and loaded pavement slabs is unjustifiable, a more consistent approach was adopted that would utilize FWD-generated test results for flexural strength as well as moduli determination.

The determination of the flexural strength of existing concrete slabs has traditionally centered around the correlation of compressive or split tensile strengths of six inch diameter core samples with the flexural strength of

field cured, cast or sawed beams. Hammitt (8), Narrow and Ullberg (43), and Greer (44) each report similar straightline correlations of the form

$$FS = ST + b \tag{7.1}$$

where FS equals the flexural strength, ST equals the split tensile strength, and b ranges between 150 and 250. Hammitt's equation

$$FS = 1.02\ (ST) + 210 \tag{7.2}$$

has been used by the Air Force for a number of years and represents a "middle of the road" correlation.

In an effort to establish the flexural strength of pavement slabs nondestructively, one to three core samples were extracted from nine of the ten test locations at Seymour-Johnson AFB, and returned to the AFESC laboratory for split tensile testing. This was done with the hope that a correlation could be found between the backcalculated dynamic elastic modulus and the flexural strength, utilizing the existing split tensile-flexural strength relationship. Obviously, a direct correlation is preferred, but the testing program required to develop such a relationship was beyond the scope of this research.

Table 7-1 presents the results of this split tensile testing and the correlation to flexural strength. In addition, the average backcalculated dynamic elastic moduli for each feature is shown, along with the number of slabs tested. The data in Table 7-1 are plotted in Figure 7-3 and suggest that a straight line fit is appropriate, at least for the limited number of data points available. The resulting equation is:

TABLE 7-1. DEVELOPMENT OF THE CORRELATION BETWEEN THE BACKCALCULATED DYNAMIC E MODULUS AND CONCRETE FLEXURAL STRENGTH

Feature	AFESC Core No.	Split Tensile Str. (psi)	Estimated Flexural Str. (psi)	Backcalculated E for Test No. (10^6 psi) 1	2	3	4	5	E_{avg} (10^6 psi)
R06C	94	354	571	1.74	1.88	1.85	1.64		1.78
	93	507	727	5.33	5.03	4.64	5.72	6.51	5.44
R09C	100	493	713	3.14	3.07	2.62	2.97		2.95
	99	415	633	2.72					2.72
T01A	141	401	619	4.89	3.38	2.98	3.71	4.18	3.83
T03A	41	488	708	5.09	5.09				5.09
	42	347	564	2.52					2.52
	43	406	695	4.98					4.98
T05A	39	537	757	5.74	5.75				5.75
T07A	153	472	692	4.16	6.40	3.72	4.42		4.67
A11B	12	520	740	6.14	5.28				5.71
	13	425	644	3.78	4.01				3.90
A12B	5	344	561	2.98					2.98

Note: The flexural strengths were obtained from the split tensile strengths using Equation 7.2.

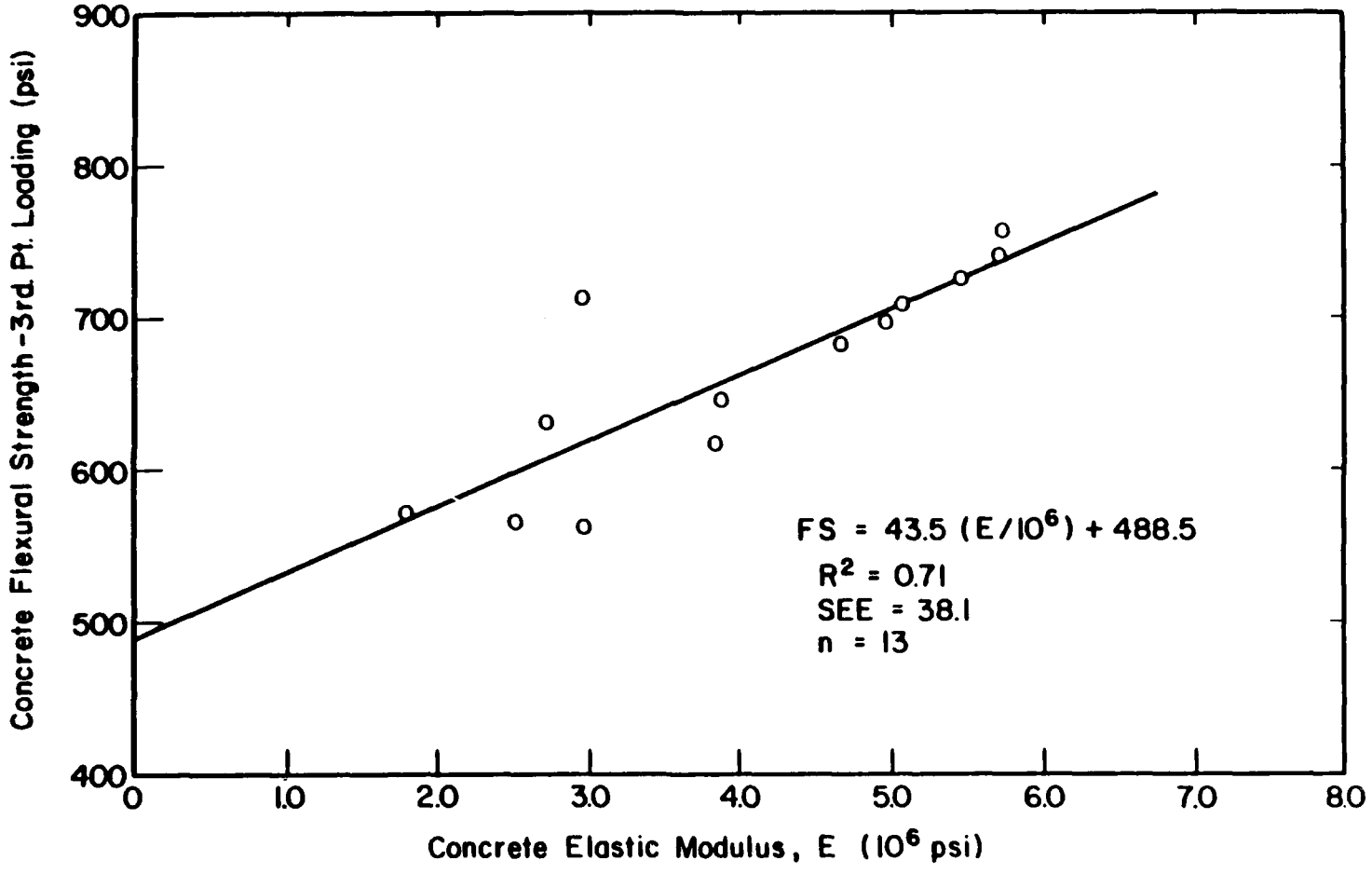

Figure 7-3. Determination of the Concrete Flexural Strength (3rd Point Loading) from the Backcalculated FWD Dynamic E Modulus

$$FS = 43.5\ (E/10^6) + 488.5 \qquad (7.3)$$

$R^2 = 0.71$
SEE =38.5

The above relationship yields reasonable flexural strengths for FWD-measured dynamic E values, and eliminates the last element of destructive testing involved in rigid pavement evaluation. Additional research is needed to verify the equation for a wider range of values, but the approach appears to be reasonable. It must be pointed out that, for the first time in the NDT & E process, static and dynamic stress modes have been interrelated; a dynamic FWD load and backcalculated dynamic E are being used to determine a static flexural strength. Normally, this is undesirable from a theoretical standpoint, since material behavior is quite different for each. However, as will be shown later in the chapter, this practice is consistent with the analysis used in the full scale, accelerated traffic tests where moving gear loads are producing dynamic stresses, but are being compared to statically determined flexural strengths.

7.3 Performance Criteria

Historically, performance criteria for design and evaluation of rigid pavements have been based on limiting the tensile stress in the PCC slab to levels such that failure occurs only after the pavement has sustained a number of load repetitions, usually the total projected for a twenty-year design life. This reasonable approach for design is accomplished by increasing concrete thickness, flexural strength, or subgrade support; in evaluation, it is done by restricting the loads placed on the pavement. As was seen in Section 7.1, however, calculating this critical stress and then relating it to some measure of performance can take many different avenues.

For the performance criteria developed in this report, the basic data will be obtained from test pavements subjected to controlled, simulated, and accelerated aircraft traffic. The following discussion outlines the specific criteria selected for this study.

7.3.1 The Strength Over Stress Ratio

For the remainder of this report, the ratio of the slab's flexural strength to its critical stress will be used in the field performance curve. The inverse of the traditional stress ratio, this "evaluation factor" has been used in several design and evaluation methodologies because it yields a straight line relationship when plotted against the $\log_{10}$ of coverages for the accelerated traffic tests. The U.S. Air Force (53) curve uses this ratio with the critical stress calculated from Westergaard's edge stress equation and then reduced by 25 percent for load transfer. The FAA (54) proposed curve utilizes interior stress from elastic layered procedures as the denominator in the ratio. ERES Consultants (36) have developed a similar curve based on a reexamination of the accelerated traffic test data using ILLI-SLAB-calculated free edge stresses, reduced by 25 percent for load transfer.

7.3.2 Coverages

The early researchers into design and evaluation of airfield pavements recognized that simply counting the number of aircraft using an airfield facility was not an adequate means of accounting for stress repetitions. Unlike highway pavements where wheel loads are highly channelized and axle configurations nearly identical, airfield pavements are subjected to a variety of gear configurations and lateral distributions of the loads. As a

result, the term coverage was introduced to reflect, in a single number, the collective influence of these and other factors on pavement performance.

Because of the vastly different mechanisms by which flexible and rigid pavements transmit loads to the subgrade, two distinct definitions of tne term "coverage" are necessary. For flexible pavement, one coverage of the feature occurs when every point on the pavement's surface over the full width of the traffic lane has received one maximum stress application. For rigid pavements, a coverage occurs when every point within the concrete slab has received one maximum stress application over the full width of the traffic lane. The distinction is made because of the overlapping of stress bulbs that occurs within the full depth of rigid pavement slabs, thus producing only a single maximum stress repetition, even for tandem gears.

This method of accounting for the total number of maximum stress applications was used in each of the full-scale tests. Traffic on the test sections was programmed so that adjacent wheel paths touched but did not overlap, thus allowing an accurate determination of the coverage levels. Obviously, some damage must have resulted at the point of maximum stress application from adjacent wheel paths, but only an extensive analysis based on Miner's damage law could reveal the extent. The Corps of Engineers merely reported the total number of passages of the load cart over the center wheel path of the traffic lane as the coverage level at failure. These reported coverage levels at failure are used in the transfer function developed herein.

7.3.3 Initial Crack Failure

The selection of the point at which the pavement has reached a failed condition is probably the most subjective aspect of the entire evaluation

process. As was pointed out earlier, failure can be based on a visual observation of crack development, upon ride quality, or any number of other schemes. For ease of determination during field tests and for simplicity of analysis, however, the "initial crack failure" criteria has been the standard for design and evaluation of rigid pavements for many years, and will be used for this evaluation methodology as well. It must be emphasized that "initial crack failure" refers to the first appearance of a load-associated crack at the surface of the slab, rather than initiation of a crack at the bottom of a slab. Failure of an entire feature occurs when 50 percent of the slabs have sustained a load associated crack.

Frequently, slabs are tested until shattered (4-6 pieces) or complete (30-35 pieces) failure levels are reached, recognizing that an initial crack does not constitute functional failure. The analysis of these slabs and the stresses that are occurring within each piece, however, would be extremely difficult with modern numerical techniques and impossible with plate or elastic layered theory. Predictions of remaining life to a shattered failure condition have been attempted, but are highly dependent on the strength of the supporting material and other factors peculiar to the test conditions. Initial crack failure criteria provides the most accurate basis for analysis and prediction of remaining life, and serves to indicate the point at which preventative maintenance techniques must be programmed if the remaining life of the pavement is to be extended.

7.4 The Full-Scale Accelerated Traffic Tests

The best information available on the performance of rigid pavements under aircraft loads comes from the full-scale test sections constructed by the Corps of Engineers between 1943 and 1973. These sections were built and

tested under very controlled circumstances at several locations in Ohio and at the Waterways Experiment Station (WES) in Vicksburgh, Mississippi. In addition to obtaining specific information on the thickness requirements of PCC slabs to support increasingly heavy military aircraft, these sections gave researchers the opportunity to evaluate the performance of several types of longitudinal and transverse joint load transfer systems.

A complete description of each test, including the design and construction of the test section, the load cart trafficking procedures, and the data collection program, is contained in References 55 through 67 and will not be presented here. Parker and Gunkel (54), however, provide a concise summary of these full-scale tests, including their strengths and limitations, which will be discussed briefly.

7.4.1 Strengths and Limitations

Although the major details of the tests were different, such as construction procedures, geographic locations, joint types, and loads, the entire range of conditions that might be experienced by a pavement were by no means covered. This fact should be recognized, but should not prevent their use in developing a general evaluation procedure.

Second, although the volume of data is substantial, it is not sufficient to define the complex relationships that undoubtedly exist. The use of data from actual tests permits a number of factors to be considered indirectly, and the resulting performance relates to the entire pavement system rather to a specific component.

Third, the accelerated traffic tests were conducted over short periods of time and the detrimental effects of exposure to the environment are not experienced. However, the beneficial effects of time, such as PCC strength

gain, are not considered either, and it is felt that the beneficial and detrimental time effects may counterbalance each other to some extent. This same counterbalancing effect may also apply to the quality of the construction. The variability normally introduced at the start of daily activities on large jobs was probably offset to some degree by the extensive manual labor and quality control required on these small sections.

Fourth, the uniqueness of each slab, or the lack of replication in the design of the test sections, prevents an independent estimate of the pure error in any statistical analysis of the data. Many of the test items contained 2, 3, or 4 slabs and would have been sufficient for the estimate of pure error if only center slab conditions were considered. The desire to test many different joint designs simultaneously, however, rendered each slab unique when analyzing the critical stresses at the joints. Therefore, each slab must be assumed to represent an average failure condition.

Finally, the volume of traffic applied to the test pavements is small when compared to the volume being experienced by modern airport facilities. At the time of these tests, however, the coverage levels applied were typical of those expected in a 20-year design life. In addition, the cost of applying large amounts of traffic was prohibitive. The net result is the requirement to extrapolate the low volume data to the current and projected high levels, a practice that is subject to error.

In summary, the use of full-scale accelerated traffic test data has certain disadvantages which undoubtedly compromise the validity of the remaining life projections being attempted. But until the results of 25 to 30 years of extensive pavement performance monitoring under a wide variety of traffic, environmental, geological, and geometrical conditions can be

completed, this alternative appears to be the only one that is generally applicable and implementable.

7.4.2 Characterization of Individual Test Slabs

The full-scale, accelerated, simulated traffic tests were made up of over 75 distinct test items grouped into 8 separate projects. Each item generally contained several slabs of constant base course and PCC thickness, material types, and reinforcement, and each was trafficked to failure by applying a number of coverages of a simulated aircraft gear load. The progress of the tests was recorded by periodic mapping of crack development in each slab, and the initial crack failure coverage level established when the slab was divided into two pieces by a load associated crack, as opposed to a curling or shrinkage crack. The entire item was deemed failed when 50 percent of the slabs were divided into two or more pieces. This coverage level has been used in the Air Force and proposed FAA design algorithms to relate the stress ratio to the number of coverages to failure.

During the preliminary stages of the reanalysis of this data, however, it quickly became apparent that each individual slab, rather that each test item, would require separate analysis. The desire on the part of the Corps of Engineers to test the performance of several joint types within each item resulted in individual pavement slabs with unique characteristics. The effect of the joint types and their load transfer efficiencies, ignored in previous analyses, must now be considered. Thus, nearly 150 distinct test slabs of plain jointed concrete were identified for ILLI-SLAB analysis, with each slab requiring a separate determination of load transfer efficiency at all four joints. Similarly, the coverage level at first crack had to be

interpreted from crack development maps that were generated at seemingly random intervals.

To compile the needed information, data contained in the original reports (References 55 through 67) were extracted for each slab and recorded onto the specially designed data form shown in Figure 7-4. Arriving at final values for the material properties was fairly straightforward. Slab dimensions and joint types were taken from the test section layout plans. PCC thicknesses were determined by averaging the lengths of core samples taken after completion of the load cart testing. Flexural strengths were obtained from the most representative data available. Generally, 28 and 90 day laboratory-cured beam strengths were reported, but field-cured, sawed or cast six-inch beam strengths were used whenever possible. These same beam specimens were also used to determine static elastic modulus and sonic dynamic modulus of each concrete slab. And finally, subbase and/or subgrade support conditions were determined by static plate load tests performed after completion of the trafficking.

The determination of the performance of the four joints in the slab, however, was very subjective in nature. In most instances, deflection guages on both sides of the joint were used to record load transfer information at sporadic intervals as the load cart rolled from the approach slab to the leave slab. These guages were placed only at selected joints, and no temperature information was reported. As a result, only average load transfer efficiencies could be calculated for each joint type and for the entire range of temperatures encountered during testing. In those cases where no load transfer information was available, estimates of typical efficiencies for specific joint types were made based on previous Corps of Engineers experience reported by Rollings (68).

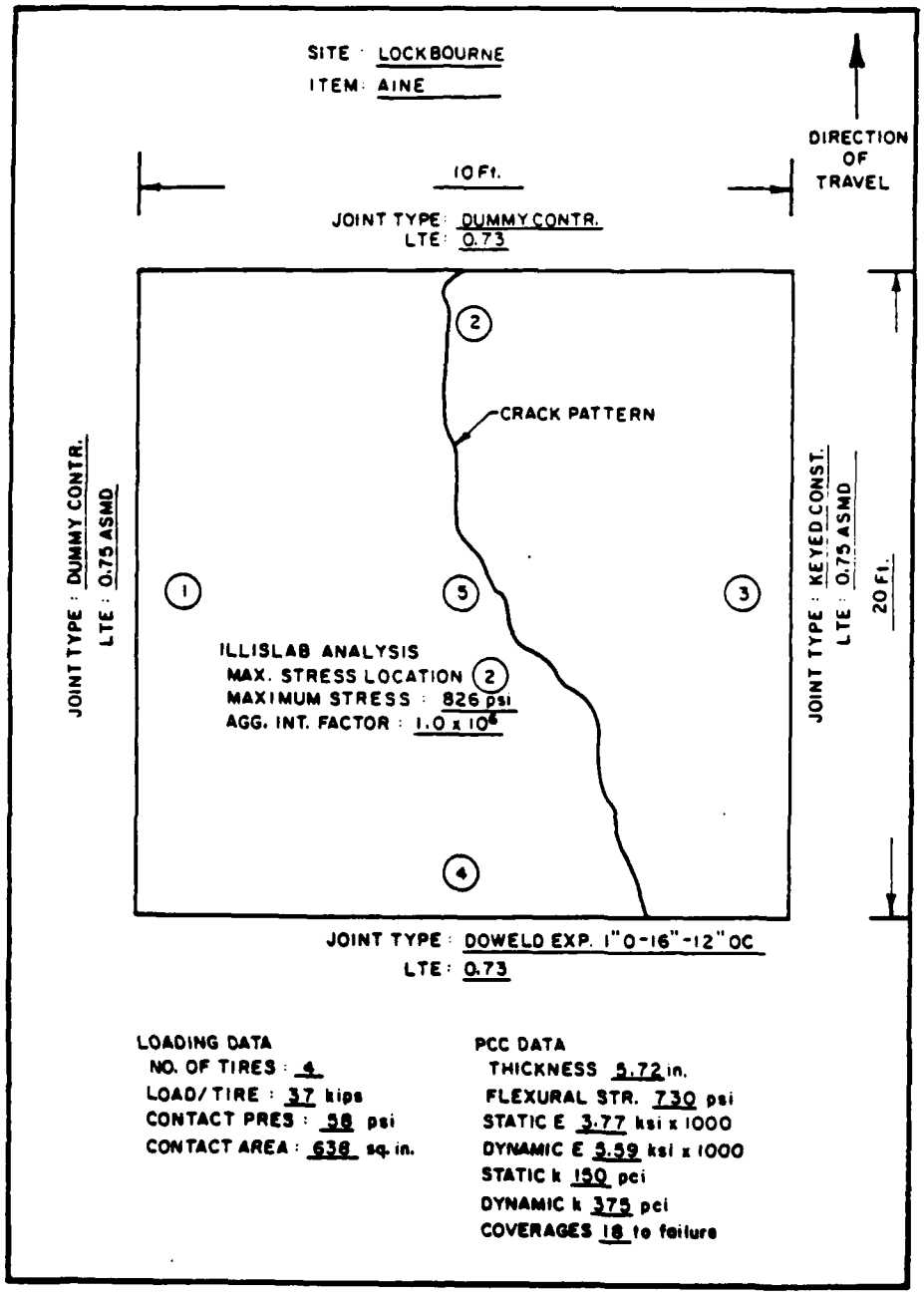

Figure 7-4. Typical Data Sheet for Reanalysis of Accelerated Traffic Test Results

Specific information was available on the load cart configurations used for each item. The number and spacing of the wheels, the load on each individual tire, and each tire's pressure and contact area were precisely measured and recorded. Finally, the propagation of the initial load crack was followed closely from the crack pattern development maps to verify the location of the critical stress point in the slab for the given loading conditions and traffic pattern.

7.4.3 ILLI-SLAB Analysis of the Original Test Data

The analysis of the full-scale test slabs using the ILLI-SLAB finite element model was considered crucial to the development of a consistent rigid pavement evaluation methodology based on dynamic FWD measurements. In keeping with this policy, dynamic elastic moduli and subgrade reaction moduli were chosen to represent the material properties of each slab under the moving loads applied during the original tests. Without the benefit of FWD testing to backcalculate these properties, however, use was made of the best information available. In the case of dynamic elastic moduli, the sonic modulus of the concrete, measured after completion of the trafficking, was used. These sonic values are very similar to the backcalculated values from FWD measurements of typical concrete slabs at Sheppard and Seymour-Johnson AFB's, and are believed to be reasonable estimates of FWD-generated dynamic moduli.

The dynamic modulus of subgrade reaction for each slab was determined through a correlation between static plate bearing moduli and backcalculated FWD moduli. This correlation was developed from a limited number of side by side tests at Seymour-Johnson and Sheppard AFB's and at McDill AFB in Tampa,

Florida. Table 7-2 presents the data, while Figure 7-5 illustrates the relationship described by the following equation:

$$k_{dyn} = 117.1 \times \log_e k_{sta} - 211.8 \qquad (7.4)$$

$$R^2 = 0.72$$
$$SEE = 46.8$$

Again, although based on only seven data points, the correlation appears to give reasonable values of dynamic subgrade modulus. Obviously, additional testing is required to verify this model for a variety of support conditions, but Equation 7.4 at least provides a foundation upon which to start. This same model will be used in Chapter 8 to permit the static analysis of pavement features, such as aircraft hardstands, where a dynamic analysis is not appropriate.

The final parameter needed for a complete analysis of the critical stress in each of the test slabs is the aggregate interlock factor that will reproduce the load transfer efficiency assumed earlier for the joint where cracking initiated. Unfortunately, this factor could only be determined by trial and error, but once resolved, results of the stress analysis at each joint were in near unanimous agreement with the observed location of crack initiation: the highest stresses were found at those joints where the cracks actually started. This evidence further substantiates the validity of the ILLI-SLAB model and, as will be shown in the next section, increases the precision of the transfer funtion when compared with Westergaard or elastic layered analyses.

TABLE 7-2. DEVELOPMENT OF THE CORRELATION BETWEEN THE PLATE BEARING-DERIVED STATIC k MODULUS AND THE FWD-DERIVED DYNAMIC k MODULUS

Installation	Feature	Static k (pci)	Dynamic k (pci)
Mc Dill	A-1-A	80	315
	1-A-1	85	375
	T-33	230	450
Sheppard	A08B	65	209
Seymour-Johnson	T05A	250	409
	T07A	180	404
	A23B	240	410

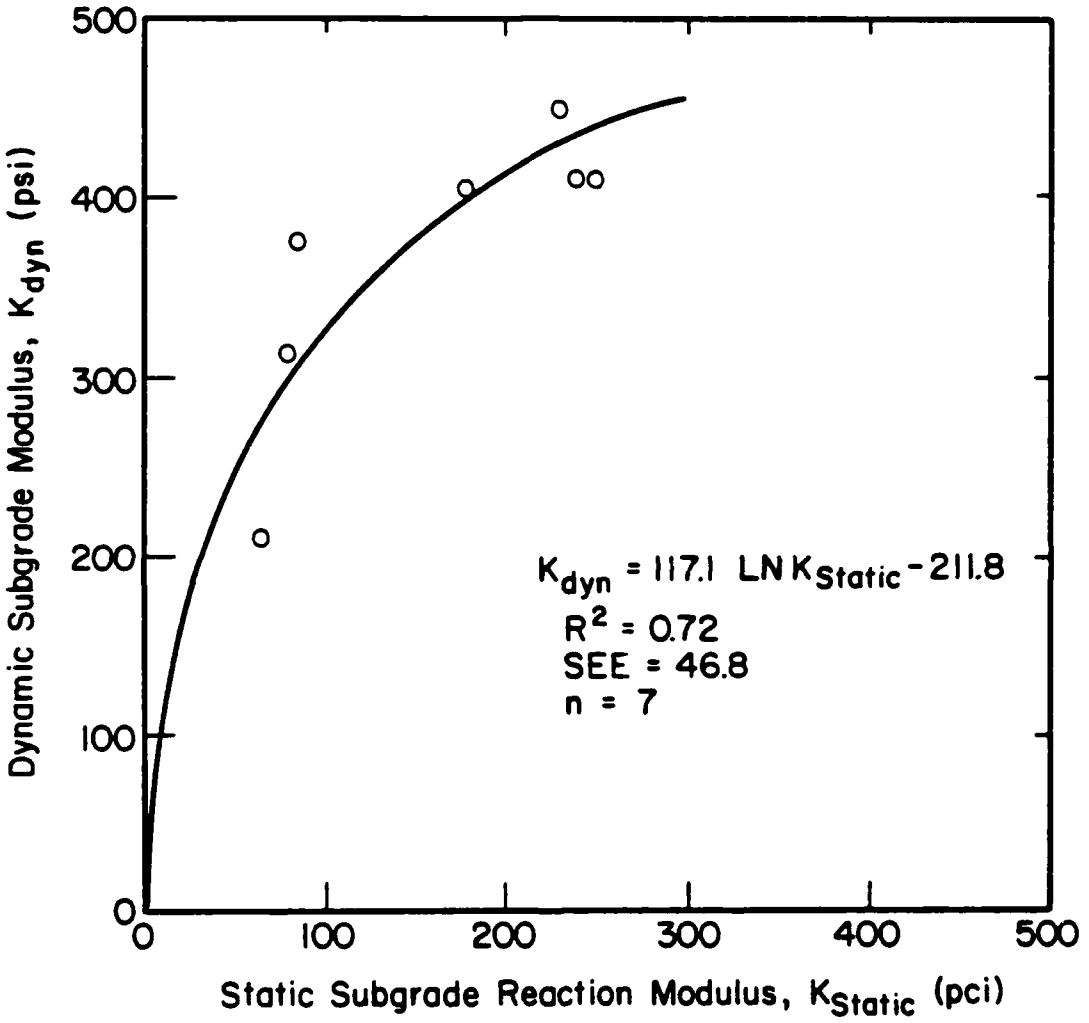

Figure 7-5. Relationship Between the Conventional Static k Modulus and the Backcalculated FWD Dynamic k Modulus

7.5 Developing the Field Performance Curve

With all of the empirical components of the field performance curve firmly established, the flexural strength of each slab was divided by the critical stress at the appropriate joint in each slab to determine the "evaluation factor." This factor was then paired with the $\log_{10}$ of the coverage level for each slab to produce the points shown on Figure 7-6. A simple least squares, linear regression was then fit through the data using the SPSS computer program. The following equation resulted:

$$\text{Log}_{10}\ \text{COV} = 1.323 \times (\text{FS/CS}) + 0.588 \qquad (7.5)$$

where COV = Coverages to Initial Crack Failure
FS = Flexural Strength
CS = Critical Stress
R^2 = 0.64
SEE = 0.52

A comparison of this field performance curve with other relationships developed from the same original test sections is shown in Figure 7-7. The wide disparity among curves comes about for several reasons. First, the basis upon which the critical stress is calculated is different for each curve. The line labeled Darter #1 is based on an ILLI-SLAB analysis of free edge stress for an entire item, reduced 25 percent for assumed load transfer. The Darter #2 line is an ILLI-SLAB analysis of interior stress for 138 individual slabs. The Parker curve is an elastic layered analysis of interior stresses, as is the Witczak curve. Second, the flexural strengths used in the Darter #1, Witczak, and Parker curves were generally based on laboratory-cured beam specimens cast during construction. The Foxworthy and Darter #2 curves are based on field-cured, cast and sawed specimens which typically produce lower strengths. Finally, the Parker and Witczak curves

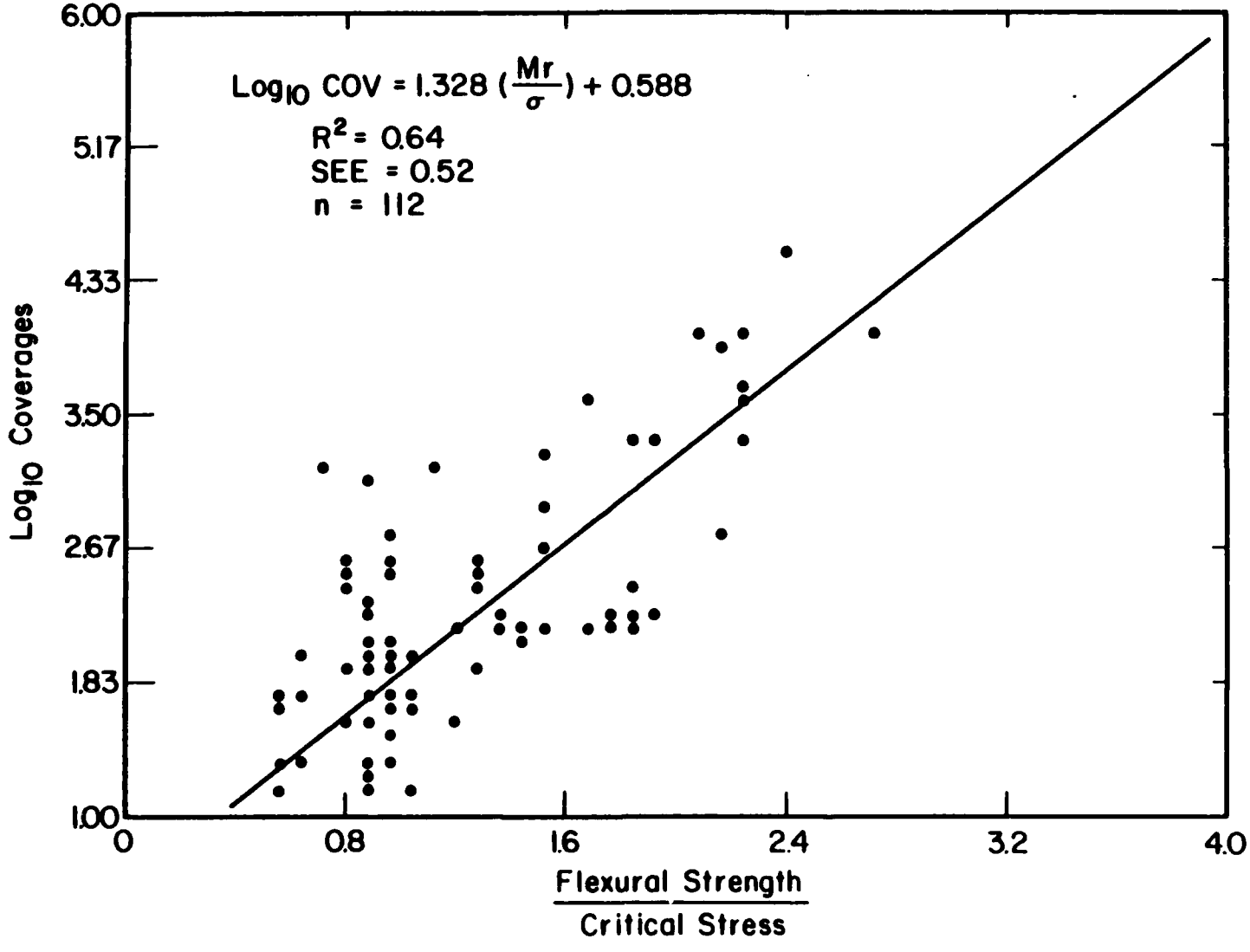

Figure 7-6. Relationship Between the Strength and Stress of Concrete Slabs and Their Field Performance - The Transfer Function

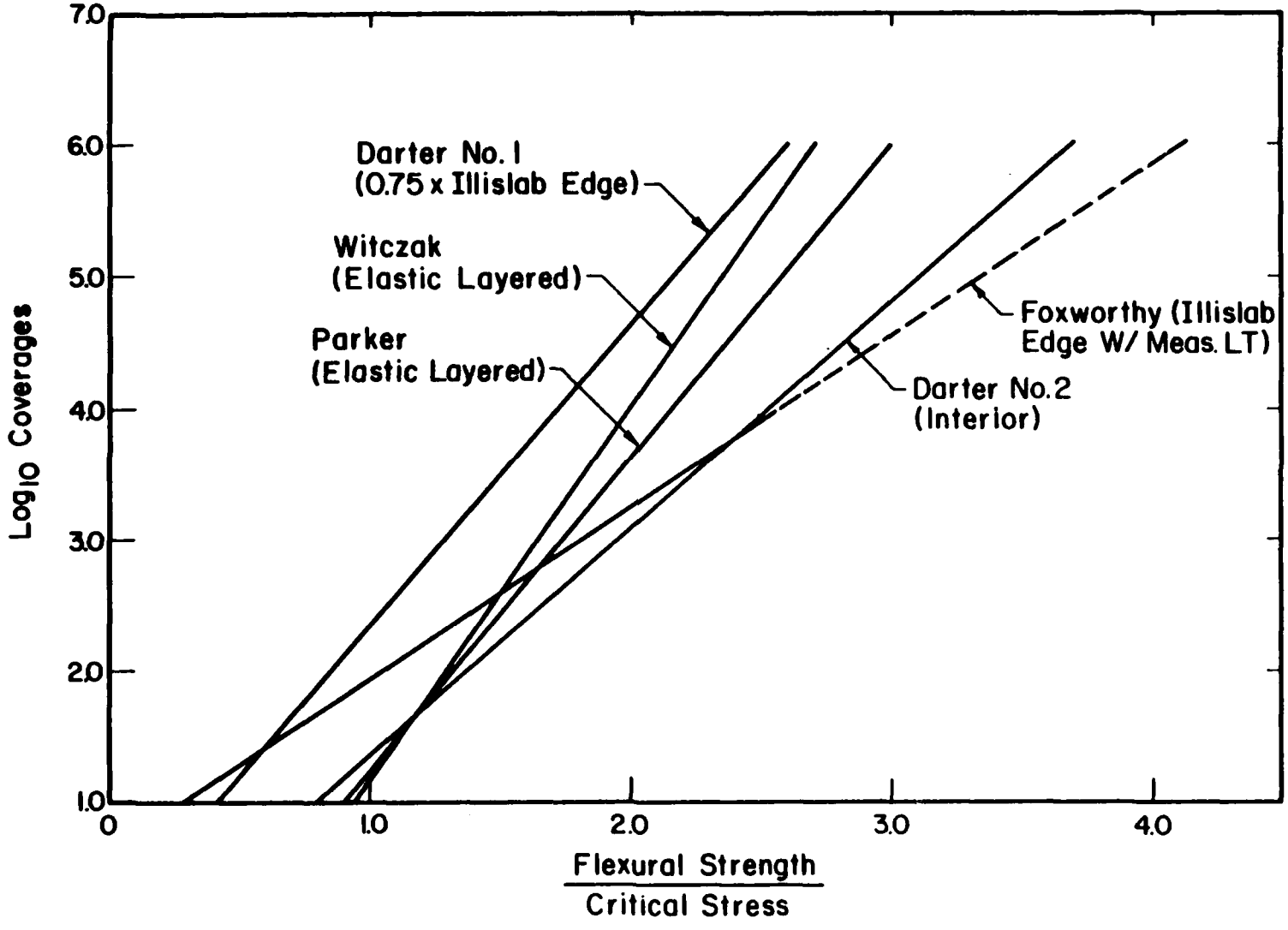

Figure 7-7. Comparison of Field Performance Models Based on Accelerated Traffic Tests

contain data points for test items that had not reached initial crack failure at the conclusion of the load cart testing, while the others do not.

It must be strongly emphasized that use of any of the field performance curves shown in Figure 7-7 must be in conjunction with the same analysis procedures that were used to develop the chosen curve. In other words, the stresses calculated from elastic layered procedures may be entirely different from those calculated by ILLI-SLAB, but when each stress is used with its appropriate curve, the resulting coverage levels should be similar. Use of a single curve for stresses computed from different theories would result in an erroneous comparison.

Figure 7-8 provides an interesting rearrangement of several of the PCC laboratory beam fatigue curves currently in use for the design of rigid pavements. These curves have been drawn using the same scale as Figure 7-7 to illustrate the tremendous increase in coverages that could conceivably be obtained when laboratory beam data is used. These differences are not easily explained, but certainly can be attributed in part to environmental conditions during curing and construction practices. The impact of using the field performance curve developed in this study over laboratory beam fatigue models can be felt most severely at the lower stress levels. The slope of the field performance curve suggests that greater damage occurs at the joints from shear numbers of aircraft operations, regardless of weight, rather than from increased stress levels, as is suggested by the laboratory beam data. This has profound implications for the lower stress producing aircraft that have heretofor been largely discounted as being harmful to rigid pavements. Conversely, the higher stresses generated by some aircraft may not be as damaging as predicted by the beam curves.

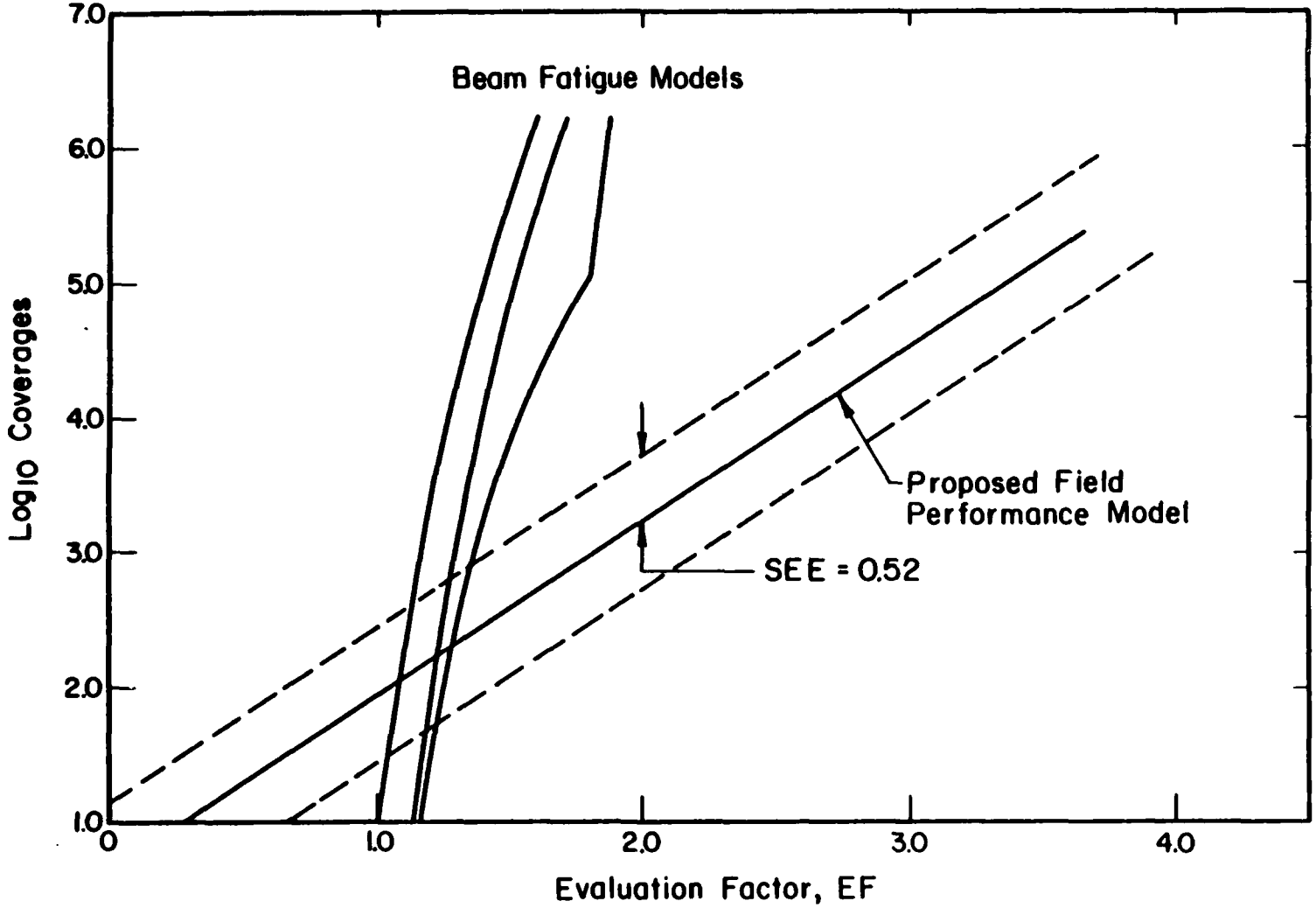

Figure 7-8. Comparison of PCC Fatigue Models Based on Laboratory Beam Tests

CHAPTER 8

THE NONDESTRUCTIVE TESTING AND EVALUATION PROCESS

It is the intent of this research effort to establish a firm basis for the NDT & E of rigid airfield pavements. Up to this point, the three major components of such a system:

(1) the field data collection equipment

(2) the field testing program

(3) the analysis package

have been identified, and detailed descriptions of each have been presented.

It now remains to formulate these components into a comprehensive methodology that will guide and direct the engineer toward realistic projections of remaining pavement life. This chapter will accomplish this objective by introducing several new concepts into the evaluation process that are intended to link the major components, and then providing specific examples from Seymour-Johnson AFB, Feature A20T, Slab No. 1, to illustrate the NDT & E process. (Appendix figure numbers contained in paraentheses are provided to illustrate the complete computer output for this feature.) The result will be a complete system upon which to expand and improve. Figure 8-1 presents a flow chart that can be used as ready reference for the entire NDT & E procedure.

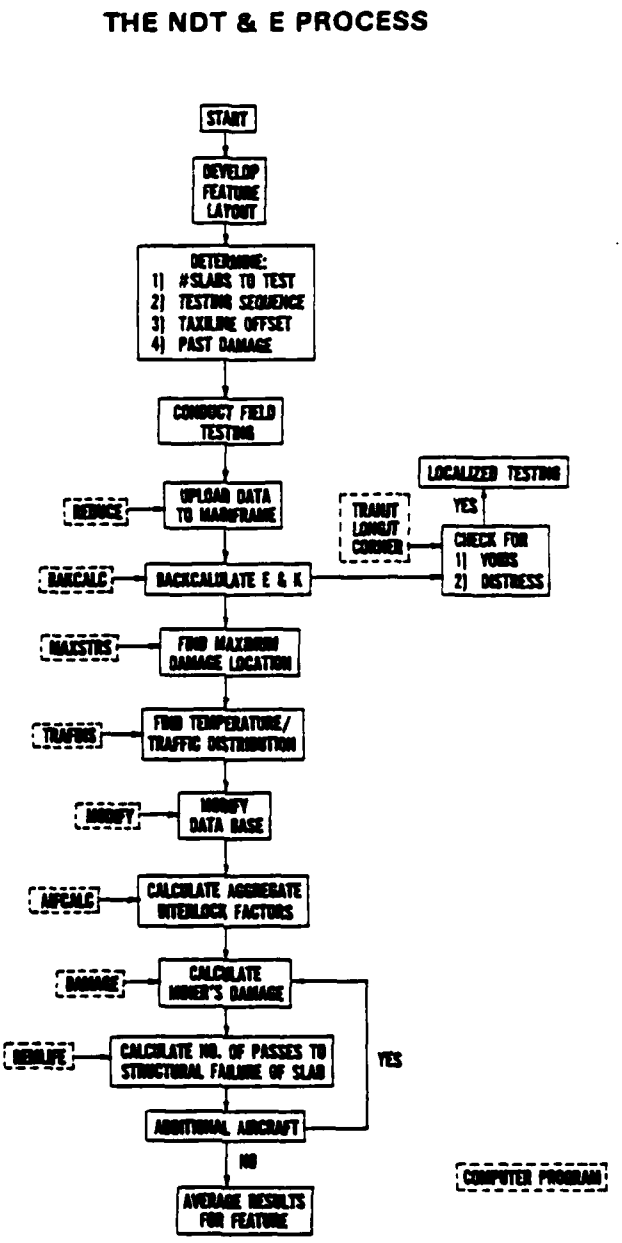

Figure 8-1. Flow Chart of the Nondestructive Testing and Evaluation Process

8.1 Planning and Conducting the Field Testing Program

The structural evaluation of any pavement network (such as all pavements at an airfield) is basically a two-fold process: general network level evaluation and specific project level evaluation. The engineer must initially be concerned with the collection and analysis of information for all identifiable pavement features on the airfield network. By necessity, such a testing program must be broad enough in scope to permit the most efficient use of limited resources, yet detailed enough to identify potential problem areas. This general network evaluation program need not be overly concerned about the underlying causes of pavement distress, but rather should provide remaining structural life predictions for each feature and identify those features warranting additional investigation during the "specific" phase of the evaluation. The methodologies described herein will address the first of these two phases, the general network evaluation.

8.1.1 Feature Identification

The tremendous challenge facing the engineer in planning and conducting an NDT & E program, touched upon in Chapter 3, must begin in much the same way as conventional destructive evaluations. All available sources of information on the design, construction, maintenance, and repair of the airfield facilities must be reviewed, along with the results of any previous testing and condition surveys, to identify each distinct group of contiguous pavement slabs that display nearly identical material properties, dimensions, construction histories, and maintenance practices. There are no limitations on the maximum or minimum feature size; however, the two primary purposes of feature designations are to 1) provide "uniform" pavement sections for ease of analysis, and 2) provide a convenient breakdown of the entire pavement

system into smaller sections for maintenance and repair planning. This suggests that features smaller than about 10 slabs should be avoided to reduce testing and analysis requirements. Similarly, large parking aprons or entire runway widths seldom require maintenance or repair over the entire surface; generally keel sections and aircraft tiedown locations would receive priority for repair. Thus, the "use" of the pavement plays an important role in feature identification.

Historically, the concept of "traffic area" has been used in design to further subdivide pavement features into sections that not only have similar material properties design and geometrics, but also have consistent loading conditions. The designation of traffic areas has been based on the degree of channelization of the traffic and whether the airplane is at full mission weight or not. In Figures 3-1 to 3-3, the last character in the feature designation represents the traffic area, as currently stipulated by Reference 6. These convenient designations have permitted reductions in the design of pavement thicknesses to take advantage of the lateral distribution of traffic along runway interiors and aprons, and lower fuel loads along ladder taxiways. In addition, construction difficulties are minimized by the designation of entire aprons and runway widths as single features. This author feels, however, that certain locations, such as alert parking areas and taxilanes within large aprons, warrant the "A" designation for design rather than "B", but these issues must be resolved administratively.

For purposes of evaluation, however, the use of current traffic area designations must be modified to more accurately reflect actual loading conditions. This will result in a substantial increase in the number of features for evaluation than were required for design, but the speed with which data can be collected and analyzed with this system completely

justifies this recommendation. For parking aprons, this will mean further subdivisions for 1) the highly channelized taxilanes, 2) the statically loaded parking "spots", and 3) the nonloaded pavement areas between parking rows and taxilines. For runways, separate features must be established for the highly channelized areas surrounding the centerline. This centerline feature may only be two slabs wide for the first 1000 feet, and then expand to a four slab width for the remainder of the runway interior to account for increased wander. The exact location of this widening point will vary with the gross loads of the mission aircraft and, therefore, can not be fixed a priori. Observation of surface distress will be the primary indicator of proper feature change points on runways as well as aprons.

Figures 8-2 and 8-3 provide examples of proposed feature designations on the Runway at Plattsburgh AFB and SAC Apron at Seymour-Johnson AFB. The "A", "B", "C", and "D" identifiers used for design have been replaced by "S", "T", and "U" designations representing static, transient, and unloaded conditions, respectively. These three categories encompass the entire spectrum of loading conditions that are encountered and readily describe the relative importance of the feature in prioritizing maintenance and repair work. When used in conjunction with pavement thickness, construction history, and distress patterns, a realistic feature layout can be developed for NDT & E of an entire airfield.

The vast majority of features on an airfield will receive either "T" or "U" designations, with only those slabs actually supporting parked aircraft falling in the "S" category. Unloaded or "U" features can, in many instances, be omitted altogether from the NDT & E program if the potential for their use by aircraft, now or in the future, is low. Later in this

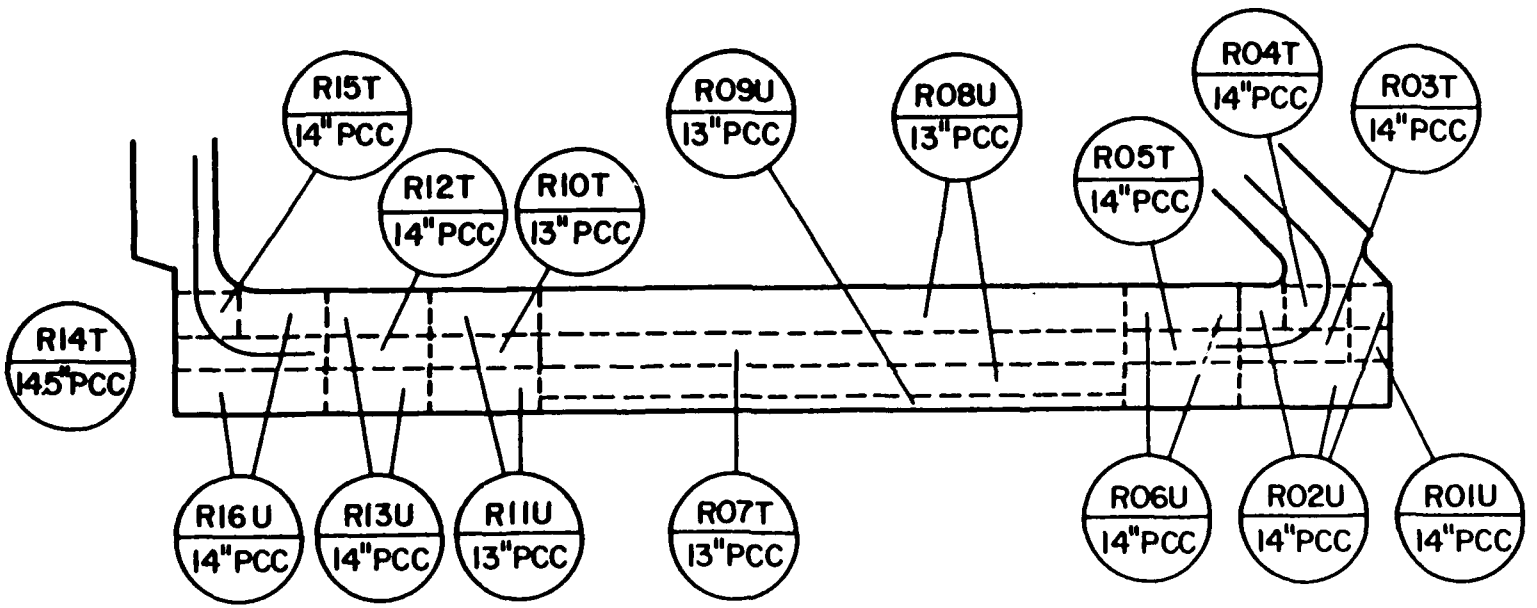

Figure 8-2. Proposed Feature Designations for Runway 17-35 at Plattsburgh Air Force Base

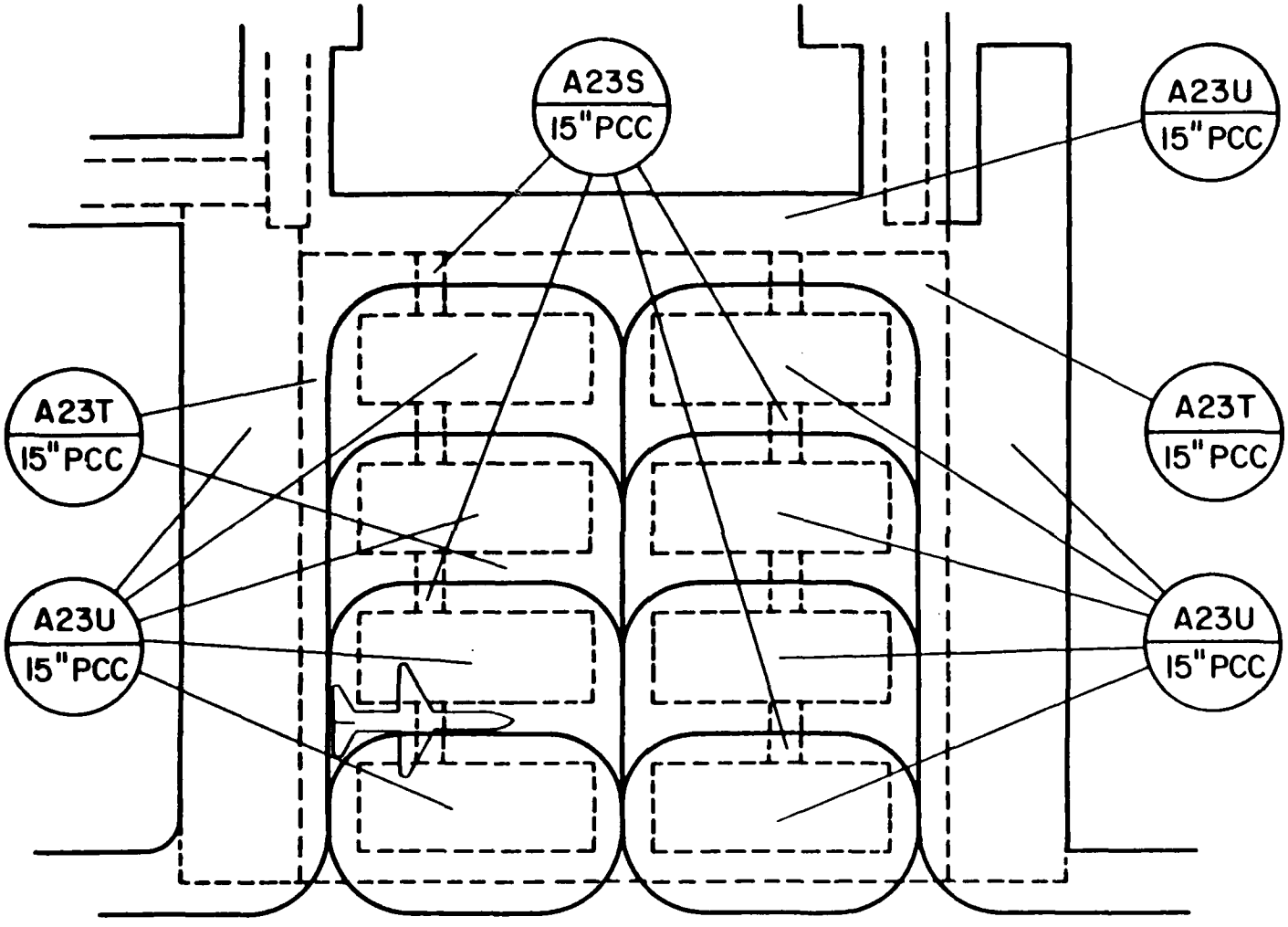

Figure 8-3. Proposed Feature Designations for the SAC Apron at Seymour-Johnson Air Force Base

chapter, the proper use of pass per coverage ratios for each of these feature designations will be discussed.

8.1.2 Random Sampling within Features

Even with the ability to collect and analyze vast amounts of data, it would be highly impractical in the "general" evaluation to test every slab in every feature. Therefore, a sampling program must be developed to systematically test each feature. This sampling program must specify, through the use of statistical concepts, the number of slabs to be tested in a feature (or the number of replications) for a given level of desired precision. Since the engineer will not likely have the opportunity to return to the site for additional tests, the procedure must include a means to determine the number of tests required based on the previously established variability of the data being collected. The sampling program presented here is similar to the program developed for the Pavement Condition Index (PCI) methodology described in Reference 69. Use of this statistical sampling plan will reduce testing requirements without significant loss of accuracy.

The number of slabs to be tested in a feature depends on:

1. How large an error (e) can be tolerated in the estimate of the mean (X_E) of the feature elastic concrete modulus E (chosen over the subgrade reaction modulus K because of its greater variability).

2. The desired probably that the estimated mean of E (X_E) will be within this limit of error (e), usually set at 95 percent.

3. An estimate of the variation of E from one slab to another within the feature, usually expressed as the variance (s^2) or the coefficient of variation (s/X_E).

4. The total number of slabs (N) in the feature.

The allowable error e must first be expressed in terms of confidence limits. If e is the allowable error in estimating the mean elastic modulus (X_E) of the feature, and the desired probability that error will not exceed e is 95 percent, the 95 percent confidence limits, computed from an approximately normally distributed sample mean, are

$$X_E \pm 2s/n^{0.5} \tag{8.1}$$

where n is the number of tested slabs. Therefore,

$$e = 2s/n^{0.5} \tag{8.2}$$

Solving for the required sample size n gives

$$n = 4s^2/e^2 \tag{8.3}$$

This expression can be used if the total number of slabs in the feature is very large (greater than 1000). However, if the computed value of n is greater than 10 percent of the total number of slabs in the feature, a modified value n' (70) should be used:

$$n' = Ns^2/((e^2/4)\ (N-1) + s^2) \tag{8.4}$$

Before Equation 8.4 can be used to compute the required number of slabs to be tested, the total number of slabs in the feature must be estimated, and the standard deviation and allowable error must be determined. From the repeatability studies on backcalculated FWD elastic modulus reported in

Chapter 5, a coefficient of variation of about 20 percent was found for dynamic E. Since E values center around $5x10^6$ psi, the standard deviation of E is approximately $1.0x10^6$ psi. If an allowable error of $0.5x10^6$ psi is permitted, the maximum number of slabs to be tested in a feature is

$$n = 4\ (1.0)^2\ /\ 0.5^2$$

$$= 16 \text{ slabs}$$

Figure 8-4 was developed from Equation 8.4 to permit a rapid determination of the number of slabs to be tested, if the total number of slabs in the feature has been estimated. Several alternatives for the allowable error, expressed as a percentage of the mean (e/X_E), are presented. A minimum of four slabs is required for every feature. As additional field verification of this procedure takes place, more accurate information on the true variance of the expected value of the mean of E will become available. This will probably result in a lower standard deviation and, therefore, a reduced testing requirement. Basing the determination of the number of slabs to be tested on the elastic modulus will insure that modulus of subgrade reaction values, which display smaller variances, are determined with more than adequate precision.

The selection of which slabs to test is as important as the number to test. Not only is a random selection required to assure an unbiased estimate of the K and E parameters, but ideally they should be tested in a random order. Such a procedure would be impractical, however, increasing travel time between test locations dramatically. Therefore, it is recommended that the testing sequence depicted in Figure 8-5 be used to systematically test the required number of slabs. A stratified random sampling procedure is

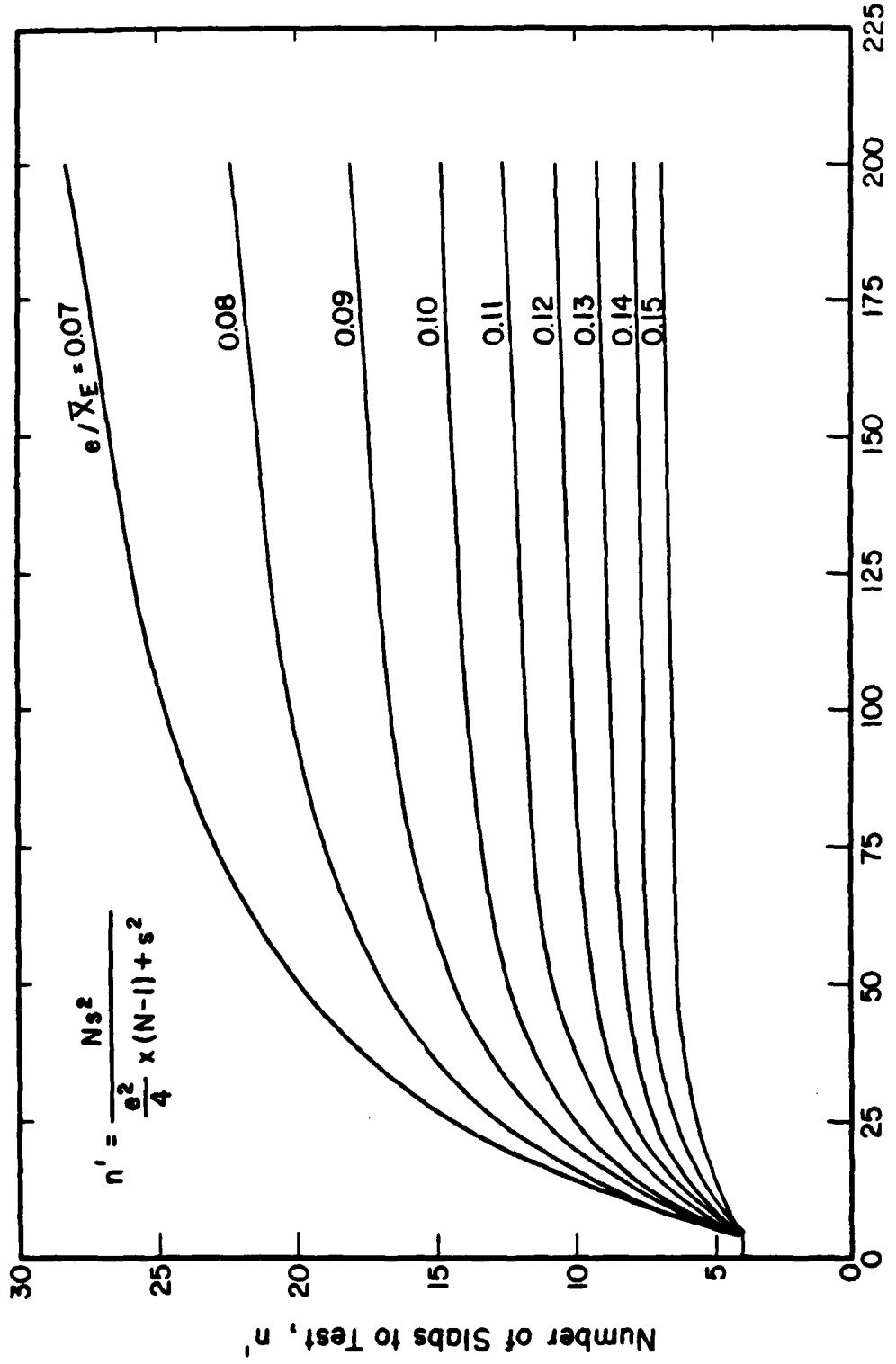

Figure 8-4. Determination of FWD Testing Requirements

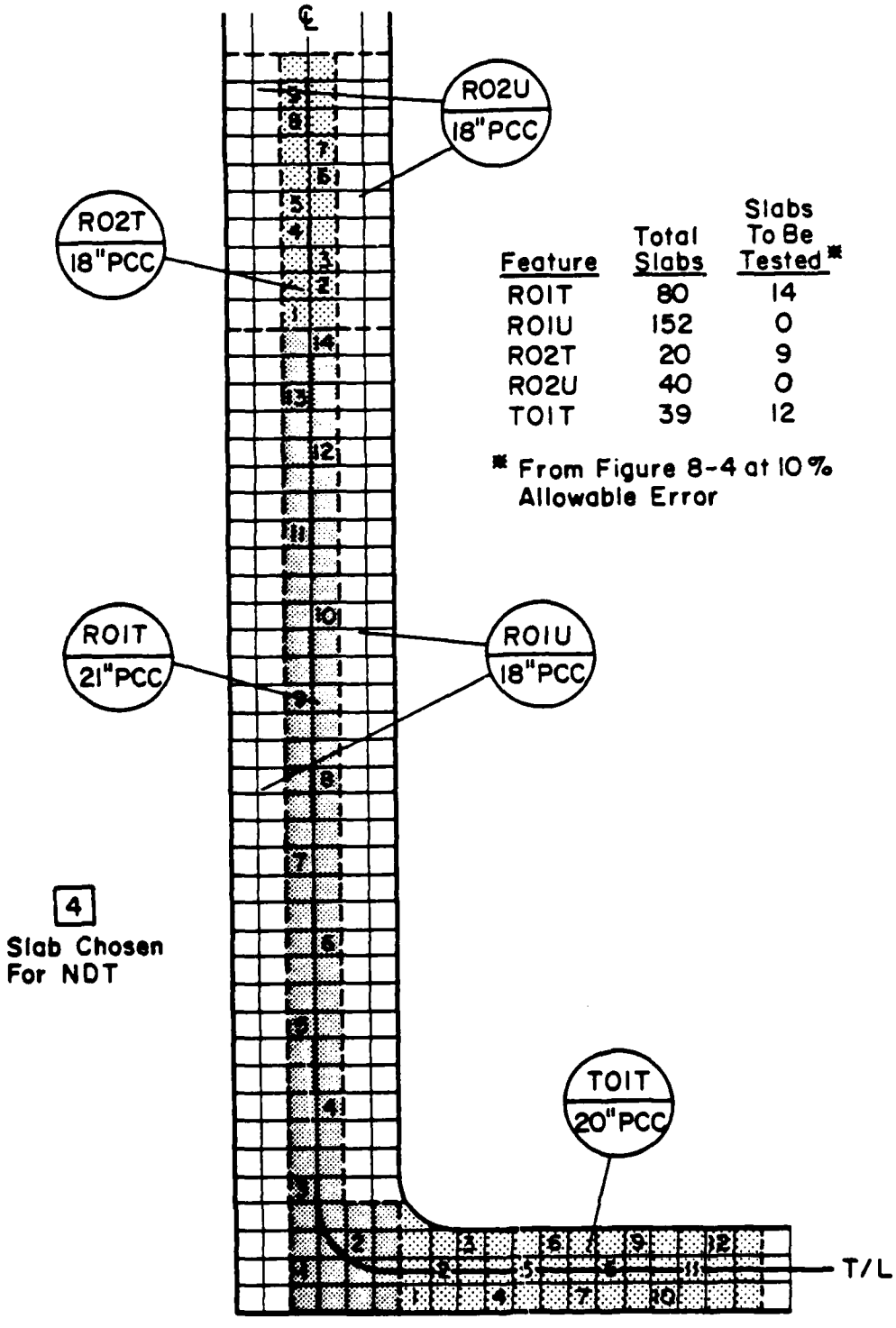

Feature	Total Slabs	Slabs To Be Tested*
R01T	80	14
R01U	152	0
R02T	20	9
R02U	40	0
T01T	39	12

* From Figure 8-4 at 10% Allowable Error

Figure 8-5. Recommended Stratified Testing Sequence

recommended. The total number of slabs in the feature (N) is divided by the number to be tested (n) to establish the number of slabs skipped in-between tests. Testing should be accomplished in both directions along the feature unless only one-directional movement of aircraft is allowed on the feature, in which case testing should proceed in that direction. Finally, only intact slabs should be tested, as they are the only slabs that can be modeled relatively easily by the finite element program. Variation from the testing sequence of Figure 8-5 by one or two slabs to avoid broken slabs will not affect the random nature of the sequence.

The Nose Dock Apron at Seymour-Johnson AFB that was chosen as an example of the NDT & E process is shown in Figure 8-6. From the observed usage of the pavement, two features have been identified; Feature A20T carries the aircraft loadings while Feature A20U remains unloaded. From Figure 8-4, 6 of the total of 24 slabs in Feature A20T are to be tested at an allowable error of 14 percent, while Feature A20U does not require evaluation. Figure 8-6 indicates which slabs were tested and the crack pattern development for the entire feature.

8.1.3 Individual Slab Testing

The testing pattern described in Section 3.3.2 and illustrated in Figure 3-5 was proven during the field research to be the most efficient method of testing the four key stations on each slab. This sequence is recommended for all general network level evaluation testing. In addition, three drops of the FWD should be made at each station from a height that will produce loads in the 24,000-pound range. These three drops can then be averaged by the computer to improve deflection gauge sensitivity and reduce testing error for the backcalculation program.

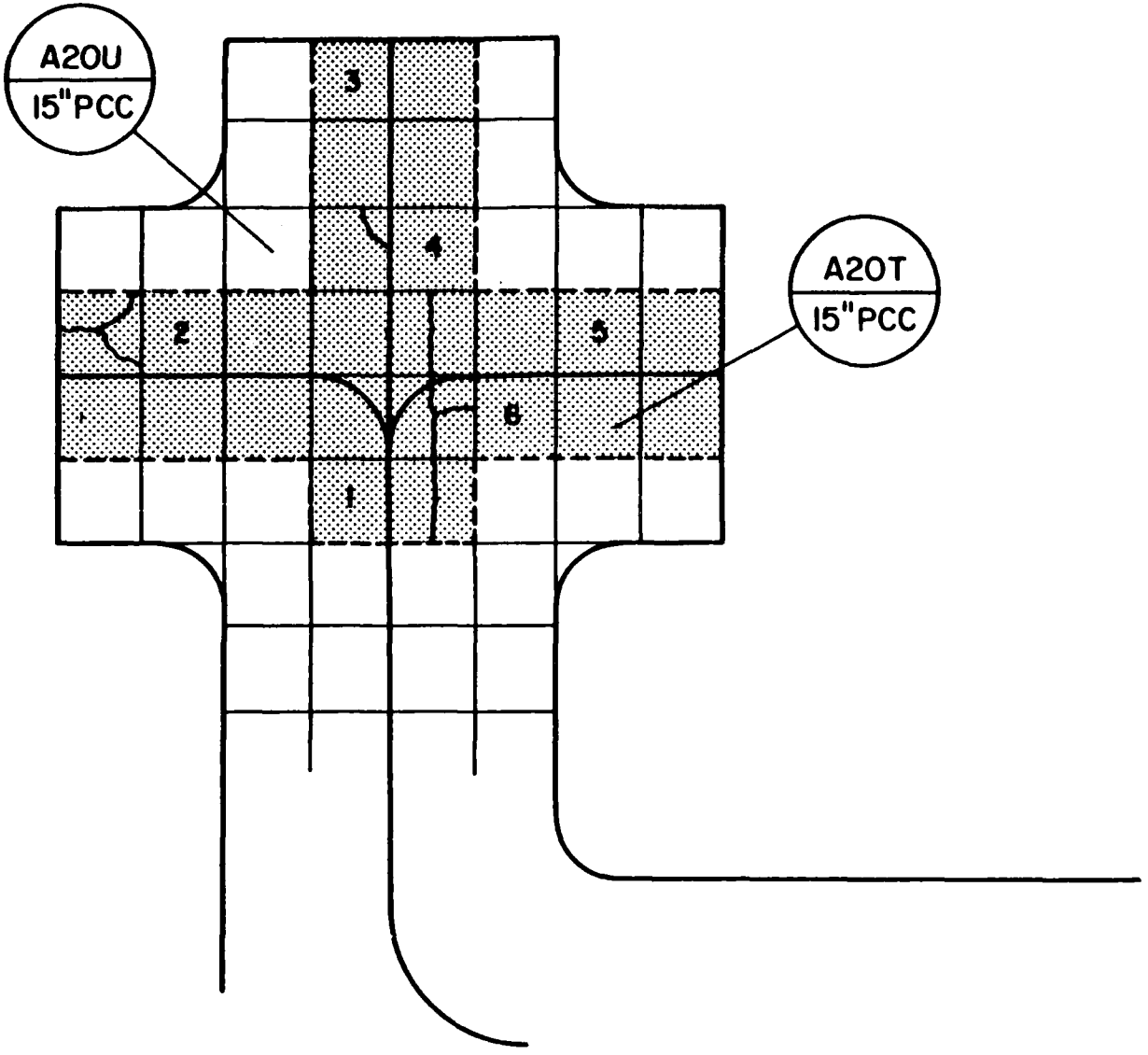

Figure 8-6. Crack Development and Testing Sequence for Feature A20T

The HP-85 computer software supplied with the FWD can be programmed to create a data file for each feature on the airfield, with the total number of slabs to be tested input prior to starting each feature. In addition, several other important pieces of information can be recorded on tape at this time for later use by the mainframe computer. These include the installation name, the feature designation, the transverse and longitudinal slab dimensions and joint types, the pavement thickness, the date and time of testing, and any remarks about the feature that may be pertinent. The air temperature will also be required, but is usually only available from the base weather station or FAA Flight Service Station at the end of each day, and will have to be added to the mainframe's comprehensive data file separately. The taxiline offset distance, the transverse offset distance, and Miner's past damage, which will be discussed in Section 8.6, can be input to the HP-85 at the time of testing and will be retained throughout the evaluation sequence.

8.2 Data Preparation

The field data collection program will typically result in the accumulation of over 100 HP-85 data files containing information on from 6 to 22 separate slabs and 12 drops per slab. These files must be transfered to a mainframe computer using a terminal emulation program supplied with the FWD. Unfortunately, this usually requires the somewhat tedious task of individually transfering each file, unless a procedure file can be written to accomplish the entire transfer automatically. In addition, the information stored on the HP-85 cassette tapes is in metric units and unformatted, making it difficult to read the information directly from the file.

To solve this problem, a computer program REDUCE was written to create new individual files for each feature, with the information formatted for input into the back-calculation program. Figures 8-7 and 8-8 (A-1) provide examples of raw and transformed data files, respectively, for Feature A20T at Seymour-Johnson AFB. The metric units are converted to pounds force and mils of deflection, and represent an average of three drops. It then became a matter of adding the appropriate air temperature to each file, and then using file manipulation commands to combine the individual data files into one comprehensive file for the entire airfield. The geometric and environmental data are listed only once for each slab, opposite the first station's averaged load and deflection values, followed by the remaining three stations' loads and deflections.

A closer examination of Figure 8-8 (A-1) reveals several interesting pieces of information about the slabs tested on Feature A20T. The corner position on slab 1 exhibits a much higher deflection than other corners, while the center slab positions for slabs 5 and 6 are unusually high. Finally, longitudinal and transverse joints perform about the same within slabs. These initial observations will be tracked throughout the remaining analysis to determine their impact on final results.

8.3 Back-calculation of E, K, and the Aggregate Interlock Factors

The back-calculation of the dynamic elastic modulus of the concrete and the dynamic modulus of subgrade reaction for each slab is performed by the computer program BAKCALC utilizing the data format shown in Figure 8-8 for Feature A20T. This program is the first in a series of programs developed to analyze the response of the pavement slab to FWD loads at the key locations. The program uses the iterative scheme described in Chapter 5, and the

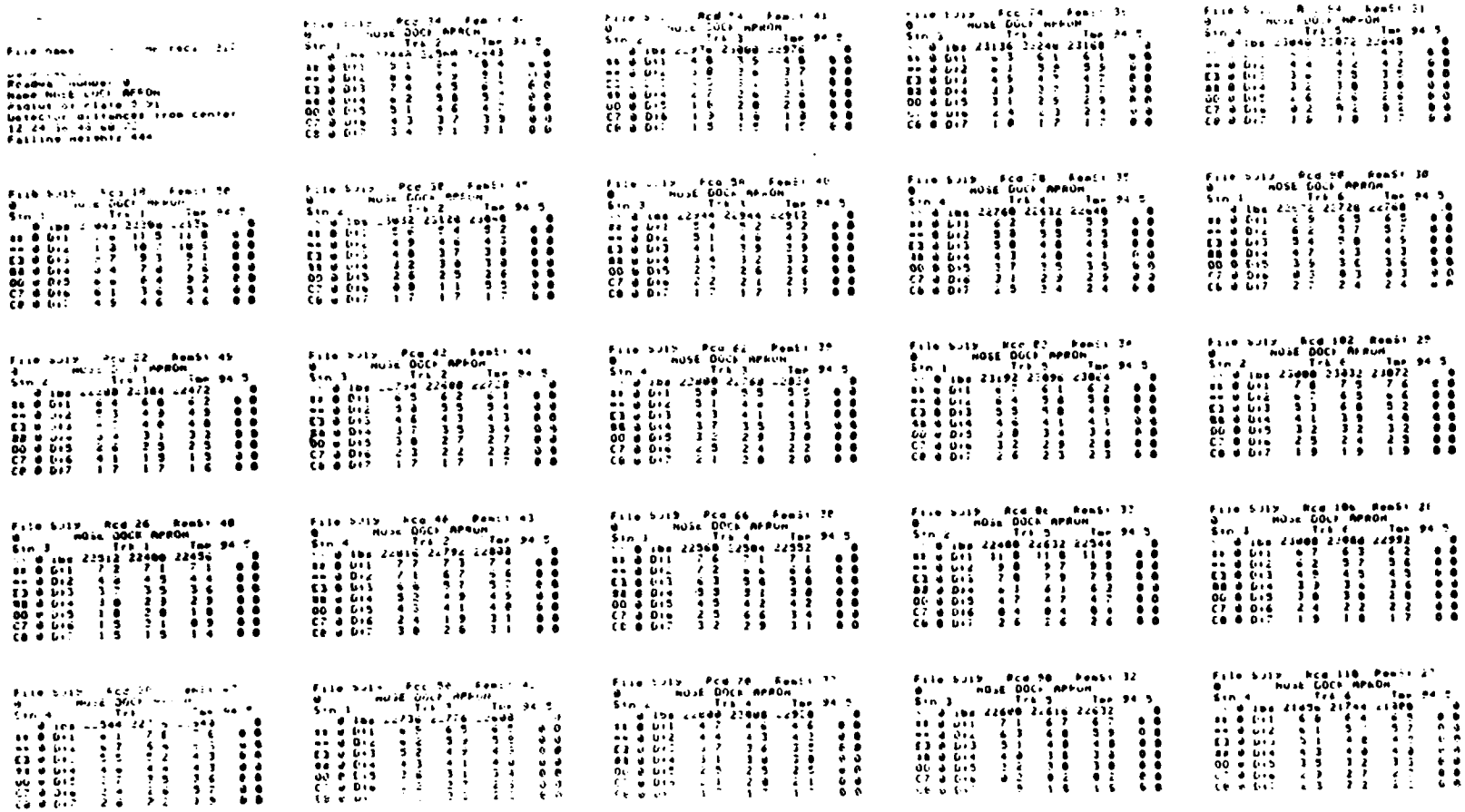

Figure 8-7. Unformatted FWD-Generated Data File

SYMBOL	VARIABLE	UNITS
BSE	THREE LETTER DESIGNATION OF BASE/INSTALLATION	
FEAT	FEATURE DESIGNATION	
S	SLAB NUMBER	
TDIM	SLAB WIDTH IN TRANSVERSE DIRECTION	FEET
LDIM	SLAB WIDTH IN LONGITUDINAL DIRECTION	FEET
THCK	SLAB THICKNESS	INCHES
AT	AIR TEMPERATURE	DEGREES F
P	POSITION OF TEST: 1=CORNER, 2=CENTER, 3=LONG JT, 4=TRAN JT	
LOAD	FORCE EXERTED ON PAVEMENT BY FALLING WEIGHT	LBF
R	RESPONSE OF PAVEMENT: M=MEASURED, P=PREDICTED	
D0	DEFLECTION AT 0.0 INCHES FROM LOADING PLATE	MILS
D1	DEFLECTION AT 12.0 INCHES FROM LOADING PLATE	MILS
D2	DEFLECTION AT 24.0 INCHES FROM LOADING PLATE	MILS
D3	DEFLECTION AT 36.0 INCHES FROM LOADING PLATE	MILS
D4	DEFLECTION AT 48.0 INCHES FROM LOADING PLATE	MILS
D5	DEFLECTION AT 60.0 INCHES FROM LOADING PLATE	MILS
D6	DEFLECTION AT 72.0 INCHES FROM LOADING PLATE	MILS
K	MODULUS OF SUBGRADE REACTION	PSI/INCH
E	YOUNG'S MODULUS OF ELASTICITY	PSI
AIF	AGGREGATE INTERLOCK FACTOR	LBF/INCH/INCH
LTE	LOAD TRANSFER EFFICIENCY: D1/D0	
TLOS	TAXILINE OFFSET DISTANCE	FEET
TJOS	TRANSVERSE JOINT OFFSET DISTANCE	FEET
MPDN	MINER'S PAST DAMAGE NUMBER	
A/C	AIRCRAFT TYPE	
P/C	PASS PER COVERAGE RATIO	
PROP	PROPORTION OF AIRCRAFT TYPE IN TOTAL MIX	
P01 TO P12	PERCENTAGE OF TRAFFIC IN EACH TEMPERATURE ZONE	PERCENT
AIF1 TO AIF12	AGGREGATE INTERLOCK FACTORS FOR TEMPERATURE ZONES	LBF/INCH/INCH
DMG100 TO DMG50	MINER'S DAMAGE PER COVERAGE	
PASS100 TO PASS50	REMAINING PASSES FOR EACH GROSS WEIGHT CATEGORY	

Figure 8-8. Reformatted Field Data File for Feature A20T, Slab No. 1

BSE	FEAT	S	TDIM	LDIM	THCK	AT	P	LOAD	R	D0	D1	D2	D3	D4	D5	D6
SEY	A20T	1	25.0	25.0	15.0	72	1	22138	M	11.400	10.733	9.400	8.000	6.433	5.767	4.700
							2	22392	M	6.267	5.067	4.100	3.267	2.600	2.100	1.700
							3	22493	M	7.167	4.600	3.633	2.933	1.900	1.633	1.500
							4	22663	M	7.900	6.733	5.367	4.433	3.633	3.000	2.267

Figure 8-8. (continued)

ILLI-SLAB finite element program as a subroutine, to determine these moduli values. These values are reinput a final time to compute the predicted deflections. Figure 8-9 (A-2) presents the results of the backcalculation process and compares measured with predicted deflections for Feature A20T. The deflections appear to be in good agreement, but the unusually high center slab deflection on slab 5 has produced an extremely low E modulus. Such an event generally indicates that testing has taken place near a full depth crack, and that the results will be unduly biased. On the whole, K values are somewhat high for this feature while E values are consistently low.

For the most part, measured and predicted deflections will be within about 2 percent of each other, particularly for the D0 reading. In the event that the two D0 deflections do not agree within this tolerance, an error in the estimation of the pavement thickness is most probably to blame. When this occurs, a trial and error solution for the correct thickness can be initiated. The correct value of thickness will produce nearly identical values of measured and predicted D0's. This technique has potential for the NDT & E of airfields where pavement thickness information is unavailable, such as COB's and captured airfields.

Three other computer programs were developed, as part of the rigid pavement evaluation process, to compare predicted and measured deflections at the transverse joint (TRANJT), longitudinal joint (LONGJT), and corner (CORNER) of the slab. These programs utilize the backcalculated moduli from the center slab position, along with the iterative solution for the aggregate interlock factor discussed in Chapter 6, to provide the engineer with supplemental information about the performance of individual joints within a feature.

AD-A165 855 CONCEPTS FOR THE DEVELOPMENT OF A NONDESTRUCTIVE TESTING AND EVALUATION S..(U) ILLINOIS UNIV AT URBANA NEWMARK CIVIL ENGINEERING LAB P T FOXWORTHY NOV 85 3/3

UNCLASSIFIED AFESC/ESL-TR-85-46 F08637-84-M-1743 F/G 14/2 NL

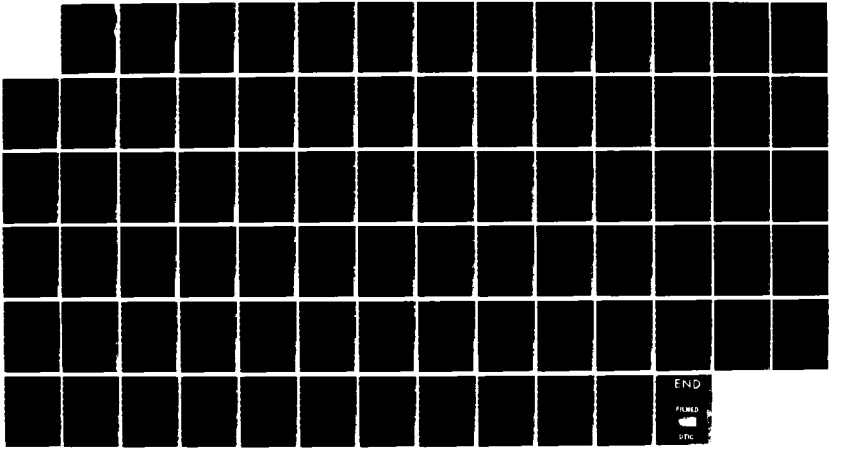

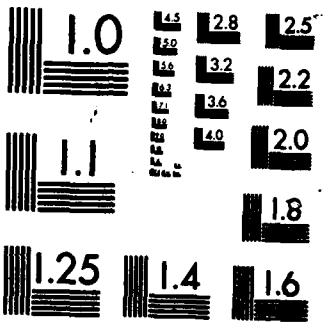

BSE	FEAT	S	TDIM	LDIM	THCK	AT	P	LOAD	R	D0	D1	D2	D3	D4	D5	D6	K	E
SEY	A20T	1	25.0	25.0	15.0	72	1	22138	M	11.400	10.733	9.400	8.000	6.433	5.767	4.700		
							2	22392	M	6.267	5.067	4.100	3.267	2.600	2.100	1.700	511.6	1305420.
									P	6.264	5.657	4.533	3.361	2.371	1.560	0.952		
							3	22493	M	7.167	4.600	3.633	2.933	1.900	1.633	1.500		
							4	22663	M	7.900	6.733	5.367	4.433	3.633	3.000	2.267		

Figure 8-9. Backcalculated E and k Result and Predicted Sensor Deflection for the Center Slab Position

Figures 8-10 (A-3) through 8-12 (A-5) illustrate the results from this series of programs for Feature A20T. The output shown in Figure 8-10 is merely a recapitulation of the results from Figure 8-9, with the addition of the iterated aggregate interlock factor, the predicted deflections along the longitudinal joint, and measured versus predicted joint load transfer efficiencies. Figure 8-11 (A-4) follows from Figure 8-10 (A-3) for the transverse joints; and finally , Figure 8-12 (A-5) depicts the measured and predicted deflections and load transfer efficiencies for all testing stations.

These computer programs were designed to utilize center slab K and E values at the joints, and then adjust the aggregate interlock factor to match the measured and predicted load transfer efficiencies to produce accurate stress calculations. Generally, this match is within 2 percent. The excellent agreement between measured and predicted deflections at these edge and corner locations was demonstrated in Chapter 6 for joints with little or no loss of support. However, several examples were encountered at Sheppard AFB where predicted joint and corner deflections were well below measured deflections, indicating that subbase or subgrade support has been lost. A consistent pattern of this type, along with some corner breaks, should alert the engineer to the potential for loss of support beneath the slab. Reference 73 provides details in void detection using the FWD. For Feature A20T, however, just the opposite is true; slabs 5 and 6 display predicted values much higher than measured in Figures A-3 to A-5. This is most probably a direct result of the very low E modulus that was transferred from the center of the slab to the edges. Such an artficially low E value would account for the discrepancy more than slab curling in this instance.

BSE	FEAT	S	TDIM	LDIM	THCK	AT	P	LOAD	R	D0	D1	D2	D3	D4	D5	D6	K	E	AIF	LTE
SEY	A20T	1	25.0	25.0	15.0	72	1	22138	M	11.400	10.733	9.400	8.000	6.433	5.767	4.700				
							2	22392	M	6.267	5.067	4.100	3.267	2.600	2.100	1.700	511.6	1306420.		
									P	6.264	5.657	4.633	3.381	2.371	1.860	0.952				
							3	22493	M	7.167	4.600	3.633	2.933	1.900	1.633	1.500				
							4	22663	M	7.900	6.733	5.367	4.433	3.633	3.000	2.267			456910.	0.85
									P	8.963	7.717	5.338	3.449	2.264	1.080	-0.105				0.86

Figure 8-10. Iterated Aggregate Interlock Factors, and Measured and Predicted Deflections and Load Transfer Efficiencies at the Transverse Joint

BSE	FEAT	S	TDIM	LDIM	THCK	AT	P	LOAD	R	D0	D1	D2	D3	D4	D5	D6	K	E	AIF	LTE
SEY	A20T	1	26.0	26.0	15.0	72	1	22138	M	11.400	10.733	9.400	8.000	6.433	5.767	4.700				
							2	22392	M	6.267	5.067	4.100	3.267	2.600	2.100	1.700	511.6	1305420.		
									P	6.264	5.657	4.533	3.361	2.371	1.560	0.952				
							3	22493	M	7.167	4.600	3.633	2.933	1.900	1.633	1.500			50583.	0.64
									P	10.090	6.487	4.527	2.941	1.930	0.918	-0.093				0.64
							4	22663	M	7.900	6.733	5.367	4.433	3.633	3.000	2.267			456910.	0.85
									P	8.963	7.717	5.338	3.449	2.264	1.080	-0.105				0.86

Figure 8-11. Iterated Aggregate Interlock Factors, and Measured and Predicted Deflections and Load Transfer Efficiencies at the Longitudinal Joint

BSE	FEAT	S	TDIM	LDIM	THCK	AT	P	LOAD	R	D0	D1	D2	D3	D4	D5	D6	K	E	AIF	LTE
SEY	A20T	1	25.0	25.0	15.0	72	1	22138	M	11.400	10.733	9.400	8.000	6.433	5.767	4.700			4766618545.	0.94
									P	10.579	9.865	7.279	5.107	3.632	2.157	0.682				0.93
							2	22392	M	6.267	5.067	4.100	3.267	2.600	2.100	1.700	511.6	1305420.		
									P	6.264	5.657	4.533	3.381	2.371	1.560	0.952				
							3	22493	M	7.167	4.600	3.633	2.933	1.900	1.633	1.500			50583.	0.64
									P	10.090	6.487	4.527	2.941	1.930	0.918	-0.093				0.64
							4	22663	M	7.900	6.733	5.367	4.433	3.633	3.000	2.267			456910.	0.85
									P	8.963	7.717	5.338	3.449	2.264	1.080	-0.105				0.86

Figure 8-12. Iterated Aggregate Interlock Factors, and Measured and Predicted Deflections and Load Transfer Efficiencies at the Slab Corner

8.4 Determination of the Critical Stress Location for Each Feature

Up to this point in the evaluation process, the primary emphasis has been on the determination of the dynamic E and K moduli. Once accomplished, this information can be used to perform critical stress computations for each aircraft operating on a given feature. Therefore, the remainder of the evaluation becomes much like a DO LOOP in a computer program; the process returns to this point, after completing remaining life calculations for one aircraft, to begin again the prediction calculations for the next. It will become evident later in this chapter how any mix of aircraft can be accommodated on a single feature.

8.4.1 Simplifying Assumptions

The next major task facing the engineer is the determination of that one key location on each feature where the critical stress is developed for each aircraft. At first glance, this might seem to be an extensive undertaking, but certain simplifying assumptions, based on evidence presented earlier, reduces this task considerably. First, aircraft do not generally operate randomly over the surface of a feature; they follow very specific paths dictated by painted taxilines. Second, the location of this taxiline remains a constant distance from the slab's longitudinal joints throughout the feature. If not, a new feature should be designated where the taxiline shifts location. Third, the load transfer efficiency along transverse and longitudinal joints remains nearly constant, as shown in Figures 4-4 through 4-12. Finally, the critical tensile stress (and thus maximum damage) in a slab will occur at a transverse joint, unless the gear travels within an average distance of about 12 inches from the longitudinal joint, in which

case the critical stress is developed midway between transverse joints along the longitudinal joint. Figure 6-2 illustrates this phenomenon.

8.4.2 Critical Gear Position

These four assumptions permit the engineer to make a rapid assessment of the critical stress location of the aircraft gear to produce the maximum damage to the concrete slab. As illustrated in Figure 8-13, the combination of fixed taxiline to longitudinal joint distance and aircraft centerline to outside of the gear distance firmly establishes the position of the gear relative to the longitudinal joint. If the gear is not within about 12 inches of this joint, the point at which it crosses the transverse joint becomes the critical stress location. On 25 foot wide slabs, about 92 percent of the critical stress locations will occur at the transverse joint.

There will undoubtedly be many occasions when a particular slab width, load transfer efficiency, taxiline location, and aircraft gear configuration combine to make the critical stress location uncertain. To assist the engineer in such an eventuality, a computer program called MAXSTRS was developed, based on the ILLI-SLAB finite element model, to calculate the maximum tensile stress at the bottom of the slab for any position of the gear. Inputs to the program include: the aircraft type, the slab dimensions, the backcalculated K, E, and aggregate interlock factors, and the distances from each joint to the nearest point on the gear. The specified type of aircraft automatically sets up the proper finite element mesh, and the offset distances from the joints specifies the gear position. Each potential critical location for the gear can then be checked quickly, including the remote possibility that it could lie in the interior of the slab if load transfer at the joints is high enough (at least 95 percent).

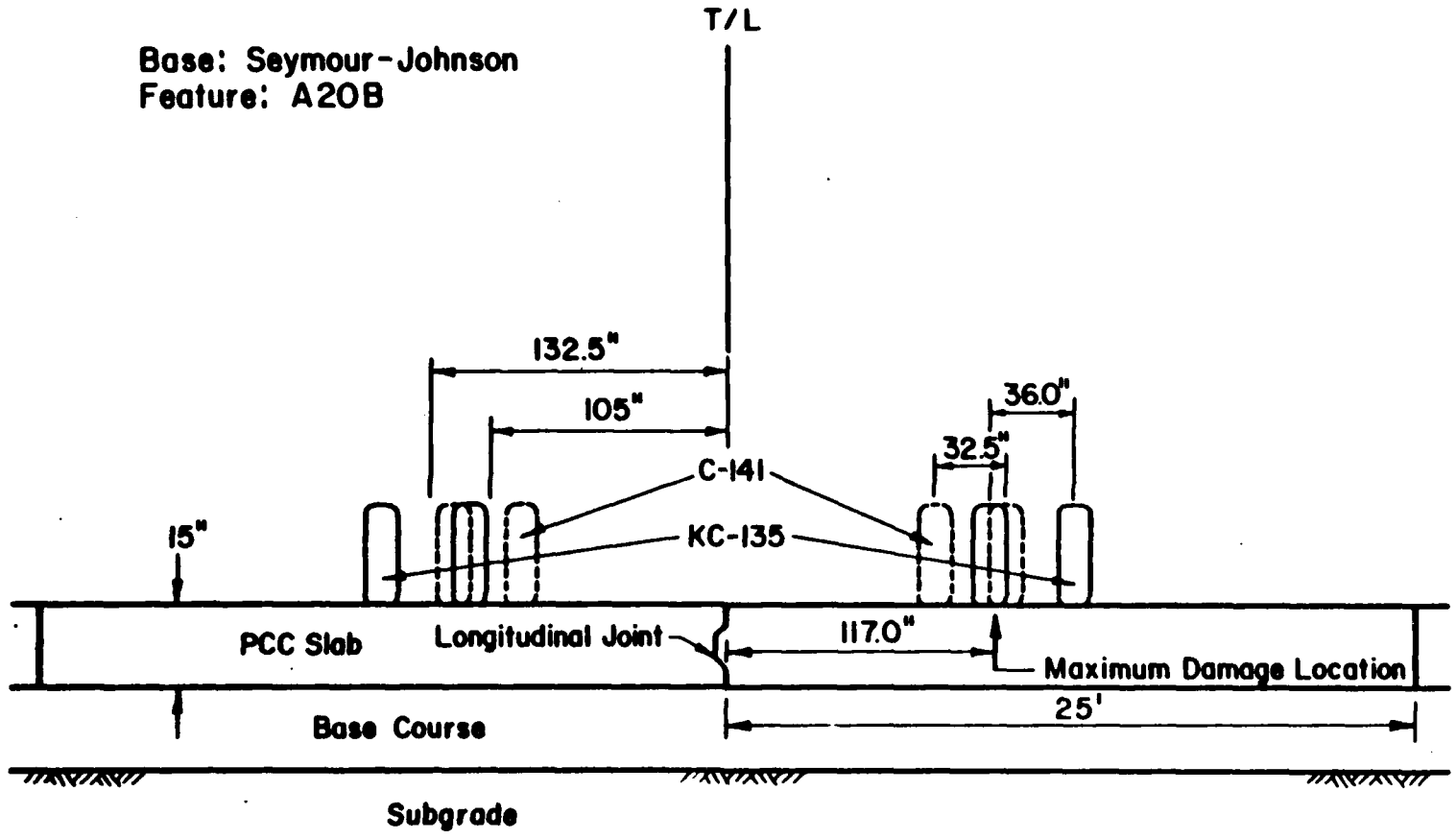

Figure 8-13. Determining the Location of Maximum Accumulated Damage for Two or More Aircraft

8.4.3 Effects of Mixed Traffic

At this stage in the evaluation process, a few comments on the effects of mixed traffic will serve to greatly reduce or even eliminate repeated stress calculations for other than the primary aircraft utilizing the pavement feature. First, the failure of a slab, defined as the appearance of the first load-associated crack throughout this evaluation procedure, begins at only one point on the bottom of the slab, the point of greatest repeated stress damage. Second, this point of greatest damage will usually occur under the mean wander point of the primary aircraft gear. Third, unless the wheel paths of two or more aircraft overlap, resulting in additive stresses at the bottom of the slab, only the primary aircraft needs to be included in the evaluation of the feature.

In special instances, such as for thicker pavements and certain aircraft mixes, the actual point of maximum stress damage might not be located directly under a wheel of either aircraft. This situation can be accomodated by analyzing the stress distribution of each gear separately and then summing the stresses to find the point of maximum total stress. This point then becomes the location of maximum damage.

The final determination of the critical aircraft gear may or may not coincide with the primary mission aircraft for the feature. It is entirely possible, for instance, that an aircraft producing high stress levels for 10 operations per day may cause more accumulated damage at its gear mean wander point than a lower stress producing aircraft, operating at 100 passes per day, would cause at some other point on the slab. Generally, the critical aircraft for a feature will be apparent from the comparison of wheel paths of all aircraft using the feature, especially if an analysis of the critical stress has been performed on other similar features. In the event two or

more wheel path mean wander points do coincide, Miner's Damage Law (71) must be used to account for the cumulative effects. This procedure will be discussed in detail later in this chapter.

8.5 Accounting for Temperature and Past Traffic Effects

As pointed out in the previous section, the determination of the critical stress location for each feature will generally result in the identification of a single aircraft upon which to base the accumulation of damage at a single point in the slab, usually at the transverse joint. Before the evaluation process continues with these results, however, two additional concepts of major significance must be brought into the picture. The first, temperature effects, has been shown to have a tremendous influence on joint behavior; the second, the effects of past traffic, will ultimately impact directly on the remaining life of the feature.

8.5.1 Traffic and Temperature Distributions

The tremendous variation of load transfer efficiencies experienced by any joint, over the range of temperatures that joint is subjected to annually, must be accounted for in the cumulative damage effects of the critical aircraft gear load. It is not sufficient to simply use an average annual load transfer efficiency exhibited by the joint when calculating the maximum stress because that stress is not linear with temperature or load transfer efficiency. Figure 8-14 typifies this relationship. It is possible, however, to distribute the total annual traffic at an installation into several temperatur zones, calculate the maximum stress that would be generated by the critical gear at the average temperature of each zone, determine Miner's damage for that stress in each zone, and then sum the

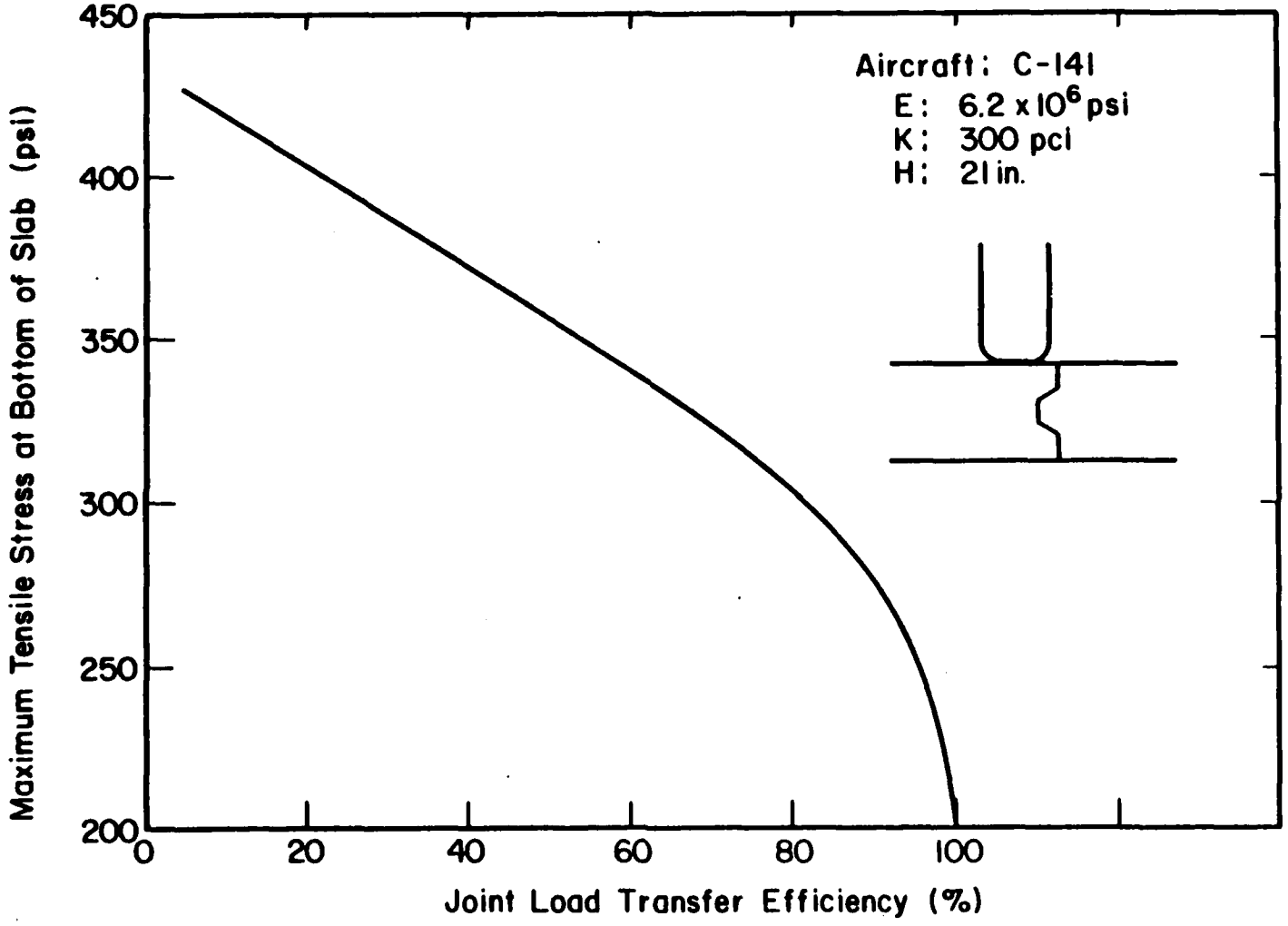

Figure 8-14. The Effect of Load Transfer Efficiency on Maximum Tensile Stress at the Bottom of a PCC Slab

damage for each temperature zone to obtain the overall damage to the pavement in a year's time. This is the approach recommended in this evaluation procedure.

Figure 8-15 shows a typical daily temperature log for Sheppard AFB at two different times of the year. Both patterns can be described approximately by the trigonometric relationship

$$T_H = ((T_{max} - T_{min})/2) \times \text{Sin}(15 \times (H - s) + T_{avg} \quad (8.5)$$

where T_H = Temperature at any hour of the day
T_{max} = Maximum daily temperature, ^oF
T_{min} = Minimum daily temperature, ^oF
H = The hour of the day from 1 to 24
s = The number of hours, from 1 to 24, between midnight and the occurrence of T_{avg}
$T_{avg} = (T_{max} + T_{min})/2$

From this relationship, the temperature at any hour of the day can be approximated. If it is assumed that the variable s remains constant throughout the year, and that T_{max} and T_{min} are relatively stable over an entire month, then the average temperature of each hour of the year could be used to place that hour into one of 12 temperature zones. These zones were established in 10 ^oF widths from 0 to 100, with temperatures below 0 ^oF and above 100 ^oF each comprising a zone, as a compromise between the accuracy of smaller intervals and the increased analysis effort. From the total number of hours in each zone, the percentage of the total hours in a year falling within each zone can easily be calculated.

If aircraft operations are assumed to be distributed evenly throughout the day, week, and year, the above percentages now become the percentages of aircraft operations on any feature within each temperature zone. Since the load transfer efficiency at any joint can be calculated for each temperature

zone, the critical stress generated by the primary aircraft can be calculated for each of the 12 temperature zones in which it might operate. A computer program called TRAFDIS was written to perform these calculations, using the maximum and minimum mean daily temperatures listed in Table 8-1 to produce the distribution shown in Table 8-2 for Feature A20T.

The three assumptions made in order to complete this analysis do not appear to compromise the accuracy of this approach. The time of the day at which maximum and minimum temperatures occur remains fairly constant from month to month, as indicated by Figure 8-15. The use of readily available monthly maximum and minimum mean daily temperatures will obviously not include those few hours of each year when temperature extremes exist, but the effect on the total percentage of these few hours is small. The greatest critisism could be levied at the assumption of evenly distributed traffic over time, especially for commercial airport operations. For military airfields, however, this assumption is not unreasonable based on their commitment to 24-hour readiness. The results of an analysis based on even distribution of traffic would probably lead to somewhat conservative estimates of remaining life since greater damage would be accumulated for night operations at colder temperatures. If an accurate traffic distribution pattern could be determined for a particular installation, it certainly could be incorporated into the computer scheme to provide a more realistic analysis.

8.5.2 Estimating Past Traffic Damage

The prediction of remaining structural life in any pavement system must begin with an estimate of the past accumulated load damage based on Miner's Law, which states that:

TABLE 8-1. MAXIMUM AND MINIMUM MEAN DAILY TEMPERATURES FOR SEYMOUR-JOHNSON AIR FORCE BASE

Month	Mean Daily Maximum (^{o}F)	Mean Daily Minimum (^{o}F)
January	51	33
February	54	34
March	62	42
April	73	51
May	79	59
June	86	66
July	88	71
August	87	70
September	83	64
October	73	52
November	64	43
December	55	35

TABLE 8-2. THE DISTRIBUTION OF TOTAL ANNUAL TRAFFIC WITHIN EACH OF TWELVE TEMPERATURE ZONES

Temperature Zone	Range (^{o}F)	Distribution of Total Traffic (%)
1	< 0	0.0
2	0-10	0.0
3	10-20	0.0
4	20-30	3.1
5	30-40	14.9
6	40-50	20.8
7	50-60	16.7
8	60-70	22.6
9	70-80	16.7
10	80-90	5.2
11	90-100	0.0
12	> 100	0.0

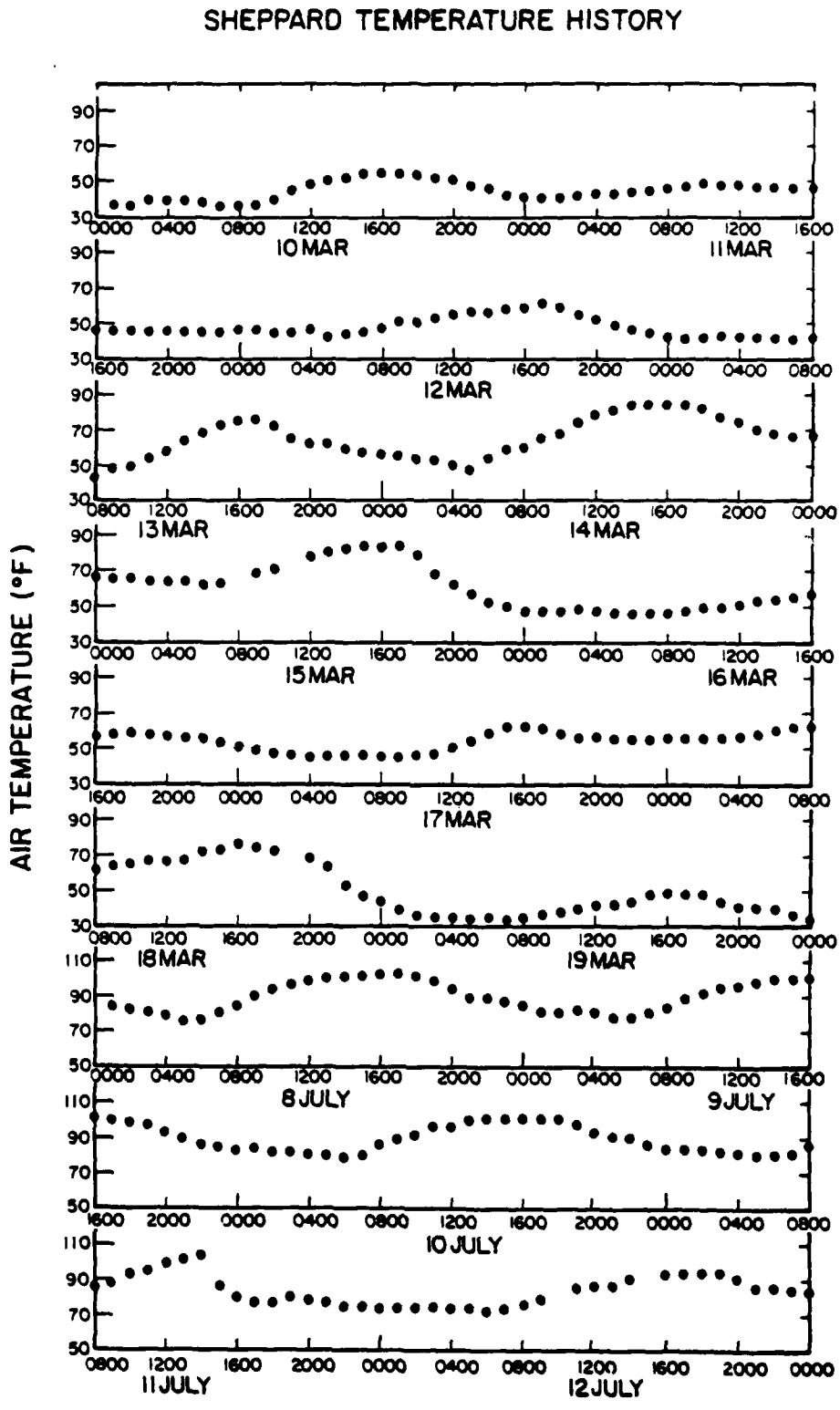

Figure 8-15. Typical Hourly Temperature Variations in the Spring and Summer at Sheppard AFB

$$\text{Total Damage} = \text{Past Damage} + \text{Future Damage}$$

$$= \frac{n_p}{N_p} + \frac{n_f}{N_f} \qquad (8.6)$$

The past damage can be estimated in two different ways, depending on the availability of past traffic loading data. If adequate data are available, then a stress analysis could be conducted for each aircraft that has used the pavement, taking into account all of the factors that influence stress levels. From this extensive analysis, a summation of load damage can be made using Miner's Damage Law. Normally, however, records on the movement of aircraft are very inadequate, particularly for taxiways and aprons. Therefore, it is recommended that the estimate of past damage be obtained using existing load-associated slab cracking information from the current PCI survey. If only load-associated damage is used, this technique will provide a quick, reasonable assessment of the accumulated damage, regardless of the type and mix of aircraft that produced it. The importance of the distress survey now becomes even more obvious.

The estimate of past damage is made by counting the number of slabs in the feature that contain any of the following distress types: corner breaks, longitudinal and transverse cracking, diagonal cracking, or shattered slabs. This number of distressed slabs is divided by the total number of slabs in the feature to arrive at the percentage of cracked slabs for the feature. Since the failure criteria used consistently throughout this report has been 50 percent of all slabs with at least one load-associated crack dividing the slab into two pieces, a percentage of cracked slabs equalling 50 constitutes a Miner's damage of 1.00. It then becomes simply a linear transformation between the percent cracked slabs (%CS) and Miner's damage number (MDN).

Expressed mathematically,

$$MDN = \%CS \times 0.02 \qquad (8.7)$$

Only in those rare instances when no load-associated cracking can be detected within the feature will an analysis of past traffic damage be necessary. In these cases, the feature would probably have been recently constructed, and such an analysis would be very feasible.

Two points must be emphasized in making this estimate of the past damage. First, care must be taken during the initial counting of the distressed slabs to avoid including slabs that have cracked from other than load associated causes. It is often difficult, for instance, to distinguish between a longitudinal crack caused primarily from load damage and a crack caused primarily from environmental or construction factors. Many cracks are caused by a combination of load and curling, warping, and shrinkage stresses. Cracking due to construction deficiencies, such as poor joint alignment or late sawing of contraction joints, must not be counted. Conversely, slabs that have been replaced must be counted (unless over half of the slabs have been replaced, in which case it becomes a new feature) as cracked slabs to avoid biasing the damage estimate for the other slabs. Good engineering judgement must be used to make this estimate because it has such a tremendous impact on the remaining life projection.

The second point of interest is the potentially unconservative nature of the final damage estimate from distress survey results. It is entirely possible that, because of the mechanics of crack propagation, load associated cracking may not have quite reached the surface of several slabs where it could be counted. Thus, a feature could possibly exhibit no load associated

distress during the survey, and two weeks later 5-10 percent of the slabs display their initial crack. Only through the long-term monitoring programs currently underway will trends of this nature be discovered. In the interim, this procedure provides the most reasonable approach to estimating past damage, certainly far better that the only other alternative.

Figure 8-6 contains the required crack development pattern to make this estimate of the total accumulated past damage. Of the 24 slabs in the feature, 5 contain a load associated crack. From Equation 8.7, Miner's damage number for Feature A20T becomes 0.42 and will be used in the remaining life predictions to follow.

8.6 Development of the Final Evaluation Data Base

Up to this point in the evaluation process, several computer programs have been introduced that utilize and make additions to the data base of information obtained from the field data collection program. Examples of this progressive buildup of information can be seen in Figures 8-8 (A-1) through 8-12 (A-5). With the supplemental information obtained in Section 8-5, the stage has been set for the development of the final data base to be used in predicting the number of aircraft passes a given feature can withstand in the future. This section will discuss the development of this final data base.

8.6.1 Additional Feature Data

The analyses conducted in Sections 8-4 and 8-5 have resulted in the establishment of three additional pieces of information, critical to the evaluation of each feature, which must be added to the data base illustrated in Figure 8-9 (A-2). The aggregate interlock factors and predicted joint

deflections of Figures 8-10 (A-3) through 8-12 (a-5) will not be required for the balance of the evaluation process.

The taxiline offset distance is the distance from the taxiline of the feature, either painted or projected, to the closest longitudinal joint. This distance is used in conjunction with the airplane's configuration to position the gear on the slab for stress calculations. The transverse joint offset distance allows the positioning of the gear at some point other than the transverse joint, if the critical stress analysis revealed, for instance, that the maximum stresses were developed along the longitudinal joint.

Finally, the past, accumulated, load-associated damage, expressed as a Miner's damage number, is added to the data base at this point if it was not input to the HP-85 computer during the field testing. A simple computer program MODIFY has been written to generate the file shown in Figure 8-16 (A-6).

8.6.2 Aggregate Interlock Factors for Each Temperature Zone

The dependence of the critical stress on air temperature, and, hence, load transfer efficiency, requires that the maximum tensile stress at the bottom of the slab be calculated for each of the 12 temperature zones. To accomplish this, aggregate interlock factors must be determined for each zone at both longitudinal and transverse joints for inclusion into the ILLI-SLAB program. Thus 24 aggregate interlock factors must be iterated for each slab tested. Fortunately, the computer program AIFCALC performs these calculations quickly and efficiently.

AIFCALC uses the modified field data file shown in Figure 8-16 (A-6) to generate the condensed file shown in Figure 8-17 (A-7). All of the FWD deflection information has been purged, and only the pertinent slab and

BSE	FEAT	S	TDIM	LDIM	THCK	AT	P	LOAD	R	D0	D1	D2	D3	D4	D5	D6	K	E
SEY	A20T	1	25.0	25.0	15.0	72	1	2136	M	1.400	0.733	9.400	6.000	6.433	5.767	4.700		
							2	22392	M	6.267	5.067	4.100	3.267	2.600	2.100	1.700	511.6	1305420.

TLOS	TJOS	MPDN
0.0	0.0	0.42

		P	6.264	5.657	4.533	3.381	2.271	1.560	0.952
3	22493	M	7.167	4.600	3.633	2.933	1.900	1.633	1.500
4	22663	M	7.900	6.733	5.367	4.433	3.633	3.000	2.267

Figure 8-16. Modified Field Data Base for Use with AIFCALC to Iterate Transverse and Longitudinal Aggregate Interlock Factors

```
**********************************************************
BSE FEAT  S TDIM LDIM THCK  AT   K         E      TLOS TJOS MPDN
**********************************************************
SEY A20T  1 25.0 25.0 15.0  72 511.6   1306420.   0.0  0.0 0.42

**********************************************************************************************************************************
     AIF1        AIF2        AIF3        AIF4        AIF5        AIF6        AIF7        AIF8        AIF9        AIF10       AIF11       AIF12
**********************************************************************************************************************************
     6703.       6703.       6703.       6730.       7383.      11252.      23667.      52743.     127870.     340869.     843703.    1385242.
     6703.       6703.       6703.       6787.       9195.      23446.      70265.     259902.     914870.3000000000.3000000000.3000000000.
```

Figure 8-17. Typical AIFCALC Output Showing Aggregate Interlock Factors for Each of Twelve Temperature Zones

feature information needed for the final computer program has been retained. Aggregate interlock factors are now included for each slab.

AIFCALC makes two assumptions in determining these aggregate interlock factors. First, load transfer efficiencies below 25 percent are elevated to 25 percent to avoid exceeding the precision capability of the computer when slopes of lines near zero are encountered. Similarly, load transfer efficiencies above 95 percent are automatically assigned an aggregate interlock value of 30×10^8 to avoid much the same problem that exists at the lower values. Secondly, the program assumes that load transfer efficiencies below 25 percent and above 95 percent, as measured in the field, have just reached these values at the time of measurement. Otherwise, no prediction of their behavior with temperature could be made. The only alternative to this assumption would be a retesting of the slab joint at another time to obtain a load transfer efficiency between 25 and 95 percent. Fortunately, this situation does not arise often if testing is accomplished between 40 and 85 ^{o}F.

8.7 Predicting the Remaining Life

The development of the data base illustrated in Figure 8-17 (A-7) has provided the foundation upon which the remaining structural life of each pavement feature can be evaluated. The following discussion outlines the internal processes of the computer programs DAMAGE, which calculates the amount of damage caused by one coverage of an aircraft, and REMLIFE, which computes the remaining passes for one or more aircraft. In addition, justification is provided for the use of new pass-coverage ratios.

8.7.1 Reporting Format

As described earlier, the evaluation of most airfield pavement features will involve only one aircraft, the one producing the most damage to a single location on the slab. However, in the event that two or more aircraft shared the same wheel paths at some point on the slab, a reporting format had to be devised that would permit the handling of mixed traffic conditions. In addition, the final presentation of results had to be meaningful to Operations personnel by presenting alternative gross weight and pass level combinations for maximum utilization of critical airfield facilities and advanced planning of maintenance and repair requirements. These considerations guided the development of the DAMAGE program, and led to the decision to report Miner's future damage number as a separate output for each aircraft. The total remaining passes for each of six gross weight categories could then be calculated by a program called REMLIFE, which combines damage results for any mix of aircraft, calculates the remaining coverages, and applies appropriate pass-to-coverage ratios to arrive at the final evaluation. The gross weight categories are based on percentages of the maximum gross weight of the aircraft and range from 50 to 100 percent in 10 percent increments.

8.7.2 The Calculation of Future Damage

The data presented in Figure 8-18 (A-8) constitutes all of the information required by the computer program DAMAGE to calculate the allowable future damage for any aircraft. This figure is identical to Figure 8-17 (A-7), except two lines of information have been added. The first line specifies the aircraft type, the appropriate pass to coverage ratio, and the proportion of the total mix for that aircraft type. The second line provides

```
**************************
 A/C          P/C       PROP
**************************
C141B        3.81       1.00

*****************************************************************
P01   P02   P03   P04   P05   P06   P07   P08   P09   P10   P11   P12
*****************************************************************
0.0   0.0   0.0   3.1   14.9  20.8  16.7  22.6  16.7  5.2   0.0   0.0

*************************************************************
BSE FEAT  S TDIM LDIM THCK  AT   K          E      TLOS TJOS MPDM
*************************************************************
SEY A20T  1 25.0 25.0 15.0  72 511.6   1305420.   0.0  0.0 0.42

*****************************************************************************************************************************
      AIF1         AIF2         AIF3         AIF4         AIF5         AIF6         AIF7         AIF8         AIF9         AIF10        AIF11        AIF12
*****************************************************************************************************************************
      6703.        6703.        6703.        6730.        7383.       11252.       23687.       52743.      127870.      340869.      843703.     1385242.
      6703.        6703.        6703.        6787.        9195.       23446.       70265.      259902.      914870.3000000000 3000000000.3000000000.
```

Figure 8-18. Modified AIFCALC Output for Use with DAMAGE

the percentage of traffic falling within each temperature zone at the particular installation. To perform the evaluation for another aircraft, only the first line needs revision. The specific information regarding each slab tested and the traffic distribution remains valid throughout subsequent evaluations.

The DAMAGE program reads the slab dimensions, backcalculated moduli, and aggregate interlock factors for the first temperature zone to calculate the maximum stress generated by the specified aircraft, with adjustments to the dynamic K moduli for static loading conditions using Equation 7.4, if necessary. This stress is used as the basis for determining the stress in each of the six gross weight categories. For example, an aircraft loaded at 80 percent of its gross weight will produce a stress at the bottom of the slab equal to 80 percent of the stress produced at its maximum gross weight.

The flexural strength of the concrete is then determined by Equation 7.3 using the backcalculated modulus of elasticity, adjusted for traffic area. When divided by the calculated stress for each gross weight category, the "evaluation factor" for each category is established. Equation 7.5 then relates the "evaluation factor" to the number of coverages that can be expected for each gross weight category in the first temperature zone. Next, the damage caused by one coverage of the aircraft is distributed among the temperature zones according to the percentage of total aircraft operations occurring in each zone. Finally, this entire process is repeated for each of the 12 temperature zones, and the damage from each zone is summed to provide the total damage resulting from one coverage of the aircraft in each gross weight category. Figure 8-19 (A-9) illustrates the output product from DAMAGE, the damage number for one coverage on Slab No. 1 of Feature A20T.

A/C	P/C	PROP
C141B	3.81	1.00

BSE	FEAT	S	TDIM	LDIM	THCK	AT	MPDN	DMG100	DMG90	DMG80	DMG70	DMG60	DMG50
SEY	A20T	1	25.0	25.0	15.0	72	0.42	0.000475648051	0.000251231814	0.000117908269	0.000043514638	0.000011719828	0.000001911235

Figure 8-19. Typical DAMAGE Output Showing Miner's Accumulated Damage for One Coverage of the C-141 at Six Gross Weight Levels

8.7.3 Relating Future Damage to Remaining Coverages

From the calculation of the damage caused by just one coverage of the specified aircraft, it remains only a simple procedure to calculate the remaining coverages to initial crack failure. REMLIFE calculates the future damage allowed for one coverage of the aircraft by subtracting the past damage from a total permitted Miner's damage of 1.0. The remaining coverage level for each gross weight category is simply the total future damage divided by the total damage for one coverage of the aircraft. This entire process is then repeated for every slab tested.

8.7.4 Pass per Coverage Ratios

The rationale behind the development of the coverages concept was discussed earlier in Section 7.3.2. Unfortunately, this convenient method of applying stress repetitions to a pavement slab during full-scale testing does not lend itself to a convenient method of accounting for aircraft operations.

Brown and Thompson (12) documented the background, development, and application of the current procedure for converting coverages to passes, and provided a limited amount of data upon which the current P-C ratios, still in use by many agencies, are based. These data were collected at several Air Force bases in 1956 and 1960, using B-47, KC-97, B-52, and KC-135 aircraft. Approximately 1176 observations of aircraft taxi, takeoff, and landing operations were made at 1000, 2000, and 5000 foot points on runways, and along curved portions of taxiways.

The primary result of the study was a method to calculate P-C ratios based on a channelized traffic wander width of 70 inches and a nonchannelized wander width of 140 inches. Recognizing that the lateral distribution was

continuously changing along the runway for each aircraft, the above wander widths were arbitrarily established for design purposes.

In 1975, the FAA sponsored an extensive research effort by HoSang (72) to determine realistic lateral distribution patterns for commercial aircraft traffic at civil airports. Data were collected at nine airports representing a wide range of operating and environmental conditions. Over 10,000 observations of lateral distribution were made at three runway locations and on parallel and high speed taxiways.

The results of this study, presented in Figure 8-20, verified the P-C ratio calculation procedures developed by Brown and Thompson, but also provided lateral distribution characteristics more representative of today's aircraft operations. Particularly noteworthy is the fact that, for all practical purposes, the standard deviations along the entire length of runways and taxiways can be assumed constant. On runways, some additional wander was evident at the point of rotation, but generally speaking, a standard deviation of 6.5 feet is representative of the entire length. On taxiways and apron taxilanes, a standard deviation of 3.0 feet is typical. The vast amount of data collected and the instrumentation utilized make this report extremely valuable in the pavement evaluation process. The P-C ratios presented in Table 8-3 were developed from the recommendations in Reference 72 and allow the user to select values that are appropriate for a given situation. The average P-C ratios stated above are used in the REMLIFE computer program.

8.7.5 The Final Evaluation

The last step performed by REMLIFE in the evaluation for a single aircraft is the application of the aircraft's P-C ratios to the calculated

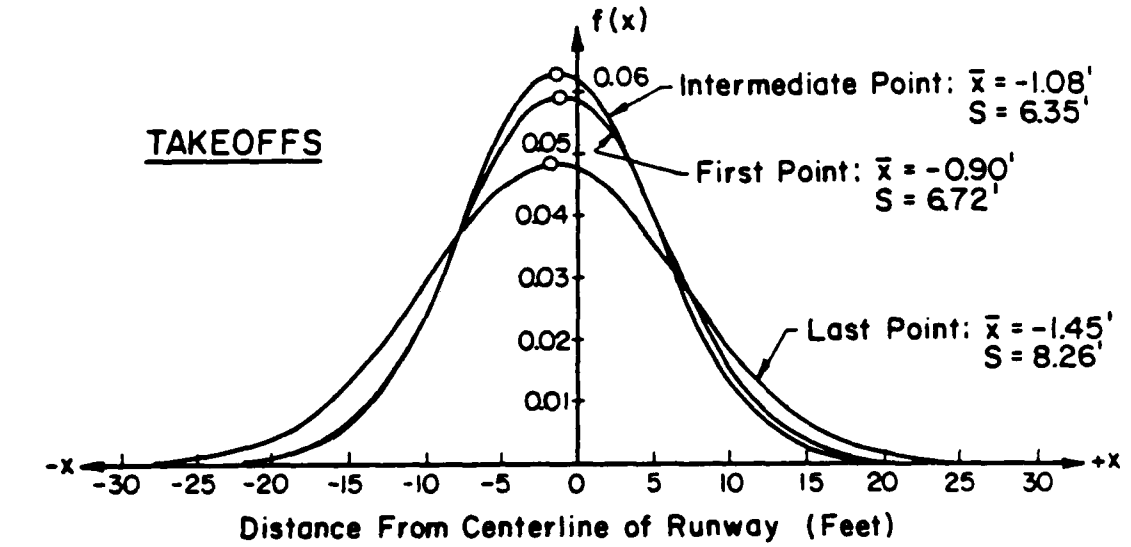

$$f(x) = \frac{1}{S\sqrt{2\pi}} e^{-(x-\bar{x})^2/2S^2}$$

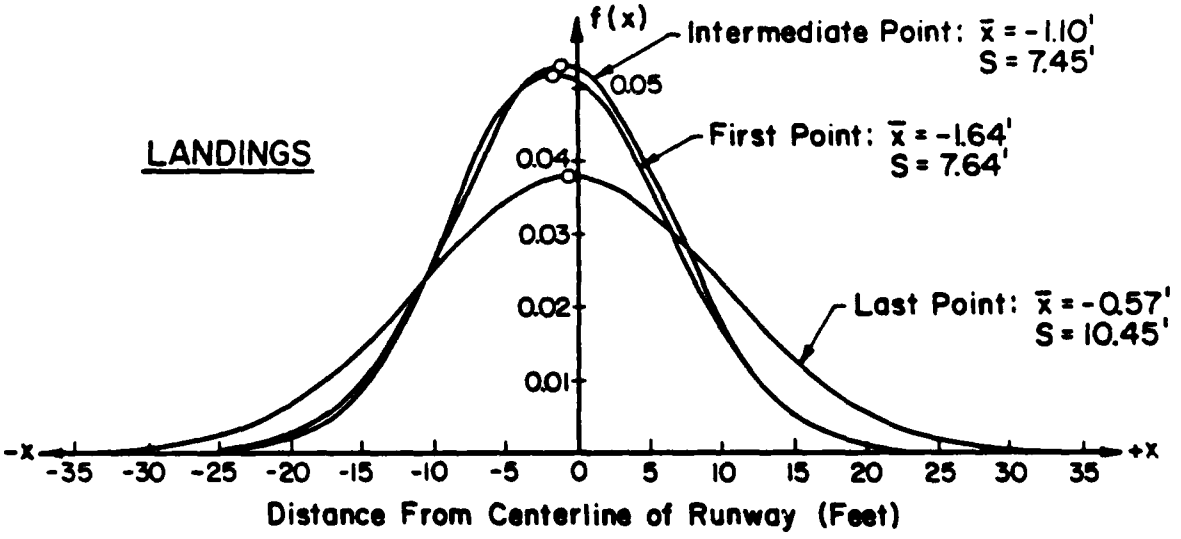

Figure 8-20. Summary of Lateral Distributions of Commercial Aircraft Along Runways at Nine Major Airports

TABLE 8-3. PASS PER COVERAGE RATIOS FOR SELECTED AIRCRAFT AT VARIOUS STANDARD DEVIATIONS OF WANDER WIDTH FOR RIGID PAVEMENTS

Aircraft	Wander Width Standard Deviations (ft.)								
	1	2	3	4	5	6	7	8	9
F-4	3.42	6.84	10.26	13.67	17.06	20.26	22.92	24.67	25.24
A-10	4.78	9.55	14.32	19.10	23.81	28.15	31.58	33.54	33.95
F-15	3.54	7.08	10.62	14.15	17.55	20.43	22.26	22.75	23.16
F-16	4.56	9.11	13.13	14.57	15.38	16.84	18.59	20.50	22.50
T-38	7.72	15.43	23.10	29.95	33.84	34.56	36.25	38.66	41.48
F-111	1.99	3.98	5.95	7.57	8.21	8.46	9.69	10.46	11.29
C-130	0.85	1.71	2.56	3.41	4.20	4.79	5.04	5.11	5.28
DC-9	2.24	3.00	4.17	5.41	6.65	7.75	8.54	8.89	8.97
B737	2.45	3.14	4.20	5.37	6.56	7.66	8.50	8.94	9.03
B727	2.17	2.99	3.76	4.72	5.72	6.70	7.54	8.14	8.41
C-141	1.16	1.50	1.98	2.53	3.09	3.61	4.02	4.26	4.31
KC135	1.10	1.48	1.89	2.39	2.91	3.44	3.95	4.41	4.77
C5	0.83	1.31	1.39	1.52	1.72	1.94	2.17	2.40	2.61
DC10	1.00	1.80	1.98	2.33	2.76	3.21	3.67	4.14	4.62
L1011	1.01	1.78	1.97	2.34	2.77	3.23	3.71	4.19	4.67
E4	1.00	1.53	1.81	2.14	2.33	2.40	2.43	2.45	2.46
B52*	0.55	0.75	0.95	1.16	1.29	1.31	1.37	1.45	1.54

* These pass-coverage ratios are one-half of the values calculated by the program to account for the large distance between the bicycle gears.

coverage level for each gross weight category. This produces the predicted number of aircraft passes remaining in each slab until initial crack failure occurs. It remains for the engineer, however, to condense these individual slab predictions into a single prediction for the entire feature.

In Figure 8-21 (A-10), a typical output for the C-141 is illustrated for Feature A20T. A second aircraft labeled "dummy" is included to indicate that only one aircraft is being evaluated for the feature. It is interesting to note that the very low E and k values for slabs 5 and 6 in Figure A-10 have apparently been offset for the most part by the very high load transfer efficiencies shown in Figure 8-12 (A-5). The end result is a remaining life prediction very similar to the other slabs tested.

Ideally, a "representative" slab could have been developed for the evaluation of each feature by averaging FWD deflections and backcalculating an overall E and k for the feature. In fact, this technique was shown as a part of this research to produce results that agree precisely with backcalculated E and k values obtained for each slab and then averaged for the entire feature. The savings in computer processing time is substantial, and such a procedure is recommended if only E and k values are desired from FWD deflections.

When the evaluation process is extended to remaining life projections, however, the "representative" slab concept will not work. The required average load transfer efficiency for each joint in such a "representative" slab would not accurately reflect the increased stresses that develop as joints open in colder temperatures. Therefore, each slab must be evaluated separately for remaining passes to failure, and then an average remaining pass level for the feature can be determined easily.

BSE	FEAT	S	TDIM	LDIM	THCK	AT	MPDN	A/C	PASS100	PASS90	PASS80	PASS70	PASS60	PASS50
SEY	A20T	1	26.0	26.0	15.0	72	0.42	C141B	4646.	8796.	18742.	50783.	188552.	1156216.
								DUMMY	0.	0.	0.	0.	0.	0.

Figure 8-21. Summary of Predicted Remaining Passes for Each Gross Weight Category of the C-141

The evaluation of the feature for a mix of aircraft requires an additional step in the REMLIFE program. The DAMAGE outputs for each aircraft must be combined in a specific manner for each gross weight category and slab to determine the total damage from the assumed traffic. The pass-coverage ratio for each aircraft and the proportion of each aircraft in the total number of operations are utilized to solve the following two sets of equations simultaneously.

$$(RP_A/PC_A \times DMG_A) + (RP_B/PC_B \times DMG_B) = RMDN \qquad (8.8)$$

where RP_A = Remaining passes for Aircraft A
PC_A = Pass-coverage ratio for Aircraft A
DMG_A = Damage for 1 coverage of Aircraft A
RP_B = Remaining passes for Aircraft B
PC_B = Pass-coverage ratio for Aircraft B
DMG_B = Damage for 1 coverage of Aircraft B
RMDN = Remaining Miner's Damage

and

$$RP_A/(RP_A + RP_B) = MP_A \qquad (8.9)$$

where MP_A = Proportion of total operations for Aircraft A

The result is an allowable number of passes for each aircraft, for that particular gross weight category and slab, that meet the assumed mix proportions. Figures 8-22 (A-11) and 8-23 (A-12) show separate inputs that have been developed for a mix of C-141 and KC-135 traffic on Feature A20T. Each aircraft is input into DAMAGE to produce Figures 8-24 (A-13) and 8-25 (A-14). REMLIFE then combines these two outputs, using the assigned P-C ratios and mix proportions, to generate the final product shown in Figure 8-26 (A-15).

The present capabilities of the REMLIFE program will permit any mix of aircraft, but the gross weight categories cannot be combined. In other

```
*************************
 A/C        P/C       PROP
*************************
C141B       3.81      0.40

*****************************************************************
P01   P02   P03   P04   P05   P06   P07   P08   P09   P10   P11   P12
*****************************************************************
0.0   0.0   0.0   3.1   14.0  20.8  16.7  22.6  16.7  5.2   0.0   0.0

*************************************************************
BSE FEAT  S TDIM LDIM THCK  AT   K         E       TLOS TJOS MPDM
*************************************************************
SEY A20T  1 26.0 26.0 16.0  72 811.6   1306420.   0.0  0.0  0.42

*****************************************************************************************************************************
      AIF1        AIF2        AIF3        AIF4        AIF5        AIF6        AIF7        AIF8        AIF9        AIF10       AIF11       AIF12
*****************************************************************************************************************************
      6703.       6703.       6703.       6730.       7383.      11252.      23667.      52743.     127870.     340869.     843703.    1385242.
      6703.       6703.       6703.       6787.       9195.      23446.      70265.     259902.     914870.3000000000.3000000000.3000000000
```

Figure 8-22. Input File to DAMAGE for a 40 Percent Mix of the C-141

```
**************************
 A/C          P/C        PROP
**************************
KC135         3.89       0.60

*****************************************************************
P01   P02   P03   P04   P05   P06   P07   P08   P09   P10   P11   P12
*****************************************************************
0.0   0.0   0.0   3.1   14.9  20.8  16.7  22.6  16.7  5.2   0.0   0.0

*************************************************************
BSE FEAT  S TDIM LDIM THCK  AT   K          E        TLOS TJOS MPDM
*************************************************************
SEY A20T  1 25.0 25.0 15.0  72 511.6   1305420.    0.0  0.0 0.42

*****************************************************************************************************************************
      AIF1         AIF2         AIF3         AIF4         AIF5         AIF6         AIF7         AIF8         AIF9         AIF10        AIF11        AIF12
*****************************************************************************************************************************
      6703.        6703.        6703.        6730.        7383.       11252.       23667.       52743.      127870.      340869.      843703.     1385242.
      6703.        6703.        6703.        6787.        9195.       23446.       70265.      259902.      914870.3000000000.3000000000.3000000000.
```

Figure 8-23. Input File to DAMAGE for a 60 Percent Mix of the KC-135

A/C	P/C	PROP
C141B	3.81	0.40

BSE	FEAT	S	TDIM	LDIM	THCK	AT MPDN	DMG100	DMG90	DMG80	DMG70	DMG60	DMG50
SEY	A20T	1	25.0	25.0	15.0	72 0.42	0.000475648051	0.000251231814	0.000117908269	0.000043514638	0.000011719828	0.000001911235

Figure 8-24. Cumulative Miner's Damage Numbers for the C-141

A/C	P/C	PROP
KC135	3.69	0.60

BSE	FEAT	S	TDIM	LDIM	THCK	AT	MPDN	DMG100	DMG90	DMG80	DMG70	DMG60	DMG50
SEY	A20T	I	25.0	25.0	15.0	72	0.42	0.000050334930	0.000021444419	0.000007787722	0.000002043259	0.000000349278	0.000000030125

Figure 8-25. Cumulative Miner's Damage Numbers for the KC-135

BSE	FEAT	S	TDIM	LDIM	THCK	AT	MPDN	A/C	PASS100	PASS90	PASS80	PASS70	PASS60	PASS50
SEY	A20T	1	25.0	25.0	15.0	72	0.42							
								C141B	3992.	7769.	17002.	47340.	180233.	1128663.
								KC135	5987.	11653.	25504.	71010.	270350.	1692994.

Figure 8-26. Remaining Passes for a 40/60 Mix of C-141/KC-135 Aircraft

words, it is not possible at this point to determine the remaining life of a pavement experiencing 40 percent C-141 traffic at 80 percent of maximum gross weight, and 60 percent KC-135 traffic at 90 percent gross weight. The results must be expressed for either 80 percent or 90 percent maximum gross weight but not a combination of both.

8.8 Sensitivity of Results

A sensitivity analysis of remaining passes in a slab or feature must necessarily be limited to those parameters which are "controlled" by the engineer, including the aircraft type, the P-C ratio, Miner's past damage, and the mix proportions. The classical approach to a sensitivity analysis, examining the effects of thickness, E, k, or load transfer, is not possible because the NDT & E system depends on actual field measurements of FWD loads and deflections on existing slabs. The response of the slab to load is fixed by the conditions at the time of the test. The following paragraphs, however, will examine those parameters which are variable to determine their effect on remaining passes.

The effect of aircraft type on the remaining life of Feature A20T, slab 1, is presented in Figure 8-27 for several aircraft. As might be expected, significant differences exist between aircraft, and these differences are directly linked to the amount of damage imparted to the slab. The F-15 can operate on the feature almost without limit, while the B-52 would cause severe damage within a short period. This method of presenting remaining life predictions vividly illustrates to airfield management the impact of operating each aircraft type on the feature.

The effect of the selected pass to coverage ratio is shown in Figure 8-28 for the C-141 on slab 1 of Feature A20T. Since the remaining coverage levels

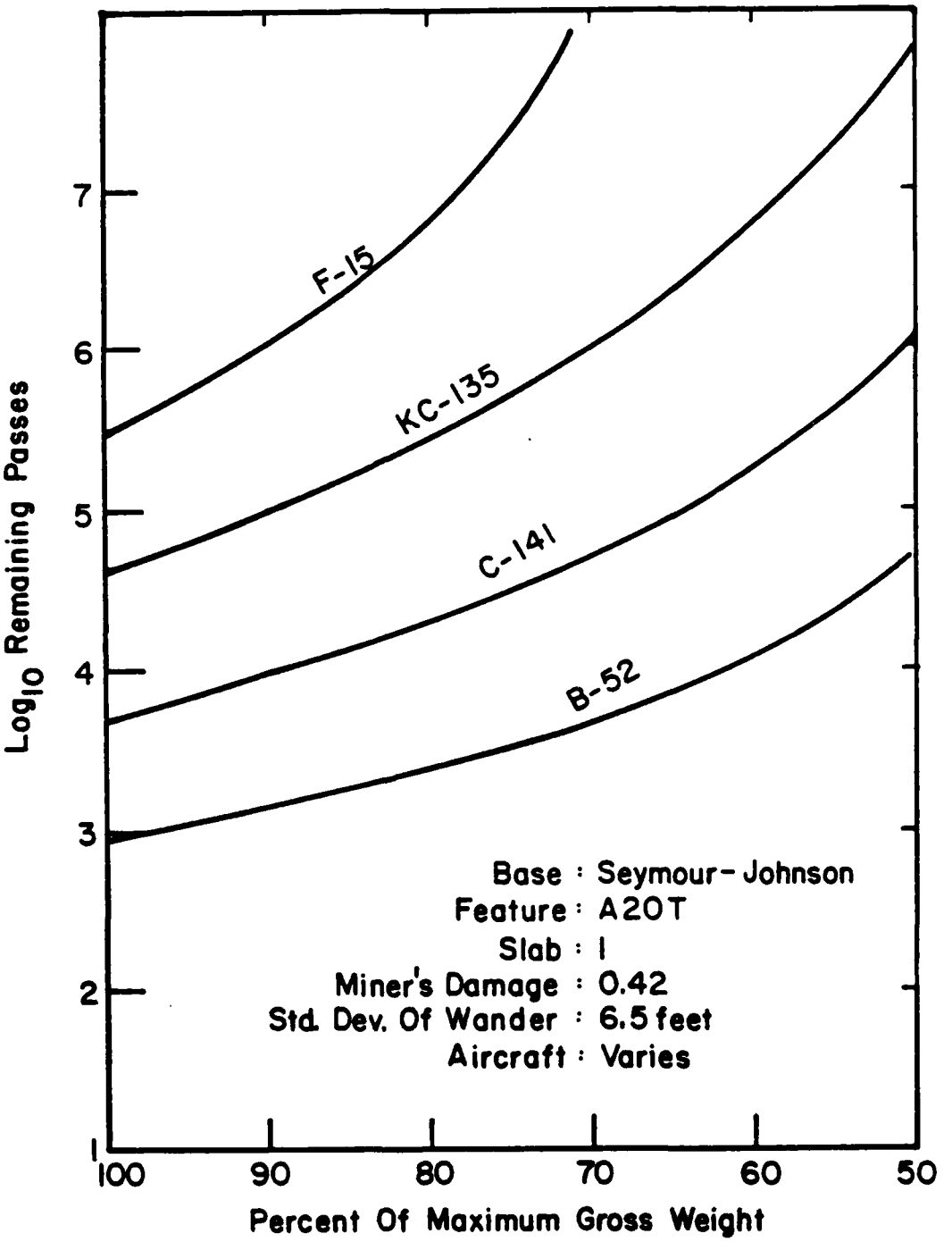

Figure 8-27. The Effect of Aircraft Type on the Remaining Life of Feature A20T

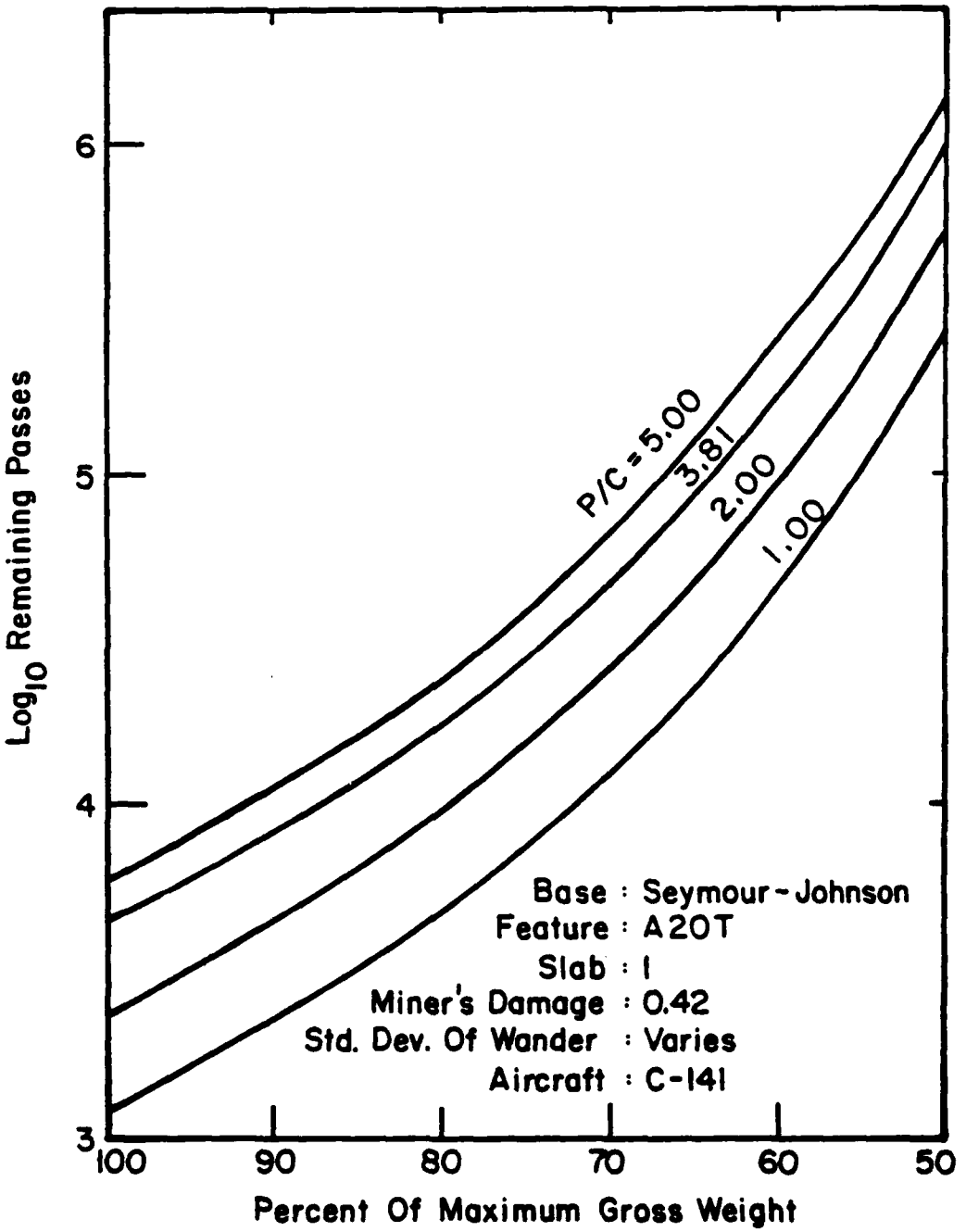

Figure 8-28. The Effect of Pass to Coverage Ratio on Remaining Structural Life for the C-141 Aircraft

for the slab are constant for a given aircraft at various percents of gross weight, the parallel nature of the curves is expected. This figure does serve to highlight the importance, however, of properly choosing the P-C ratio for a realistic estimate of remaining structural life.

Figure 8-29 illustrates the impact that Miner's past damage estimate has on the remaining structural life of a slab. Approximately one order of magnitude additional passes are available from a feature with no visible damage than from a feature in which 45 percent of the slabs contain a load associated crack. This simple analysis, however, assumes that the same pavement response to FWD loading would have resulted regardless of the feature's condition, an assumption that probably is not valid over a wide range of condition.

Finally, one of the more interesting comparisons is that of different proportions of mixed traffic. Figure 8-30 depicts the total available operations of the C-141 and KC-135 on Feature A20T for the entire range of mix proportions available. The significantly greater damage caused by the C-141 is reflected by the curvature of the lines. Increased operations of C-141 aircraft comes at a tremendous reduction in available operations of both aircraft, a tradeoff that airfield management might not be willing to make.

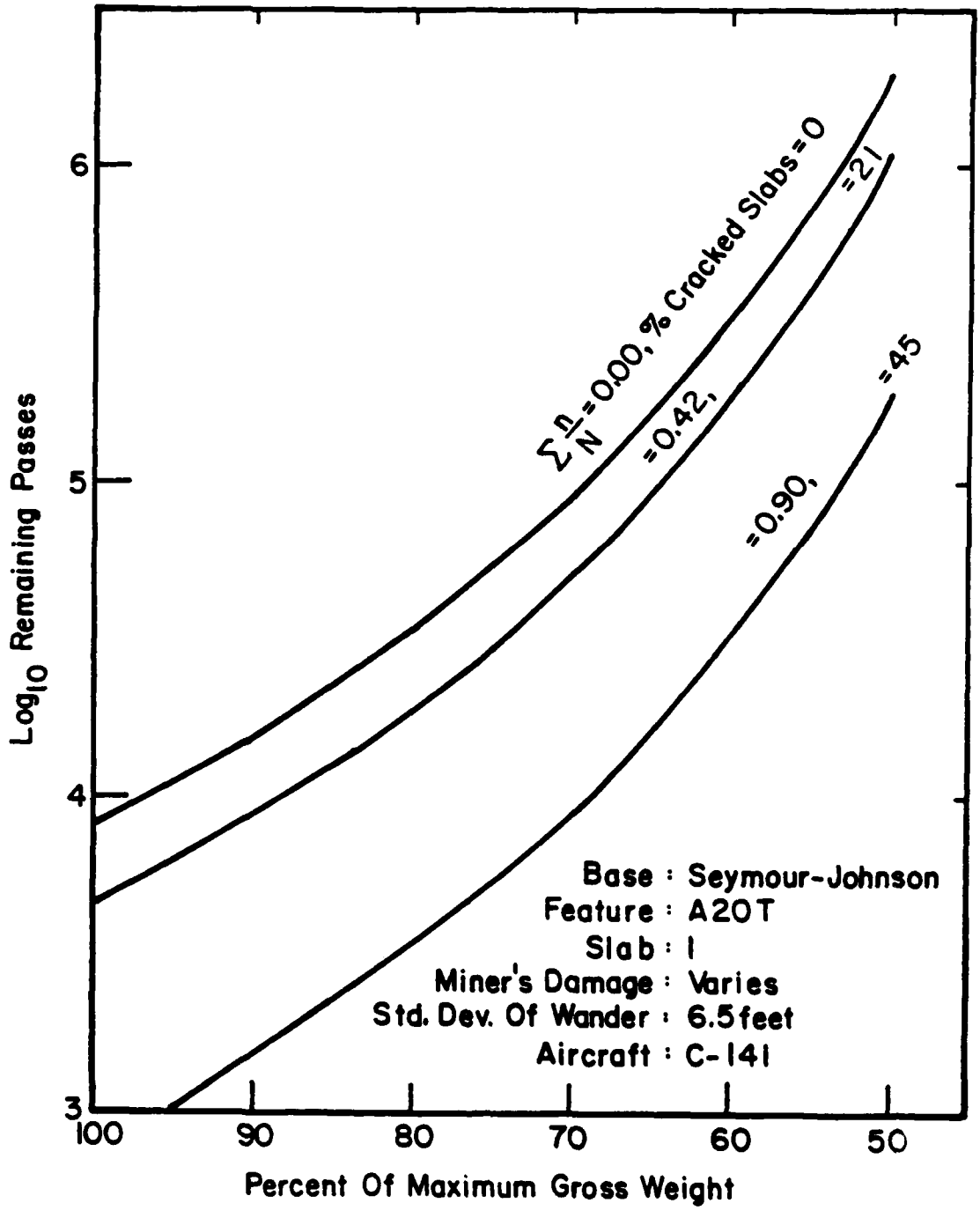

Figure 8-29. The Effect of Miner's Damage Number on the Remaining Structural Life of Feature A20T

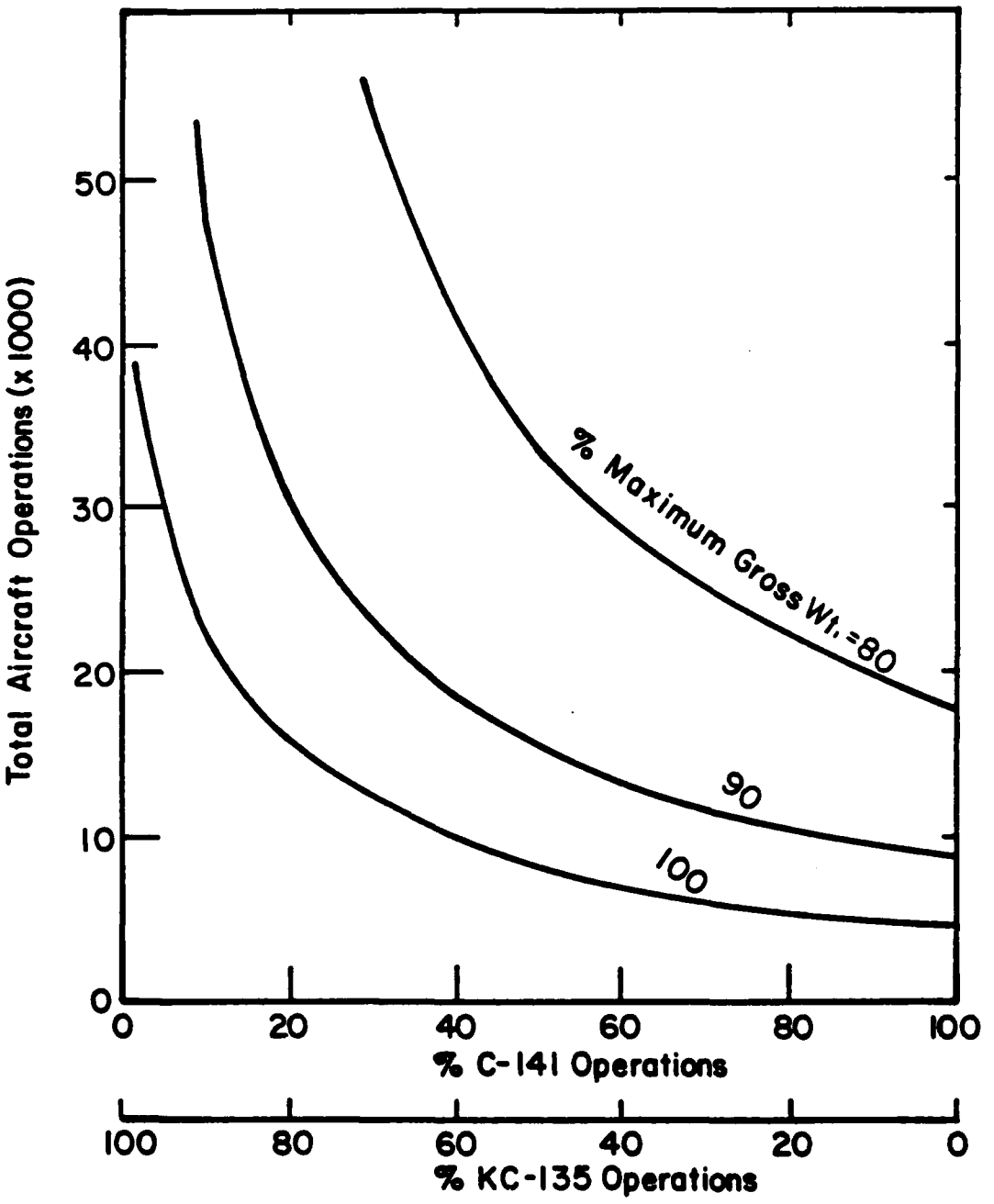

Figure 8-30. The Effect of Different Mix Proportions on the Total Available Aircraft Operations

CHAPTER 9

SUMMARY, CONCLUSIONS, AND NEEDED RESEARCH

Throughout the course of this research effort, numerous findings and areas requiring further investigation were uncovered, as is the case in most major studies. This chapter begins with a brief summary of the data collection and analyses, recaps the major findings and conclusions, and then presents specific suggestions for further research and improvement of this work.

9.1 Summary of the Research

This research project began with the intention of developing the concepts necessary for a complete nondestructive testing and evaluation system for rigid airfield pavements that was capable of testing and analyzing the many distinct features that typically exist on modern commercial and military airfields. Past destructive methodologies and present elastic layered analysis procedures are not capable of assessing the true impact of aircraft operations at rigid pavement joints under a variety of temperature conditions. After an extensive review of presently available NDT equipment and mechanistic models, the Dynatest Model 8000 Falling Weight Deflectometer and the ILLI-SLAB finite element program were chosen for their tremendous versatility. To collect the field data necessary for system development, three Air Force installations were selected for testing, and the Army's Waterways Experiment Station was requested to collect the FWD data.

Testing initially centered around the establishment of FWD load and deflection measurement repeatability under constant and changing temperature conditions. Testing patterns were developed for specific situations that

eventually would lead to the most efficient pattern for large-scale data collection. With a high degree of repeatability demonstrated for center slab testing, efforts turned toward the determination of joint behavior under various tempeature conditions. The consistency of load transfer efficiencies along the entire length of transverse and longitudinal joints was investigated, and the effect of load magnitude used to measure load transfer efficiency was established. Finally, the effect of temperature on load transfer efficiency was studied extensively for a variety of slab thicknesses, temperature conditions, and load transfer mechanisms. This effort resulted in analytical models that predict the load transfer efficiency of a joint at any temperature.

The research next moved into the development of a computerized scheme to backcalculate the concrete elastic modulus and the modulus of subgrade reaction. The scheme utilizes the ILLI-SLAB finite element model as a subroutine to iterate these values which are then used to compare measured and predicted center slab deflections. Repeatability of backcalculated moduli under constant and changing temperature conditions was also investigated. These moduli values were then transferred to the joints, and an iterative solution for appropriate aggregate interlock factors was devised to compare measured and predicted deflections and load transfer efficiencies across joints. From the E, k, and aggregate interlock factor, the critical stress under an aircraft gear could be calculated using ILLI-SLAB.

The next phase of the research related the critical stress developed at the bottom of the slab to the performance that should be expected from that slab in the future. This was done by reanalyzing the accelerated, full-scale traffic test data collected by the Corps of Engineers over a 30-year period. ILLI-SLAB was used to estimate stress levels that existed under the

load carts used in the tests, which was then combined with reported flexural strengths to develop the transfer function needed to make the remaining structural life predictions. In the process of development of this transfer function, correlations were established that allowed the determination of concrete flexural strengths from backcalculated concrete elastic moduli, and that permit the analysis of pavement features subjected to static loading conditions.

In an effort to apply these analysis techniques to actual rigid pavement systems, new concepts for identifying airfield features were presented that reflected the true nature of the loading conditions, and techniques were provided for statistically determining the number and sequence of slabs to be tested in each feature. The assessment of the maximum damage location for each feature was facilitated by the development of an ILLI-SLAB-based computer program that automatically positions the gear and generates the proper loaded areas given the aircraft type and the distances to the joints. Each aircraft utilizing the feature can then be checked quickly to determine which one or combination of aircraft produces the greatest stress in the slab.

The influence of temperature in generating these stresses was accomodated by distributing the total annual aircraft operations into twelve temperature zones and then calculating the Miner's damage produced in each zone. The damage in each zone is weighted by the percent of traffic in that zone and then summed to obtain the total damage for one aircraft coverage. When combined with estimates of the total past accumulated damage based on distress survey results, the remaining number of coverages to 50 percent cracked slabs can be calculated. Finally, more realistic aircraft wander patterns were incorporated into the analysis in the form of pass to coverage

ratios to determine the remaining structural life in terms of aircraft operations. The final reporting format will handle any assumed proportion of maximum image-producing aircraft.

9.2 Findings and Conclusions

The following specific report findings are presented as a concise summary of those contained throughout the text.

1. The falling weight deflectometer (FWD) is capable of reproducing center slab load and deflection measurements with coefficients of variation of one and four percent, respectively, at load levels above 23,000 lbf and temperatures above 40 ^{o}F. Temperatures below this level result in a stiffening of the buffer system and subsequently higher load measurements. Deflection measurements do not appear to be significantly affected by temperature extremes.

2. Joint load transfer measurements indicated that efficiencies are independent of load magnitude between 7000 and 25,000 lbf, providing a basis from which to extrapolate load transfer efficiencies under actual gear loads.

3. Directional effects of traffic on load transfer efficiency of joints is not significant on airfield pavements, and aircraft wander about centerlines and taxilines is great enough to minimize localized differences in load transfer efficiencies along the edge of a slab.

4. Significant increases in joint performance accompany air and pavement temperature increases, and this behavior can be described mathematically for either by S-shaped curves between efficiencies of 25 and 100 percent. The type of load transfer mechanism affects the slope of this curve.

5. The deflection basin created and measured by the seven sensor FWD defines a unique combination of concrete stiffness (E) and subgrade reaction modulus (k) that can be used by the ILLI-SLAB finite element model to accurately predict deflections under rapid loading conditions. These moduli can be backcalculated by the computer to eliminate interpolation errors prevalent in the labor-intensive manual graphical procedures.

6. For interior loading conditions, no apparent relationship exists between the magnitude of load and backcalculated k, at least within the load range of 7-25 kips. The hefty nature of the slabs tested and the load levels used, however, may have precluded the appearance of any stress dependency. Prototype loads at joints and corners may very well display stress-dependent tendencies. Backcalculated k values exhibit coefficients of variation around 8 percent at constant as well as changing temperatures, indicating that temperature does not significantly affect k.

7. Consistently higher and often unrealistic E values are backcalculated for load levels at the lower range of the FWD (7-8 kips). Greater consistency is available at the higher load levels. Over a wide range of temperatures, E values measured at higher load levels display coefficients of variation around 12 percent, about 4 percent higher than for the constant temperature case.

8. Slab size can significantly affect the interior stresses developed under aircraft loadings, particularly for thinner pavements. Maximum tensile stresses increase significantly as the gear load approaches the free edge of a slab.

9. A given aggregate interlock factor, used by ILLI-SLAB to model joint efficiency, can produce a wide range of load transfer efficiencies depending on slab thickness, E, and k. Backcalculated center slab E and k can be used

to iterate the aggregate interlock factor that will produce reasonable predictions of FWD deflections across joints. The measured deflections agree very well with predicted deflections using backcalculated k and E (from center slab) and measured load transfer

10. Backcalculated E can be correlated indirectly to concrete flexural strength through the previously established split tension-modulus of rupture relationship. This permits an expedient means to estimate concrete flexural strengths from backcalculated E moduli in lieu of any better information.

11. Static and dynamic k values were correlated through side-by-side testing with the FWD and conventional plate bearing equipment, and a regression equation was developed.

12. Large discrepancies exist among several concrete pavement field performance models developed on the basis of accelerated traffic tests. These differences are caused by differences in critical stress locations, flexural strengths used, and use of data points for which failure had not been reached. There are also large differences between field and laboratory beam performance models.

13. Significant differences in measured and predicted deflections at joints can expose potential problem areas requiring additional investigation. Similar differences at center slab locations signify that incorrect pavement thicknesses have been selected.

The following major conclusions have been developed from the specific findings outlined above.

1. The falling weight deflectometer is an excellent tool for the rapid collection of large volumes of rigid pavement evaluation data. It can be used to accurately measure pavement response to simulated aircraft movement

at the center and along joints of airfield concrete slabs. All seven deflection sensors are required to adequately define the deflection basin on thick rigid pavements.

2. The consistency of load transfer efficiency measurements along the length of both transverse and longitudinal slab joints provides some tolerance in the positioning of the FWD along the joint. The nondirectional nature of load transfer efficiencies along transverse joints on airfield pavements permits good flexibility in planning and conducting a field testing program, but testing of longitudinal joints must take into account the history of loading conditions, as well as the present mission aircraft, to assess load transfer efficiency in the proper direction.

3. FWD testing should be accomplished between 40 and 90 ^{o}F to minimize the stiffening effect on the rubber buffers of the device and to provide more consistent loads, deflections, and backcalculated parameters.

4. The ability of ILLI-SLAB to accurately model FWD deflections at slab centers and across joints establishes high levels of confidence in the accuracy of ILLI-SLAB-computed stresses under all types of aircraft loadings.

5. The present knowledge of fatigue mechanisms in concrete is not sufficient to warrant any basis other than empirical, full-scale field tests and/or other performance data for the development of the transfer function relating critical stress to performance. The results of long term pavement performance monitoring now underway should be incorporated into the transfer function as they become available.

6. The methods of testing, analysis, and model development must be consistent if meaningful evaluations of pavement performance are to be obtained.

7. The first appearance of load associated cracking on the surface of concrete slabs should continue to serve as the basis for preventative maintenance and evaluation of rigid pavements until computer-efficient mechanistic models can be developed to analyze shattered slab conditions.

8. The reanalysis of accelerated traffic test data using the ILLI-SLAB model for edge loading conditions suggests that additional structural life of concrete slabs is available for higher stress producing combinations of gear load and pavement thickness than would be predicted by laboratory beam fatigue models. Conversely, less structural life is predicted, using this edge loading curve, for lower stress generating circumstances. Thus, the breakdown in load transfer efficiency at joints, and therefore more rapid accumulation of damage, appears to be more closely linked to the shear number of operations of aircraft over the joint rather than to higher stress levels.

9. The use of static, transient, and unloaded designations for airfield feature identification more realistically describes actual pavement loading conditions and aids in the efficient planning and use of limited maintenance and repair expenditures.

10. Statistically-based determinations of FWD testing requirements will permit rapid and efficient utilization of valuable airfield facility down time and provide the degree of accuracy warranted by inherent variability.

11. The failure of rigid airfield pavement slabs generally results from the accumulation of damage at only one point on the slab and can be attributed, in most cases, to just one aircraft. Only in the event that mean wander paths of two or more aircraft wheels overlap is an evaluation for mixed traffic justified.

12. The use of pavement distress survey results to estimate accumulated past damage eliminates a tremendous amount of analysis of past traffic data

that is often speculative, but somewhat unconservative estimates are likely.

13. More recent studies of aircraft wander tendencies provide the basis for eliminating the nonchannelized designation for runway interiors and ladder taxiways. More realistic pass to coverage ratios are available that reflect actual aircraft movements along various airfield facilities, particularly on apron features.

14. The analysis of a single "representative" slab for each feature does not adequately take into account the variablity of joint load transfer that exists within a feature. Several individual slabs (determined from statistical analysis) must be evaluated for remaining structural life and the results averaged for the entire feature.

15. The system developed from this research effort is capable of providing realistic predictions of pavement performance for the many features on today's airfields under a variety of aircraft loading and environmental conditions. The somewhat computer-intensive analysis package appears insignificant when compared with the effort required to obtain the same quality of information from present systems.

9.3 Suggestions for Further Research

The following areas have been identified for additional research to both improve upon this effort and to advance the state of knowledge in pavement performance.

1. The effects of load magnitude on load transfer efficiencies and backcalculated E and k moduli should be investigated for loads in the range of those produced by larger aircraft. The stress dependency of cohesive and granular materials under rigid airfield pavements should be determined and included in the analysis, if it is significant.

2. Further study of the behavior of all joint types with changes in temperature is needed. Correlations should be developed between soil types and the minimum degree of load transfer available just from inherent shear strength.

3. The effects of soil moisture and its seasonal fluctuations on backcalculated moduli should be researched and incorporated into the NDT & E system.

4. Additional, more controlled field tests are required for substantiation of the flexural strength-backcalculated E correlation. Direct correlation with flexural strength, as opposed to the indirect correlation through split tension results, is preferred.

5. Predictive models of pavement performance to shattered slab conditions should be developed to take advantage of the tremendous amount of pavement performance remaining in cracked slabs, particularly those constructed on stabilized materials.

6. The NDT & E system should be expanded to include the evaluation of overlayed rigid pavement. Both flexible and rigid overlays of rigid pavement must be considered.

7. Extensive monitoring of the long term performance of rigid airfield pavements in a variety of geological and environmental conditions is required if improved transfer functions are to be developed. Accurate records of aircraft operations and loads must be maintained if improved estimates of accumulated damage are to be made.

8. The methodologies for evaluating both statically loaded and dynamically loaded pavement features with the FWD should be well defined. The appropriateness of using static third point flexural strengths for the evaluation of dynamically loaded slabs should be investigated, as should the

use of backcalculated dynamic E values for statically loaded slabs.

9. The comparison of center slab measured and predicted deflection basins for the determination of concrete slab thickness should be researched for potential use in locations where thickness information is unavailable.

10. More accurate daily distributions of traffic should be mathematically modeled and incorporated into the analysis to better reflect actual conditions. The uniform distribution assumed in this research probably results in conservative predictions of remaining life.

11. The concepts presented in this report must undergo extensive field verification to establish their validity and identify unforeseen problems. A wide variety of conditions must be included in the validation study, and side-by-side testing with other systems is desireable.

12. The computer programs written for the various analyses included in this system should be examined for maximum efficiency and recoded if necessary to improve performance. Adaptation of the analysis procedures for the micro-computer would greatly increase the utility of the system, particularly for use in contingency situations where quick results are imperative.

REFERENCES

1. Air Force Regulation 30-1, Air Force Standards, May 1985.

2. Nielson, John P. and Baird, Glenn T., Pavement Evaluation System-Final Report, AFCEC-TR--76-28, Air Force Civil Engineering Center, Tyndall AFB, Florida, October 1976.

3. Bush, Albert J. III and Hall, Jim W. Jr., Experience With Nondestructive Structural Evaluation of Airfield Pavements, Proceedings, 2nd International Conference on Concrete Pavement Design, Purdue University, April 1981.

4. Hall, Jim W. Jr., Comparitive Study of Nondestructive Pavement Testing-Mac Dill Air Force Base, U.S. Army Engineer Waterways Experiment Station, Vicksburg, Mississippi, 1984.

5. Moore, W.M., Hanson, D.I., and Hall, J.W. Jr., An Introduction to Nondestructive Structural Evaluation of Pavements, Transportation Research Circular No. 189, Transportation Research Board, National Academy of Sciences, January 1978.

6. Air Force Manual 88-24, Chapter 3, Rigid Airfield Pavement Evaluation, February 1959.

7. Air Force Manual 89-3, Materials Testing, February 1971.

8. Hammit, G.M. II, Concrete Strength Relationships, U. S. Army Engineer Waterways Experiment Station, Vicksburg, Mississippi, December 1971.

9. Air Force Manual 86-3, Chapter 3, Rigid Pavements for Airfields Other Than Army, August 1979.

10. Westergaard, H.M., Stresses in Concrete Pavements Computed by Theoretical Analyses, Public Roads, Volume 7, No. 2, 1926.

11. Westergaard, H.M., New Formulas for Stresses in Concrete Pavements of Airfields, Transactions, American Society of Civil Engineers, Volume 113, 1948.

12. Brown, D.N. and Thompson, O.O., Lateral Distribution of Aircraft Traffic, Miscellaneous Paper S-73-56, U. S. Army Engineer Waterways Experiment Station, Vicksburg, Mississippi, July 1973.

13. Hall, J.W. Jr. and Elsea, D.R., Small Aperture Testing for Airfield Pavement Evaluation, Miscellaneous Paper S-74-3, U. S. Army Engineer Waterways Experiment Station, Vicksburg, Mississippi, February 1974.

14. Pickett, G. and Ray, G.K., Influence Charts for Concrete Pavements, Transactions, American Society of Civil Engineers, Volume 116, 1951.

15. Kreger, W.C., Computerized Aircraft Ground Flotation Analysis-Edge Loaded Rigid Pavement, EER-FW-572, General Dynamics, Fort Worth, Texas, 1967

16. Arntzen, D.M., Barenberg, E.J., and Krauce, R., Airfield Pavement Demonstration Validation Study, Journal, American Society of Civil Engineers, Volume 106, No. TE6, November 1980.

17. Federal Aviation Administration Circular 150, Airport Pavement Design and Evaluation, December 1978.

18. Smith, Roger E. and Lytton, Robert L., Synthesis Study of Nondestructive Testing Devices for Use in Overlay Thickness Design of Flexible Pavements, ERES Consultants, Champaign, Illinois, November 1983.

19. Bush, Albert J. III, Nondestructive Testing for Light Aircraft Pavements, Phase I, U.S. Army Engineer Waterways Experiment Station, Vicksburg, Mississippi, January 1980.

20. Hall, Jim W. Jr., Comparitive Study of Nondestructive Pavement Testing-MacDill Air Force Base, U.S. Army Engineer Waterways Experiment Station, Vicksburg, Mississippi, Undated.

21. Burmister, D.M., The Theory of Stresses and Displacements in Layered Systems and Application to the Design of Airport Runways, Proceedings, Highway Research Board, 1943.

22. Burmister, D.M., The General Theory of Stresses and Displacements in Layered Soil Systems, Journal of Applied Physics, Volume 16, 1945.

23. Yoder, E.J. and Witczak, M.W., Principles of Pavement Design, 2nd Edition, John Wiley and Sons, 1975.

24. Ioannides, A.M., Donnelly, J., Thompson, M.R., and Barenberg, E.J., Analysis of Slabs-On-Grade for a Variety of Loading and Support Conditions, AFOSR-83-0143, Air Force Office of Scientific Research, Washington, D.C., September 1984.

25. Parker, Frazier, Jr., Development of a Structural Design Procedure for Rigid Airport Pavements, U.S. Army Engineer Waterways Experiment Station, Vicksburg, Mississippi, May 1977.

26. Bush, Albert J. III, Nondestructive Testing for Light Aircraft Pavements, Phase II, U.S. Army Engineer Waterways Experiment Station, Vicksburg, Mississippi, November 1980.

27. Uddin, W., Meyer, A.H., Hudson, W.R., and Stokoe, K.H. II, A Rigid Pavement Structural Evaluation System Based on Dynamic Deflections, Proceedings, 3rd International Conference on Concrete Pavement Design and Rehabilitation, Purdue University, April 1985.

28. Winkler, E., The Theory of Elasticity and Stiffness, H. Dominicus, Prague, 1867.

29. Zienkiewicz, O.C., The Finite Element Method, 3rd Edition, MacGraw-Hill, 1977.

30. Cook, R.D., Concepts and Applications of Finite Element Analysis, 2nd Edition, John Wiley and Sons, 1981.

31. Desai, C.S. and Christian, J.T., Numerical Methods in Geotechnical Engineering, MacGraw-Hill, 1977.

32. Ang, A.H.S. and Newmark, N.M., A Numerical Procedure for the Analysis of Continuous Plates, Proceedings, 2nd Conference on Electronic Compulation, Structural Division, American Society of Civil Engineers, September 1960.

33. Tabatabaie-Raissi, A.M., Structural Analysis of Concrete Pavement Joints, Ph.D. Thesis, University of Illinois, 1977.

34. Nie, Norman H., et al, Statistical Package for the Social Sciences, 2nd Edition, MacGraw-Hill, 1975.

35. Hoffman, M.S. and Thompson, M.R., Mechanistic Interpretation of Non-destructive Pavement Testing Deflections, Project IHR-508, University of Illinois, June 1981.

36. ERES Consultants, Nondestructive Structural Evaluation of Airfield Pavements, Champaign, Illinois, December 1982.

37. Tabatabaie, A.M., Barenberg, E.J., and Smith, R E., Longitudinal Joint Systems in Slip-Formed Rigid Pavements, Volume II-Analysis of Load Transfer Systems for Concrete Pavements, FAA-RD-79-4, Federal Aviation Administration, November 1979.

38. Thompson, M.R. and Dempsey, B.J., Development of a Preliminary ALRS Stabilization Material Pavement Analysis System (SPAS), ESL-TR-83-84, U.S. Air Force Engineering and Services Center, Tyndall AFB, Florida, March 1984.

39. Nordby, G.M., Fatigue of Concrete-A Review of Research, Journal of the American Concrete Institute, Volume 55, No.2, August 1958.

40. American Concrete Institute, Fatigue of Concrete, Committee 215, Bibliography No. 3, Detroit, Michigan, 1960.

41. Murdock, J.W., A Critical Review of Research on Fatigue of Plain Concrete, Engineering Experiment Station Bulletin 215, University of Illinois, February 1965.

42. Ople, F.S. and Hulsbos, C.L., Probable Fatigue Life of Plain Concrete With Stress Gradient, Journal of the American Concrete Institute, Volume 63, No. 1, January 1966.

43. Narrow, I. and Ullberg, E., Correlation Between Tensile and Splitting Strength and Flexural Strength of Concrete, American Concrete Institute Proceedings,, Vol 60, January 1968.

44. Greer, W.C. Jr., The Estimation of Concrete Flexural Strength From Other Types of Strength Tests, Special Technical Publication M-5, Law Engineering Testing Company, Atlanta, Georgia, Undated.

45. Darter, M.I., Design of Zero-Maintenance Plain Jointed Concrete Pavements, Volume 1, FHWA-RD-77-11, Federal Highway Administration, June 1977.

46. Packard, Robert G., Design of Concrete Airport Pavements, Engineering Bulletin 050.03P, Portland Cement Association, Skokie, Illinois, 1973

47. Trebig, H.J., McCullough, B.F., Smith, P., and Van Quintas, H., Overlay Design and Reflection Cracking Analysis for Rigid Pavements, Volume 1, Development of a New Design Criteria, FHWA-RD-77-76, Federal Highway Administration, 1977.

48. Vesic, A.S. and Saxena, S.K., Analysis of Structural Behavior of Road Test Rigid Pavements, Highway Research Board Record 291, 1969.

49. Majidzadeh, K. and Ilves, G.J., Evaluation of Rigid Pavement Overlay Design Procedure, Development of the OAR Procedure, Final Report, DTFH-11-9489, 1983.

50. Majidzadeh, K., Ilves, G.J., and Sklyut, H., RISC - A Mechanistic Method of Rigid Pavement Design, Proceedings, 3rd International Conference on Concrete Pavement Design, Purdue University, 1985.

51. Raithby, K.D. and Galloway, J.W., Effect of Moisture Condition, Age, and Rate of Loading on Fatigue of Plain Concrete, SP-41, American Concrete Institute, 1974.

52. Ballinger, C.A., Cumulative Fatigue Damage Characteristics of Plain Concrete, Highway Research Board Record 370, 1977.

53. Ahlvin, R.G., et al, Multiple-Wheel Heavy Gear Load Pavement Tests, AFWL-TR-70-113, Volumes 1 and 2, Air Force Weapons Laboratory, Kirtland AFB, New Mexico, November 1971.

54. Parker, F. Jr. and Gunkel, R.C., Development of a Structural Design Procedure for Rigid Airport Pavements, FAA-RD-77, May 1977.

55. U.S. Army Corps of Engineers, Ohio River Division Laboratories, Design and Construction Report: Lockbourne Test Track, Mariemont, Ohio, June 1944.

56. U.S. Army Corps of Engineers, Ohio River Division Laboratories, Lockbourne No. 1 Test Track: Report of Reconstruction, Mariemont, Ohio, January 1945.

57. U.S. Army Corps of Engineers, Ohio River Division Laboratories, Lockbourne No. 1 Test Track: Final Report, Mariemont, Ohio, March 1946.

58. U.S. Army Corps of Engineers, Ohio River Division Laboratories, Lockbourne No. 2; 300,000 Pound Experimental Mat: Report of Construction, Mariemont, Ohio, June 1945.

59. U.S. Army Corps of Engineers, Ohio River Division Laboratories, Lockbourne No. 2; Experimental Mat: Final Report, Mariemont, Ohio, May 1950.

60. U.S. Army Corps of Engineers, Ohio River Division Laboratories, Lockbourne No. 3; Overlay Mat Pavement Overlay Investigation: Report of Construction, Mariemont, Ohio, June 1948.

61. U.S. Army Corps of Engineers, Ohio River Division Laboratories, Lockbourne No. 3; Pavement Overlay Investigation: Final Report, Mariemont, Ohio, March 1951.

62. U.S. Army Corps of Engineers, Ohio River Division Laboratories, Channelized Test Tracks, Sharonville, Ohio: Report of Construction, Technical Report 4-7, Mariemont, Ohio, March 1957.

63. U.S. Army Corps of Engineers, Ohio River Division Laboratories, Heavy Load Test Tracks: Report of Construction, Technical Report 4-17, Mariemont, Ohio, February 1961.

64. Mellinger, F.M., Sale, J.P., and Wathen, T.R., Heavy Wheel Load Traffic on Concrete Pavements, Proceedings, Highway Research Board, Volume 36, 1957.

65. Ahlvin, R.G., et al, Multiple-Wheel Heavy Gear Load Pavement Tests, AFWL-TR-70-113, Volumes 3 and 4, Air Force Weapons Laboratory, Kirtland AFB, New Mexico, November 1971.

66. Grau, R.W., Strengthening of Keyed Longitudinal Construction Joints in Rigid Pavements, FAA-RD-72-106, Federal Aviation Administration, August 1972.

67. Burns, C.D., et al, Comparitive Performance of Structural Layers in Pavement Systems; Volume I, Design, Construction, and Behavior Under Traffic of Pavement Test Sections, FAA-RD-73-198, Federal Aviation Administration, June 1974.

68. Rollings, R.S., Corps of Engineers Design Procedures for Rigid Airfield Pavements, Proceedings, 2nd International Conference on Concrete Pavement Design, Purdue University, 1981.

69. Shahin, M.Y., Darter, M.I., and Kohn, S.D., Development of a Pavement Maintenance Management System, Volume I, AFCEC-TR-76-27, Tyndall AFB, Florida, November 1976.

70. Snedecor, G.W. and Cochran, W.G., Statistical Methods, 6th Edition, Iowa State Press, 1967.

71. Miner, M.A., Cumulative Damage in Fatigue, Journal of Applied Mechanics, September 1945.

72. HoSang, V.A., Field Survey and Analysis of Aircraft Distribution on Airport Pavements, FAA-RD-74-36, Federal Aviation Administration, February 1975.

73. Crovetti, J.A. and Darter, M.I., Joint Repair Methods for Portland Cement Concrete Pavements, Appendic C, Void Detection Procedures, University of Illinois, March 1985.

APPENDIX A

EXAMPLE COMPUTER PRODUCTS

SYMBOL	VARIABLE	UNITS
BSE	THREE LETTER DESIGNATION OF BASE/INSTALLATION	
FEAT	FEATURE DESIGNATION	
S	SLAB NUMBER	
TDIM	SLAB WIDTH IN TRANSVERSE DIRECTION	FEET
LDIM	SLAB WIDTH IN LONGITUDINAL DIRECTION	FEET
THCK	SLAB THICKNESS	INCHES
AT	AIR TEMPERATURE	DEGREES F
P	POSITION OF TEST: 1=CORNER, 2=CENTER, 3=LONG JT, 4=TRAN JT	
LOAD	FORCE EXERTED ON PAVEMENT BY FALLING WEIGHT	LBF
R	RESPONSE OF PAVEMENT: M=MEASURED, P=PREDICTED	
D0	DEFLECTION AT 0.0 INCHES FROM LOADING PLATE	MILS
D1	DEFLECTION AT 12.0 INCHES FROM LOADING PLATE	MILS
D2	DEFLECTION AT 24.0 INCHES FROM LOADING PLATE	MILS
D3	DEFLECTION AT 36.0 INCHES FROM LOADING PLATE	MILS
D4	DEFLECTION AT 48.0 INCHES FROM LOADING PLATE	MILS
D5	DEFLECTION AT 60.0 INCHES FROM LOADING PLATE	MILS
D6	DEFLECTION AT 72.0 INCHES FROM LOADING PLATE	MILS
K	MODULUS OF SUBGRADE REACTION	PSI/INCH
E	YOUNG'S MODULUS OF ELASTICITY	PSI
AIF	AGGREGATE INTERLOCK FACTOR	LBF/INCH/INCH
LTE	LOAD TRANSFER EFFICIENCY: D1/D0	
TLOS	TAXILINE OFFSET DISTANCE	FEET
TJOS	TRANSVERSE JOINT OFFSET DISTANCE	FEET
MPDN	MINER'S PAST DAMAGE NUMBER	
A/C	AIRCRAFT TYPE	
P/C	PASS PER COVERAGE RATIO	
PROP	PROPORTION OF AIRCRAFT TYPE IN TOTAL MIX	
P01 TO P12	PERCENTAGE OF TRAFFIC IN EACH TEMPERATURE ZONE	PERCENT
AIF1 TO AIF12	AGGREGATE INTERLOCK FACTORS FOR TEMPERATURE ZONES	LBF/INCH/INCH
DMG100 TO DMG50	MINER'S DAMAGE PER COVERAGE	
PASS100 TO PASS50	REMAINING PASSES FOR EACH GROSS WEIGHT CATEGORY	

Figure A-1. Reformatted Field Data File for Feature A20T

BSE	FEAT	S	TDIM	LDIM	THCK	AT	P	LOAD	R	D0	D1	D2	D3	D4	D5	D6
SEY	A20T	1	25.0	25.0	15.0	72	1	22138	M	11.400	10.733	9.400	8.000	6.433	5.767	4.700
							2	22392	M	6.267	5.067	4.100	3.267	2.600	2.100	1.700
							3	22493	M	7.167	4.600	3.633	2.933	1.900	1.633	1.500
							4	22663	M	7.900	6.733	5.367	4.433	3.633	3.000	2.267
SEY	A20T	2	25.0	25.0	15.0	72	1	22493	M	8.633	8.233	6.867	5.900	4.800	4.067	3.200
							2	23076	M	5.433	4.600	3.867	3.133	2.633	2.200	1.733
							3	22742	M	6.333	5.600	4.400	3.533	2.867	2.333	1.767
							4	22816	M	7.533	6.833	5.833	5.033	4.167	3.433	2.967
SEY	A20T	3	25.0	25.0	15.0	72	1	22710	M	6.667	6.000	5.033	4.167	3.367	2.667	2.233
							2	22986	M	4.000	3.733	3.167	2.700	2.100	1.833	1.500
							3	22949	M	5.267	4.933	4.033	3.333	2.667	2.133	1.733
							4	22806	M	5.633	4.933	4.200	3.567	3.067	2.367	2.067
SEY	A20T	4	25.0	25.0	15.0	72	1	22551	M	7.367	6.833	6.067	5.200	4.400	3.467	3.067
							2	22917	M	4.667	4.333	3.600	3.033	2.533	2.067	1.700
							3	23198	M	6.200	5.967	4.833	3.833	3.033	2.400	1.833
							4	22684	M	6.067	5.600	4.867	4.200	3.567	2.967	2.467
SEY	A20T	5	25.0	25.0	15.0	72	1	23124	M	6.400	6.000	5.133	4.267	3.567	2.967	2.400
							2	22562	M	11.833	9.800	7.867	6.133	4.700	3.400	2.600
							3	22626	M	6.867	6.067	4.900	3.967	3.100	2.267	1.900
							4	23002	M	4.867	4.267	3.567	3.100	2.667	2.200	1.833
SEY	A20T	6	25.0	25.0	15.0	72	1	22731	M	6.633	5.867	5.133	4.433	3.733	3.333	2.600
							2	23044	M	7.667	6.633	5.567	4.033	3.200	2.500	1.933
							3	23039	M	6.433	5.867	4.633	3.700	3.000	2.267	1.833
							4	21809	M	6.633	5.833	4.933	4.100	3.367	2.800	2.233

Figure A-1. (continued)

BSE	FEAT	S	TDIM	LDIM	THCK	AT	P	LOAD	R	D0	D1	D2	D3	D4	D5	D6	K	E
SEY	A20T	1	25.0	25.0	15.0	72	1	22138	M	11.400	10.733	9.400	8.000	6.433	5.767	4.700		
							2	22392	M	6.267	5.067	4.100	3.267	2.600	2.100	1.700	511.6	1305420.
									P	6.264	5.667	4.533	3.381	2.371	1.560	0.952		
							3	22493	M	7.167	4.800	3.633	2.933	1.900	1.633	1.500		
							4	22663	M	7.900	6.733	5.367	4.433	3.633	3.000	2.267		
SEY	A20T	2	25.0	25.0	15.0	72	1	22493	M	8.633	8.233	6.867	5.900	4.800	4.067	3.200		
							2	23076	M	5.433	4.600	3.867	3.133	2.633	2.200	1.733	473.6	2027716.
									P	5.432	5.001	4.174	3.287	2.467	1.767	1.203		
							3	22742	M	6.333	5.600	4.400	3.533	2.867	2.333	1.767		
							4	22816	M	7.533	6.833	5.833	5.033	4.167	3.433	2.967		
SEY	A20T	3	25.0	25.0	15.0	72	1	22710	M	6.667	6.000	5.033	4.167	3.367	2.667	2.233		
							2	22986	M	4.000	3.733	3.167	2.700	2.100	1.633	1.500	467.9	3862056.
									P	4.012	3.768	3.282	2.733	2.196	1.707	1.281		
							3	22949	M	5.267	4.933	4.033	3.333	2.667	2.133	1.733		
							4	22806	M	5.633	4.933	4.200	3.567	3.067	2.367	2.067		
SEY	A20T	4	25.0	25.0	15.0	72	1	22551	M	7.367	6.833	6.067	5.200	4.400	3.467	3.067		
							2	22917	M	4.667	4.333	3.600	3.033	2.533	2.067	1.700	419.0	3163554.
									P	4.666	4.371	3.786	3.130	2.494	1.919	1.423		
							3	23198	M	6.200	5.967	4.833	3.833	3.033	2.400	1.833		
							4	22684	M	6.067	5.800	4.867	4.200	3.567	2.967	2.467		
SEY	A20T	5	25.0	25.0	15.0	72	1	23124	M	8.400	8.000	5.133	4.267	3.567	2.967	2.400		
							2	22562	M	11.833	9.800	7.867	6.133	4.700	3.400	2.600	287.3	660204.
									P	11.828	10.635	8.446	6.221	4.295	2.770	1.646		
							3	22626	M	6.867	6.067	4.900	3.967	3.100	2.267	1.900		
							4	23002	M	4.867	4.267	3.567	3.100	2.667	2.200	1.833		
SEY	A20T	6	25.0	25.0	15.0	72	1	22731	M	6.633	5.867	5.133	4.433	3.733	3.333	2.600		
							2	23044	M	7.667	6.633	5.567	4.033	3.200	2.500	1.933	392.0	1211163.
									P	7.739	7.042	5.735	4.370	3.148	2.144	1.369		
							3	23039	M	6.433	5.867	4.633	3.700	3.000	2.267	1.833		
							4	21809	M	6.633	5.833	4.933	4.100	3.367	2.800	2.233		

Figure A-2. Backcalculated E and k Results and Predicted Sensor Deflections for the Center Slab Position

BSE	FEAT	S	TDIM	LDIM	THCK	AT	P	LOAD	R	D0	D1	D2	D3	D4	D5	D6	K	E	AIF	LTE
SEY	A20T	1	25.0	25.0	15.0	72	1	22138	M	11.400	10.733	9.400	8.000	6.433	5.767	4.700				
							2	22392	M	6.267	5.067	4.100	3.267	2.600	2.100	1.700	511.6	1305420.		
									P	6.264	5.657	4.533	3.381	2.371	1.560	0.952				
							3	22493	M	7.167	4.600	3.633	2.933	1.900	1.633	1.500				
							4	22663	M	7.900	6.733	5.367	4.433	3.633	3.000	2.267			456910.	0.85
									P	8.963	7.717	5.338	3.449	2.264	1.080	-0.105				0.86
SEY	A20T	2	25.0	25.0	15.0	72	1	22493	M	8.633	8.233	6.867	5.900	4.800	4.067	3.200				
							2	23076	M	5.433	4.600	3.867	3.133	2.633	2.200	1.733	473.6	2027716.		
									P	5.432	5.001	4.174	3.287	2.467	1.767	1.203				
							3	22742	M	6.333	5.600	4.400	3.533	2.867	2.333	1.767				
							4	22816	M	7.533	6.833	5.833	5.033	4.167	3.433	2.967			1650365.	0.91
									P	7.579	6.915	5.016	3.461	2.408	1.356	0.303				0.91
SEY	A20T	3	25.0	25.0	15.0	72	1	22710	M	6.667	6.000	5.033	4.167	3.367	2.667	2.233				
							2	22986	M	4.000	3.733	3.167	2.700	2.100	1.833	1.500	467.9	3882056.		
									P	4.012	3.768	3.282	2.733	2.196	1.707	1.281				
							3	22949	M	5.267	4.933	4.033	3.333	2.667	2.133	1.733				
							4	22806	M	5.633	4.933	4.200	3.567	3.067	2.367	2.067			643574.	0.88
									P	5.822	5.175	3.979	2.952	2.192	1.433	0.674				0.89
SEY	A20T	4	25.0	25.0	15.0	72	1	22551	M	7.367	6.833	6.067	5.200	4.400	3.467	3.067				
							2	22917	M	4.667	4.333	3.600	3.033	2.533	2.067	1.700	419.0	3163554.		
									P	4.666	4.371	3.786	3.130	2.494	1.919	1.423				
							3	23198	M	6.200	5.967	4.833	3.833	3.033	2.400	1.833				
							4	22684	M	6.067	5.600	4.867	4.200	3.567	2.967	2.467			2431272.	0.92
									P	6.593	6.129	4.662	3.419	2.516	1.613	0.710				0.93
SEY	A20T	5	25.0	25.0	15.0	72	1	23124	M	6.400	6.000	5.133	4.267	3.567	2.967	2.400				
							2	22562	M	11.833	9.800	7.867	6.133	4.700	3.400	2.600	287.3	660204.		
									P	11.828	10.635	8.446	6.221	4.295	2.770	1.646				
							3	22626	M	6.867	6.067	4.900	3.967	3.100	2.267	1.900				
							4	23002	M	4.867	4.267	3.567	3.100	2.667	2.200	1.833			566874.	0.88
									P	16.696	14.835	10.118	6.428	4.166	1.904	-0.358				0.89
SEY	A20T	6	25.0	25.0	15.0	72	1	22731	M	6.633	5.867	5.133	4.433	3.733	3.333	2.600				
							2	23044	M	7.667	6.633	5.567	4.033	3.200	2.500	1.933	392.0	1211163.		
									P	7.739	7.042	5.735	4.370	3.148	2.144	1.369				
							3	23039	M	6.433	5.867	4.633	3.700	3.000	2.267	1.833				
							4	21809	M	6.633	5.833	4.933	4.100	3.367	2.800	2.233			688637.	0.88
									P	10.204	9.081	6.394	4.237	2.845	1.452	0.060				0.89

Figure A-3. Iterated Aggregate Interlock Factors, and Measured and Predicted Deflections and Load Transfer Efficiencies at the Transverse Joints

BSE	FEAT	S	TDIM	LDIM	THCK	AT	P	LOAD	R	D0	D1	D2	D3	D4	D5	D6	K	E	AIF	LTE
SEY	A20T	1	25.0	25.0	15.0	72	1	22138	M	11.400	10.733	9.400	8.000	6.433	5.767	4.700				
							2	22392	M	6.267	5.067	4.100	3.267	2.600	2.100	1.700	511.6	1305420.		
									P	6.264	5.657	4.533	3.381	2.371	1.560	0.952				
							3	22493	M	7.167	4.600	3.633	2.933	1.900	1.633	1.500			50583.	0.64
									P	10.090	6.487	4.527	2.941	1.930	0.916	-0.093				0.64
							4	22663	M	7.900	6.733	5.367	4.433	3.633	3.000	2.267			456910.	0.85
									P	8.963	7.717	5.338	3.449	2.264	1.080	-0.105				0.86
SEY	A20T	2	25.0	25.0	15.0	72	1	22493	M	8.633	8.233	6.867	5.900	4.800	4.067	3.200				
							2	23076	M	5.433	4.600	3.867	3.133	2.633	2.200	1.733	473.6	2027716.		
									P	5.432	5.001	4.174	3.287	2.467	1.767	1.203				
							3	22742	M	6.333	5.600	4.400	3.533	2.867	2.333	1.767			825347.	0.88
									P	7.630	6.819	4.956	3.423	2.382	1.342	0.301				0.89
							4	22816	M	7.533	6.833	5.833	5.033	4.167	3.433	2.967			1650365.	0.91
									P	7.579	6.915	5.016	3.461	2.408	1.356	0.303				0.91
SEY	A20T	3	25.0	25.0	15.0	72	1	22710	M	6.667	6.000	5.033	4.167	3.367	2.667	2.233				
							2	22986	M	4.000	3.733	3.167	2.700	2.100	1.833	1.500	467.9	3882056.		
									P	4.012	3.768	3.282	2.733	2.196	1.707	1.281				
							3	22949	M	5.267	4.933	4.033	3.333	2.667	2.133	1.733			5258063.	0.94
									P	5.704	5.357	4.101	3.033	2.251	1.469	0.687				0.94
							4	22806	M	5.633	4.933	4.200	3.567	3.067	2.367	2.067			643574.	0.88
									P	5.822	5.175	3.979	2.952	2.192	1.433	0.674				0.89
SEY	A20T	4	25.0	25.0	15.0	72	1	22551	M	7.367	6.833	6.067	5.200	4.400	3.467	3.067				
							2	22917	M	4.667	4.333	3.600	3.033	2.533	2.067	1.700	419.0	3163554.		
									P	4.666	4.371	3.786	3.130	2.494	1.919	1.423				
							3	23198	M	6.200	5.967	4.833	3.833	3.033	2.400	1.833			3000000000.	0.96
									P	6.710	6.299	4.786	3.507	2.581	1.654	0.727				0.94
							4	22684	M	6.067	5.600	4.867	4.200	3.567	2.967	2.467			2431272.	0.92
									P	6.593	6.129	4.662	3.419	2.516	1.613	0.710				0.93
SEY	A20T	5	25.0	25.0	15.0	72	1	23124	M	6.400	6.000	5.133	4.267	3.567	2.967	2.400				
							2	22562	M	11.833	9.800	7.867	6.133	4.700	3.400	2.600	287.3	660204.		
									P	11.828	10.635	8.446	6.221	4.295	2.770	1.646				
							3	22626	M	6.867	6.067	4.900	3.967	3.100	2.267	1.900			692865.	0.88
									P	16.379	14.635	9.977	6.336	4.106	1.877	-0.353				0.89
							4	23002	M	4.867	4.267	3.567	3.100	2.667	2.200	1.833			566874.	0.88
									P	16.696	14.835	10.118	6.428	4.166	1.904	-0.358				0.89
SEY	A20T	6	25.0	25.0	15.0	72	1	22731	M	6.633	5.867	5.133	4.433	3.733	3.333	2.600				
							2	23044	M	7.667	6.633	5.567	4.033	3.200	2.500	1.933	392.0	1211163.		
									P	7.739	7.042	5.735	4.370	3.148	2.144	1.369				
							3	23039	M	6.433	5.867	4.633	3.700	3.000	2.267	1.833			2164537.	0.91
									P	10.643	9.727	6.831	4.521	3.034	1.548	0.062				0.91
							4	21809	M	6.633	5.833	4.933	4.100	3.367	2.800	2.233			688637.	0.88
									P	10.204	9.081	6.394	4.237	2.845	1.452	0.060				0.89

Figure A-4. Iterated Aggregate Interlock Factors, and Measured and Predicted Deflections and Load Transfer Efficiencies at the Longitudinal Joints

BSE	FEAT	S	TDIM	LDIM	THCK	AT	P	LOAD	R	D0	D1	D2	D3	D4	D5	D6	K	E	AIF	LTE
SEY	A20T	1	25.0	25.0	15.0	72	1	22138	M	11.400	10.733	9.400	8.000	6.433	5.767	4.700			4766618545.	0.94
									P	10.579	9.885	7.279	5.107	3.632	2.157	0.682				0.93
							2	22392	M	6.267	5.067	4.100	3.267	2.600	2.100	1.700	511.6	1305420.		
									P	6.264	5.657	4.533	3.381	2.371	1.560	0.952				
							3	22493	M	7.167	4.600	3.633	2.933	1.900	1.633	1.500			50583.	0.64
									P	10.090	6.487	4.527	2.941	1.930	0.918	-0.093				0.64
							4	22663	M	7.900	6.733	5.367	4.433	3.633	3.000	2.267			456910.	0.85
									P	8.963	7.717	5.338	3.449	2.264	1.080	-0.105				0.86
SEY	A20T	2	25.0	25.0	15.0	72	1	22493	M	8.633	8.233	6.867	5.900	4.600	4.067	3.200			3000000000.	0.95
									P	9.318	8.815	6.778	5.022	3.741	2.460	1.179				0.95
							2	23076	M	5.433	4.600	3.867	3.133	2.633	2.200	1.733	473.6	2027716.		
									P	5.432	5.001	4.174	3.287	2.467	1.767	1.203				
							3	22742	M	6.333	5.600	4.400	3.533	2.867	2.333	1.767			825347.	0.88
									P	7.630	6.819	4.956	3.423	2.382	1.342	0.301				0.89
							4	22816	M	7.533	6.833	5.833	5.033	4.167	3.433	2.967			1650365.	0.91
									P	7.579	6.915	5.016	3.461	2.408	1.356	0.303				0.91
SEY	A20T	3	25.0	25.0	15.0	72	1	22710	M	6.667	6.000	5.033	4.167	3.367	2.667	2.233			1104033.	0.90
									P	7.436	6.806	5.431	4.235	3.315	2.394	1.474				0.92
							2	22986	M	4.000	3.733	3.167	2.700	2.100	1.833	1.500	467.9	3882056.		
									P	4.012	3.768	3.282	2.733	2.196	1.707	1.281				
							3	22949	M	5.267	4.933	4.033	3.333	2.667	2.133	1.733			5258063.	0.94
									P	5.704	5.357	4.101	3.033	2.251	1.469	0.687				0.94
							4	22806	M	5.633	4.933	4.200	3.567	3.067	2.367	2.067			643574.	0.88
									P	5.822	5.175	3.979	2.952	2.192	1.433	0.674				0.89
SEY	A20T	4	25.0	25.0	15.0	72	1	22551	M	7.367	6.833	6.067	5.200	4.400	3.467	3.067			2429168.	0.93
									P	8.403	7.879	6.276	4.873	3.792	2.710	1.629				0.94
							2	22917	M	4.667	4.333	3.600	3.033	2.533	2.067	1.700	419.0	3163554.		
									P	4.666	4.371	3.786	3.130	2.494	1.919	1.423				
							3	23198	M	6.200	5.967	4.833	3.833	3.033	2.400	1.833			3000000000.	0.96
									P	6.710	6.299	4.786	3.507	2.581	1.654	0.727				0.94
							4	22684	M	6.067	5.600	4.867	4.200	3.567	2.967	2.467			2431272.	0.92
									P	6.593	6.129	4.662	3.419	2.516	1.613	0.710				0.93
SEY	A20T	5	25.0	25.0	15.0	72	1	23124	M	6.400	6.000	5.133	4.267	3.567	2.967	2.400			7802778463.	0.94
									P	20.560	19.156	13.970	9.682	6.816	3.950	1.084				0.93
							2	22562	M	11.833	9.800	7.867	6.133	4.700	3.400	2.600	287.3	660204.		
									P	11.828	10.635	8.446	6.221	4.295	2.770	1.646				
							3	22626	M	6.867	6.067	4.900	3.967	3.100	2.267	1.900			692865.	0.88
									P	16.379	14.635	9.977	6.336	4.106	1.877	-0.353				0.89
							4	23002	M	4.867	4.267	3.567	3.100	2.667	2.200	1.833			566874.	0.88
									P	16.696	14.835	10.118	6.428	4.166	1.904	-0.358				0.89

Figure A-5. Iterated Aggregate Interlock Factors, and Measured and Predicted Deflections and Load Transfer Efficiencies at the Slab Corners

BSE	FEAT	S	TDIM	LDIM	THCK	AT	P	LOAD	R	D0	D1	D2	D3	D4	D5	D6	K	E
			TLOS	TJOS	MPDN													
SEY	A20T	1	25.0	25.0	15.0	72	1	2138	M	1.400	0.733	9.400	8.000	6.433	5.767	4.700		
							2	22392	M	6.267	5.067	4.100	3.267	2.600	2.100	1.700	511.6	1305420.
			0.0	0.0	0.42				P	6.264	5.857	4.533	3.381	2.371	1.560	0.952		
							3	22493	M	7.167	4.600	3.633	2.933	1.900	1.633	1.500		
							4	22663	M	7.900	6.733	5.367	4.433	3.633	3.000	2.267		
SEY	A20T	2	25.0	25.0	15.0	72	1	2493	M	8.833	8.233	6.867	5.900	4.800	4.067	3.200		
							2	23076	M	5.433	4.600	3.867	3.133	2.633	2.200	1.733	473.6	2027716.
			0.0	0.0	0.42				P	5.432	5.001	4.174	3.287	2.467	1.767	1.203		
							3	22742	M	6.333	5.600	4.400	3.533	2.867	2.333	1.767		
							4	22818	M	7.533	6.833	5.833	5.033	4.167	3.433	2.967		
SEY	A20T	3	25.0	25.0	15.0	72	1	2710	M	6.667	6.000	5.033	4.167	3.367	2.667	2.233		
							2	22986	M	4.000	3.733	3.167	2.700	2.100	1.833	1.500	467.9	3882056.
			0.0	0.0	0.42				P	4.012	3.768	3.282	2.733	2.196	1.707	1.281		
							3	22919	M	5.267	4.933	4.033	3.333	2.667	2.133	1.733		
							4	22806	M	5.633	4.933	4.200	3.567	3.067	2.367	2.067		
SEY	A20T	4	25.0	25.0	15.0	72	1	2551	M	7.367	6.833	6.067	5.200	4.400	3.467	3.067		
							2	22917	M	4.667	4.333	3.600	3.033	2.533	2.067	1.700	419.0	3163554.
			0.0	0.0	0.42				P	4.666	4.371	3.786	3.130	2.494	1.919	1.423		
							3	23198	M	6.200	5.967	4.833	3.833	3.033	2.400	1.833		
							4	22684	M	6.067	5.600	4.667	4.200	3.567	2.967	2.467		
SEY	A20T	5	25.0	25.0	15.0	72	1	3124	M	6.400	6.000	5.133	4.267	3.567	2.967	2.400		
							2	22562	M	11.833	9.800	7.867	6.133	4.700	3.400	2.600	287.3	660204.
			0.0	0.0	0.42				P	11.828	10.635	8.446	6.221	4.295	2.770	1.646		
							3	22626	M	6.867	6.067	4.900	3.967	3.100	2.267	1.900		
							4	23002	M	4.867	4.267	3.567	3.100	2.667	2.200	1.833		
SEY	A20T	6	25.0	25.0	15.0	72	1	2731	M	6.633	5.867	5.133	4.433	3.733	3.333	2.600		
							2	23044	M	7.667	6.633	5.567	4.033	3.200	2.600	1.933	392.0	1211163.
			0.0	0.0	0.42				P	7.739	7.042	5.735	4.370	3.148	2.144	1.369		
							3	23039	M	6.433	5.867	4.633	3.700	3.000	2.267	1.833		
							4	21809	M	6.633	5.833	4.933	4.100	3.367	2.800	2.233		

Figure A-6. Modified Field Data Base for Use with AIFCALC to Iterate Transverse and Longitudinal Aggregate Interlock Factors

```
**********************************************************************************************************************************

BSE FEAT  S TDIM LDIM THCK  AT    K          E      TLOS TJOS MPDN

   AIF1         AIF2         AIF3         AIF4         AIF5         AIF6         AIF7         AIF8         AIF9         AIF10        AIF11        AIF12

**********************************************************************************************************************************

SEY A20T  1 25.0 25.0 15.0  72 511.6    1305420.   0.0  0.0 0.42
      6703.        6703.        6703.        6730.        7383.       11252.       23667.       52743.      127870.      340869.      843703.     1385242.
      6703.        6703.        6703.        6787.        9195.       23446.       70265.      259902.      914870.3000000000.3000000000.3000000000.

SEY A20T  2 25.0 25.0 15.0  72 473.6    2027716.   0.0  0.0 0.42
      6667.        6904.        9272.       18604.       43026.      107503.      302250.      798063.     1381656.3000000000.3000000000.3000000000.
      6665.        6665.        6673.        7558.       15592.       46084.      161588.      622157.     1385466.3000000000.3000000000.3000000000.

SEY A20T  3 25.0 25.0 15.0  72 467.9    3882056.   0.0  0.0 0.42
      7715.       11483.       25169.       58749.      152289.      444196.     1138056.3000000000.3000000000.3000000000.3000000000.3000000000.
      7247.        7247.        7247.        7503.       11873.       33021.       98522.      380118.     1254660.3000000000.3000000000.3000000000.

SEY A20T  4 25.0 25.0 15.0  72 419.0    3163554.   0.0  0.0 0.42
     10190.       22179.       53335.      150837.      444330.     1061565.3000000000.3000000000.3000000000.3000000000.3000000000.3000000000.
      6501.        6501.        6538.        8208.       19353.       58445.      222324.      805510.3000000000.3000000000.3000000000.3000000000.

SEY A20T  5 25.0 25.0 15.0  72 287.3     660204.   0.0  0.0 0.42
      2970.        3093.        4354.        9457.       24804.       68862.      185957.      399002.      381691.3000000000.3000000000.3000000000.
      2968.        2968.        2969.        3100.        5301.       16563.       61690.      223253.      462618.3000000000.3000000000.3000000000.

SEY A20T  6 25.0 25.0 15.0  72 392.0    1211163.   0.0  0.0 0.42
      4772.        5621.       10040.       23189.       60320.      169773.      457510.      871679.3000000000.3000000000.3000000000.3000000000.
      4733.        4733.        4734.        4962.        8430.       23953.       83737.      318756.      850202.3000000000.3000000000.3000000000.
```

Figure A-7. Typical AIFCALC Output Showing Aggregate Interlock Factors for Each of Twelve Temperature Zones

```
**********************************************************************************************************************************

 A/C          P/C        PROP

P01    P02    P03    P04    P05    P06    P07    P08    P09    P10    P11    P12

B&E FEAT  S TDIM LDIM THCK  AT    K          E       TLOS TJOS MPDM

       AIF1         AIF2         AIF3         AIF4         AIF5         AIF6         AIF7         AIF8         AIF9         AIF10        AIF11        AIF12

**********************************************************************************************************************************

C141B        3.81        1.00

0.0    0.0    0.0    3.1    14.9   20.8   16.7   22.8   16.7   5.2    0.0    0.0

SEY A20T  1 25.0 25.0 15.0  72 511.6    1305420.   0.0  0.0 0.42
       6703.        6703.        6703.        6730.        7383.       11252.       23667.       52743.      127870.      340869.      843703.     1385242.
       6703.        6703.        6703.        6787.        9195.       23446.       70265.      259902.      914870.3000000000.3000000000.3000000000.

SEY A20T  2 25.0 25.0 15.0  72 473.6    2027716.   0.0  0.0 0.42
       6667.        6904.        9272.       18604.       43026.      107503.      302250.      798063.     1381656.3000000000.3000000000.3000000000.
       6665.        6665.        6673.        7558.       15592.       46084.      161588.      622157.     1385466.3000000000.3000000000.3000000000.

SEY A20T  3 25.0 25.0 15.0  72 467.9    3882056.   0.0  0.0 0.42
       7715.       11483.       25169.       58749.      152289.      444196.     1138058.3000000000.3000000000.3000000000.3000000000.3000000000.
       7247.        7247.        7247.        7503.       11873.       33021.       98522.      380118.     1254660.3000000000.3000000000.3000000000.

SEY A20T  4 25.0 25.0 15.0  72 419.0    3163554.   0.0  0.0 0.42
      10190.       22179.       53335.      150837.      444330.     1061565.3000000000.3000000000.3000000000.3000000000.3000000000.3000000000.
       6501.        6501.        6538.        8208.       19353.       58445.      222324.      805510.3000000000.3000000000.3000000000.3000000000.

SEY A20T  5 25.0 25.0 15.0  72 287.3     660204.   0.0  0.0 0.42
       2970.        3093.        4354.        9457.       24804.       68862.      185957.      399002.      381691.3000000000.3000000000.3000000000.
       2968.        2968.        2969.        3100.        5301.       16563.       61690.      223253.      462618.3000000000.3000000000.3000000000.

SEY A20T  6 25.0 25.0 15.0  72 392.0    1211163.   0.0  0.0 0.42
       4772.        5621.       10040.       23189.       60320.      169773.      457510.      871679.3000000000.3000000000.3000000000.3000000000.
       4733.        4733.        4734.        4962.        8430.       23953.       83737.      318756.      850202.3000000000.3000000000.3000000000.
```

Figure A-8. Modified AIFCALC Output for Use with DAMAGE

A/C	P/C	PROP									
BSE	FEAT	S	TDIM	LDIM	THCK	AT	MPDN	DMG100	DMG90	DMG80	DMG70	DMG60	DMG50
C141B			3.81		1.00								
SEY	A20T	1	25.0	25.0	15.0	72	0.42	0.000475648051	0.000251231814	0.000117908269	0.000043514638	0.000011719828	0.000001911235
SEY	A20T	2	25.0	25.0	15.0	72	0.42	0.000588021976	0.000319465868	0.000155415089	0.000060370088	0.000017495094	0.000003184591
SEY	A20T	3	25.0	25.0	15.0	72	0.42	0.001086658107	0.000625898388	0.000325746658	0.000137929324	0.000044598882	0.000009392049
SEY	A20T	4	25.0	25.0	15.0	72	0.42	0.000814814610	0.000458592224	0.000232745835	0.000095670196	0.000029906286	0.000006057774
SEY	A20T	5	25.0	25.0	15.0	72	0.42	0.000481683384	0.000256502772	0.000121779077	0.000045754137	0.000012663037	0.000002154629
SEY	A20T	6	25.0	25.0	15.0	72	0.42	0.000607209627	0.000330413359	0.000160873119	0.000062450258	0.000018032927	0.000003251979

Figure A-9. Typical DAMAGE Output Showing Miner's Accumulated Damage for One Coverage of the C-141 at Six Gross Weight Levels

BSE	FEAT	S	TDIM	LDIM	THCK	AT	MPDN	A/C	PASS100	PASS90	PASS80	PASS70	PASS60	PASS50
SEY	A20T	1	25.0	25.0	15.0	72	0.42	C141B	4646.	8796.	16742.	50783.	188552.	1156216.
								DUMMY	0.	0.	0.	0.	0.	0.
SEY	A20T	2	25.0	25.0	15.0	72	0.42	C141B	3758.	6917.	14219.	36604.	126310.	693904.
								DUMMY	0.	0.	0.	0.	0.	0.
SEY	A20T	3	25.0	25.0	15.0	72	0.42	C141B	2034.	3531.	6784.	16021.	49548.	235284.
								DUMMY	0.	0.	0.	0.	0.	0.
SEY	A20T	4	25.0	25.0	15.0	72	0.42	C141B	2712.	4819.	9494.	23098.	73891.	364787.
								DUMMY	0.	0.	0.	0.	0.	0.
SEY	A20T	5	25.0	25.0	15.0	72	0.42	C141B	4588.	8615.	18146.	48297.	174508.	1025606.
								DUMMY	0.	0.	0.	0.	0.	0.
SEY	A20T	6	25.0	25.0	15.0	72	0.42	C141B	3639.	6688.	13736.	35385.	122543.	679525.
								DUMMY	0.	0.	0.	0.	0.	0.

Figure A-10. Summary of Predicted Remaining Passes for Each Gross Weight Category of the C-141

```
**********************************************************************************************************************************

 A/C          P/C        PROP

PQ1    PQ2    PQ3    PQ4    PQ5    PQ6    PQ7    PQ8    PQ9    P10    P11    P12

BSE FEAT  S TDIM LDIM THCK  AT    K          E      TLOS TJOS MPDM

       AIF1          AIF2          AIF3          AIF4          AIF5          AIF6          AIF7          AIF8          AIF9          AIF10         AIF11         AIF12

**********************************************************************************************************************************

C141B        3.81        0.40

0.0    0.0    0.0    3.1    14.9   20.8   16.7   22.6   16.7   5.2    0.0    0.0

SEY A20T  1 25.0 25.0 15.0  72 511.6    1305420.   0.0  0.0 0.42
        6703.          6703.          6703.          6730.          7383.          11252.         23667.         52743.         127870.        340869.        843703.        1385242.
        6703.          6703.          6703.          6787.          9195.          23446.         70265.         259902.        914870.3000000000.3000000000.3000000000.

SEY A20T  2 25.0 25.0 15.0  72 473.6    2027716.   0.0  0.0 0.42
        6667.          6904.          9272.          18604.         43026.         107503.        302250.        798063.        1381656.3000000000.3000000000.3000000000.
        6665.          6665.          6673.          7858.          15592.         46084.         161588.        622157.        1385466.3000000000.3000000000.3000000000.

SEY A20T  3 25.0 25.0 15.0  72 467.9    3882056.   0.0  0.0 0.42
        7715.         11483.         25169.         58749.         152289.        444196.        1138058.3000000000.3000000000.3000000000.3000000000.3000000000.
        7247.          7247.          7247.          7503.          11873.         33021.         98522.         380118.        1254660.3000000000.3000000000.3000000000.

SEY A20T  4 25.0 25.0 15.0  72 419.0    3163554.   0.0  0.0 0.42
       10190.         22179.         53335.        150837.        444330.        1061565.3000000000.3000000000.3000000000.3000000000.3000000000.3000000000.
        6501.          6501.          6538.          8208.          19353.         58445.         222324.        805510.3000000000.3000000000.3000000000.3000000000.

SEY A20T  5 25.0 25.0 15.0  72 287.3     660204.   0.0  0.0 0.42
        2970.          3093.          4354.          9457.          24804.         68862.         185957.        399002.        381691.3000000000.3000000000.3000000000.
        2968.          2968.          2969.          3100.          5301.          16563.         61690.         223253.        462618.3000000000.3000000000.3000000000.
SEY A20T  6 25.0 25.0 15.0  72 392.0    1211163.   0.0  0.0 0.42
        4772.          5621.         10040.         23189.         60320.         169773.        457510.        871679.3000000000.3000000000.3000000000.3000000000.
        4733.          4733.          4734.          4962.          8430.          23953.         83737.         318756.        850202.3000000000.3000000000.3000000000.
```

Figure A-11. Input File to DAMAGE for a 40 Percent Mix of the C-141

```
**********************************************************************************************************************************

 A/C          P/C       PROP

P01   P02    P03   P04   P05   P06   P07   P08   P09   P10   P11   P12

BSE FEAT  S TDIM LDIM THCK  AT    K          E       TLOS TJOS MPDM

      AIF1         AIF2         AIF3         AIF4         AIF5         AIF6         AIF7         AIF8         AIF9         AIF10        AIF11        AIF12

**********************************************************************************************************************************

KC135        3.69        0.60

0.0   0.0    0.0   3.1   14.9  20.8  16.7  22.6  16.7  5.2   0.0   0.0

SEY A20T  1 25.0 25.0 15.0  72 511.6    1305420.   0.0  0.0 0.42
       6703.        6703.        6703.        6730.        7383.       11252.       23667.       52743.      127870.      340869.      843703.     1385242.
       6703.        6703.        6703.        6787.        9195.       23446.       70265.      259902.      914870.3000000000.3000000000.3000000000.

SEY A20T  2 25.0 25.0 15.0  72 473.6    2027716.   0.0  0.0 0.42
       6667.        6904.        9272.       18604.       43026.      107503.      302250.      798063.     1381656.3000000000.3000000000.3000000000.
       6665.        6665.        6673.        7558.       15592.       46084.      161588.      622157.     1385466.3000000000.3000000000.3000000000.

SEY A20T  3 25.0 25.0 15.0  72 467.9    3082056.   0.0  0.0 0.42
       7715.       11483.       25169.       58745.      152289.      444196.     1138058.3000000000.3000000000.3000000000.3000000000.3000000000.
       7247.        7247.        7247.        7503.       11873.       33021.       98522.      380118.     1254660.3000000000.3000000000.3000000000.

SEY A20T  4 25.0 25.0 15.0  72 419.0    3163554.   0.0  0.0 0.42
      10190.       22179.       53335.      150837.      444330.     1061565.3000000000.3000000000.3000000000.3000000000.3000000000.3000000000.
       6501.        6501.        6538.        8208.       19353.       58445.      222324.      805510.3000000000.3000000000.3000000000.3000000000.

SEY A20T  5 25.0 25.0 15.0  72 287.3     660204.   0.0  0.0 0.42
       2970.        3093.        4354.        9457.       24804.       68862.      185957.      399002.      381691.3000000000.3000000000.3000000000.
       2968.        2968.        2969.        3100.        5301.       16563.       61690.      223253.      462618.3000000000.3000000000.3000000000.

SEY A20T  6 25.0 25.0 15.0  72 392.0    1211163.   0.0  0.0 0.42
       4772.        5621.       10040.       23189.       60320.      169773.      457510.      871679.3000000000.3000000000.3000000000.3000000000.
       4733.        4733.        4734.        4962.        8430.       23953.       83737.      318756.      850202.3000000000.3000000000.3000000000.
```

Figure A-12. Input File to DAMAGE for a 60 Percent Mix of the KC-135

A/C	P/C		PROP								
BSE FEAT	S	TDIM	LDIM	THCK	AT	NPDN	DMG100	DMG90	DMG80	DMG70	DMG60	DMG50
C141B		3.81		0.40								
SEY A20T	1	25.0	25.0	15.0	72	0.42	0.000475648051	0.000251231814	0.000117908269	0.000043514638	0.000011719828	0.000001911235
SEY A20T	2	25.0	25.0	15.0	72	0.42	0.000588021976	0.000319465868	0.000155415089	0.000060370088	0.000017495094	0.000003184591
SEY A20T	3	25.0	25.0	15.0	72	0.42	0.001086658107	0.000625898368	0.000325746658	0.000137929324	0.000044598682	0.000009392049
SEY A20T	4	25.0	25.0	15.0	72	0.42	0.000814814610	0.000458592224	0.000232745835	0.000095670196	0.000029906286	0.000006057774
SEY A20T	5	25.0	25.0	15.0	72	0.42	0.000481683384	0.000256502772	0.000121779077	0.000045754137	0.000012663037	0.000002154629
SEY A20T	6	25.0	25.0	15.0	72	0.42	0.000607209627	0.000330413359	0.000160873119	0.000062450258	0.000018032927	0.000003251979

Figure A-13. Cumulative Miner's Damage Numbers for the C-141

A/C BSE	FEAT	S	P/C TDIM	LDIM	PROP THCK	AT	MPDN	DMG100	DMG90	DMG80	DMG70	DMG60	DMG50
KC135			3.69		0.60								
SEY	A20T	1	25.0	25.0	15.0	72	0.42	0.000050334930	0.000021444419	0.000007787722	0.000002043259	0.000000349278	0.000000030125
SEY	A20T	2	25.0	25.0	15.0	72	0.42	0.000077452017	0.000035114755	0.000013771229	0.000004016058	0.000000793975	0.000000084513
SEY	A20T	3	25.0	25.0	15.0	72	0.42	0.000209183077	0.000103389073	0.000044820051	0.000014876867	0.000003476386	0.000000464310
SEY	A20T	4	25.0	25.0	15.0	72	0.42	0.000138282706	0.000066517087	0.000028017849	0.000008994921	0.000002024198	0.000000258905
SEY	A20T	5	25.0	25.0	15.0	72	0.42	0.000051294377	0.000022127189	0.000008177455	0.000002203159	0.000000391597	0.000000035808
SEY	A20T	6	25.0	25.0	15.0	72	0.42	0.000075180828	0.000033723251	0.000013040332	0.000003725010	0.000000714389	0.000000072552

Figure A-14. Cumulative Miner's Damage Numbers for the KC-135

BSE	FEAT	S	TDIM	LDIM	THCK	AT	MPDN	A/C	PASS100	PASS90	PASS80	PASS70	PASS60	PASS50
SEY	A20T	1	25.0	25.0	15.0	72	0.42							
								C141B	3992.	7769.	17002.	47340.	180233.	1128663.
								KC135	5987.	11653.	25504.	71010.	270350.	1692994.
SEY	A20T	2	25.0	25.0	15.0	72	0.42							
								C141B	3121.	5911.	12503.	33185.	118015.	666509.
								KC135	4682.	8866.	18754.	49778.	177022.	999764.
SEY	A20T	3	25.0	25.0	15.0	72	0.42							
								C141B	1567.	2811.	5592.	13728.	44211.	218551.
								KC135	2350.	4217.	8388.	20592.	66316.	327826.
SEY	A20T	4	25.0	25.0	15.0	72	0.42							
								C141B	2148.	3935.	8002.	20162.	66880.	342140.
								KC135	3221.	5902.	12004.	30243.	100320.	513210.
SEY	A20T	5	25.0	25.0	15.0	72	0.42							
								C141B	3936.	7600.	16437.	44945.	166532.	999870.
								KC135	5907.	11400.	24655.	67418.	249798.	1499805.
SEY	A20T	6	25.0	25.0	15.0	72	0.42							
								C141B	3054.	5775.	12204.	32393.	115458.	656829.
								KC135	4581.	8663.	18306.	48589.	173188.	985243.

Figure A-15. Remaining Passes for a 40/60 Mix of C-141/KC-135 Aircraft

END

FILMED

DTIC